Supplementary Information

A comprehensive genomic history of extinct and living elephants

Eleftheria Palkopoulou[a,b,1], Mark Lipson[a], Swapan Mallick[a,b], Svend Nielsen[c], Nadin Rohland[a], Sina Baleka[d], Emil Karpinski[e,f], Atma M. Ivancevic[g], Thu-Hien To[g], R. Daniel Kortschak[g], Joy M. Raison[g], Zhipeng Qu[g], Tat-Jun Chin[g], Kurt W. Alt[h,i], Stefan Claesson[j], Love Dalen[k], Ross MacPhee[l], Harald Meller[m], Alfred L. Roca[n], Oliver Ryder[o], David Heiman[b], Sarah Young[b], Matthew Breen[p], Christina Williams[p], Bronwen L. Aken[q,r], Magali Ruffier[q,r], Elinor Karlsson[b,s], Jeremy Johnson[b], Federica Di Palma[t], Jessica Alfoldi[b], David L. Adelson[g], Thomas Mailund[c], Kasper Munch[c], Kerstin Lindblad-Toh[b,u,2], Michael Hofreiter[d,2], Hendrik Poinar[e,2] and David Reich[a,b,v,1,2]

[a]Department of Genetics, Harvard Medical School, Boston, MA 02115, USA

[b]Broad Institute of MIT and Harvard, Cambridge, MA 02142, USA

[c]Bioinformatics Research Centre, Aarhus University, Aarhus, Denmark

[d]Faculty of Mathematics and Life Sciences, Institute of Biochemistry and Biology, Unit of General Zoology–Evolutionary Adaptive Genomics, University of Potsdam, Potsdam, 14476 Germany

[e]McMaster Ancient DNA Centre, Departments of Anthropology, Biology, Biochemistry and the Michael G. DeGroote Institute for Infectious Disease Research, McMaster University, Hamilton, ON, Canada

[f]Department of Biology, McMaster University, 1280 Main St. West, Hamilton, Ontario, Canada, L8S 4K1

[g]Department of Genetics and Evolution, School of Biological Sciences, The University of Adelaide, Adelaide, SA, 5005, Australia.

[h]Center of Natural and Cultural History of Man, Danube Private University, Krems, Austria

[i]Department of Biomedical Engineering, University Spital, and Integrative Prehistory and Archaeological Science, University of Basel, Switzerland

[j]Institute of Maritime History, Tall Timbers, Maryland, 20690, USA

[k]Department of Bioinformatics and Genetics, Swedish Museum of Natural History, SE-10405 Stockholm, Sweden

[l]Division of Vertebrate Zoology/Mammalogy, American Museum of Natural History, New York, NY, USA

[m]State Office for Heritage Management and Archaeology, Halle (Saale), Germany

[n]Department of Animal Sciences and Institute for Genomic Biology, University of Illinois at Urbana-Champaign, Urbana, Illinois 61801, USA

[o]Institute for Conservation Research, San Diego Zoo, Escondido, California 92027, USA

[p]Department of Molecular Biomedical Sciences, College of Veterinary Medicine, North Carolina State University

[q]Wellcome Trust Sanger Institute, Wellcome Genome Campus, Hinxton, Cambridge, CB10 1SD

[r]European Molecular Biology Laboratory, European Bioinformatics Institute, Wellcome Genome Campus, Hinxton, Cambridge, CB10 1SD

[s]Program in Bioinformatics and Integrative Biology, University of Massachusetts Medical School, Worcester MA 01655, USA

[t]Earlham Institute, Norwich, UK

[u]Science for Life Laboratory, Department of Medical Biochemistry and Microbiology, Uppsala University, Uppsala, Sweden

[v]Howard Hughes Medical Institute, Harvard Medical School, Boston, MA 02115, USA

[1]To whom correspondence should be addressed. Email:

Eleftheria_Palkopoulou@hms.harvard.edu; reich@genetics.med.harvard.edu

[2]K.L.T., M.H., H.P. and D.R. equally supervised this work.

Table of contents

Supplementary Note 1

***De novo* genome assembly of the savanna elephant**

The African savannah elephant (*Loxodonta africana*) genome was constructed from high molecular weight DNA derived from a single female wild-born savanna elephant named Swazi (animal ID: KB13542, North American studbook number 532) that was provided from the San Diego Wild Animal Park, Escondido, CA, USA. The DNA was extracted from blood. Sanger sequencing paired-end reads were generated on ABI 3700 sequencers from 4 kilobases (kb) and 10 kb plasmids, as well as 40 kb fosmids (corresponding to 6.1x, 0.7x and 0.9x sequence coverage, respectively), totaling 33,364,995 Sanger reads. In addition, we generated 458,208 Sanger reads (0.1x) from a bacterial artificial chromosomes (BAC) library (VMRC-15) derived from a male African elephant. These reads, along with the BAC reads, were assembled via the Assemblez module of the Arachne software package using the following command (default settings):

> Assemblez PRE=/seq/assembly_analysis/mammals ATA=projects/Loxodonta_africana RUN=20081105_Assemblez num_cpus=2 num_cpus_pi=2 FORCE_VERSION=True REMOVE_INTERMEDIATES=True remove_duplicate_reads=True n_haplotypes=2 maxcliq1=120 THREE_KILLER_PATCHES=False

Fluorescence in-situ hybridization (FISH) was conducted on ~200 of the BAC clones to anchor 85% of the assembly to chromosomes (Table S1.1). The FISH mapped assembly is named *LoxAfr4* and is available at NCBI and UCSC.

Table S1.1. Statistics for the savanna elephant genome assembly.

Basic Assembly Statistics	
Contig N50	69.0 kb
Contig #	95,866
Scaffold N50	46.4 Mb
Scaffold #	2352
Assembly size (including gaps)	3.19 Gb
FISH chromosome anchoring (*LoxAfr4*)	
Scaffolds mapped #	77
Total bp mapped	2.7 Gb
% assembly anchored	84.60%

Repeat content

RepeatMasker was run on the assembly by the team at the UCSC Genome Browser (University of California, Santa Cruz.) identifying a typical mammalian amount of repeat sequences (Table S1.2).

Table S1.2. Repeat content of the savanna elephant genome assembly.

Repeat class	**% of assembly**
LINE	28.88
SINE	8.67
LTR	6.68
Simple repeat	0.46
Misc. classes	2.99
Total repeat content	47.68

Gene Annotation

Gene annotation was completed by Ensembl and the genome annotation is available on their site: (http://www.ensembl.org/Loxodonta_africana/Info/Annotation). A total of 20,033 coding genes were identified consisting of 28,846 transcripts. In addition, a total of 2,644 non-coding genes and 568 pseudogenes were identified.

Supplementary Note 2

Sample description

Modern specimens

The African savanna elephant (*Loxodonta africana*) sample (*L. africana_B*) was obtained from a wild-born female elephant named Watoto from the Woodland Park Zoological Gardens, Seattle, WA, USA, with the assistance of Bruce Upchurch and Teri Hermann (Table S2.1). The second African savanna elephant sample (*L. africana_C*) was obtained from the same elephant (Swazi) from which the reference genome was generated. The Asian elephant (*Elephas maximus*) samples were obtained from a female elephant named Moola (North American studbook number 42; *E. maximus_D*) from the Dickerson Park Zoo, Springfield, MO, USA with the assistance of Melissa Dickson and a wild-born female elephant named Chendra (North American studbook number 519; *E. maximus_E*) from the Oregon Zoo, Portland, OR, USA with the assistance of David Shepherdson. Fresh blood was drawn directly from living zoo specimens, in conjunction with veterinarians at the respective Association of Zoos and Aquariums (AZA) zoos and following all the appropriate procedures under the Institutional Animal Care and Use Committee (IACUC). Blood draws were performed as a part of regular blood draws for each individual elephant. Genomic DNA was extracted from the blood draws for whole genome sequencing.

The Central African forest elephant (*L. cyclotis*) sample (DS1546; *L. cyclotis_A*) was collected by Nicholas J. Georgiadis (Center for Urban Waters, University of Washington, Tacoma). DNA samples for both African forest elephants (DS1546 and Coco, SL0001; *L. cyclotis_F*) were provided by Prof. Alfred Roca (Department of Animal Sciences and Institute for Genomic Biology, University of Illinois at Urbana-Champaign).

Ancient specimens

Most of the ancient specimens sequenced in this study have been described previously and characterized for part of their nuclear genome and/or their mitochondrial genome (2005-915 (1, 2), *M. primigenius_G*; IK-99-70 (1, 2), *M. primigenius_H*; IK-99-237 (3, 4), *M. americanum_I*; NEPEC (5), *P. antiquus_N;* Lyuba (2, 6), *M. primigenius_S*; Rawlins (2, 7), *M. columbi_U*; UW20579 (2), *Mammuthus*_V; MAS2 (8), *M. americanum_X*; Table S2.1).

Previously published data analyzed in this study

In addition to the specimens sequenced in this study, we re-analyzed publicly available genome-wide data from four Asian elephants (Pavarthy (9), *E. maximus_L;* Asha (9), *E. maximus_M;* Uno (9), *E. maximus_Y*; Jayaprakash (10), E. maximus_Z), two woolly mammoths (Oimyakon (11), *M. primigenius_P;* Wrangel (11), *M. primigenius_Q*) and a straight-tusked elephant (NEU2A (5), *P. antiquus_O*). Information about these specimens is given in Table S2.2.

Published radiocarbon dates were re-calibrated in OXCAL (12) v.4.2 using the IntCal 13 calibration curve (13). Posterior calibrated ranges (99.7%) are given in Tables S2.1, S.2.2.

Table S2.1. Specimens sequenced for this study. Radiocarbon (^{14}C) and calibrated ages are given in years before present (YBP). Abbreviated IDs are given inside parentheses in the ID column.

ID	Specimen	Species	Geographic origin	Material	^{14}C date ± error	99.7% calibrated range (YBP)
L. cyclotis_A (LcycA)	DS1546	*Loxodonta cyclotis*	Congolian forest block, Dzanga-Sangha, Central Africa Republic	Skin biopsy dart	- (modern)	- (modern)
L. africana_B (LafrB)	Watoto NA studbook #78	*Loxodonta africana*	Kenya	Blood	- (modern)	- (modern)
L. africana_C (LafrC)	Swazi KB13542 NA studbook #532	*Loxodonta africana*	Kruger National Park, South Africa	Blood	- (modern)	- (modern)
E. maximus_D (EmaxD)	Moola NA studbook #42	*Elephas maximus*	Myanmar	Blood	- (modern)	- (modern)
E. maximus_E (EmaxE)	Chendra OR-ZOO-ISS-99270 NA studbook #519	*Elephas maximus*	Malaysia (Borneo)	Blood	- (modern)	- (modern)
L. cyclotis_F (LcycF)	Coco SL0001	*Loxodonta cyclotis*	Guinean forest block, Sierra Leone	Blood	- (modern)	- (modern)
M. primigenius_G (MpriG)	2005-915	*Mammuthus primigenius*	Taimyr Peninsula, Russia	Bone	27,740 ± 220	31,026 – 32,596
M. primigenius_H (MpriH)	IK-99-70	*Mammuthus primigenius*	Upper Ikpikpuk River, Alaska, USA	Tooth	41,510 ± 80	44,430 – 45,491
M. americanum_I (MameI)	IK-99-237	*Mammut americanum*	Northern Alaska, USA	Teeth	> 50,000	~50,000 - 150,000
P. antiquus_N (PantN)	NEPEC	*Paleoloxodon antiquus*	Neumark-Nord, Germany	Petrous bone	NA	~120,000
M. primigenius_S (MpriS)	Lyuba	*Mammuthus primigenius*	Yamal Peninsula, Russia	Soft tissue	41,910 ± 550	43,850 – 47,070
M. columbi_U (McolU)	Rawlins	*Mammuthus columbi*	Wyoming, USA	Teeth	11,560 ± 60	13,220 – 13,576
Mammuthus_V (MpriV)	UW20579	*Mammuthus sp.*	Wyoming, USA	Tusk	38,260 ± 790	40,719 – 44,738
M. americanum_X (MameX)	MAS2	*Mammut americanum*	Gulf of Maine, USA	Teeth	11570 ± 60	13581 – 13235

NA studbook #: studbook numbers from the 2011 edition of the North American Region studbook for the African elephant and 2014 edition of the North American Regional studbook for the Asian elephant.

Table S2.2. Specimens sequenced in earlier studies and included in our dataset. Radiocarbon (^{14}C) and calibrated ages are given in years before present (YBP). Abbreviated IDs are given inside parentheses in the ID column.

ID	Specimen	Species	Geographic origin	Material	^{14}C date ± error	99.7% calibrated range	Reference
E. maximus_L (EmaxL)	Pavarthy	*Elephas maximus*	India*	NA	- (modern)	- (modern)	Lynch *et al.* (2015)
E. maximus_M (EmaxM)	Asha	*Elephas maximus*	India*	NA	- (modern)	- (modern)	Lynch *et al.* (2015)
P. antiquus_O (PantO)	NEU2A	*Paleoloxodon antiquus*	Neumark-Nord, Germany	Molar	NA	~120,000	Meyer *et al.* (2017)
M. primigenius_P (MpriP)	Oimyakon	*Mammuthus primigenius*	Oimyakon, Russia	Soft tissue	41,300 ± 900	42,753 – 48,045	Palkopoulou *et al.* (2015)
M. primigenius_Q (MpriQ)	Wrangel	*Mammuthus primigenius*	Wrangel Island, Russia	Molar	3,905 ± 47	4,147 – 4,523	Palkopoulou *et al.* (2015)
E. maximus_Y (EmaxY)	Maya (Uno)	*Elephas maximus*	Assam, India	NA	- (modern)	- (modern)	Lynch *et al.* (2015)
E. maximus_Z (EmaxZ)	Jayaprakash	*Elephas maximus*	Bandipur National Park, Karnataka, India	Blood	modern	- (modern)	Reddy *et al.* (2015)

** The geographic origins of E. maximus_L and E. maximus_M are unknown. They are located in the Kodanadu Elephant training center in southwestern India and in Lynch et al. (9) they are referred to as Indian elephants and so we also assume that they derive from India.*

Supplementary Note 3

DNA extraction, library preparation and sequencing of ancient specimens

Generation of DNA Libraries for Mammuthus sp. and IK-99-237 specimens

Approximately 30 to 85 mg subsamples were taken from five specimens: 2005_915 [bone]; IK-99-237 [tooth]; Lyuba [abdominal and subcutaneous fat]; Rawlins [tooth]; and UW20579 [tusk].

Extract Preparation:

Samples 2005_915 and Lyuba

Subsamples were digested using 1 ml of 0.5 M EDTA for 24 hours at room temperature while shaking at 700 rpm. Sample tubes were spun down for 5 minutes at 16,000 G and demineralized supernatants removed and saved prior to digestion with 750 µl of digestion solution (Final conc: Tris-Cl – 0.01 M; Sarcosyl – 0.5%; Proteinase K – 0.25 mg/ml; $CaCl_2$ – 0.005 M; DTT – 50 mM; PVP – 1%; PTB – 2.5 mM). Digestion was carried out for 21 hours at 45°C with shaking at 700 rpm. Samples were spun down for 5 minutes at 16,000 G and supernatants transferred to sterile 2 ml tubes.

Following digestion, 375 µl of digestion supernatant was removed, combined with 5 volumes PB buffer, and bound to MinElute PCR Purification spin columns for 30 seconds at 8,000 G. Columns were washed with PE buffer twice: first with 750 µl (30s; 8,000 G) then with 720 µl (30s; 16,000 G). Samples underwent a dry spin, before being eluted with 2x 20 µl of EBT (Buffer EB with 0.0005% Tween-20).

Five microliters of 1 M Tris-Cl were added to the remaining digestion supernatants and incubated for 22 hours at room temperature with shaking (700 rpm). The remaining volumes of digestion supernatant were purified as above, except using 700 µl PE buffer for both washes.

Extracts from both rounds were subsequently combined. Twenty microliters of the combined 2005_915 extract was further purified over MinElute PCR Purification spin columns using 6 volumes buffer PB. Samples were bound to the column by spinning for 1 minute at 3,300 G, washed twice with 700 µl buffer PE (1 minute at 4,500 G), and dried by spinning at max speed for 1.5 minutes. Purified extracts were eluted in 22 µl buffer EB.

Sample IK-99-237

Samples were demineralized with 1 ml of 0.5 M EDTA for 22 hours at room temperature with shaking (700 rpm for 30 minutes; 600 rpm remainder). Following incubation, samples were spun down for 5 minutes at 16,000 G and the supernatant was removed and collected in sterile 2 ml tubes. Digestion occurred with 900 µl of digestion solution (Final conc: Tris-Cl – 0.01 M; Sarcosyl – 0.5%; Proteinase K – 0.25 mg/ml; $CaCl_2$ – 0.005 M; DTT – 50 mM; PVP – 1%; PTB – 2.5 mM) for 19 hours at 55°C (shaking at 750 rpm for 14 hours then rotation). Tubes were

again spun down and supernatants saved. All samples underwent a second round of demineralization (19 hours) and digestion (5 hours) except with rotation. Supernatants from the second demineralization and digestion were purified separately, using 500 µl of both PCI (phenol/chloroform/isoamyl alcohol) (pH 8) and chloroform. Digestion supernatants underwent a second round of PCI purification (900 µl) due to the presence of a large interphase. Aqueous phases were concentrated over pre-wet (0.1xTE) 30kDa Ultra-0.5 Centrifugal Filter tubes, and washed twice with 450 µl of 0.1xTE. Final extracts generated from both supernatants were pooled and purified over MinElute spin columns in an identical fashion to 2005_915, except in 44 µl buffer EB.

Sample Rawlins

Samples were pre-digested using 300 µl of a pre-digestion solution (Final conc: 0.5 M EDTA; 0.1% Sarcosyl; 0.25 mg/ml Proteinase K) for 45 minutes at 1000 rpm. Tubes were centrifuged at 1,000 G for 1 minute and the pre-digestion solution was removed.

Samples underwent three rounds of alternating demineralization and digestion steps. Demineralization was carried out using 500 µl of 0.5 M EDTA, while digestion was carried out using 350 µl of a digestion solution (Final conc: Tris-Cl – 0.01 M; Proteinase K – 0.25 mg/ml; $CaCl_2$ – 0.005 M; DTT – 50 mM; PVP – 1%; PTB – 2.5 mM). Samples were centrifuged at 10,000 G for 5 minutes following each incubation and the supernatants were collected in sterile 2 ml tubes. All incubations were carried out at room temperatures for 22 – 24 hours shaking at 1000-1100 rpm.

Samples were purified using 1.6 ml each of PCI and chloroform. Aqueous phases were concentrated over pre-wet (0.1xTE) 10kDa Ultra-0.5 Centrifugal Filter tubes, washing twice with 450 µl of 0.1xTE. Twenty microliters of final extract was further purified over MinElute PCR Purification spin columns in an identical manner to 2005_915.

Sample UW20579

Samples underwent two subsequent rounds (24 hours first round; 16 hours second round) of demineralization using 1 ml of 0.5 M EDTA at room temperature with rotation. Tubes were spun after each round and supernatants removed and saved in sterile 2 ml tubes. Following both demineralization rounds, samples were digested once using 980 µl of digestion solution (Final conc: Tris-Cl – 0.01 M; Sarcosyl – 0.5%; Proteinase K – 0.25 mg/ml; $CaCl_2$ – 0.005 M; DTT – 50 mM; PVP – 1%) at 50°C for 6 hours.

Second round demineralization and digestion supernatants were purified individually using 500 µl and 980 µl of PCI respectively, followed by 500 µl of chloroform. Aqueous phases were then concentrated over pre-wet (0.1xTE) 30kDa Ultra-0.5 Centrifugal Filter tubes, and washed twice with 450 µl of 0.1xTE. Final extracts were raised to 60 µl using 0.1x TTE, combined, and

purified over MinElute PCR purification spin columns in an identical manner to 2005_915, except in 44 µl buffer EB.

Library Preparation:

Final extracts were converted into UDG-treated libraries using established protocols (14, 15), with the modification listed in Karpinski *et al.* (16), except using a final adapter concentration of 1 µM.

Two reactions of 15 µl heat-inactivated library each were indexed for 10 cycles using the following protocol: 95°C for 2 minutes; 10 cycles of 95°C for 15 seconds, 60°C for 30 seconds, 68°C for 1 minute; 68°C for 1.5 minutes; 4°C for 30 seconds. Indexing reactions were conducted using Accuprime Pfx polymerase with the following final concentrations: 10x Accuprime Pfx rxn mix – 1x; forward and reverse indexing primers – 500 nM; EvaGreen – 0.75x; Accuprime Pfx – 0.042 U/µl. Both indexing reactions per library were pooled and combined with ~6 volumes of PB buffer, and purified over MinElute PCR purification spin columns. Columns were washed once with 720 µl buffer PE and eluted twice, first with 20 µl buffer EB, and a second time with 20 µl buffer EBT.

Generation of additional libraries

Ten additional subsamples each (~100mg each) were taken from specimens 2005_915 [bone], IK_99-237 [tooth], Lyuba [soft tissue], and Rawlins [bone] as well as 7 for IK_99-70 [bone]. Samples were pulverized to small crumbles or chunks using a hammer. Subsamples from each specimen were accompanied by a *Mylodon darwinii* carrier blank and an extraction blank to monitor contamination.

Subsamples and blanks underwent an initial wash with 0.5 M EDTA at 600 rpm for 20 minutes, after which samples were centrifuged and the wash supernatant collected. This was followed by a demineralization step using 1 ml of 0.5 M EDTA for 16-24 hours at 600 rpm and room temperature. All tubes were centrifuged to pellet any residual material and the supernatant was removed and stored at -20°C in sterile 2 ml tubes. Samples were then digested using 0.75 ml of Proteinase K digestion buffer (Final conc: Tris-Cl (pH 9.0) – 0.1 M; Sarcosyl – 0.20%; Proteinase K – 0.25 mg/ml; $CaCl_2$ – 0.01 M) for 1.5 to 5 hours at 45°C. Tubes were again centrifuged to pellet any residual material, and the supernatant removed and combined with the demineralization supernatant. All subsamples and blanks underwent two rounds of alternating demineralization and digest under the above conditions, with supernatants within rounds being pooled.

Second round demineralization and digestion supernatants were extracted using an organic extraction protocol using 800 µl of PCI (phenol/chloroform/isoamyl alcohol) (pH 8) and 700 µl chloroform. Aqueous phases from 3 to 5 subsamples corresponding to the same specimen were combined and concentrated over pre-wet (350 µl 1xTE) 30kDa Amicon Ultra-0.5 Centrigugal

Filter tubes, producing 2 to 3 extracts per specimen. 30 µl of extract was further purified over MinElute PCR Purification Kit spin columns to remove any residual traces of phenol that may have been introduced during extraction. Purifications were preformed according to the manufacturer's recommend protocol except with an additional wash with PE buffer, and elution in 25 µl of TEB (EDTA added to 1mM final concentration).

Extracts were converted into UDG-treated libraries using a double stranded library preparation protocol described previously (14, 15) with modifications as described in Karpinski *et al.* (16), except with a final adapter concentration of 0.25 µM. Libraries were constructed using 24 µl of extract alongside a library preparation blank to monitor contamination introduced at this step.

Sample specific indices were added to each library through four identical indexing reactions (5 µl library as template per reaction), to account for the high concentration of input template. Indexes were added in 20 µl final reactions with the following concentrations: KAPA SYBR®FAST qPCR Master Mix – 1x; forward indexing primer – 800 nM; reverse indexing primer – 800 nM. Indexing was carried out using the following protocol: 95°C for 3 minutes; 6 cycles of 95°C for 15 seconds, 60°C for 30 seconds, 68°C for 60 seconds; 68°C for 2 minutes; 8°C for 30 seconds. Pairs of indexed libraries were subsequently purified over MinElute PCR Purification Kit spin columns. Purification was performed as per manufacturer's recommend protocol except with an additional wash with PE buffer, and elution in 13 µl of TEB. Pairs of purified eluted indexed libraries were then further combined for a final volume of 26 µl of indexed library.

Generation of DNA libraries for straight-tusked and MAS2 specimens.

DNA extraction and library preparation methods for *P. antiquus_N* (NEPEC) are described in Meyer *et al.* (5). For *M. americanum_X,* we extracted DNA and prepared a barcoded single-stranded library following the same protocols as in Claesson *et al. (8)*.

Sequencing

A pool of 7 libraries from 7 samples (2005_915, IK-99-237, Lyuba, Rawlins, UW20579 and 2 additional samples not analyzed in this study) were sequenced on a single Illumina MiSeq run for 2x75bp cycles and dual index reads. After a manual gel cut from a 2% NuSieve GTG agarose gel to remove short fragments and cleanup with MinElute Gel Extraction Kit (Qiagen), libraries from IK-99-237, Lyuba, Rawlins and UW20579 were submitted for sequencing at Illumina FastTrack Services for 2×100bp cycles on Illumina HiSeqs. A total of 10 lanes were sequenced for IK-99-237, 3 lanes for Lyuba, 2 lanes for Rawlins and 10 lanes for UW20579. New libraries for 2005-915 (3 libraries) and additional libraries for IK-99-237 (3 libraries), as well as 2 libraries from another sample (IK-99-70) were pooled in equimolar ratios and sequenced on one NextSeq 500 run (2x76bp cycles). After data analysis, another NextSeq 500 run (2x75bp cycles) was performed for the 3 libraries of IK-99-237.

Low coverage shotgun sequencing data for NEPEC and NEU2A were previously reported in Meyer *et al.* (5). MAS2 was sequenced during that initial sequencing of NEPEC and NEU2A (together with another sample not analyzed in this study) as part of two library pools on 2 NextSeq500 flowcells (2x76bp cycles).

Additional sequences were generated for NEPEC after the library was subjected to an automatic gel cut using a Pippin Prep and a 3% gel cassette for an insert size of 35-50bp for one NextSeq500 run (2x76bp cycles) at Harvard Medical School, followed by 12 NextSeq 500 runs (2x42bp cycles) at the Broad Institute.

Supplementary Note 4

Processing and mapping ancient sequence data

Raw reads were processed in the following way: bcl2fastq v.2.15 was used to convert bcl files to fastq files and de-multiplex reads based on their indexes. Trimming of adapters and merging of paired-end reads was performed with SeqPrep v.1.1 (https://github.com/jstjohn/SeqPrep) using default parameters except for a minor modification to the source code that takes the best possible quality score of the bases in the merged region instead of aggregating them. Merged reads with a minimum length of 30bp were retained. Merged reads were aligned against the African savanna elephant reference genome (*LoxAfr4*; downloaded from ftp://ftp.broadinstitute.org/distribution/assemblies/mammals/elephant/loxAfr4/) with BWA (17) v.0.7.8 using the 'aln' algorithm and the 'samse' command. The following parameters were implemented –l 16500 –n 0.01 –o 2 to deactivate seeding, allow for more substitutions and permit up to two gaps (as recommended in Kircher M. (18)). Alignments were converted to bam format with SAMtools (19) v.0.1.19 and PCR duplicates at the library level were discarded using a custom python script that removes merged reads with identical coordinates at both 5' and 3' end and takes into account the orientation of the reads.

In addition to the sequence data generated for this study, we included previously published genome data from two woolly mammoths that were sequenced at high coverage (11) (Wrangel and Oimyakon) and previously published low-coverage data from two *P. antiquus* samples (5) (NEPEC and NEU2A). For Wrangel and Oimyakon, we used bam files generated in Palkopoulou *et al.* (11) prior to the step removing duplicate reads; this step was instead conducted using the custom python script mentioned above. This resulted in a higher number of retained unique reads compared to using SAMtools' 'rmdup' command with the '-s' option that was implemented in the original paper, which takes into account only the 5'end coordinates of reads to mark PCR duplicates. The average coverage of the Wrangel and Oimyakon genomes therefore increased to ~19-fold and ~13-fold, respectively (Table S4.1). Woolly mammoths M4 and M25, which had been sequenced at high coverage by Lynch *et al.* (9) were not included in our dataset since it has been suggested that they may have been contaminated by other elephantid DNA(20). For NEPEC, the low-coverage shotgun sequence data published by Meyer *et al.* (5) was merged with higher-coverage sequence data generated at the Broad Institute and Harvard Medical School for this study. Sequencing characteristics, alignment statistics and average depth of coverage for each sample are given in Table S4.1.

We used PMDtools (21) v.0.59 to identify post-mortem degradation profiles for each library with the option '--platypus' that estimates deamination rates across sequence reads and in CpG dinucleotides in parallel. Overall, double-stranded libraries that were treated with the USER enzyme prior to sequencing exhibit negligible frequencies of cytosine to thymine and guanine to adenine substitutions at the 5' and 3' ends, respectively (solid lines in Figure S4.1). In contrast, nucleotide misincorporation frequencies are higher in a CpG context (intermittent lines in Figure

S4.1) since deaminated methylated cytocines lead to thymines that cannot be removed by enzymes that treat uracils (22). On the other hand, uracil-treatment is less efficient even in a non-CpG context in single-stranded libraries that exhibit cytosine to thymine misincorporations at both the 5' and 3' end of the reads (solid lines in Figure S4.2) as expected (23).

To infer the sex of each specimen, we calculated the ratio of reads that aligned to the X-chromosome to the number of reads that aligned to chromosome 8, which has a size comparable to that of the X-chromosome, normalized by the length of the respective chromosomes. Because females carry two X chromosomes, this ratio is expected to be close to 1 in females, whereas for males that carry only one X chromosome, the ratio is expected to be close to 0.5. Using this method, we were able to predict the sex of unidentifiable specimens and genetically verify the sex of specimens that were morphologically characterized as males or females (Table S4.1).

Table S4.1. Sequencing statistics of ancient DNA data processed or re-processed in this study.

ID	Library protocol	UDG-treatment	Sequencing	# mapped reads	Duplication rate	# unique reads	Mean read length (bp)	Average coverage	Sex
MpriG	ds	+	HMS	54,587,646	0.688	17,053,464	109	0.60	M
MpriH	ds	+	HMS	26,871,928	0.026	26,174,677	58	0.49	F
MameI	ds	+	HMS, IFT	398,860,978	0.506	197,037,643	63	3.96	M
PantN	ss	+	Broad Institute, HMS & data from Meyer *et al*. (2017)	1,399,425,736	0.172	1,158,622,813	39	14.64	M
PantO	ss	+	data from Meyer *et al.* (2017)	12,136,348	0.021	11,879,136	38	0.14	F
MpriP	ds	+	data from Palkopoulou *et al.* 2015	901,920,079	0.185	734,754,790	54	12.77	M
MpriQ	ds	+	data from Palkopoulou *et al.* 2015	959,343,713	0.083	879,274,567	67	19	M
MpriS	ds	+	HMS, IFT	131,600,567	0.639	47,513,405	60	0.91	F
McolU	ds	+	HMS, IFT	121,781,498	0.058	114,746,258	41	1.53	M
MpriV	ds	+	HMS, IFT	829,957,506	0.481	430,601,883	42	5.86	M

MameX	ss	+	HMS	70,829,305	0.276	51,314,205	48	0.79	F

ds/ss: double-stranded / single-stranded library preparation protocol
HMS: sequencing performed at Harvard Medical School
Broad Institute: sequencing performed at the Broad Institute
IFT: sequencing performed at Illumina Fast Track Services
 # unique reads: number of reads after removal of PCR duplicates
Mean read length: mean read length of unique reads
M/F: male/ female sex identification based on the normalized number of reads that mapped to chrX

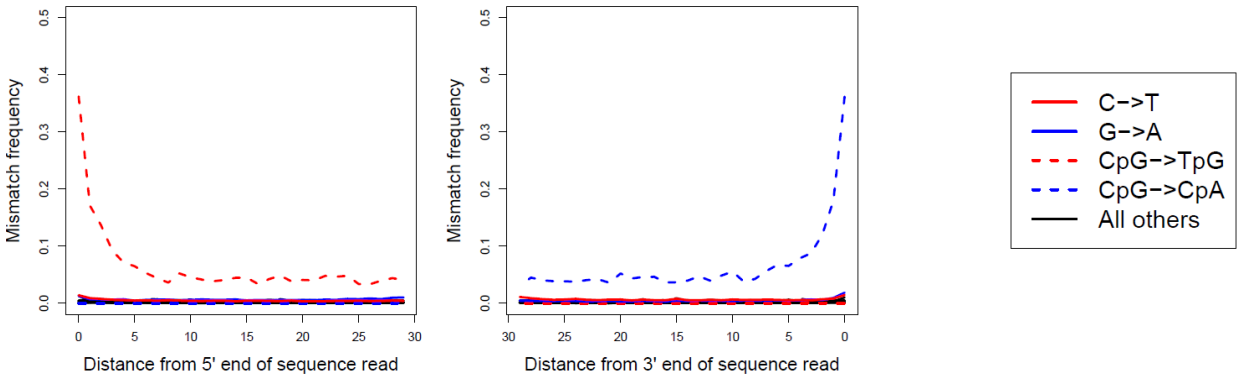

Figure S4.1. Post-mortem damage profiles for *Mammuthus_V.* Similar damage profiles are observed for all the double-stranded libraries sequenced in this study.

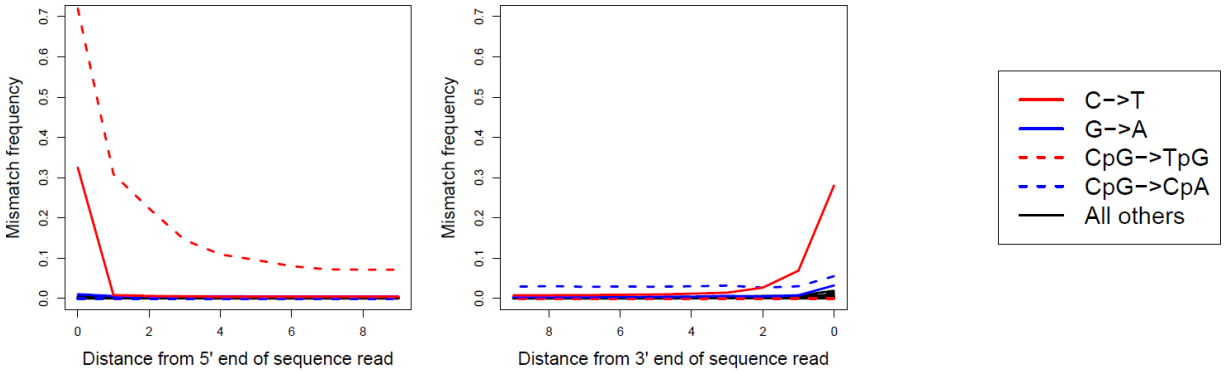

Figure S4.2. Post-mortem damage profiles for *P. antiquus_N.* Higher rates of cytocine to thymine misincorporations are observed at both 5' and 3' ends. Note that in CpG context, cytocine to thymine misincorporations are estimated towards the 5' end of the reads only (left plot). Similar damage profiles are observed for all the single-stranded libraries sequenced in this study.

Supplementary Note 5

Sequencing and processing of modern elephant data

Illumina fragment libraries were constructed from genomic DNA of the 2 African savanna, 2 African forest and 2 Asian elephants, and sequenced to 30x on Illumina HiSeq2000 with v3 chemistry and 101bp paired-end reads. Reads were de-multiplexed with Broad Institute's Picard (http://broadinstitute.github.io/picard/) pipeline. Adapters were trimmed with SeqPrep v.1.1 (https://github.com/jstjohn/SeqPrep) using default parameters without merging overlapping reads. Paired-end reads were aligned to the African savanna elephant reference genome using BWA (17) v.0.7.8, employing the 'aln' algorithm with default parameters (separately for read 1 and read 2) and the 'sampe' command. SAMtools (19) v.0.1.19 was used to convert alignments to bam files, merge bam files derived from the same library and remove PCR duplicate reads using the command 'rmdup' with default parameters.

In addition to the sequence data generated at the Broad Institute for this study, we included previously published genome data from four Asian elephants (Pavarthy, Asha, Maya (9); Jayaprakash (10)). Sequencing reads were downloaded in SRA format (SRA projects PRJNA281811, PRJNA301482, respectively), converted to fastq files with SRAtoolkit v.2.3.5 and processed using the pipeline described above. Sequencing characteristics, alignment statistics and average depth of coverage for each sample are given in Table S5.1.

As described in Supplementary Note 4, we genetically determined the sex of each specimen. By calculating the expected number of reads aligning to chromosome X for a male or female and comparing it to the actual number of reads aligned to chromosome X, we could confirm the sex of all modern specimens, as shown in Table S5.1.

Table S5.1. Sequencing statistics of modern elephant data processed or reprocessed in this study.

ID	Library protocol	Sequencing	# reads	# mapped reads	Mean read length (bp)	Duplication rate	# unique reads	Average coverage	Sex
LcycA	ds	Broad Institute	1,003,840,320	905,978,933	101	0.031	877,722,371	27.78	F
LafrB	ds	Broad Institute	1,147,337,718	1,000,856,392	101	0.024	976,964,325	30.44	F
LafrC	ds	Broad Institute	1,219,881,062	1,114,442,274	101	0.041	1,068,611,598	33.42	F
EmaxD	ds	Broad Institute	1,367,459,696	1,283,115,660	101	0.055	1,212,733,645	38.94	F
EmaxE	ds	Broad Institute	1,193,281,098	1,107,077,600	101	0.089	1,008,964,513	32.20	F
LcycF	ds	Broad Institute	1,205,810,958	1,073,866,040	101	0.039	1,031,992,089	32.06	M

EmaxL	ds	Seq. data from Lynch *et al.* 2015	939,546,024	888,615,529	101	0.055	840,083,119	27.02	F
EmaxM	ds	Seq. data from Lynch *et al.* 2015	1,065,619,302	1,013,574,726	101	0.071	941,145,955	30.27	F
EmaxY	ds	Seq. data from Lynch *et al.* 2015	1,349,450,838	1,238,676,303	95	0.039	1,190,011,505	35.90	F
EmaxZ	ds	Seq. data from Reddy *et al.* 2015	534,073,404	446,551,000	108	0.060	419,643,596	14.58	M

Broad Institute: sequencing performed at the Broad Institute
 # unique reads: number of reads after removal of PCR duplicates
Mean read length: mean read length of unique reads
M/F: male/ female sex identification based on the normalized number of reads that mapped to chrX

Supplementary Note 6

Filtering and genotype calling

Standard filters

Throughout the analyses presented in this paper we applied filters consisting of minimum base quality = 30 and minimum mapping quality = 30 or 37 (for modern and ancient sequencing data, respectively). We further developed and applied two mappability filters similar to the genome alignability filter described in Prüfer *et al.* (24) to exclude regions that can lead to ambiguous alignments of short sequences. We used programs developed by Heng Li and described in http://lh3lh3.users.sourceforge.net/snpable.shtml to identify positions in the reference genome (*LoxAfr4*) for which at least 50% (for the 50% stringency filter) or 90% (for the 90% stringency filter) of all possible 35mers that overlap these regions do not find a match to any other position, allowing for up to one mismatch. The mappability filter with 50% stringency masks ~829 million base pairs (Mbp; 26.59%) of the reference genome while the 90% stringency filter masks ~1,192Mbp (38.22%) of the reference genome. The latter more conservative filter was applied in most analyses.

The mapping quality threshold (MQ ≥ 30) resulted in the removal of a substantial number of reads in some of the extant elephants. In particular, the average coverage of *L. africana_B* decreased from 30.44-fold to 16.75-fold, of *L. africana_C* from 33.42-fold to 14.5-fold, and of *L. cyclotis_F* from 32.06-fold to 14.7-fold. All extant elephants sequenced in this study were processed under the same conditions in the lab and using the same bioinformatics pipeline (Figure S6.1). Since the average coverage of these individuals is still higher than 10-fold after the removal of reads with MQ < 30, we decided to keep this stringent mapping quality filter for all modern elephant genomes.

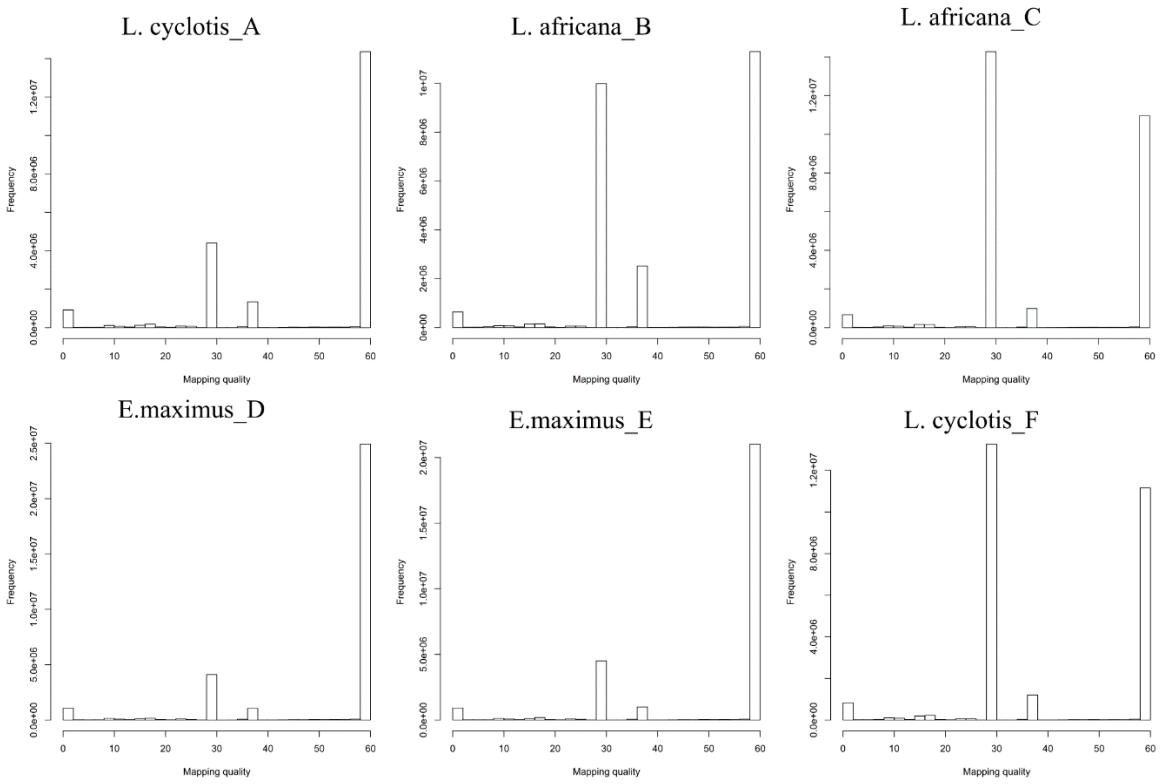

Figure S6.1. Mapping quality distribution of reads in extant elephants sequenced for this study. Approximately half the number of reads in *L. africana_B, L. africana_C* and *L. cyclotis_F* are filtered out when the minimum mapping quality threshold is equal to 30.

Genotype calling

Most analyses presented in this paper used single, randomly sampled alleles per site unless stated otherwise. This strategy was employed to exploit all samples, including those with low average depth of coverage (even < 1x) for which reliable diploid calls could not be produced, and to alleviate potential biases from alignment to the African savanna elephant reference genome (*LoxAfr4*, which originates from the same elephant as the genome sequence of *L. africana_C*), with the drawback that randomly sampled alleles introduce a higher sequencing error rate. To quantify such biases and the sequencing error rate, we generated two types of pseudo-haploid sequences: *i)* with random allele calls (from here on referred to as random sequences) and *ii)* with majority allele calls (from here on referred to as majority sequences), and estimated sequence divergence to the reference genome for each type of sequence. For ancient DNA data, we also trimmed 5bp from both 5' and 3' ends of the reads to exclude sites with post-mortem damage.

Alignment biases are expected to be more prevalent in majority sequences since reads with alleles identical to the reference sequence will preferentially align to the reference compared to reads with alternative alleles, leading to a higher number of reference-matching alleles at

polymorphic sites. In random sequences on the other hand, alignment biases are expected to be weaker while sequencing errors are expected to have a stronger effect, since single random alleles are sampled per site. However, in genomes with low average sequencing depth (<1x), most sites will be covered by at most one read, and therefore the effects of sequencing errors should be similar in random vs. majority sequences while the effects of alignment biases should be overall lower.

As expected based on the above assumptions, sequence divergence to the reference genome is higher for random sequences than for majority sequences (with the exception of *M. primigenius_G*; Table S6.1). Their difference ranges from 2.31×10^{-4} – 1.28×10^{-3} in genomes with higher average coverage and from 1.7×10^{-5} – 8.08×10^{-5} in genomes with low average coverage (<1x). For higher coverage genomes, this is due to the combined effect of stronger alignment biases in the majority sequences and a higher rate of sequencing errors in the random sequences, whereas for low-coverage genomes, the differences are much smaller because very few sites will be covered by more than one read (reference bias becomes worse for higher coverage data). A similar pattern is observed when excluding transitions but with overall lower estimates of divergence to the reference genome for both random and majority sequences relative to those obtained from all substitutions (Table S6.1).

We devised a method that uses the empirical divergence estimates for all sites and for transversions, from random and majority sequences of high-coverage genomes, to obtain a rough estimate of the sequencing error rate, under the assumptions that random sequences eliminate most or all of the reference bias, while majority sequences eliminate most or all of the sequencing errors. The variables of our model are:

E = sequencing error rate, assumed for simplicity to only affect randomly-called sequences
B = reference bias effect, assumed for simplicity to only affect majority-called sequences
D = true divergence parameter (for all sites)
f = the ratio of divergence for transversions to divergence for all sites

Under this model, and assuming that sequencing error is equally likely for all sites and that reference bias is equally strong at all polymorphic sites, the parameters from the data are:

pi_allsites_random = D + E
pi_allsites_majority = D – B
pi_tv_random = fD + E
pi_tv_majority = fD - fB

where pi_allsites and pi_tv are the empirical sequence divergence estimates for all sites and transversions, respectively (Table S6.1). Given these estimates, we can solve as follows:

f = pi_tv_majority/pi_allsites_majority
D = (pi_allsites_random - pi_tv_random)/(1-f)

E = pi_allsites_random - D
B = D - pi_allsites_majority

We performed these calculations for each high-coverage sample and obtained estimates of the sequencing error rate (9.17×10^{-5} – 4.44×10^{-4}) and reference bias (1.83×10^{-4} – 1.19×10^{-3}; Table S6.1). We should note that these are approximate estimates since there is potentially still some remaining reference bias in the random sequences and sequencing errors in the majority sequences. In most cases, the estimated approximate reference bias is slightly higher than the respective sequencing error rate. For ancient samples, we are probably underestimating sequencing error rate and overestimating reference bias since the assumptions described above are not really true: residual damage affects mostly transitions, so the sequencing error rate is higher for transitions compared to transversions, a behavior attributed to reference bias but not errors under our model. In the most extreme example, for *P. antiquus_N* for instance, the reference bias (1.19×10^{-3}) is estimated to be ~13-fold higher than the sequencing error rate (9.17×10^{-5}). In fact, some of the former likely represents sequencing errors due to ancient DNA damage.

Table S6.1. Sequence divergence to the African savanna elephant reference genome (*LoxAfr4*) and approximate estimates of sequencing error rate and reference bias. Sequence divergence was estimated from sequences with random allele calls (π_{random}) and sequences with majority allele calls ($\pi_{majority}$) for all sites and transversions. $f_{majority}$ is the ratio of divergence for transversions to divergence for all sites with majority allele calls, and D is the estimated true divergence for all sites taking into account sequencing error rate (E) and reference bias (B). These parameters were calculated as described in the text for high-coverage genomes only, for which reference biases have a stronger effect in majority sequences while sequencing errors have a stronger effect in random sequences.

	All substitutions			**Transversions**						
	π_{random}	**$\pi_{majority}$**	**$\pi_{random} - \pi_{majority}$**	**π_{random}**	**$\pi_{majority}$**	**$\pi_{random} - \pi_{majority}$**	**$f_{majority}$**	**D**	**E**	**B**
LcycA	0.00641	0.00598	4.27E-04	0.00207	0.00184	2.24E-04	0.30801	0.00628	1.34E-04	2.93E-04
LafrB	0.00181	0.00093	8.79E-04	0.00086	0.00031	5.43E-04	0.33518	0.00144	3.74E-04	5.05E-04
LafrC	0.00122	0.00046	7.54E-04	0.00064	0.00017	4.68E-04	0.36506	0.00091	3.03E-04	4.51E-04
EmaxD	0.00832	0.00777	5.45E-04	0.00278	0.00244	3.44E-04	0.31342	0.00807	2.52E-04	2.93E-04
EmaxE	0.00833	0.00781	5.17E-04	0.00278	0.00244	3.39E-04	0.31251	0.00807	2.58E-04	2.59E-04
LcycF	0.00704	0.00600	1.05E-03	0.00248	0.00185	6.30E-04	0.30799	0.00660	4.44E-04	6.04E-04
MpriG	0.00796	0.00890	-9.37E-04	0.00259	0.00261	-1.70E-05				
MpriH	0.00894	0.00890	3.91E-05	0.00265	0.00264	1.07E-05				
MameI	0.01717	0.01636	8.17E-04	0.00523	0.00504	1.93E-04				
EmaxL	0.00820	0.00774	4.52E-04	0.00270	0.00243	2.75E-04	0.31326	0.00800	1.94E-04	2.57E-04
EmaxM	0.00823	0.00777	4.63E-04	0.00272	0.00244	2.85E-04	0.31384	0.00803	2.03E-04	2.60E-04
EantN	0.00778	0.00650	1.28E-03	0.00239	0.00195	4.47E-04	0.29951	0.00769	9.17E-05	1.19E-03
EantO	0.00717	0.00715	1.70E-05	0.00271	0.00270	1.00E-05				

MpriP	0.00826	0.00764	6.16E-04	0.00266	0.00234	3.22E-04	0.30580	0.00807	1.92E-04	4.25E-04
MpriQ	0.00831	0.00767	6.37E-04	0.00266	0.00236	2.98E-04	0.30728	0.00816	1.48E-04	4.89E-04
MpriS	0.00849	0.00844	4.88E-05	0.00283	0.00280	2.80E-05				
McolU	0.00855	0.00832	2.31E-04	0.00290	0.00277	1.27E-04				
MamV	0.00827	0.00766	6.16E-04	0.00270	0.00239	3.03E-04				
MameX	0.01603	0.01595	8.08E-05	0.00514	0.00510	4.37E-05				
EmaxY	0.00822	0.00773	4.90E-04	0.00273	0.00242	3.14E-04	0.31253	0.00799	2.34E-04	2.56E-04
EmaxZ	0.00806	0.00766	3.91E-04	0.00264	0.00238	2.65E-04	0.31023	0.00785	2.08E-04	1.83E-04

To investigate reference-alignment bias further and explore its relationship to coverage, we estimated *D*-statistics (25) as described in Supplementary Note 11 using majority allele calls, and assessed the effect of read coverage using a method similar to that in Prüfer *et al.* (24) (Supplementary Information 16a). We calculated the cumulative distribution function of coverage in each genome by estimating depth of coverage at each position of the genome that passed our filters. Based on this function, we ranked positions in the genome to deciles of coverage and used positions from each decile to calculate *D*-statistics. Alignment biases appear to have an effect on *D*-statistics estimated from majority allele calls, and this effect is stronger at sites with higher read coverage (Figure S6.2). For example, when computing *D (L. africana_C, L. cyclotis_A; E. maximus_D, E. maximus_E)*, restricting to sites with higher read coverage in *E. maximus_D*, we obtain significantly positive *D*-statistics, while restricting to sites with higher coverage in *E. maximus_E* leads to significantly negative *D*-statistics, suggesting in each case attraction between the higher-coverage Asian elephant and the source of the reference genome (*L. africana_C*).

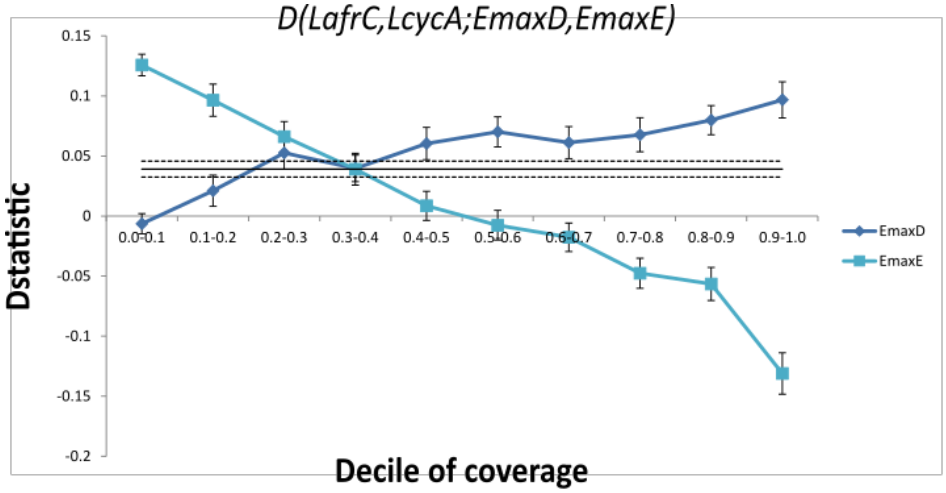

Figure S6.2. *D*-statistic estimates as a function of decile in read coverage for the test *D (L. africana_C, L. cyclotisA; E. maximus_D, E. maximus_E)*. Solid black lines indicate the mean genome-wide *D*-statistic with one standard error indicated by dotted lines. Error bars give one standard error.

Based on these observations, we decided to use random allele calls instead of majority allele calls to minimize biases induced by alignment to the reference genome since the effect of reference bias can be more detrimental in analyses of shared genetic drift compared to random sequencing errors. However, as discussed in Supplementary Notes 11 and 12, reference biases still exist to some extent in the random sequences, contributing to excess genetic affinities to *L. africana* (the origin of the reference genome), and therefore we are cautious with interpreting such statistics as signals of gene flow.

Supplementary Note 7

Mitochondrial genome sequences and contamination estimates

Mitochondrial phylogeny

The mitochondrial genome sequence of a woolly mammoth (NC007596) was added to the savanna elephant reference genome (*LoxAfr4*) prior to read alignment to obtain both nuclear and mitochondrial (mt) DNA sequences. As described in Prufer *et al*. (24), using BWA (17) for alignment to a circular genome would lead to reduced coverage at the beginning and end of the mt genome. Hence, to facilitate mapping at these regions, we added the first 240bp of the mt reference genome at the end of it. Using a mapping quality filter of 30 for modern samples and 37 for ancient samples, we obtained complete and partial mt genomes with average coverage ranging from 0.39- to over 1000-fold (Table S7.1).

We called consensus sequences with SAMtools (19) v.0.1.19 using the 'mpileup' command and the 'vcf2fq' command from vcfutils.pl applying the following filters: minimum base quality of 30, minimum mapping quality of 30 for modern samples and 37 for ancient samples, minimum root-mean-squared mapping quality of 30, minimum depth of 3 reads and filtering out 5bp around indels. The generated sequences were aligned to publicly available mt genome sequences of 3 savanna, 8 forest, 3 Asian and 4 straight-tusked elephants, 96 woolly, 16 Columbian and 43 *Mammuthus sp.* (comprised of 1 *M. exilis,* 2 *M. jeffersonii* and 40 undetermined *Mammuthus* specimens), and one American mastodon, using MAFFT (26, 27) with the option –ginsi. Note that some of the previously published sequences originate from the same specimens sequenced in this study.

We performed maximum likelihood phylogenetic analysis on the dataset described above with RAxML (28) v.8.2 using the GTRGAMMA model of nucleotide substitution and 100 bootstrap replicates (Figure S7.1). The obtained phylogeny was visualized in FigTree v.1.4.3. (http://tree.bio.ed.ac.uk/software/figtree/).

As originally described in Meyer *et al.* (5), the straight-tusked elephant mt genome sequences fall within the mt diversity of forest elephants (clade *F*). The mt genome sequences from the Neumark-Nord (NN; ~120,000 years old) specimens are most closely related to the western subclade of clade *F* (*L. cyclotis_F*, NC020759 and JN673264). Note that sequence *L. cyclotis_F* was generated from the same elephant (Coco) from Sierra Leone, West Africa, as were sequences NC020759 and JN673264. Similarly, sequences KY499555 and KY499556 were generated from the same specimens (NEPEC and NEU2A, respectively) as *P. antiquus_N* and *P. antiquus_O*, respectively, but their sequences are not identical due to the low mt coverage of the latter obtained in this study from shotgun sequencing data. The mt genome sequence from the straight-tusked elephant from Weimar-Ehringsdorf (WE; ~244,000 years old) is placed basal to

the western and west-central subclades of clade *F*, while *L. cyclotis_A* groups within the north-central subclade of clade *F*.

L. africana_B and *L. africana_C* from Kenya and South Africa, respectively, cluster within the African savanna elephant *S* clade and are a sister lineage to forest/straight-tusked elephants.

E. maximus_L, E. maximus_M and *E. maximus_Z* from India group together with high bootstrap support and *E. maximus_E* from Malaysian Borneo is placed basal to this group. *E. maximus_D* from Myanmar groups together with sequences EF588275 and DQ316068 from Thailand and Myanmar (Burma), respectively, while *E. maximus_Y* from Assam, India, together with sequence AJ428946 fall basal to all sequences described above. Asian elephants form a sister lineage to mammoths.

As previously described in Palkopoulou *et al.* (29), Enk *et al.* (2) and Chang *et al.* (30), we identify three major clades within *Mammuthus*: clade I (haplogroups C, D, E, F), clade II (haplogroup A) and clade III (haplogroups B1, B2). *M. primigenius_G* from Taimyr, Russia and *M. primigenius_Q* from Wrangel Island fall within clade I (haplogroups D & E). *M. primigenius_H* from Alaska falls within the North American mammoth haplogroup C (clade I). *M. primigenius_P* from Oimyakon, Russia falls within clade II (haplogroup A). *M. primigenius_S* from Yamal Peninsula, Russia falls within clade III (haplogroup B2). *M. columbi_U* from Wyoming falls within the Columbian mammoth haplogroup F (clade I), while *Mammuthus_V* falls basal to haplogroups C and F (clade I), as shown in Enk *et al.* (2).

Finally, *M. americanum_I* and *M. americanum_X* group together with the previously published mt genome sequence of the American mastodon, which was generated from the same specimen as *M. americanum_I*, but note that their sequences are not identical due to the low mt coverage of the latter.

Table S7.1. Statistics for read alignment to the mitochondrial reference genome (NC007596).

ID	# mapped reads	average read length	mt average coverage
LcycA	50,848	101	301.01
LafrB	546	100	3.21
LafrC	260	99	1.51
EmaxD	34,930	101	207.18
EmaxE	30,727	101	182.16
LcycF	15,505	100	91.57
MpriG	9,280	105	57.29
MpriH	19,745	67	78.07
MameI	580	77	2.63
EmaxL	14,257	101	84.65
EmaxM	15,575	101	92.45

PantN	6,072	44	15.87
PantO	166	40	0.39
MpriP	780,497	86	3962.36
MpriQ	172,701	75	765.12
MpriS	1,097,724	110	7113.11
McolU	14,359	50	42.50
MpriV	66,138	53	206.62
MameX	685	56	2.25
EmaxY	139,656	96	787.54
EmaxZ	2,233	109	14.25

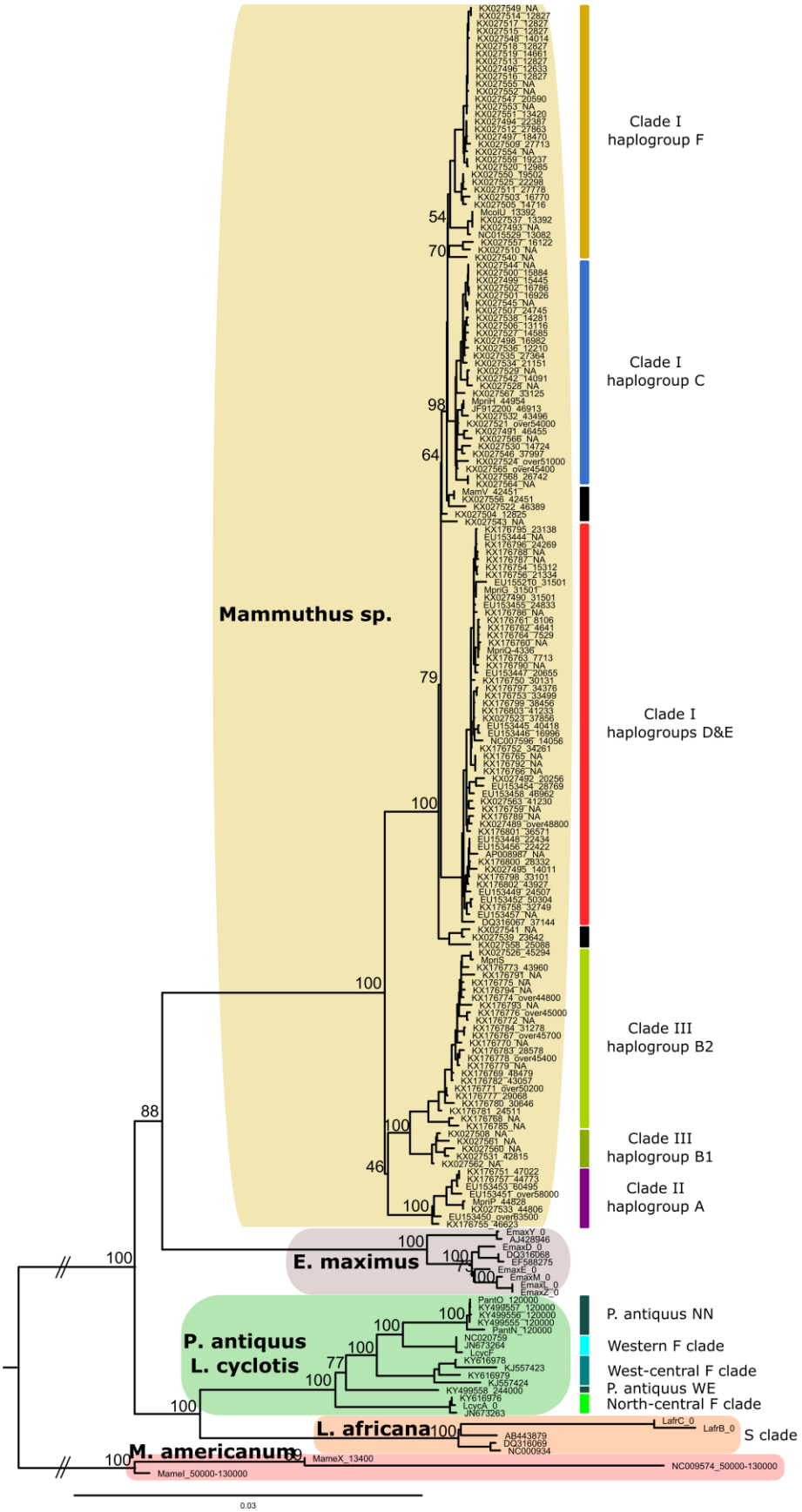
Mammuthus sp.
E. maximus
P. antiquus
L. cyclotis
L. africana
M. americanum
Clade I haplogroup F
Clade I haplogroup C
Clade I haplogroups D&E
Clade III haplogroup B2
Clade III haplogroup B1
Clade II haplogroup A
P. antiquus NN
Western F clade
West-central F clade
P. antiquus WE
North-central F clade
S clade
0.03

Figure S7.1. Maximum likelihood phylogeny of proboscidean mitochondrial genome sequences. Bootstrap support values from 100 replicates are shown on top of major nodes.

Mitochondrial contamination estimates

We estimated mtDNA contamination for the mammoth samples using the software 'calico' (https://github.com/pontussk/calico). This tool uses a method (31) that compares a 'test' sequence against a 'reference' dataset and estimates the proportion of reads that carry the derived (private) allele at sites that are private in the 'test' sequence. This method requires high coverage mtDNA and hence could not be used for other ancient samples in our dataset.

A consensus sequence was generated from all publicly available mammoth mt genome sequences with NC007596 as the reference sequence, using BWA (17) v.0.7.8 with the option 'bwasw', SAMtools (19) v.0.1.19 and the python script 'mpilup2consensusfasta.py' (https://github.com/pontussk/calico) setting the minor allele frequency at 5% for calling polymorphic sites. This consensus sequence served as the 'reference dataset'. The mtDNA reads of each 'test' sample where then re-aligned to the consensus sequence using BWA v.0.7.8 with the 'aln' option and SAMtools v.0.1.19. Contamination rates were then estimated using SAMtools v.0.1.19 with the 'mpileup' option and the extended BAQ computation (-E) and the python script 'calico.0.2.py' (https://github.com/pontussk/calico). All mammoth samples exhibit contamination rates < 5% (confidence intervals [CI]: 0 – 0.14; Table S.7.3).

Table S7.3. Contamination estimates for mammoth samples using the method 'calico'.

ID	# inform. sites	# maj. alleles	# min. alleles	Contamination rate	CI_low	CI_up
MpriG	1	56	1	0.018	0	0.053
MpriH	7	465	3	0.006	0	0.013
MpriP	5	1379	33	0.023	0.015	0.031
MpriQ	3	2294	45	0.019	0.013	0.025
MpriS	1	20	1	0.048	0	0.139
McolU	20	1082	10	0.009	0.003	0.015
MpriV	6	1111	23	0.02	0.012	0.028

Supplementary Note 8

Sequence divergence and proboscidean phylogeny

To investigate the phylogenetic relationships within the family Elephantidae, we estimated sequence divergence between all pairs of genome sequences and built a Neighbor-joining (NJ) tree from the resulting distance matrix. We generated pseudo-haploid sequences for all autosomes of each specimen by sampling a random allele per site to eliminate biases introduced by the alignment of reads to the reference genome, as explained in more detail in Supplementary Note 6. For ancient DNA data, we trimmed 5bp from both the 5' and 3' ends of the reads to exclude sites with post-mortem damage. Standard filters described in Supplementary Note 6 were applied for all sequences, including the 90% stringent mappability filter. We estimated the number of differences per site for each pairwise sequence comparison and used the resulting distance matrix to construct a NJ tree with PHYLIP (32) version 3.696. We performed 100 bootstrap analyses by splitting all autosomes in blocks of 5Mb and randomly sampling blocks with replacement. From the resulting replicate trees, we built a majority-rule consensus tree with support values on each node indicating the number of times a particular node was observed in the replicates.

We identified a total of 67,142,732 single nucleotide polymorphisms (SNPs) among all samples, of which 24,544,936 were transversions. All specimens within each taxon form distinct reciprocally monophyletic groups (Figure S8.1). African forest and African savanna elephants form two highly diverged lineages, supporting their distinction as separate species (33-36). Straight-tusked elephants are most closely related to African elephants, and in particular, they appear to be a sister lineage to forest elephants, as originally shown from the analysis of low-coverage genomic data from the same specimens (5). However, admixture analyses reveal a more complex picture, with the straight-tusked elephant being the product of three-way admixture between three lineages: an ancestral lineage that splits off basal to the common ancestor of forest and savanna elephants, a lineage related to woolly mammoths and a lineage related to the West African forest elephant (*L. cyclotis_F*; see Supplementary Note 12 for more details). The topology obtained from the pairwise distance NJ tree, placing the straight-tusked elephants as a sister lineage to forest elephants, suggests a considerable proportion of admixture from the forest elephant-related population into the straight-tusked elephant. We estimate this proportion at ~37% using f_4-ratio tests (Table S11.9) and admixture graphs (Figure S12.1).

Woolly mammoths and the Columbian mammoth form a sister lineage to Asian elephants, in agreement with results from Rohland *et al.* (4), although no Columbian mammoths had been included in that study. The Columbian mammoth (*M. columbi_U*) appears to be sister to all woolly mammoths, while the other mammoth specimen from the same geographic location (*Mammuthus_V* from Wyoming), which lacks diagnostic morphological characters and thus has not been formally assigned to a specific *Mammuthus* taxon, groups within the woolly mammoth lineage with high bootstrap support. The placement of the latter sequence suggests that this

specimen was genetically a woolly mammoth. In Supplementary Note 11, we use admixture tests to show that the majority of the ancestry of *Mammuthus_V* originates from woolly mammoths, with a modest proportion from Columbian mammoths. Therefore, from here on, we consider this specimen as a member of the woolly mammoth lineage. Overall, we obtain virtually identical topologies when using all substitutions or only transversions, with slight differences only within the woolly mammoth clade (Figure S8.1).

As expected, interspecific pairwise sequence divergence is higher than intraspecific divergence, except for the relatively low divergence between woolly and Columbian mammoths. Among present-day elephants, average divergence is highest within African forest elephants (0.49%) and lowest within Asian elephants and African savanna elephants (0.22 and 0.24%, respectively; Table S8.1). These findings are consistent with previous studies that have found higher genetic diversity within forest elephants than within savanna elephants (4, 33, 34). Among extinct taxa, mastodons and straight-tusked elephants exhibit relatively high levels of pairwise sequence divergence (0.43% and 0.44%, respectively) whereas woolly mammoths have intermediate average pairwise sequence divergence (0.36%).

All elephantids show high levels of sequence divergence to the mastodon sequences (average: 1.72%). Straight-tusked elephants display an average divergence of 0.73% to African forest elephants and 0.82% to African savanna elephants. Despite fossil morphology-based arguments that the straight-tusked elephant is most closely related to Asian elephants and therefore a member of the genus *Elephas* (37, 38), we find that the average pairwise sequence divergence between these two taxa (0.89%) is higher compared to the divergence between straight-tusked elephants and any of the African elephants. Likewise, divergence between mammoths and straight-tusked elephants (0.93%) is higher than that between African elephants and straight-tusked elephants, and similar to that between Asian elephants and straight-tusked elephants, which is expected given that mammoths and Asian elephants are sister taxa. The same pattern is observed when examining only transversions, but divergence estimates are overall lower since transversions exhibit a lower mutation rate compared to transitions. Sequence divergence between the two African elephants (average: 0.74%) is higher than that between Asian elephants and mammoths (average: 0.65%), confirming with complete nuclear genome sequences previous findings based on limited nuclear data (Rohland *et al.* (4)) that African forest and savanna elephants are deeply diverged despite incongruent phylogenetic patterns in their mitochondrial DNA (4, 33, 34, 36, 39, 40). The Columbian mammoth (*M. columbi_U*) is most closely related to woolly mammoths (average pairwise sequence divergence: 0.47%).

Table S8.1. Pairwise sequence divergence between all specimens. Divergence estimates using all substitutions are shown in the lower diagonal and divergence estimates using transversions only are shown in the upper diagonal.

	LcycA	**LafrB**	**LafrC**	**EmaxD**	**EmaxE**	**LcycF**	**MpriG**	**MpriH**	**MameI**	**EmaxL**	**EmaxM**
LcycA	0	0.0025	0.0025	0.0028	0.0029	0.0019	0.0027	0.0028	0.0053	0.0028	0.0028

LafrB	0.0071	0	0.0013	0.0032	0.0032	0.0029	0.0031	0.0031	0.0057	0.0031	0.0032
LafrC	0.0070	0.0024	0	0.0032	0.0032	0.0029	0.0030	0.0031	0.0056	0.0031	0.0031
EmaxD	0.0084	0.0090	0.0089	0	0.0011	0.0032	0.0022	0.0023	0.0055	0.0010	0.0010
EmaxE	0.0084	0.0090	0.0089	0.0025	0	0.0032	0.0022	0.0023	0.0055	0.0011	0.0011
LcycF	0.0049	0.0077	0.0076	0.0090	0.0090	0	0.0031	0.0032	0.0058	0.0032	0.0032
MpriG	0.0081	0.0087	0.0086	0.0060	0.0060	0.0088	0	0.0013	0.0055	0.0021	0.0021
MpriH	0.0092	0.0097	0.0096	0.0071	0.0071	0.0098	0.0039	0	0.0055	0.0022	0.0022
MameI	0.0173	0.0179	0.0178	0.0174	0.0174	0.0179	0.0174	0.0184	0	0.0054	0.0054
EmaxL	0.0083	0.0089	0.0088	0.0022	0.0024	0.0089	0.0059	0.0070	0.0173	0	0.0009
EmaxM	0.0083	0.0089	0.0088	0.0022	0.0024	0.0089	0.0059	0.0071	0.0173	0.0020	0
EantN	0.0071	0.0085	0.0084	0.0092	0.0092	0.0076	0.0091	0.0101	0.0184	0.0091	0.0091
EantO	0.0069	0.0081	0.0080	0.0089	0.0089	0.0076	0.0086	0.0098	0.0175	0.0088	0.0088
MpriP	0.0084	0.0090	0.0089	0.0062	0.0063	0.0090	0.0028	0.0039	0.0175	0.0062	0.0062
MpriQ	0.0085	0.0090	0.0089	0.0063	0.0063	0.0091	0.0028	0.0040	0.0175	0.0062	0.0062
MpriS	0.0088	0.0092	0.0091	0.0067	0.0068	0.0094	0.0036	0.0048	0.0178	0.0066	0.0067
McolU	0.0089	0.0093	0.0092	0.0068	0.0068	0.0095	0.0044	0.0054	0.0183	0.0067	0.0067
MpriV	0.0085	0.0090	0.0089	0.0064	0.0064	0.0091	0.0032	0.0042	0.0176	0.0063	0.0063
MameX	0.0164	0.0168	0.0167	0.0165	0.0165	0.0170	0.0165	0.0176	0.0043	0.0164	0.0164
EmaxY	0.0083	0.0089	0.0088	0.0022	0.0024	0.0089	0.0060	0.0071	0.0173	0.0021	0.0021
EmaxZ	0.0082	0.0088	0.0087	0.0021	0.0024	0.0088	0.0059	0.0070	0.0172	0.0019	0.0020

	EantN	**EantO**	**MpriP**	**MpriQ**	**MpriS**	**McolU**	**MpriV**	**MameX**	**EmaxY**	**EmaxZ**
LcycA	0.0023	0.0027	0.0028	0.0028	0.0030	0.0031	0.0028	0.0053	0.0028	0.0027
LafrB	0.0028	0.0033	0.0031	0.0031	0.0033	0.0034	0.0032	0.0056	0.0032	0.0031
LafrC	0.0028	0.0032	0.0031	0.0031	0.0033	0.0033	0.0031	0.0056	0.0031	0.0030
EmaxD	0.0030	0.0035	0.0022	0.0022	0.0025	0.0025	0.0023	0.0055	0.0010	0.0010
EmaxE	0.0030	0.0035	0.0022	0.0022	0.0025	0.0025	0.0023	0.0055	0.0011	0.0011
LcycF	0.0026	0.0032	0.0032	0.0032	0.0034	0.0034	0.0032	0.0057	0.0032	0.0031
MpriG	0.0029	0.0033	0.0012	0.0011	0.0015	0.0019	0.0013	0.0055	0.0021	0.0021
MpriH	0.0030	0.0035	0.0013	0.0013	0.0016	0.0019	0.0014	0.0056	0.0022	0.0022
MameI	0.0056	0.0060	0.0054	0.0054	0.0057	0.0059	0.0056	0.0013	0.0054	0.0054
EmaxL	0.0029	0.0034	0.0022	0.0022	0.0024	0.0025	0.0022	0.0054	0.0009	0.0009
EmaxM	0.0029	0.0034	0.0022	0.0022	0.0024	0.0025	0.0023	0.0054	0.0010	0.0009
EantN	0	0.0018	0.0029	0.0029	0.0032	0.0033	0.0030	0.0056	0.0030	0.0029
EantO	0.0044	0	0.0034	0.0034	0.0036	0.0036	0.0034	0.0060	0.0034	0.0034
MpriP	0.0092	0.0089	0	0.0011	0.0015	0.0018	0.0013	0.0054	0.0022	0.0022
MpriQ	0.0092	0.0089	0.0029	0	0.0014	0.0018	0.0013	0.0054	0.0022	0.0022
MpriS	0.0097	0.0091	0.0036	0.0036	0	0.0022	0.0016	0.0057	0.0024	0.0024
McolU	0.0098	0.0093	0.0044	0.0044	0.0052	0	0.0019	0.0058	0.0025	0.0025
MpriV	0.0093	0.0089	0.0032	0.0032	0.0040	0.0047	0	0.0055	0.0023	0.0022
MameX	0.0175	0.0166	0.0166	0.0166	0.0170	0.0174	0.0167	0	0.0054	0.0054
EmaxY	0.0091	0.0088	0.0062	0.0062	0.0067	0.0067	0.0063	0.0164	0	0.0009
EmaxZ	0.0090	0.0086	0.0061	0.0062	0.0066	0.0067	0.0063	0.0163	0.0020	0

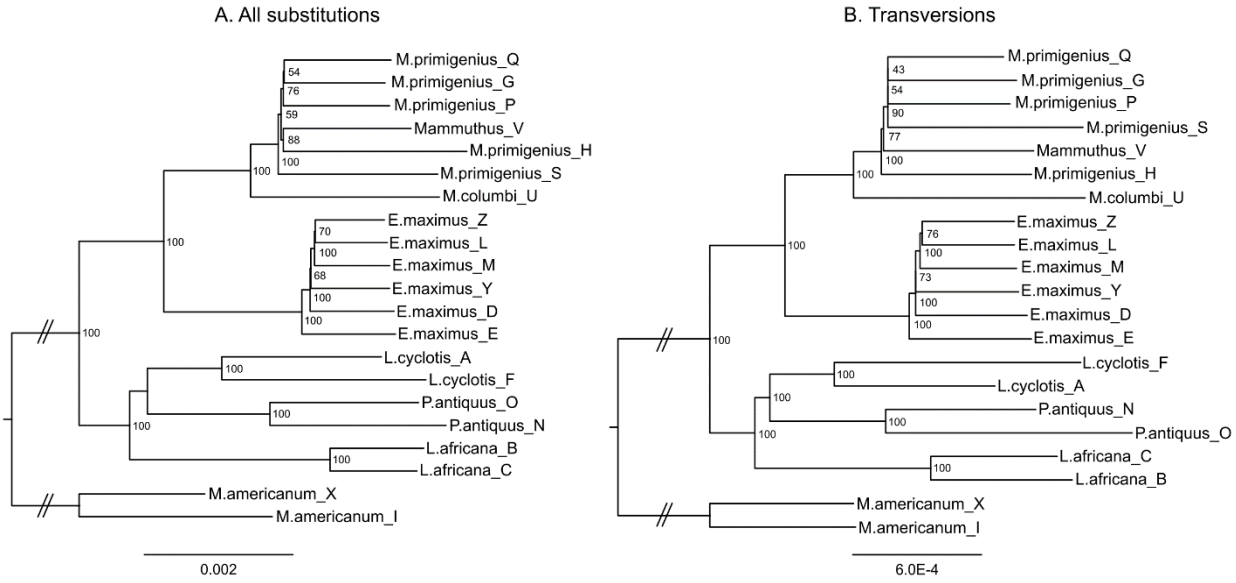

Figure S8.1 Pairwise genetic distance NJ tree of proboscidean genome sequences using all substitutions (A) or only transversions (B). Support values from 100 bootstrap analyses are given inside each node. The scale bar indicates the number of substitutions or transversions per site.

Supplementary Note 9

Using repetitive elements to infer species relationships

Single nucleotide polymorphisms (SNPs) are often used as genetic markers to identify differences between species and individuals. In this note, we present an alternative approach utilising the `dark matter' of the genome: repetitive elements. Huge portions of eukaryotic genomes are made up of non-coding, ancient repeats, which can be used to describe ancestral species relationships. Our model is simple: use the repetitive intervals in each genome to identify binary variance (presence versus absence) and thus infer phylogenetic relationships. Using the provided dataset of 21 modern and ancient elephantids, we compare our results to the previously established pairwise genetic distance phylogeny and discuss the advantages and limitations of a repeat-based approach.

Introduction

Before the advent of genome sequencing technologies, scientists devoted their attention to protein-coding genes and proteins. Since then, over a hundred mammalian genomes have been sequenced - revealing the prevalence of non-coding, repeat-derived sequences. The vast majority of repeats are remnants of insertion events that occurred millions of years ago. This provides a genetic footprint of evolutionary relationships between different species and individuals.

The most frequently used method for resolving genome differences is by looking at single nucleotide polymorphisms (41) (SNPs). However, SNP-based approaches are not always robust because they rely on single alleles. Similarly, human genome projects sometimes use transposable element polymorphisms (polyTEs) from recent insertions to infer ancestry (42). This method was primarily designed for use between individuals of the same species - it does not take into account ancient repeats. We propose an alternative approach: using a reference genome, identify all of the repetitive intervals and compare them between genomes to find binary variance (presence versus absence). Variant intervals are then used to infer a phylogeny of the species relationships. Due to its binary nature, our method executes quickly and can be used on any dataset of genomic sequences, including those with no known SNP variants.

To test our approach, we used the set of 21 ancient and modern elephantids from diverse geographic backgrounds. An evolutionary phylogeny of this dataset has already been inferred using pairwise genetic distance data (see Figure S.8.1). Using the publicly available chromosome-level assembly of *Loxodonta africana* as a reference (*LoxAfr4*), we characterised the interspersed repeats in the genome, mapped them onto the genomic data of the 20 other elephantids and compared our results to the genetic distance-based phylogeny. Various criteria were tested to determine the optimal parameters, particularly when dealing with ancient DNA.

Methods

Reference genome: repeat identification, annotation and analysis

Ab initio repeat identification and annotation

Loxodonta africana (KB13542, chromosome-level assembly *LoxAfr4*) was used as the reference genome. Entire *LoxAfr4* chromosome sequences were locally aligned with the krishna program (43, 44) (http://godoc.org/code.google.com/p/biogo.examples/krishna) using the default parameters. Alignments identified by krishna were clustered by the igor program (43, 44) (http://godoc.org/code.google.com/p/biogo.examples/igor) using default parameters, except for the "-overlap-strictness=1" parameter to prevent inclusion of overlapping features. The minimum accepted cluster size was two members. Sequences corresponding to members of alignment clusters were extracted from the *LoxAfr4* sequence and aligned using MUSCLE (45, 46) with default parameters; only members within 95% of the length of the longest member were aligned and when clusters contained more than 100 members, 100 randomly chosen sequences satisfying the length constraint were included in the alignment. A consensus for each cluster was constructed from its MUSCLE alignment and subsequently used in the repeat annotation process.

CENSOR (47) was used to annotate identifiable repeats. WU-BLAST (48) was further used with a comprehensive retroviral and retrotransposon protein database assembled from the National Center for Biotechnology Information (49) to further annotate repeats, and with swissprot to identify known protein-coding genes from large gene families inappropriately included in the repeat set. Consensus sequences identified as either simple sequence repeats (SSRs) or protein-coding sequences, but not similar to retrotransposon or endogenous retrovirus protein-coding sequences, were removed from the consensus set.

LTR class identification

Initially, the *LoxAfr4* genome assembly was analysed using CENSOR (47) with the long terminal repeat (LTR) records from RepBase (50) version 20140131. The output from CENSOR was then run through censormerge; briefly, this program merges adjacent repeat features with matching annotation allowing for limited insertions by different elements or backtracking within the annotating repeat sequence, or until a significant fraction of the annotating repeat sequence has been covered. Merged sequences identified by censormerge were tested for the presence of GAG- or POL-encoding sequence by BLAST (51) alignment against databases containing representatives of these protein sequences, using an e-value threshold of 1E-12.

Repeat analysis

The genome was divided into 1.5 Mb contiguous bins and the number of each of the features within each bin was counted. Genomic features analysed include: interspersed repeat groups, obtained from running CENSOR (47) with the mammal library and our elephant repeat library and grouping based on the repeat sequence classification, genes, CpG islands and G4s. The count data was transformed by first dividing by the number of known base pairs (A,C,T,G) in the bin and then taking the square root. For each bin, the CpG coverage was calculated and an arcsine transformation taken, and the GC content was calculated. Bins that had less than 500,000 known

base pairs (bp) were excluded from the analysis. For each feature, outlier bins within the genome were identified using a 2-tail t-test at the 5% significance level.

To identify ancient and recent regions of the genome, a principal components analysis was performed on the transformed bin data. The principal component with high weights for the ancient repeats MIR, L2 and CR1 was selected as the indicator for 'ancientness'. For each bin in the analysis, the average value of the principal component (in a 5-bin window centered on the bin) was calculated. If this value was significantly greater than zero the bin was classified as ancient; if it was significantly less than zero the bin was classified as recent. Significance tests were based on 2-tail t-tests at the 5% significance level. Window variance was used unless there was only one bin in the window; in that case, the variance of the principal component was used.

Extraction of repetitive intervals from elephantid genomic data

All interspersed repeats identified and annotated in the reference assembly were used to produce BED intervals (>50 bp) for each major repeat class (DNA, ERV, LINE, SINE; total of 4,353,898 interspersed repeat intervals). The BED intervals were used to extract BAM slices from the provided whole genome data of 21 elephantids (2 *Loxodonta cyclotis*, 2 *Loxodonta africana*, 6 *Elephas maximus*, 6 *Mammuthus primigenius*, 1 *Mammuthus columbi*, 2 *Mammut americanum* and 2 *Paleoloxodon antiquus*). Extraction was performed using BEDTools (52) with default parameters for intersecting a BAM alignment with features in BED format, irrespective of strand.

Phylogenetic inference of species relationships using variant sites

The intersected BAM slices were converted to BED format, sorted with respect to chromosome name and start/end position, and merged to form a set of unique, non-redundant repeat intervals for each genome. Intervals were then transformed into a binary system for each individual, where '1' indicated presence of that interval and '0' indicated absence (see Figure S9.1). Each elephantid had a distinct signature of 1's and 0's to compare to the reference. The binary signatures were compared across all elephantids to find persistent sites (i.e. present in all taxa) and variant sites (absent from some taxa). Only the variant sites were used to infer a phylogeny.

RAxML (28) and PAUP (53) were used to infer maximum likelihood (ML) and maximum parsimony (MP) phylogenies from the binary sequences. The RAxML model used was BINCAT: a memory and time efficient approximation for the standard GAMMA model of rate heterogeneity from binary data. Bootstrapping was used to estimate confidence values.

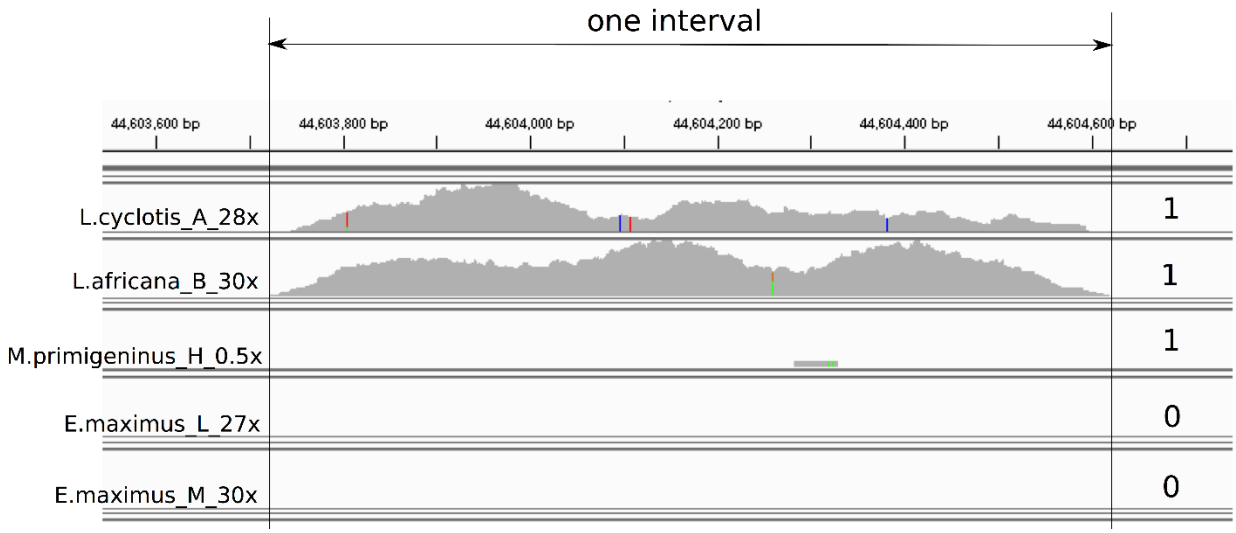

Figure S9.1. Variant site example. Shows an interval, which would be classified 'variant' because it is present in some elephantids (labelled '1') but absent in others (labelled '0'). In this trivial example, an interval is 'present' if there is at least 1 bp in the specified region.

Parameter testing for quality control

The aim of this project was to use a repeat-based approach to infer phylogenetic relationships. To determine the optimal parameters for an accurate phylogeny, we needed to take into account external factors that differ between genomes (e.g. level of coverage, or ancient DNA versus modern DNA). Several criteria were tested for defining presence/absence of an interval: (1) presence is indicated by at least 1 bp in the expected interval; (2) setting a minimum length of 20 bp for each interval (such that any intervals containing <20 bp are considered absent, not present); (3) as per (1) but only including taxa with >5x coverage; (4) as per (2) but only including taxa with >5x coverage.

Other tests included a triplets analysis for incomplete lineage sorting (54): in brief, this test performs groupings by counting the number of intervals present in two species and absent in the third. Every possible combination of three elephantids was inspected to find the most likely grouping, and determine whether this grouping was due to repeat content or data quality.

We also considered setting other genomes as the reference (e.g. *M. columbi_U* or *M. americanum_I*), although this was limited by the fact that *L. africana_C* was the original reference, so repeats specific to ancient elephantids could not be observed.

Similarly, we tried to minimise bias due to coverage by imputing common intervals from high coverage elephantids to low coverage elephantids.

Finally, the absent intervals in each elephantid were categorised by repeat class (e.g. DNA, ERV, LINE, SINE), to see if there was an under-representation of some repeats in certain species compared to others.

Results

Repeat coverage and ancient regions in Loxodonta africana

The total repeat coverage of the reference elephant genome was found to be about 50% (Table S9.1), which is comparable to other mammalian genomes. However, the non-LTR retrotransposon fraction of the genome is significantly higher in the elephant compared to other placental mammals. Non-LTR over-representation may be attributable to the presence of LINE retrotransposons, which are horizontally transferred in higher organisms (55, 56). Correlations between different repeat groups are shown in Figure S9.2.

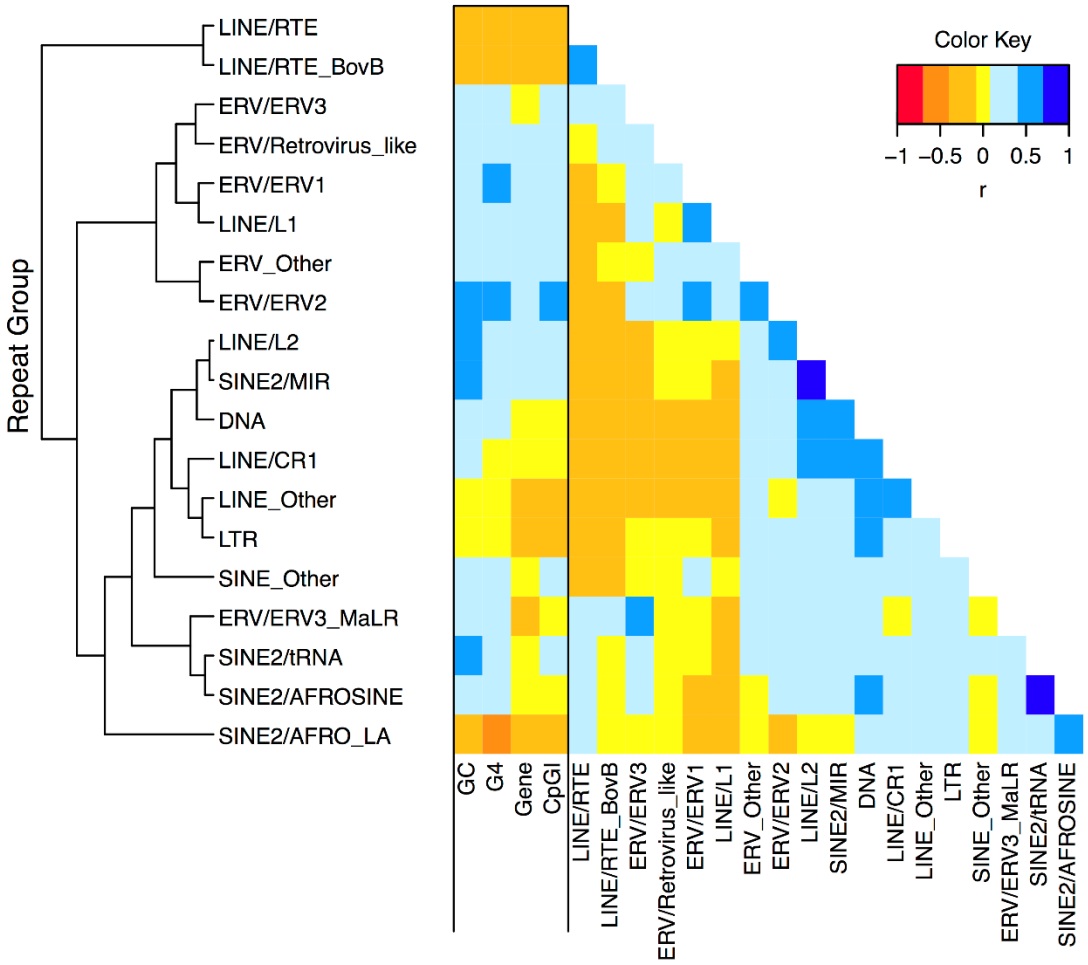

Figure S9.2. Correlations among repeat groups. Heatmap showing correlations between repeat groups in the reference elephant genome (*LoxAfr4*).

Our identification of Ancient Genomic Regions (AGR) through principal component analysis indicates that AGR exist in the elephant genome as they do in the bovine genome (57). AGR seldom contain recent, clade-specific repeats (Figure S9.3, Figure S9.4). In contrast, regions of low Ancient Repeat density tend to contain many recent, clade-specific repeats.

Table S9.1. Repeat coverage. Simple and interspersed repeats in the reference elephant genome (*LoxAfr4*), as annotated by CENSOR.

			Percent Coverage of Genome						
Group	**Number**	**Total bp**	**Elephant**	**Human**	**Bovine**	**Horse**	**Dog**	**Opossum**	**Platypus**
Non-LTR retrotransposons									
LINE L1	986,136	666,082,855	20.358	16.045	12.314	15.661	15.186	19.105	0.131
LINE RTE	382,385	298,221,273	9.115	0.001	0.033	0.021	0.005	1.385	0.760
LINE L2	312,620	60,957,649	1.863	2.017	1.587	3.155	1.946	4.455	18.217
LINE RTE_BovB	54,446	17,739,670	0.542	0.000	13.592	0.012	0.006	0.055	0.178
LINE CR1	20,719	3,430,136	0.105	0.174	0.089	0.178	0.100	1.576	0.714
LINE Other	9,665	1,832,187	0.056	0.054	0.046	0.089	0.052	0.015	0.022
	1,765,971	1,048,263,770	32.039	18.291	27.661	19.116	17.294	26.590	20.022
SINEs									
SINE AFROSINE	699,084	114,655,966	3.504	0.000	0.000	0.000	0.000	0.000	0.000
SINE AFRO_LA	599,613	88,296,626	2.699	0.000	0.000	0.000	0.000	0.000	0.000
SINE MIR	408,591	53,741,261	1.643	1.769	1.449	2.557	1.694	8.474	18.319
SINE tRNA	67,079	15,999,561	0.489	0.002	1.841	0.124	0.266	0.865	0.237
SINE Other	4,783	401,145	0.012	10.094	6.421	3.455	7.162	0.742	0.599
	1,779,150	273,094,559	8.347	11.864	9.711	6.135	9.122	10.080	19.155
ERVs									
LTR ERV3	428,290	151,727,987	4.637	2.017	1.044	1.855	1.373	0.137	0.133
LTR ERV3_MaLR	134,810	30,067,032	0.919	2.957	0.980	1.673	1.296	0.001	0.000
LTR ERV1	102,880	23,043,092	0.704	2.267	1.735	1.779	1.030	5.664	0.202
LTR ERV2	16,401	1,261,492	0.039	0.296	0.229	0.110	0.051	0.364	0.058
LTR Retrovirus_like	3,788	767,845	0.023	N/A	N/A	N/A	N/A	N/A	N/A
LTR ERV_Other	7,940	912,769	0.028	0.385	0.071	0.105	0.094	3.382	0.021
	694,109	207,780,217	6.351	7.922	4.060	5.523	3.844	9.549	0.414
DNA transposons									
DNA All	324,199	56,138,861	1.716	3.183	1.622	2.552	1.915	1.609	0.765
LTR Other									
LTR Other	21,580	3,492,951	0.107	0.663	0.300	0.183	0.097	0.210	0.014
Di-nucleotide SSR									
Di AG	555,906	5,321,258	0.163	0.172	0.128	0.186	0.658	0.461	0.223
Di AC	553,097	6,490,071	0.198	0.259	0.248	0.208	0.273	0.194	0.144
Di AT	369,874	4,261,246	0.130	0.199	0.179	0.131	0.177	0.288	0.075
Di CG	7,431	70,438	0.002	0.003	0.003	0.002	0.004	0.001	0.003
	1,486,308	16,143,013	0.493	0.633	0.558	0.529	1.113	0.945	0.445
Tri-neucleotide SSR									
Tri AAC	456,643	5,335,331	0.163	0.058	0.065	0.047	0.050	0.065	0.029
Tri AAG	352,392	3,462,209	0.106	0.067	0.068	0.081	0.085	0.115	0.058
Tri AAT	271,242	2,916,210	0.089	0.130	0.086	0.100	0.122	0.181	0.617
Tri AGG	150,641	1,532,725	0.047	0.064	0.071	0.074	0.076	0.073	0.137
Tri AGC	132,185	1,327,413	0.041	0.043	0.141	0.048	0.040	0.029	0.047
Tri ACC	126,603	1,321,090	0.040	0.076	0.038	0.039	0.038	0.028	0.030
Tri ATC	93,230	949,327	0.029	0.039	0.029	0.036	0.037	0.049	0.087
Tri ACT	63,392	629,733	0.019	0.012	0.012	0.012	0.014	0.032	0.027
Tri CCG	12,986	154,853	0.005	0.008	0.008	0.005	0.014	0.005	0.013
Tri ACG	1,719	17,135	0.001	0.000	0.001	0.001	0.001	0.001	0.005
	1,661,033	17,646,026	0.539	0.498	0.518	0.444	0.476	0.578	1.050
Tetra/penta-neucleotide SSR									
Tetra.penta All	3,292,319	40,618,455	1.241	1.486	1.324	1.224	2.101	1.863	1.720
Unclassified/chimeric									
Unclassified/chimeric	673,649	108,628,553	3.320						
Interspersed repeat total	4,585,009	1,588,770,358	48.560	41.923	43.352	33.509	32.271	48.038	40.372
SSR total	6,439,660	74,407,494	2.274	2.617	2.400	2.196	3.690	3.386	3.215
			32717930	3E+007	3E+007	2E+007	2E+007	35984260	19967942

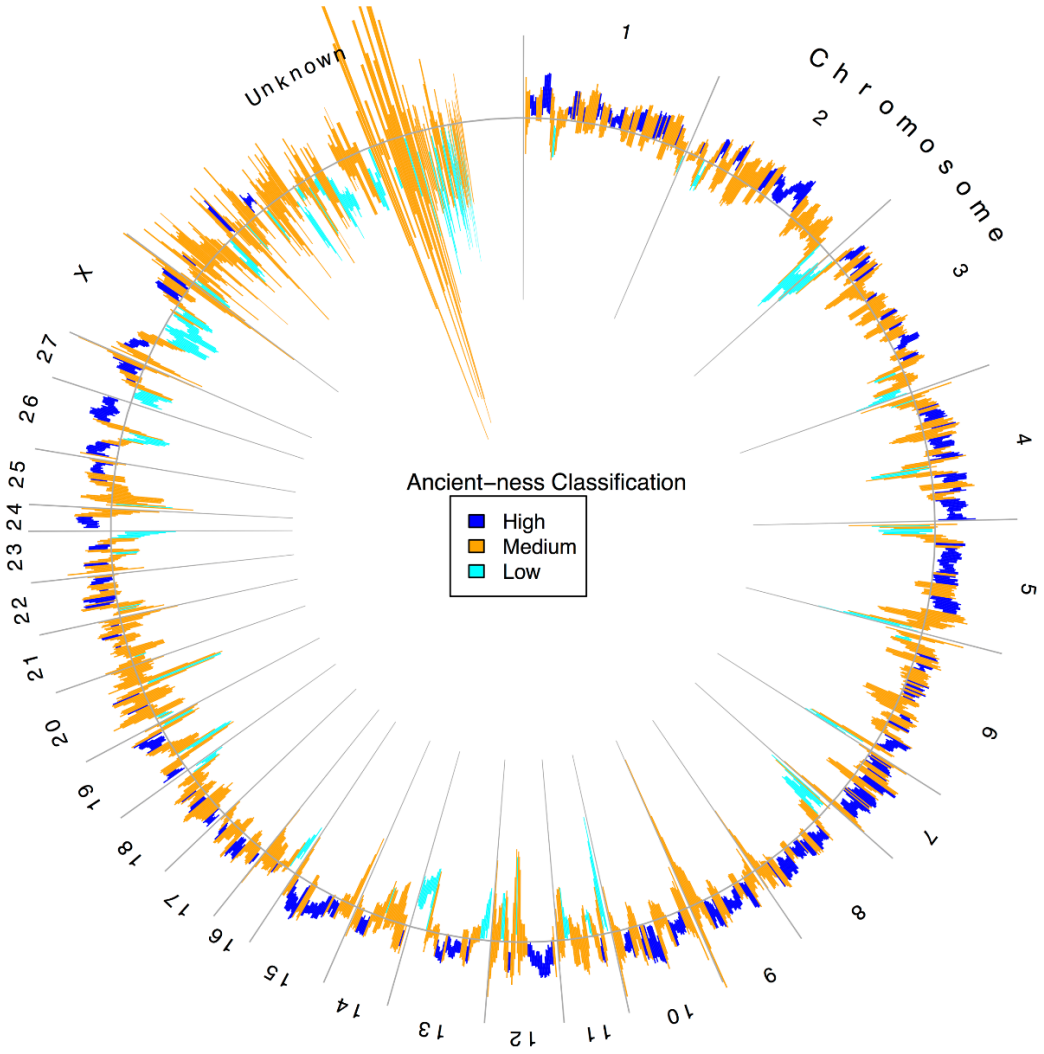

Figure S9.3. Ancient-ness classification for *Loxodonta africana*: PCA analysis of ancient repeat regions in the reference genome (*LoxAfr4*).

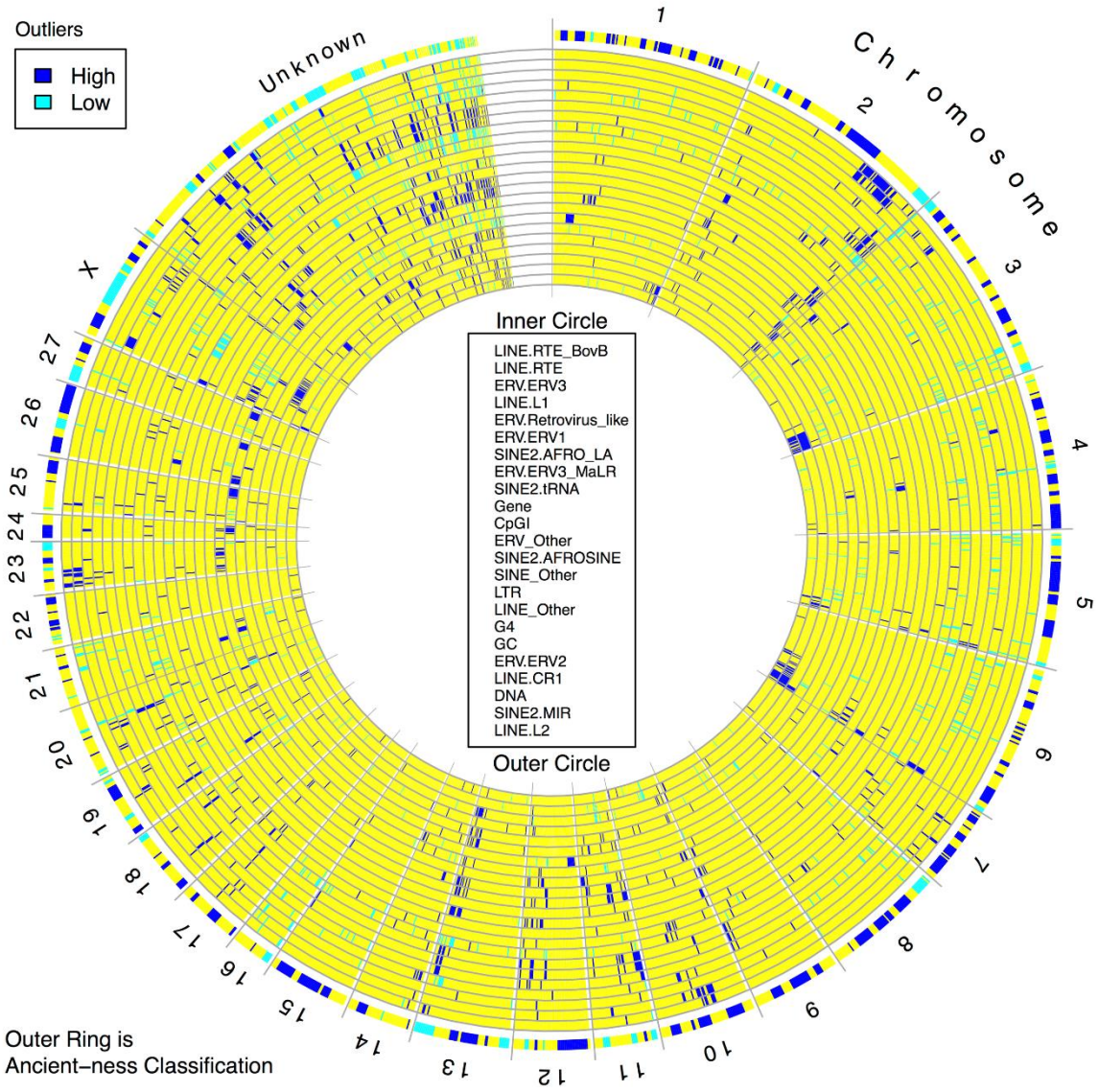

Figure S9.4. Ancient-ness classification and feature outlier bins: Classification of repeats into high and low density regions in the reference elephant genome (*LoxAfr4*).

Initial subset of full-length LINEs as genomic markers

As a preliminary test, we used a subset of full-length BovB and LINE-1 repeat intervals (4929 BovB, 10697 L1) to identify variant sites between the elephantids. The subset was too small for reliable phylogenetic inference because the binary sequence analysis reduced the dataset to a mere 18 variant sites (Figure S9.5). This suggests that full-length retrotransposons, particularly active ones, tend to persist in elephantids.

	# intervals	# intervals (after merging)	# variant intervals
BovB	4929	4776	11
L1	10697	9460	7
L1-active	234	202	0

```
L.cyclotis_A_28x        11111111111111111
L.africana_B_30x        11111111111111111
L.africana_C_33x        11111111111111111
E.maximus_D_39x         10111110111100101
E.maximus_E_32x         01111110111101000
L.cyclotis_F_32x        11111111111111111
M.primigenius_G_0.3x    11000011100011111
M.primigenius_H_0.5x    11111111111111111
E.maximus_L_27x         11111110010101101
E.maximus_M_30x         11011100110101101
P.antiquus_N_15x        11111111111111111
M.primigenius_P_13x     11111111111111111
M.primigenius_Q_19x     11111111111111111
M.primigenius_S_0.9x    11111111111111111
M.columbi_U_1.5x        11111111111111111
Mammuthus_V_5.9x        11111111111111111
E.maximus_Y_36x         11011110111111111
```

PAUP* (ML)

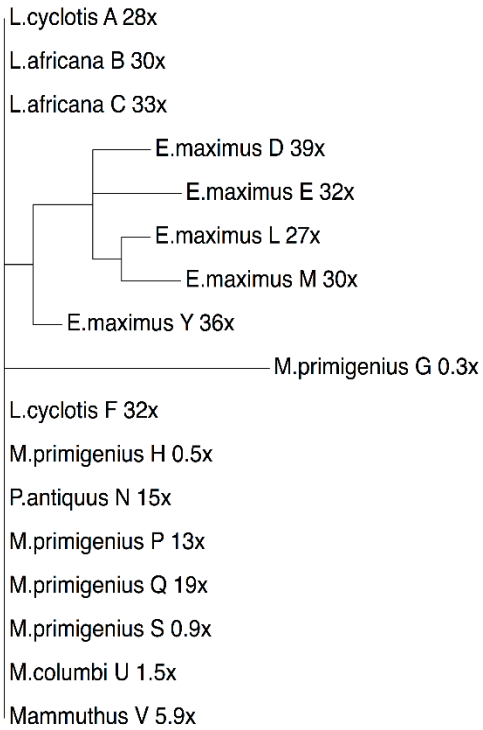

Figure S9.5. Results from the initial subset of full-length LINEs. Only 18 variant sites were found using this subset. The subsequent phylogeny (inferred using PAUP, maximum likelihood) is only useful in regards to the *E. maximus* elephants.

Full dataset of interspersed repeats

Using the entire interspersed repeats collection was more successful, variant sites increased from 18 to over 3 million. Many possible phylogenies were produced depending on the filtering parameters. To simplify discussion, we will use specific test cases to demonstrate differences due to coverage, minimum interval length, and repeat class.

Trivial case: all 21 elephantids, no filtering

The trivial case involved no filtering: all 21 elephantids were used, despite some having very low coverage and only 1 bp was needed to classify an interval as 'present' (as shown in Figure S9.1). This produced 3,037,698 variant sites. Elephantids with low coverage (e.g. *M. americanum_X*, *P. antiquus_O*, *M. columbi_U*, *M. primigenius_G*, *M. primigenius_H*, *M. primigenius_S*) stand out as having a huge number of absent intervals (Figure S9.6a), and are thus, grouped together in the inferred phylogenies (Figures S9.6b, S9.6c). Ignoring these, most of the other elephantids uphold previous species relationships. The main difference between the ML (Figure S9.6b) and MP (Figures S9.6c) phylogenies is the placement of *P. antiquus* N. The MP tree agrees with the original phylogeny (Figure S8.1), with *P. antiquus* N sister to the *L. cyclotis* group, while the ML tree places it closer to *E. maximus* elephants. Both ML and MP trees show *E. maximus* Y as an outgroup to the other *E. maximus* elephants; a placement not seen in the original tree.

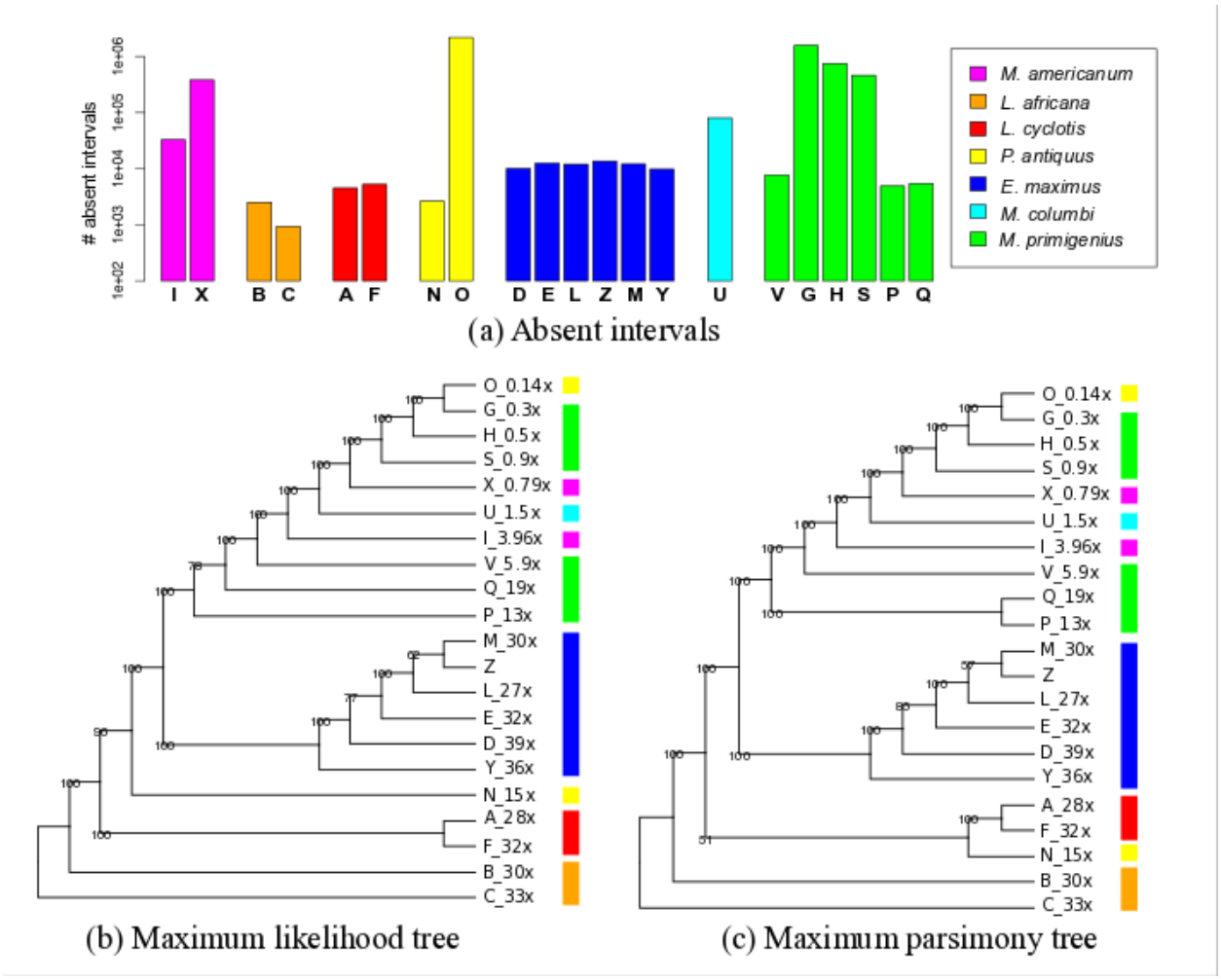

Figure S9.6. All elephantids, no filtering. (a) shows the number of absent intervals in each elephantid, coloured by species and labelled with the appropriate initial. Note that the y-axis is a log scale. (b) and (c) show the inferred phylogenies from these absent intervals. The trees are rooted with *L. africana* C (reference genome). Coloured bars represent different species, using the legend from (a). Bootstrap support values are shown; branch lengths are not shown because the low coverage species were too long.

All elephantids, minimum length of 20 bp per interval

Setting a minimum threshold of 20 bp for each interval increased the total number of variant sites to 3,235,889. The difference was largely attributed to the low coverage species, which showed a huge increase in the number of absent intervals (Figure S9.7a). Consequently, the topology did not change at all for the low coverage elephantids; they still grouped together in order of lowest coverage.

However, there was one difference in the high coverage elephantids. Previously (Figure S9.6), the ML and MP trees differed in their placement of *P. antiquus_N*. With a 20 bp minimum, the

ML and MP trees now agree that *P. antiquus* N should be distinct from the *Loxodonta* elephants (Figure S9.7). This is the only test case where the ML and MP trees concur.

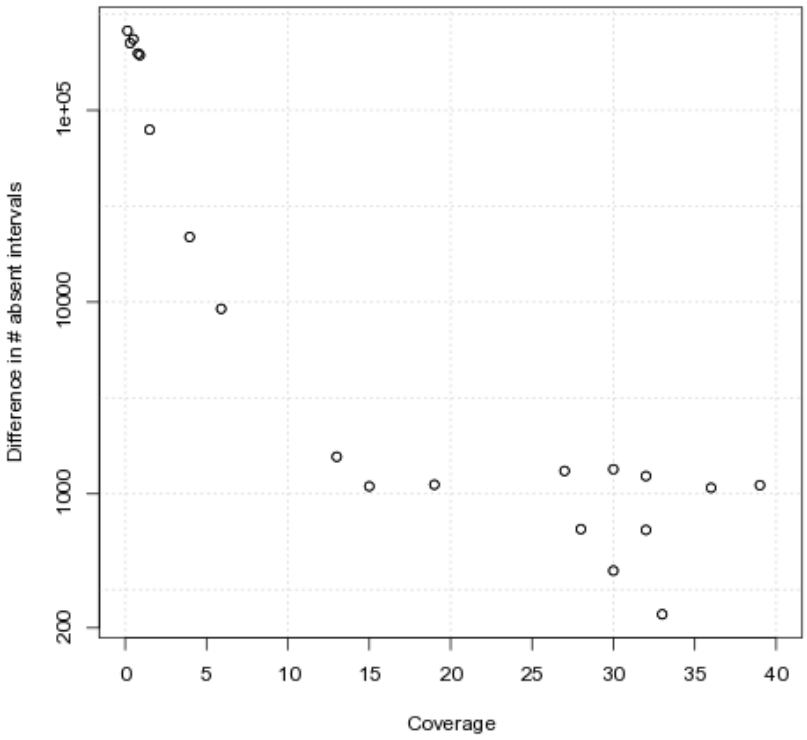

Figure S9.7. All elephantids, minimum length of 20 bp per interval. (a) shows that increasing the minimum interval length from 1 bp to 20 bp drastically affects the low coverage species. More intervals in these elephantids are classified as 'absent'. (b) shows the inferred topology seen using both a maximum likelihood and maximum parsimony approach. Low coverage species are not shown because they grouped by lowest coverage instead of repeat content, as seen previously in Figure S9.6.

All elephantids, triplets test

The triplets test was inconclusive. It confirmed the obvious topologies seen in the high coverage, modern elephants (e.g. *L. africana* is more closely related to *L. cyclotis* than *E. maximus*). It was also useful for resolving the placement of *P. antiquus_N* as sister to *L. cyclotis* elephants, supporting the genetic distance-based phylogeny (Figure S8.1). However, it could not sensibly resolve the low coverage elephantids. This, along with the previous tests, suggested that the only way to infer a high-confidence phylogeny would be to exclude low coverage species.

High coverage elephantids only

If we remove genomes with <5x coverage and do not set a minimum interval length, 34,175 variant sites remain. It is clear that *E. maximus* elephants are missing the largest number of repeat intervals (Figure S9.8). *E. maximus* are a modern species, with abundant genomic data available, so the absence of repeat intervals is not due to poor coverage or mapping quality. The trees (Figures S9.8b, S9.8c) mirror that seen previously in Figures S9.6b, S9.6c. The *E. maximus* subgroup is markedly distinct from the other elephantids, with *E. maximus_Y* acting as the species outgroup. *P. antiquus_N* is separate from *L. africana* and *L. cyclotis* in the ML tree, but clustered with *L. cyclotis* in the MP tree. Using only high coverage elephantids increased the support values and produced more reliable phylogenies.

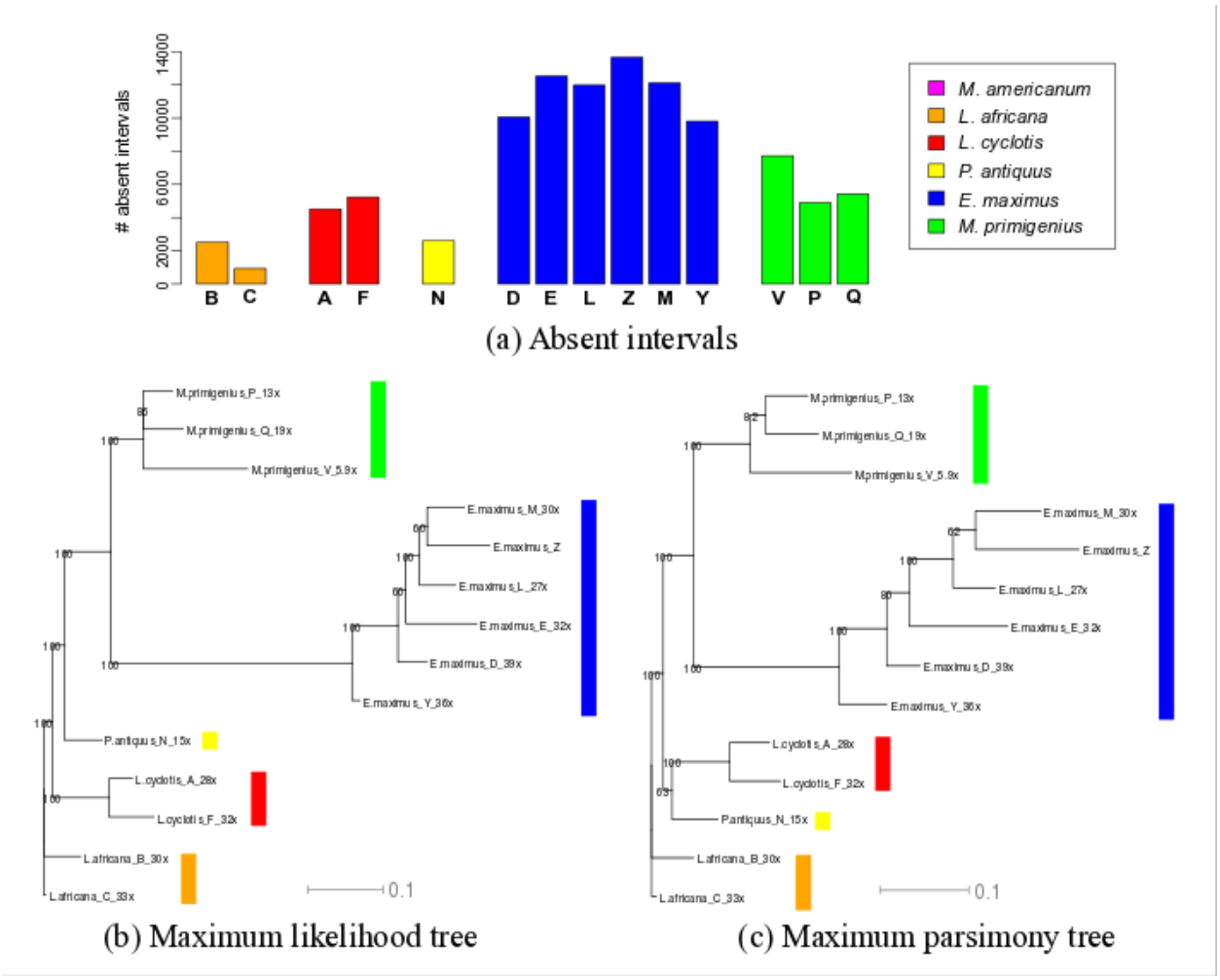

Figure S9.8. High coverage elephantids only. (a) shows the number of absent intervals in each elephantid, coloured by species and labelled by initial. (b) and (c) show the inferred phylogenies from these absent intervals. The trees are rooted with *L. africana_C* (reference genome). Coloured bars represent different species, using the legend from (a). Bootstrap support values and branch lengths are shown.

High coverage elephantids only, separated by repeat class

Next, we separated the absent intervals by repeat class to look for under-represented repeats between species. We wanted to know if the missing intervals in *E. maximus* elephants belonged to a certain repeat group. Figure S9.9 shows the breakdown of 4 major repeat classes: DNA (e.g. DNA transposons such as mariner elements); ERV (including LTRs); LINE (BovBs, LINE-1s, etc); and SINE (7SL, tRNA, 5S, etc), as categorised by CENSOR.

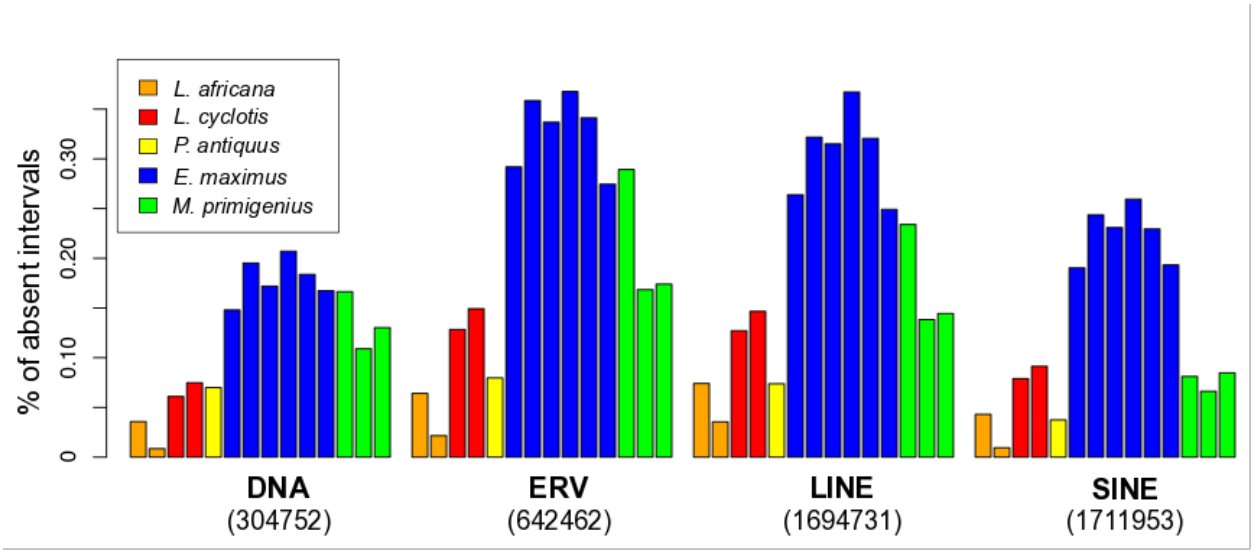

Figure S9.9. Variance between high coverage elephantids, categorised by repeat class. The x-axis shows the repeat class (e.g. ERV) and total number of intervals belonging to that repeat class (e.g. 642462). The y-axis shows the percentage of absent intervals (i.e. number of absent ERV intervals/total number of ERV intervals × 100). Elephantids are coloured by species and appear in the same order as seen previously (e.g. Figure S9.8a).

There does not appear to be a specific bias towards any category of repeats. *E. maximus* elephants consistently have the largest proportion of absent intervals. In particular, SINE repeats are very under-represented. Each member of the *E. maximus* group is missing more than twice as many SINE sites as any other elephantid.

Imputing intervals from high coverage elephantids to low coverage elephantids

Repeatedly, we observed bias due to low coverage. High-confidence phylogenies could only be produced by excluding low coverage elephantids. This does not help us resolve the topology of the mammoths.

As a final test, we tried imputing common intervals from the high coverage elephantids to the low coverage elephantids. Consider the *E. maximus*/*Mammuthus* clade. *M. columbi_U* has by far the most absent intervals in this clade, due to the 1.5x coverage (Figure S9.10a). In contrast, the high coverage (>5x) elephantids share 4,328,440 common intervals. If we assign these common intervals to the low coverage elephantids (*M. columbi_U* and *M. primigenius_V*), we can obtain a more realistic barplot (Figure S9.10b), with the total number of variant sites being 24,261. The corresponding trees differ slightly in their placement of *M. primigenius_V*, but largely support the genetic distance-based phylogeny (Figure S8.1).

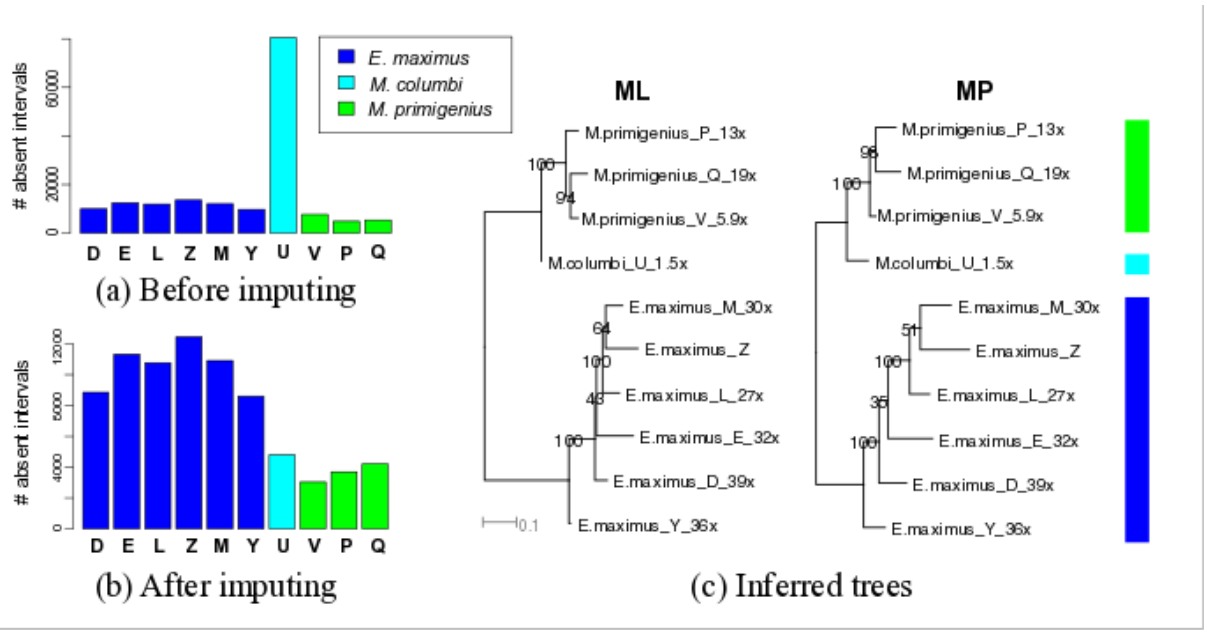

Figure S9.10. Resolving the mammoths. (a) shows the number of absent intervals in each elephantid, coloured by species as before. (b) shows the number of absent intervals after imputing common intervals on the two low coverage elephantids. (c) shows the maximum likelihood (left) and maximum parsimony (right) trees generated with RAxML and PAUP, respectively.

Recurring topology

The tests detailed above indicate that the ideal parameters on this data are to exclude low coverage species. Changing the minimum interval cutoff from 1 bp to 20 bp only resulted in minor differences. Likewise, there is no particular bias to any repeat class, but using all interspersed repeat intervals is the most effective. The recurring tree topology is shown below (Figure S9.11).

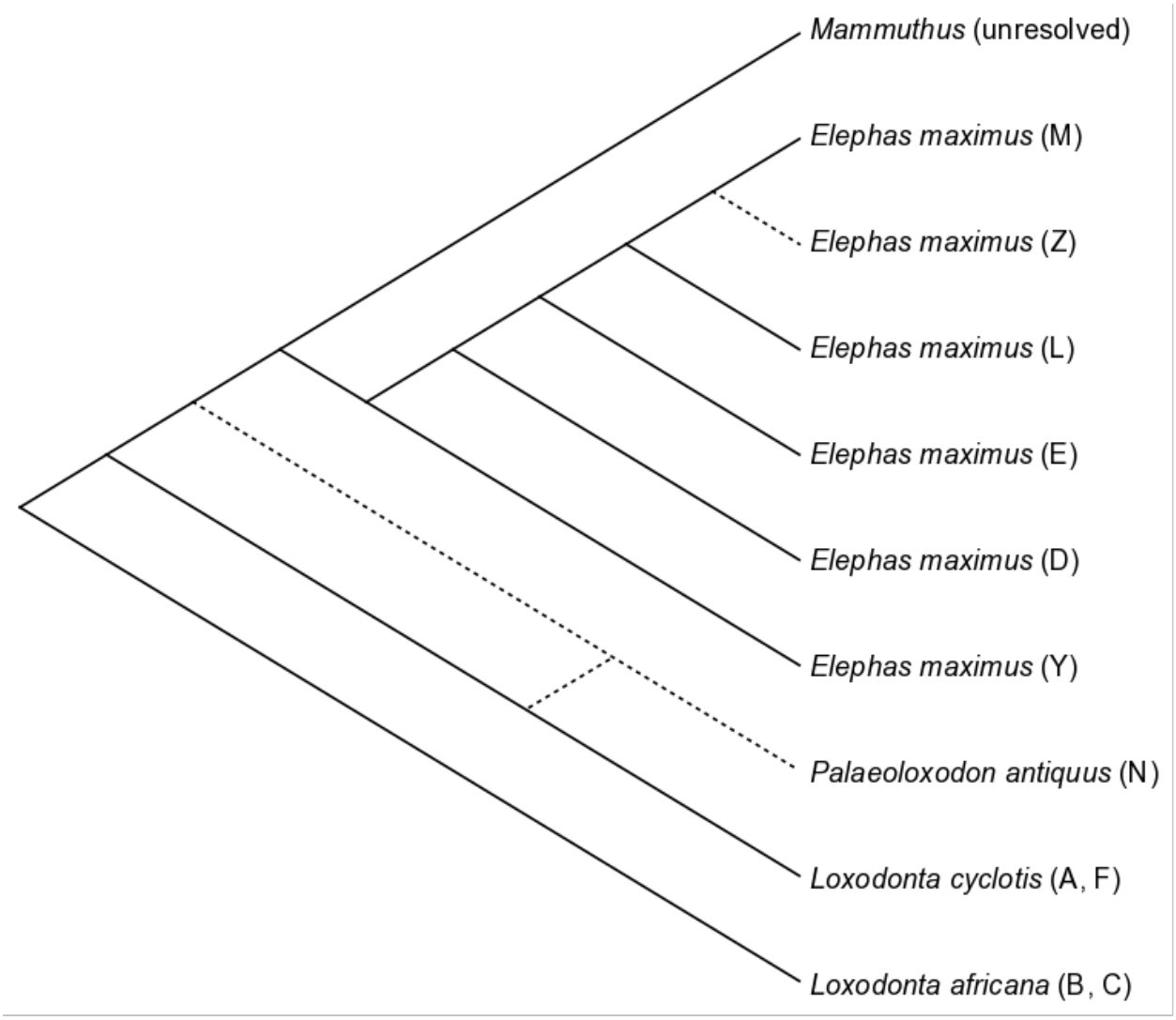

Figure S9.11. Recurring tree topology. *L. africana_C* was used as the reference genome, so differences between *L. africana_B* and *L. africana_C* are likely due to individual polymorphism. *L. cyclotis_A* and *L. cyclotis_F* are always seen grouped together. The position of *P. antiquus_N* changes depending on the approach used (within the *Loxodonta* elephants with a maximum parsimony approach; closer to the *E. maximus* elephants with a maximum likelihood approach). *E. maximus_Y* is always outgroup to the other *E. maximus* elephants (this was even true for the initial subset of full-length LINEs, which only contained 18 variant sites). *E. maximus_Z* is most often seen as a sibling to *E. maximus_M*, but with low support. The *Mammuthus* genus is unresolved in terms of inter-species relationships due to low coverage.

Discussion

Do elephantid genomes only carry dead LINEs?

The initial test using full-length BovB and LINE-1 retrotransposons failed to produce a reliable phylogeny. However, the lack of differences is an interesting finding. It means that even extinct

elephantids have all of the full-length repeats. Considering we used a modern elephant (*Loxodonta africana*) as the reference, the most likely explanation is that there has not been any recent retrotransposition in the elephantid lineage (if there had been, we would expect the modern elephants to have more full-length intervals than the ancient ones). There are a number of L1s in the *L. africana* genome that appear active, based on their structural characteristics. If they are not truly active, then they have persisted as conserved artefacts throughout the entire elephantid lineage.

Distinct differences between Asian and African elephants

Nuclear and mitochondrial DNA analyses have shown that Asian elephants are the closest living relatives of mammoths (4). The repeat-based phylogenies generated above provide supporting evidence. The most striking differences in repeat content occur in the modern Asian elephants (*E. maximus*), which stand out as having a huge number of absent intervals compared to the other elephantids. The SINE repeat class is particularly lacking (Figure S9.9): the *E. maximus* subgroup are missing more than twice as many intervals as any other elephantid (including mammoths).

Does this mean that Asian elephants are less repeat-dense? Or are their repeats found in different locations to the African elephants (and are thus undetectable with an African elephant reference)? In order to resolve this, we would need to use a modern Asian elephant as the reference and map those repeat intervals back against the other elephantids.

Changes from the original phylogeny revolve around Elephas and Paleoloxodon elephants

Our repeat-based model (results summarised in Figure S9.11) consistently produced two deviations from the genetic distance-based phylogeny (Figure S8.1). Firstly, the elephant from Assam, India *E. maximus_Y*, always appears as an outgroup to the rest of the *E. maximus* clade. The original tree has a support value of 68/73 at this node, suggesting that it may be misplaced. In an attempt to resolve this, we added a second Indian elephant *E. maximus_Z*, which groups with *E. maximus_M* and *E. maximus_L*. However, *E. maximus_Y* remained resolutely distinct, indicating that there may be repeat-specific differences in this genome, which distinguish it from the other Asian elephants.

Secondly, our maximum likelihood trees place *P. antiquus_N* outside of the *Loxodonta* elephants. *P. antiquus_O* could not be used to confirm this due to its low coverage. Placement of *P. antiquus_N* changed according to the method used (maximum likelihood versus maximum parsimony). Due to lack of further evidence, the genetic-distance-based phylogeny should be accepted.

The limitations of a reference-based binary system

Using a reference genome is never ideal. For example, the human genome project provided a high-quality DNA sequence that could be used to develop computational tools and databases, detect risk alleles, and measure conservation between species. Yet even the human reference is incomplete, and does not adequately represent the diversity of the human population.

In our case, using a reference restricts the dataset to intervals found on the *L. africana* genome. We cannot determine if other species have additional repetitive elements at different positions. Given a modern elephant as the reference, we cannot detect any repeats that were present in ancient elephantids and lost over time, or any new insertions in other, significantly diverged modern elephantids (case in point: *Elephas maximus*). We were able to distinguish between highly divergent elephantids (where the repeat-based tree mimicked the SNP-based results), but further testing is needed to improve reliability between closely related species and individuals.

Using ancient DNA raises other problems due to low coverage. By creating a system of presence/absence of intervals at given sites, and defining variance based on the absent intervals, we are making an implicit assumption that each genome is represented at equivalent coverage and quality to the reference. In reality, most genomes will be far worse than *L. africana* C (33x). Unfortunately, this problem is not easily resolved due to the low availability and high degradation of ancient DNA data. Hence, we cannot make a confident prediction about the *Mammuthus* and *Mammut* proboscideans.

Ideally, this method should be used for datasets with adequate (>5x) genome coverage and multiple high-quality reference genomes available. Using multiple references would take into account a wider range of retrotransposon diversity and give support to branches that cluster consistently regardless of the reference. An alternative strategy would be to use multiple reference genomes to generate a 'master' reference (reminiscent of the strategy in the human genome project), which would generate a more informative binary sequence for each species. Finally, one could use an outgroup (e.g. tenrec, another Afrotherian mammal) as the sole reference genome. This would remove the biases associated with using a modern elephant and restrict the analysis to ancestral repeats (where "missing" repeats act as the measure of evolutionary change). In any case, the approach we have used is complementary to the SNP-based analysis, and is also useful for providing insight into retrotransposition bursts over time.

Conclusions

This experiment has shown that repeats can be used as complementary variant site markers for determining species relationships but the results should be interpreted carefully to assess potential bias due to low coverage. We recommend this method be used together with SNP-based approaches as a way of confirming or resolving branches with low support. In cases where there are no known SNP variants, this method can be used to quickly surmise evolutionary relationships and pinpoint species, which require further testing.

Supplementary Note 10

Population genetic differentiation (F_{ST})

We calculated population genetic differentiation (F_{ST}) using the default --FST option from the software POPSTATS (https://github.com/pontussk/popstats), which computes Hudson's F_{ST} (58). We restricted this analysis to high-coverage genomes, for which we generated diploid calls per site across autosomes. We applied the standard filters described in Supplementary Note 6 including the 90% stringent mappability filter, excluded sites with read depth lower than 3 to avoid missing heterozygous sites and trimmed 5bp from both ends of ancient DNA reads. Our calculations were restricted to transversion polymorphisms to avoid residual damage-derived errors. Table S10.1 reports F_{ST} estimates among individual genomes and their standard errors. We also pooled together intraspecific genomes and estimated F_{ST} among taxa (Table S10.2).

As expected, F_{ST} values within taxa (0.05 – 0.67; Tables S10.1, S10.2) are generally lower than those among taxa (0.62 – 0.93). The highest intraspecific F_{ST} values are observed between *E. maximus_E* from Malaysian Borneo and other, mainland Asian elephants (0.44 – 0.67), suggesting that the Malaysian Borneo elephant population is highly differentiated. However, *E. maximus_E* also exhibits extremely low heterozygosity (see Table S13.1 and Figure S13.1), indicative of inbreeding and strong genetic drift, which is most likely the main reason for the high F_{ST} values. Similarly, F_{ST} between the ~45,000 year-old *M. primigenius_P* from mainland northeastern Siberia (Oimyakon) and the ~4,300 year-old *M. primigenius_Q* from Wrangel Island (0.35) is higher than many other within-taxa values, most likely because of the strong bottleneck reflected by the low heterozygosity in *M. primigenius_Q* (see Table S13.1 and Figure S13.1). Among Asian elephants, F_{ST} values follow a trend that could be explained by greater differentiation as a function of geographic distance between populations, but which could also be driven by differences in population-specific genetic drift. For example, *E. maximus_D* from Myanmar and *E. maximus_Y* from Assam in northeastern India exhibit the lowest F_{ST} (0.05) and highest heterozygosity estimates (Table S13.1 and Figure S13.1). *E. maximus_L* and *E. maximus_M*, which we assume originated in from India but whose sampling locations origins are unknown (see Table S2.2), exhibit intermediate F_{ST} values to *E. maximus_D* and to each other (0.07 – 0.17) as well as intermediate heterozygosity estimates. Finally, *E. maximus_Z* from southern India exhibits the highest F_{ST} to all the other Asian elephants (0.20 – 0.28) and the lowest heterozygosity. Genetic differentiation within forest and within savanna elephants is intermediate (0.18 and 0.14 respectively), suggesting some population structure in the two African elephant species.

Table S10.1. Pairwise F_{ST} between individual genomes and their standard errors estimated from transversion polymorphisms.

	LcycA	**LafrB**	**LafrC**	**EmaxD**	**EmaxE**	**LcycF**	**EmaxL**	**EmaxM**	**EantN**	**MpriP**	**MpriQ**	**EmaxY**	**EmaxZ**
LcycA		0.6476	0.6554	0.6809	0.7495	0.1835	0.6942	0.7002	0.6222	0.7020	0.7044	0.6871	0.7245
LafrB	0.0031		0.1439	0.8505	0.9202	0.7159	0.8661	0.8701	0.8854	0.8748	0.8749	0.8568	0.9014
LafrC	0.0028	0.0062		0.8569	0.9263	0.7238	0.8715	0.8766	0.8927	0.8811	0.8808	0.8630	0.9080
EmaxD	0.0024	0.0015	0.0012		0.4373	0.7332	0.0752	0.1288	0.8606	0.7602	0.7591	0.0525	0.2195
EmaxE	0.0023	0.0014	0.0012	0.0043		0.8030	0.5027	0.5338	0.9340	0.8618	0.8569	0.4713	0.6678
LcycF	0.0051	0.0039	0.0037	0.0030	0.0029		0.7469	0.7524	0.6949	0.7567	0.7577	0.7399	0.7797
EmaxL	0.0025	0.0017	0.0015	0.0061	0.0059	0.0031		0.1111	0.8753	0.7807	0.7795	0.0940	0.1980
EmaxM	0.0027	0.0017	0.0015	0.0061	0.0060	0.0032	0.0098		0.8804	0.7896	0.7866	0.1547	0.2725
EantN	0.0027	0.0020	0.0017	0.0015	0.0014	0.0040	0.0017	0.0018		0.8833	0.8824	0.8667	0.9135
MpriP	0.0027	0.0016	0.0013	0.0015	0.0015	0.0032	0.0020	0.0020	0.0015		0.3519	0.7708	0.8317
MpriQ	0.0027	0.0018	0.0016	0.0020	0.0020	0.0033	0.0023	0.0024	0.0018	0.0048		0.7683	0.8301
EmaxY	0.0025	0.0016	0.0014	0.0049	0.0051	0.0031	0.0069	0.0071	0.0016	0.0017	0.0021		0.2420
EmaxZ	0.0025	0.0016	0.0014	0.0059	0.0055	0.0032	0.0094	0.0098	0.0016	0.0018	0.0022	0.0073	

F_{ST} values are shown in the upper diagonal and their standard errors in the lower diagonal.

Table S10.2. F_{ST} among taxa (sorted by value) and their standard errors (SE) estimated from transversion polymorphisms. Number of individuals pooled within taxa are given inside parentheses.

Pop1	Pop2	F_{ST}	SE
Lcyc (2)	Eant (1)	0.619651	0.002561
Lcyc (2)	Lafr (2)	0.643013	0.002882
Mpri (2)	Lcyc (2)	0.679757	0.002825
Lcyc (2)	Emax (6)	0.681397	0.002456
Mpri (2)	Emax (6)	0.726472	0.001552
Lafr (2)	Emax (6)	0.848423	0.001283
Mpri (2)	Lafr (2)	0.850073	0.001534
Mpri (2)	Eant (1)	0.857299	0.001688
Emax (6)	Eant (1)	0.859915	0.001418
Lafr (2)	Eant (1)	0.881143	0.001783

Supplementary Note 11

Tests for admixture within the family Elephantidae

D-statistics

To investigate whether there has been gene flow between different elephantid taxa, we computed *D*-statistics (25), which estimate allele sharing between populations to test if tree-like population histories can explain the data. Using quartets of populations with the topology (((*A*, *B*), *X*), *O*), where *O* represents an outgroup, we computed the normalized product of the allele differences for populations A and B, and *X* and the outgroup, averaged over all SNPs. Assuming that the simple tree topology is correct, this statistic should be consistent with zero. Deviations from zero indicate an excess of shared derived alleles between populations *A* and *X* (positive values) or between populations *B* and *X* (negative values). *D*-statistics are not biased by population-specific genetic drift since a single lineage is sampled per population: under the null hypothesis of no gene flow, the lineages must coalesce at a more ancient point than the respective population split times, and therefore shared alleles between A and X, or B and X, can only be due to incomplete lineage sorting, which is expected to be symmetric between the two population pairs. We used the population genomics program POPSTATS (https://github.com/pontussk/popstats), which computes *D*-statistics as in Green *et al.* (59) and Patterson *et al.* (25) and implements a block jackknife procedure to estimate standard errors by splitting chromosomes into 5Mb blocks (weighting blocks by the number of polymorphic positions). To avoid reference-alignment biases (see Supplementary Note 6), which can distort these statistics (25), we sampled a random allele per site from each genome (as described in Supplementary Note 8).

We first merged individuals into taxon-specific groups and computed *D*-statistics for chromosomes 1-27 to test for admixture using tests of the form *D (A, B; X, Y)* where *A, B, X* and *Y* represent different taxa. Most of these statistics deviate from zero with high absolute values and highly significant *Z*-scores reflecting the phylogenetic relationships observed in the pairwise-distance NJ tree (Figure S8.1). However, we also observe tests that produce *D*-values of lower magnitude and lower *Z*-scores – but still significant ($|Z| > 3$) – indicating genetic affinities between taxa that are not consistent with the topology of the NJ tree. Although some of these genetic affinities are likely signals of true admixture between different elephantid taxa, we caution that some of them could also be due to artifacts. *D*-statistics were developed and shown to be robust for error rates and similarity of genome structure typical of within-species comparisons, and certain assumptions could be violated for comparisons of different species (60) (e.g., presence of repeat mutations). We therefore interpret nominally significant results with caution. In particular, alignment biases to the reference genome *(LoxAfr4*, which originates from the same savanna elephant as the genomic sequences for *L. africana_C*), or damage-derived errors in ancient samples, could bias *D*-statistic estimates, although the latter process should not affect statistics computed from transversions only. Exclusion of transitions further allowed us to minimize parallel substitutions in different elephantid lineages, since transversions accumulate at

a slower rate. For these reasons, only estimates from transversion polymorphisms are reported in the text.

Cognizant of these challenges, we make the following observations:

i) There is excess genetic affinity between African forest and African savanna elephants compared to the expectation of forest and straight-tusked elephants forming a clade. Specifically, statistics of the form *D (P. antiquus, L. cyclotis; L. africana, X)*, where *X* stands for all other proboscidean lineages, produce significantly negative values ($0.23 \leq |D| \leq 0.31$, $50 < |Z| < 61$; Table S12.1). Tests of the form *D (L. africana, L. cyclotis; P. antiquus, X)* also produce significantly negative values ($0.33 \leq |D| \leq 0.41$, $58 \leq |Z| < 74$) and tests of the form *D* (*P. antiquus, L. africana; L. cyclotis, X*) produce positive values ($0.07 \leq D \leq 0.11$, $9 \leq Z \leq 17$). Given these statistics, none of the three possible tree-like topologies relating forest, savanna, and straight-tusked elephants fit the data, suggesting a history of gene flow between two of the species. However, based on these statistics alone, it is not possible to resolve which lineages were involved.

ii) There is excess genetic affinity between straight-tusked elephants and Asian elephants, straight-tusked elephants and woolly mammoths, and straight-tusked elephants and the Columbian mammoth ($0.02 \leq D \leq 0.13$, $4 \leq Z \leq 30$; Table S11.1). If these signals are true, they could be due to admixture between a population related to the straight-tusked elephant and a population related to Asian elephants and/or mammoths. This is an interesting possibility since straight-tusked elephants have conventionally been grouped together with Asian elephants based on cranium and dentition morphological criteria (37, 38), and hence possible gene flow between them in their ancestry could be consistent with their shared morphological features.

iii) There is excess affinity between savanna elephants and Asian elephants, savanna elephants and woolly mammoths, and savanna elephants and the Columbian mammoth ($0.03 \leq |D| \leq 0.11$, $6 \leq |Z| \leq 30$; Table S11.1). Although these signals are nominally significant, they could possibly be artifacts associated with alignment biases to the reference genome (that of a savanna elephant), and hence we do not highlight these observations as clear findings of the study.

iv) There is excess affinity between forest elephants and Asian elephants (*D* (*M. primigenius, E. maximus; L. cyclotis, M. americanum*) = -0.03, $|Z| = 9$; Table S11.1). This signal is not consistent across tests and could also be associated with alignment biases to the reference genome due to similarity between forest elephants and savanna elephants.

Table S11.1. Autosomal *D*-statistics for tests of the form *D (A, B; X, Y)* where *A, B, X, Y* indicate different taxa (including two or more individuals). *D*-statistics that exhibit affinities between taxa that are not consistent with the topology of the pairwise-distance NJ tree are indicated in bold font.

				All sites				Only transversions			
A	***B***	***X***	***Y***	***D***	**SE**	***Z***	**nSNPs**	***D***	**SE**	***Z***	**nSNPs**
Pant	**Lcyc**	**Lafr**	**Mame**	**-0.235**	**0.004**	**-60.37**	**2,016,622**	**-0.229**	**0.005**	**-49.73**	**535,237**
Pant	**Lcyc**	**Emax**	**Mame**	**0.039**	**0.004**	**11.00**	**1,437,557**	**0.076**	**0.004**	**17.94**	**371,372**
Pant	**Lcyc**	**Mpri**	**Mame**	**0.073**	**0.004**	**19.59**	**1,479,029**	**0.135**	**0.005**	**29.69**	**354,235**
Pant	**Lcyc**	**Mcol**	**Mame**	**0.059**	**0.004**	**16.54**	**770,183**	**0.130**	**0.005**	**27.44**	**177,815**
Pant	Lafr	Lcyc	Mame	0.093	0.006	15.10	2,656,479	0.115	0.007	16.73	719,017
Pant	**Lafr**	**Emax**	**Mame**	-0.006	0.003	-1.80	1,343,859	**0.021**	**0.004**	**5.04**	**336,514**
Pant	**Lafr**	**Mpri**	**Mame**	**0.017**	**0.004**	**4.80**	**1,409,235**	**0.054**	**0.004**	**12.32**	**335,375**
Pant	**Lafr**	**Mcol**	**Mame**	**-0.016**	**0.003**	**-4.51**	**736,809**	**0.017**	**0.005**	**3.64**	**169,884**
Pant	Emax	Lcyc	Mame	0.590	0.005	108.69	2,987,775	0.640	0.006	112.86	819,245
Pant	Emax	Lafr	Mame	0.409	0.006	63.08	2,198,680	0.466	0.007	65.85	583,354
Pant	Emax	Mpri	Mame	-0.621	0.004	-158.25	2,647,310	-0.649	0.004	-146.31	698,782
Pant	Emax	Mcol	Mame	-0.611	0.004	-157.95	1,364,134	-0.647	0.005	-141.99	346,618
Pant	Mpri	Lcyc	Mame	0.599	0.005	110.09	3,038,733	0.661	0.006	114.83	793,478
Pant	Mpri	Lafr	Mame	0.413	0.007	63.55	2,272,154	0.476	0.007	65.76	574,041
Pant	Mpri	Emax	Mame	-0.634	0.004	-179.57	2,646,534	-0.671	0.004	-167.38	688,506
Pant	Mpri	Mcol	Mame	-0.885	0.002	-579.17	2,282,649	-0.919	0.002	-559.56	612,749
Pant	Mcol	Lcyc	Mame	0.587	0.005	107.79	1,627,782	0.660	0.006	112.22	421,590
Pant	Mcol	Lafr	Mame	0.380	0.007	56.93	1,180,196	0.446	0.008	57.86	295,505
Pant	Mcol	Emax	Mame	-0.628	0.003	-185.69	1,326,365	-0.677	0.004	-167.54	336,855
Pant	Mcol	Mpri	Mame	-0.884	0.001	-597.12	2,246,514	-0.920	0.002	-577.85	608,872
Lafr	Lcyc	Pant	Mame	-0.321	0.005	-61.38	2,178,358	-0.335	0.006	-57.78	586,820
Lafr	**Lcyc**	**Emax**	**Mame**	**0.043**	**0.003**	**14.33**	**1,631,590**	**0.039**	**0.004**	**10.86**	**460,386**
Lafr	**Lcyc**	**Mpri**	**Mame**	**0.055**	**0.003**	**19.33**	**1,630,098**	**0.067**	**0.003**	**19.31**	**424,819**
Lafr	**Lcyc**	**Mcol**	**Mame**	**0.085**	**0.003**	**30.13**	**840,043**	**0.110**	**0.004**	**29.55**	**210,088**
Lcyc	Emax	Pant	Mame	0.564	0.006	88.19	2,980,491	0.593	0.007	88.81	808,204
Lcyc	Emax	Lafr	Mame	0.532	0.006	91.96	3,186,705	0.554	0.006	91.82	897,604
Lcyc	Emax	Mpri	Mame	-0.655	0.004	-181.54	3,251,241	-0.682	0.004	-176.40	902,085
Lcyc	Emax	Mcol	Mame	-0.643	0.004	-176.87	1,657,753	-0.680	0.004	-168.74	440,322
Lcyc	Mpri	Pant	Mame	0.550	0.007	83.24	3,098,030	0.578	0.007	82.74	815,702
Lcyc	Mpri	Lafr	Mame	0.532	0.006	92.01	3,273,465	0.555	0.006	91.25	893,061
Lcyc	Mpri	Emax	Mame	-0.640	0.003	-192.47	3,327,421	-0.662	0.004	-184.92	930,437
Lcyc	Mpri	Mcol	Mame	-0.896	0.001	-611.66	2,687,040	-0.924	0.002	-607.70	740,163
Lcyc	Mcol	Pant	Mame	0.547	0.007	84.05	1,679,559	0.579	0.007	82.74	442,245
Lcyc	Mcol	Lafr	Mame	0.506	0.006	83.52	1,729,835	0.528	0.007	80.76	466,458
Lcyc	Mcol	Emax	Mame	-0.638	0.003	-198.84	1,672,969	-0.679	0.004	-186.55	453,057
Lcyc	Mcol	Mpri	Mame	-0.895	0.001	-657.72	2,677,802	-0.925	0.001	-650.79	746,480
Lafr	Emax	Pant	Mame	0.414	0.007	59.33	2,183,549	0.449	0.007	60.95	581,641
Lafr	Emax	Lcyc	Mame	0.562	0.005	104.82	3,191,098	0.581	0.005	105.96	915,669
Lafr	Emax	Mpri	Mame	-0.640	0.004	-173.56	2,964,263	-0.666	0.004	-165.34	826,618
Lafr	Emax	Mcol	Mame	-0.619	0.004	-159.98	1,494,452	-0.650	0.004	-147.58	398,020
Lafr	Mpri	Pant	Mame	0.399	0.007	55.56	2,307,411	0.433	0.008	56.11	589,077

Lafr	Mpri	Lcyc	Mame	0.570	0.005	106.60	3,250,431	0.600	0.005	109.48	886,815
Lafr	Mpri	Emax	Mame	-0.632	0.003	-182.15	3,021,543	-0.659	0.004	-173.69	835,481
Lafr	Mpri	Mcol	Mame	-0.890	0.002	-562.29	2,516,788	-0.918	0.002	-551.20	694,281
Lafr	Mcol	Pant	Mame	0.394	0.007	55.44	1,171,348	0.432	0.008	55.31	299,229
Lafr	Mcol	Lcyc	Mame	0.567	0.005	105.15	1,658,237	0.603	0.006	108.24	446,122
Lafr	Mcol	Emax	Mame	-0.628	0.003	-185.99	1,464,513	-0.670	0.004	-173.66	393,855
Lafr	Mcol	Mpri	Mame	-0.892	0.001	-621.36	2,466,540	-0.922	0.002	-607.87	690,288
Mpri	**Emax**	**Pant**	**Mame**	**0.021**	**0.003**	**6.61**	**1,230,678**	**0.040**	**0.004**	**9.25**	**275,766**
Mpri	**Emax**	**Lcyc**	**Mame**	**-0.025**	**0.003**	**-8.12**	**1,559,632**	**-0.035**	**0.004**	**-9.03**	**403,256**
Mpri	**Emax**	**Lafr**	**Mame**	**-0.014**	**0.003**	**-4.35**	**1,374,720**	-0.012	0.004	-2.87	341,552
Mpri	Emax	Mcol	Mame	0.774	0.003	262.72	1,894,446	0.810	0.003	260.10	514,895
Mcol	**Emax**	**Pant**	**Mame**	**0.028**	**0.003**	**8.66**	**580,326**	**0.054**	**0.005**	**11.36**	**128,947**
Mcol	Emax	Lcyc	Mame	-0.009	0.003	-2.75	724,177	-0.002	0.004	-0.42	179,852
Mcol	**Emax**	**Lafr**	**Mame**	**0.015**	**0.003**	**4.50**	**642,805**	**0.036**	**0.005**	**7.59**	**156,108**
Mcol	Emax	Mpri	Mame	0.767	0.003	260.45	1,892,595	0.809	0.003	261.00	527,072
Mpri	Mcol	Pant	Mame	0.002	0.003	0.55	417,051	-0.006	0.006	-1.06	73,576
Mpri	Mcol	Lcyc	Mame	0.004	0.003	1.44	484,240	-0.009	0.005	-1.72	95,559
Mpri	**Mcol**	**Lafr**	**Mame**	-0.009	0.003	-2.91	438,677	**-0.031**	**0.005**	**-5.83**	**85,394**
Mpri	**Mcol**	**Emax**	**Mame**	**0.016**	**0.003**	**4.55**	**654,814**	0.005	0.005	0.99	150,662

We further tested whether individuals within taxa are symmetrically related to other taxa by performing tests of the form *D (A_1, A_2; X, Y),* in which A_1, A_2 indicate different individuals within taxon *A,* while *X, Y* indicate different taxa (including one or more individuals). We expect these tests to be symmetric ($D = 0$; $|Z| < 3$) if all lineages are reciprocally monophyletic. Indeed, the majority of these tests do not significantly deviate from zero, but there are some exceptions. Here too, we consider only transversions. We make the following observations:

v) There is excess genetic affinity between one of the forest elephants and straight-tusked elephants, with *D (L. cyclotis_A, L. cyclotis_F; P. antiquus, X)* ranging from -0.03 to -0.04, where *X* indicates all other proboscidean lineages ($7 \leq |Z| \leq 9$; Table S11.2). *L. cyclotis_F* originates from the Guinean forest block in West Africa whereas *L. cyclotis_A* originates from the Congolian forest block in Central Africa. Although the two forest blocks are geographically separated by the intervening Dahomey/Benin Gap, it is unknown whether gene flow has been limited between the elephant populations inhabiting these regions (61). Earlier genetic studies hypothesized that West African forest elephant populations represent a third, distinct species in Africa (62, 63) but more recent analyses based on a larger number of nuclear markers failed to assign them to a distinct genetic cluster, and thus did not support this hypothesis (36). Assuming that the two forest elephants derive from isolated populations, the excess affinity between *L. cyclotis_F* and *P. antiquus* could be explained by gene flow between their ancestral populations, which occurred after substructure between the ancestors of West and Central African forest elephant

populations had already begun to develop. Moreover, if we assume that gene flow occurred from a population related to *L. cyclotis_F* into the straight-tusked elephant population (as suggested by the admixture graphs in Supplementary Note 12), there is a lower bound for the date of admixture at ~120,000 years before present (BP), which is the inferred age of the *P. antiquus* samples.

The asymmetric relatedness of the two forest elephants to the straight-tusked elephant is also evident in their mitochondrial genomes. *P. antiquus_N* and *P. antiquus_O* carry mtDNA that groups within the mitochondrial diversity of forest elephants (clade F) and in particular most closely related to the western subclade of clade F, which is carried by *L. cyclotis_F* (Figure S7.1; Meyer *et al.* (5)). The mtDNA of an older straight-tusked elephant from Weimar-Ehringsdorf (WE; ~244,000 years BP) reported in Meyer *et al.* (5), however, does not group together with that of *P. antiquus_N* and *P. antiquus_O* (younger straight-tusked elephants from Neumark-Nord [NN]; ~120,000 years BP) but forms a separate lineage within forest elephants that is basal to the western and west-central subclades of clade F. Our Central African forest elephant, *L. cyclotis_A*, carries a still more deeply diverged mtDNA lineage that belongs to the north-central subclade within clade F. The lack of nuclear data from the ~244,000 year-old straight-tusked elephant (WE) prevents us from obtaining an estimate of forest elephant-related ancestry in its nuclear genome. The presence of forest elephant-related mtDNA in straight-tusked elephants could either be explained by incomplete lineage sorting in the common ancestral population of forest and straight-tusked elephants or mtDNA introgression. The high fraction of forest elephant-derived ancestry in *P. antiquus* (~⅓ of its nuclear genome), inferred from f_4 ratio tests (Table S11.8) and admixture graphs (Figures S12.1 – S12.4) suggests that mtDNA introgression is more likely, with straight-tusked elephants acquiring their mtDNA via gene flow from a population that was a clade with contemporary West and West-Central African forest elephants. Given the age of the oldest straight-tusked elephant, such admixture must have occurred earlier than ~244,000 years BP, which is plausible in light of the deep split time of the two forest elephant populations (inferred to have occurred at 609,000 - 463,000 years ago in Supplementary Note 15).

Table S11.2. Autosomal *D*-statistics for tests of the form *D (L. cyclotis_A, L. cyclotis_F; P. antiquus, X)* where *X* indicates all other proboscidean taxa (including one or more individuals).

D (L. cyclotis_A, L. cyclotis_F; P. antiquus, X)								
	All substitutions				**Transversions**			
X	***D***	**SE**	***Z***	**nSNPs**	***D***	**SE**	***Z***	**nSNPs**
Emax	-0.034	0.004	-8.76	1,172,101	-0.035	0.004	-8.49	360,689
Lafr	-0.041	0.006	-6.62	1,356,486	-0.043	0.006	-6.75	393,498
Mame	-0.032	0.004	-8.79	981,781	-0.035	0.004	-8.67	266,860

Mcol	-0.036	0.004	-9.11	602,135	-0.039	0.005	-8.30	165,396
Mpri	-0.036	0.004	-9.19	1,132,112	-0.037	0.004	-8.85	320,616

vi) There is excess affinity between the taxonomically unassigned North American mammoth specimen (*Mammuthus_V*) and woolly mammoths with *D (M. columbi_U, Mammuthus_V; M. primigenius$_1$, X)* ranging from -0.49 to -0.50, where *M. primigenius$_1$* stands for all woolly mammoths except for *Mammuthus_V,* and *X* stands for all other proboscidean lineages ($84 \leq |Z| \leq 87$; Table S11.3). These *D*-statistics together with the phylogenetic position of *Mammuthus_V* within the woolly mammoth lineage in the pairwise-distance NJ tree (Figure S8.1) confirm that this specimen is genetically a woolly mammoth. However, tests of the form *D (Mammuthus_V, M. primigenius_ind; M. columbi_U, X)* where *M. primigenius_ind* stands for each woolly mammoth in turn (except for *Mammuthus_V* and *M. primigenius_H*) and *X* for all other proboscidean lineages, are significantly positive ($0.03 \leq D \leq 0.11$, $7 \leq Z \leq 14$; Table S11.3), indicating excess genetic affinity between *Mammuthus_V* and *M. columbi_U*. This signal suggests that *Mammuthus_V* has both woolly mammoth and Columbian mammoth genetic components.

vii) *M. primigenius_H* from Alaska also shows excess genetic affinity to *M. columbi_U*, with *D (M. primigenius_H, M. primigenius_ind; M. columbi_U, X)* being significantly positive ($0.05 \leq D \leq 0.14$, $7 < Z < 14$; Table S11.3), where *M. primigenius_ind* stands for each woolly mammoth in turn, excluding *M. primigenius_H* and *Mammuthus_V,* and *X* stands for all other proboscidean lineages. No other woolly mammoth in our dataset shows excess affinity to *M. columbi_U*, suggesting that only the mammoths from North America (*Mammuthus_V* and *M. primigenius_H*) have woolly and Columbian mammoth ancestry. The admixed North American mammoths appear to form a clade with respect to the Columbian mammoth and most Eurasian woolly mammoths with *D* (*M. primigenius_H, Mammuthus_V; M. columbi_U, M. primigenius_ind$_2$*) not deviating from zero significantly , where *M. primigenius_ind$_2$* stands for each Eurasian woolly mammoth in turn, excluding *M. primigenius_Q*. We use f_4-ratio tests later in this note to estimate the proportions of their ancestry.

Our discovery of Columbian mammoth ancestry in the nuclear genomes of *Mammuthus_V* and *M. primigenius_H* provides support for theories of interbreeding between Columbian and North American (NA) woolly mammoths, which was postulated to account for fossils with intermediate morphology (some of them referred to as *M. jeffersonii*) in regions where the two species encountered each other (64, 65), as well as for the similarity in their mtDNA (2, 66). Most NA woolly mammoths have been found to carry mtDNA that is more closely related to that of

Columbian mammoths (haplogroups C and F within mammoth clade I, respectively) than to other woolly mammoths, suggesting Columbian mammoth mtDNA introgression (2) into NA *M. primigenius*. The mtDNA lineage of *M. primigenius_H* is nested within haplogroup C, that of *M. columbi_U* within haplogroup F and that of *Mammuthus_V* basal to haplogroups C and F (Figure S7.1).

viii) *D* (*M. primigenius_S*, *M. primigenius_ind*$_3$; *M. columbi_U*, *X*), where *M. primigenius_ind*$_3$ stands for each woolly mammoth in turn, excluding *M. primigenius_S,* and *X* for all other proboscidean lineages, is significantly negative ($0.03 \leq |D| \leq 0.14$, $3 < |Z| < 17$; Table S11.3), suggesting that *M. primigenius_S* may have ancestry from a lineage that split off prior to the separation of Columbian and woolly mammoth ancestors. Also, most tests of the form *D* (*M. primigenius_S*, *M. primigenius*$_3$; *X, Y*) where *M. primigenius*$_3$ stands for all woolly mammoths except for *M. primigenius*_S, and *X*, *Y* stand for all other proboscidean lineages, significantly deviate from zero, suggesting different genetic affinities between *M. primigenius_S* and other proboscidean lineages. *M. primigenius_S* is a female mammoth calf found in the Yamal Peninsula in northwest Siberia (known as Lyuba), which carries a mitochondrial haplotype that belongs to the deeply diverged mammoth mtDNA clade III (haplogroup B2; Figure S7.1). Moreover, it exhibits a cline in its relatedness to the remaining woolly mammoths with higher genetic affinity to *M. primigenius_G*, *M. primigenius_P* and *M. primigenius_Q* from Eurasia compared to *M. primigenius_H* and *Mammuthus_V* from North America (Table S11.4).

Table S11.3. Autosomal *D*-statistics for tests of the form *D (M. columbi_U, Mammuthus_V; M. primigenius*$_1$*, X), D (Mammuthus_V, M. primigenius*$_2$*; M. columbi_U, X), D (M. primigenius_H, M. primigenius*$_1$*; M. columbi_U, X)* and *D (M. primigenius_S, M. primigenius*$_3$*; M. columbi_U, X)* where *X* stands for all other proboscidean taxa*, M. primigenius*$_1$ stands for all *M. primigenius* merged together excluding *Mammuthus_V*, *M. primigenius*$_2$ stands for all *M. primigenius* merged together excluding *Mammuthus_V* and *M. primigenius_H*, and *M. primigenius*$_3$ for all *M. primigenius* merged together excluding *M. primigenius_S*. *D*-statistic values in the text above refer to tests with individual woolly mammoths in turn, while *D*-statistic values in the table below refer to tests with merged woolly mammoth individuals.

	All substitutions				**Transversions**			
	D	**SE**	***Z***	**nSNPs**	***D***	**SE**	***Z***	**nSNPs**
X	***D (M. columbi_U, Mammuthus_V; M. primigenius*$_1$*, X)***							
Lafr	-0.479	0.005	-88.88	998,111	-0.497	0.006	-86.80	285,368
Lcyc	-0.480	0.005	-88.71	1,016,094	-0.496	0.006	-85.85	289,331
Emax	-0.486	0.006	-86.37	1,014,754	-0.496	0.006	-83.81	292,569
Pant	-0.463	0.005	-88.35	912,361	-0.495	0.006	-84.69	253,838
Mame	-0.446	0.005	-87.93	943,571	-0.493	0.006	-84.94	258,484

X	*D (Mammuthus_V, M. primigenius$_1$; M. columbi_U, X)*							
Lafr	0.025	0.004	6.86	621,942	0.045	0.004	10.09	174,857
Lcyc	0.031	0.004	8.75	661,647	0.051	0.004	11.55	184,871
Emax	0.041	0.004	10.42	667,702	0.051	0.005	11.01	192,053
Pant	0.012	0.004	3.40	575,613	0.045	0.005	9.44	154,722
Mame	0.007	0.003	1.97	622,982	0.052	0.004	11.54	160,913
X	*D (M. primigenius_H, M. primigenius$_1$; M. columbi_U, X)*							
Lafr	0.050	0.004	12.00	209,662	0.063	0.006	10.66	58,416
Lcyc	0.053	0.004	12.83	223,395	0.065	0.006	10.94	61,632
Emax	0.058	0.004	12.95	224,831	0.065	0.006	10.68	63,430
Pant	0.052	0.004	12.57	192,917	0.069	0.006	11.02	51,633
Mame	0.038	0.004	9.78	212,377	0.066	0.006	11.13	54,585
X	*D (M. primigenius_S, M. primigenius$_3$; M. columbi_U, X)*							
Lafr	-0.071	0.004	-18.13	256,054	-0.066	0.005	-12.28	72,453
Lcyc	-0.061	0.004	-15.88	271,796	-0.057	0.005	-10.83	76,407
Emax	-0.041	0.004	-10.17	273,653	-0.036	0.006	-6.50	78,841
Pant	-0.065	0.004	-16.96	232,485	-0.060	0.006	-10.30	63,133
Mame	-0.086	0.004	-22.08	259,125	-0.082	0.006	-14.71	67,830

Table S11.4. Autosomal *D*-statistics for tests of the form *D (M. primigenius_ind$_x$, M. primigenius_ind$_y$; M. primigenius_S, M. americanum)* where *M. primigenius_ind$_{x,y}$* stands for each woolly mammoth in turn excluding *M. primigenius_S*.

				All sites				**Only transversions**			
A	***B***	***X***	***Y***	***D***	**SE**	***Z***	**nSNPs**	***D***	**SE**	***Z***	**nSNPs**
MpriG	MpriH	MpriS	Mame	0.079	0.006	12.93	39,828	0.055	0.010	5.75	10,735
MpriG	MpriP	MpriS	Mame	0.015	0.005	3.10	108,570	0.009	0.007	1.30	30,202
MpriG	MpriQ	MpriS	Mame	0.001	0.005	0.28	111,175	-0.004	0.007	-0.55	31,421
MpriG	MpriV	MpriS	Mame	0.119	0.005	25.92	114,204	0.090	0.007	13.11	31,254
MpriH	MpriP	MpriS	Mame	-0.070	0.005	-13.79	89,683	-0.057	0.008	-7.45	24,184
MpriH	MpriQ	MpriS	Mame	-0.079	0.005	-15.81	93,415	-0.072	0.007	-9.85	25,595
MpriH	MpriV	MpriS	Mame	0.043	0.005	8.57	87,999	0.027	0.008	3.57	22,913
MpriP	MpriQ	MpriS	Mame	-0.013	0.004	-3.05	268,397	-0.016	0.005	-3.00	75,173
MpriP	MpriV	MpriS	Mame	0.108	0.004	26.79	269,695	0.082	0.005	15.65	73,304
MpriV	MpriQ	MpriS	Mame	-0.119	0.004	-27.17	282,700	-0.097	0.005	-17.71	77,175

vi) The two savanna elephants are symmetrically related to forest elephants (*D* (*L. africana_B, L. africana_C; L. cyclotis, X*) ~ 0, where *X* indicates all other proboscidean lineages, $|Z| < 3$). Similarly, the two forest elephants are symmetrically related to savanna elephants (*D* (*L. cyclotis_A, L. cyclotis_F; L. africana, X*) ~ 0, where *X* indicates all other proboscidean lineages except for straight-tusked elephants, $|Z| < 2$, and *D* (*L. africana_B, L. africana_C; L. cyclotis_A, L. cyclotis_F*)

~ 0, $|Z| < 2$). This suggests that if there has been admixture between the two species, either the mixture proportions were too small to detect, or admixture must have occurred before the ancestors of *L. africana_B* and *L. africana_C*, and the ancestors of *L. cyclotis_A* and *L. cyclotis_F* began to differentiate, or admixture was from a population ancestral to forest elephants into both savanna elephant lineages in approximately equal proportions (or vice versa).

vii) Other tests of the form *D* (A_1, A_2; *X, Y*) that significantly deviate from zero are listed in Table S11.5. However, the apparent genetic affinities in these tests could potentially be explained by alignment biases to the reference genome or data quality issues.

Table S11.5. Autosomal significant *D*-statistics for tests of the form *D* (A_1, A_2; *X, Y*), where A_1, A_2 indicate different individuals within taxon *A,* while *X, Y* indicate different taxa (including one or more individuals).

				All sites				Only transversions			
A1	***A2***	***X***	***Y***	***D***	**SE**	***Z***	**nSNPs**	***D***	**SE**	***Z***	**nSNPs**
LafrB	LafrC	Emax	Mcol	0.029	0.007	4.23	66,999	0.042	0.009	4.61	22,104
LafrB	LafrC	Emax	Mpri	0.014	0.006	2.42	159,394	0.041	0.007	6.06	58,749
PantN	PantO	Lafr	Emax	-0.065	0.008	-8.19	28,290	-0.085	0.014	-6.02	7,315
PantN	PantO	Lafr	Mame	-0.058	0.007	-8.49	27,496	-0.044	0.014	-3.10	5,494
PantN	PantO	Lafr	Mpri	-0.057	0.008	-6.80	32,012	-0.066	0.014	-4.77	7,792
PantN	PantO	Lcyc	Lafr	0.069	0.008	8.79	33,355	0.088	0.013	6.96	8,850
PantN	PantO	Lcyc	Mame	-0.002	0.007	-0.27	37,008	0.038	0.013	3.03	8,242
PantN	PantO	Lcyc	Mcol	0.015	0.009	1.69	21,622	0.053	0.015	3.46	5,355
EmaxD	EmaxM	Pant	Lcyc	0.012	0.005	2.63	162,822	0.022	0.005	4.02	61,162
EmaxD	EmaxE	Lafr	Mame	0.020	0.005	4.37	180,618	0.027	0.007	4.07	49,781
EmaxD	EmaxM	Lafr	Lcyc	0.015	0.004	3.71	214,302	0.017	0.004	3.82	91,996
EmaxD	EmaxE	Mpri	Lafr	-0.019	0.006	-3.51	333,080	-0.018	0.006	-3.24	114,535
EmaxD	EmaxL	Mpri	Lafr	-0.016	0.005	-3.19	296,720	-0.017	0.005	-3.29	104,481
EmaxD	EmaxY	Mpri	Lcyc	-0.010	0.004	-2.28	341,533	-0.013	0.004	-3.06	128,878
EmaxE	EmaxM	Pant	Lcyc	0.013	0.005	2.74	177,072	0.022	0.006	3.81	63,531
EmaxE	EmaxM	Lafr	Mame	-0.020	0.005	-4.20	182,266	-0.024	0.007	-3.71	49,959
EmaxE	EmaxY	Lafr	Mame	-0.019	0.005	-4.03	180,323	-0.022	0.007	-3.21	49,609
EmaxE	EmaxZ	Lafr	Mame	-0.023	0.005	-4.58	174,555	-0.025	0.007	-3.72	46,764
EmaxE	EmaxM	Lcyc	Mame	-0.019	0.004	-4.64	217,409	-0.023	0.006	-4.04	64,745
EmaxE	EmaxZ	Lcyc	Mame	-0.015	0.004	-3.52	205,987	-0.018	0.006	-3.00	59,403
EmaxE	EmaxM	Mpri	Lcyc	0.014	0.005	2.75	386,934	0.017	0.005	3.43	139,837
EmaxE	EmaxZ	Mpri	Lafr	0.020	0.006	3.28	313,661	0.022	0.006	3.38	102,856
EmaxL	EmaxY	Pant	Lcyc	-0.009	0.004	-1.96	156,190	-0.020	0.006	-3.60	58,785
EmaxL	EmaxY	Lafr	Lcyc	-0.014	0.004	-3.32	205,324	-0.014	0.004	-3.08	88,255

EmaxL	EmaxZ	Mpri	Lafr	0.016	0.005	3.12	250,034	0.020	0.006	3.45	85,097
EmaxM	EmaxY	Pant	Lcyc	-0.015	0.005	-3.30	159,871	-0.029	0.005	-5.29	59,895
EmaxM	EmaxY	Lafr	Lcyc	-0.013	0.004	-3.01	209,618	-0.018	0.005	-3.90	89,763
EmaxM	EmaxY	Mpri	Lcyc	-0.012	0.005	-2.62	345,035	-0.017	0.004	-3.94	129,818
MpriP	MpriQ	Pant	Lcyc	0.010	0.004	2.25	198,680	0.023	0.006	3.74	51,469
MpriV	MpriG	Pant	Lcyc	0.075	0.005	13.67	77,437	0.032	0.009	3.43	17,344
MpriV	MpriG	Emax	Lafr	-0.045	0.005	-8.43	142,741	-0.024	0.007	-3.18	38,849
MpriV	MpriG	Lafr	Lcyc	0.036	0.005	6.67	81,752	0.039	0.009	4.43	20,624
MpriV	MpriH	Pant	Lcyc	0.058	0.005	11.38	63,451	0.036	0.010	3.42	13,110
MpriV	MpriP	Emax	Lafr	-0.040	0.005	-8.55	375,488	-0.030	0.006	-5.20	108,462
MpriV	MpriP	Lafr	Mame	-0.038	0.004	-10.32	249,395	0.021	0.006	3.61	50,566
MpriV	MpriP	Lafr	Lcyc	0.029	0.004	7.16	211,037	0.034	0.006	5.70	55,665
MpriV	MpriQ	Pant	Lcyc	0.053	0.005	11.64	206,422	0.028	0.006	4.25	48,658
MpriV	MpriQ	Emax	Lafr	-0.046	0.005	-9.79	389,765	-0.037	0.006	-6.14	114,417
MpriV	MpriQ	Emax	Pant	-0.054	0.005	-11.28	356,869	-0.028	0.006	-4.38	95,638
MpriV	MpriQ	Lafr	Mame	-0.026	0.004	-7.07	257,676	0.029	0.006	4.59	52,894
MpriV	MpriQ	Lafr	Lcyc	0.038	0.004	8.61	218,551	0.042	0.007	6.49	58,776
MameI	MameX	Pant	Emax	-0.099	0.005	-19.99	51,704	-0.098	0.017	-5.74	4,903
MameI	MameX	Pant	Lcyc	-0.107	0.006	-19.34	41,999	-0.058	0.018	-3.24	3,392
MameI	MameX	Pant	Mcol	-0.079	0.006	-12.87	29,332	-0.087	0.023	-3.78	1,820
MameI	MameX	Pant	Mpri	-0.081	0.005	-17.05	61,968	-0.087	0.016	-5.41	4,847
MameI	MameX	Emax	Lafr	0.058	0.005	11.36	50,289	0.149	0.014	10.67	6,900
MameI	MameX	Emax	Lcyc	0.014	0.005	2.76	54,347	0.055	0.014	4.00	7,003
MameI	MameX	Lafr	Lcyc	-0.055	0.005	-9.98	39,367	-0.117	0.015	-7.93	4,827
MameI	MameX	Lafr	Mcol	-0.020	0.007	-3.07	26,515	-0.080	0.022	-3.58	2,485
MameI	MameX	Lafr	Mpri	-0.038	0.005	-7.57	61,960	-0.128	0.014	-9.43	6,864
MameI	MameX	Lcyc	Mpri	0.002	0.005	0.49	66,072	-0.040	0.013	-3.02	7,068

D-statistics for chromosome X

We computed *D*-statistics as described above for the X chromosome. For tests of the form *D (A, B; X, Y)* where *A, B, X, Y* indicate different taxa (including two or more individuals), we detect excess affinities with high *D*-statistic values and highly significant *Z*-scores between taxa that are most closely related, consistent with the topology of the pairwise-distance NJ tree (Table S11.6). However, we also observe significant signals of genetic affinities between taxa that are not expected:

i) There is excess genetic affinity between forest and savanna elephants (*D (P. antiquus, L. cyclotis; L. africana, X)* ranges between -0.15 and -0.26, $5 < |Z| < 10$, where *X* stands for all other proboscidean taxa; Table S11.6) compared to the expectation from the NJ tree, similar to the signal observed in the autosomes.

ii) There is excess genetic affinity between straight-tusked elephants and woolly mammoths, and between straight-tusked elephants and the Columbian mammoth (D = 0.09, $3 < Z < 4$; Table S11.6), but these signals are not consistent across tests. Moreover, compared to the signals observed in the autosomes, Asian elephants are not significantly more closely related to straight-tusked elephants than to forest or savanna elephants.

iii) There is excess genetic affinity between savanna and Asian elephants, and between savanna elephants and woolly/Columbian mammoths ($0.07 < |D| < 0.12$, $4 < |Z| < 5$; Table S11.6) but these signals could potentially be explained by alignment biases to the reference genome.

iv) There is excess genetic affinity between forest and Asian elephants ($0.14 < |D| < 0.15$, $4 < |Z| < 6$; Table S11.6) but this signal could potentially also be an artifact associated with alignment biases to the reference genome.

Table S11.6. *D*-statistics from chromosome X for tests of the form *D (A, B; X, Y)* where *A, B, X, Y* indicate different taxa (including two or more individuals). *D*-statistics discussed in the text above are indicated in bold font.

				All sites				Only transversions			
A	***B***	***X***	***Y***	***D***	**SE**	***Z***	**nSNPs**	***D***	**SE**	***Z***	**nSNPs**
Pant	Lcyc	Emax	Mame	-0.083	0.017	-4.92	16,909	-0.035	0.025	-1.41	4,374
Pant	**Lcyc**	**Lafr**	**Mame**	**-0.221**	**0.021**	**-10.68**	**25,085**	**-0.207**	**0.025**	**-8.17**	**6,476**
Pant	**Lcyc**	**Mcol**	**Mame**	-0.009	0.018	-0.49	6,843	**0.090**	**0.030**	**3.05**	**1,453**
Pant	**Lcyc**	**Mpri**	**Mame**	-0.025	0.014	-1.72	17,036	**0.090**	**0.021**	**4.20**	**3,738**
Pant	**Lafr**	**Emax**	**Mame**	**-0.093**	**0.014**	**-6.83**	**17,082**	**-0.072**	**0.017**	**-4.11**	**4,223**
Pant	Lafr	Lcyc	Mame	0.351	0.048	7.36	43,434	0.407	0.051	7.94	11,952
Pant	Lafr	Mcol	Mame	-0.083	0.014	-5.86	7,090	-0.031	0.023	-1.35	1,564
Pant	Lafr	Mpri	Mame	-0.071	0.014	-5.28	17,663	-0.018	0.021	-0.87	3,879
Pant	Emax	Lafr	Mame	0.620	0.039	15.86	44,630	0.679	0.040	17.18	12,249
Pant	Emax	Lcyc	Mame	0.773	0.028	28.10	63,834	0.822	0.026	31.98	18,138
Pant	Emax	Mcol	Mame	-0.739	0.026	-28.21	18,569	-0.791	0.029	-27.22	4,904
Pant	Emax	Mpri	Mame	-0.785	0.021	-37.42	49,696	-0.820	0.023	-35.58	13,654
Pant	Mpri	Emax	Mame	-0.771	0.023	-33.80	50,151	-0.818	0.024	-33.65	13,525
Pant	Mpri	Lafr	Mame	0.630	0.039	16.21	45,750	0.704	0.039	17.85	11,791
Pant	Mpri	Lcyc	Mame	0.786	0.026	29.67	64,429	0.851	0.024	34.91	17,351
Pant	Mpri	Mcol	Mame	-0.912	0.012	-75.60	33,812	-0.947	0.011	-89.63	9,511
Pant	Mcol	Emax	Mame	-0.731	0.027	-26.83	18,344	-0.800	0.028	-29.02	4,820
Pant	Mcol	Lafr	Mame	0.566	0.046	12.29	16,940	0.641	0.050	12.90	4,275
Pant	Mcol	Lcyc	Mame	0.755	0.031	24.56	24,436	0.828	0.031	27.01	6,498
Pant	Mcol	Mpri	Mame	-0.916	0.012	-75.63	33,313	-0.949	0.010	-97.67	9,427

Lafr	Lcyc	Pant	Mame	-0.531	0.037	-14.22	37,947	-0.566	0.039	-14.45	10,485
Lafr	Lcyc	Emax	Mame	0.018	0.011	1.62	21,192	0.016	0.014	1.10	6,507
Lafr	**Lcyc**	**Mcol**	**Mame**	**0.098**	**0.014**	**7.14**	**7,982**	**0.120**	**0.026**	**4.58**	**1,980**
Lafr	**Lcyc**	**Mpri**	**Mame**	**0.059**	**0.009**	**6.85**	**19,924**	**0.083**	**0.016**	**5.29**	**5,180**
Lcyc	Emax	Pant	Mame	0.805	0.029	28.18	62,079	0.833	0.029	28.44	17,444
Lcyc	Emax	Lafr	Mame	0.704	0.032	21.88	57,649	0.718	0.032	22.14	16,836
Lcyc	Emax	Mcol	Mame	-0.761	0.026	-29.05	21,658	-0.809	0.026	-30.86	5,983
Lcyc	Emax	Mpri	Mame	-0.795	0.021	-38.22	58,095	-0.824	0.021	-40.01	16,883
Lcyc	Mpri	Pant	Mame	0.795	0.029	27.71	64,498	0.824	0.030	27.60	17,578
Lcyc	Mpri	Emax	Mame	-0.749	0.024	-31.09	60,980	-0.767	0.024	-31.70	17,969
Lcyc	Mpri	Lafr	Mame	0.703	0.032	22.25	59,357	0.724	0.032	22.30	16,594
Lcyc	Mpri	Mcol	Mame	-0.924	0.011	-82.74	39,155	-0.951	0.009	-111.87	11,273
Lcyc	Mcol	Pant	Mame	0.758	0.034	22.26	24,532	0.797	0.037	21.77	6,633
Lcyc	Mcol	Emax	Mame	-0.703	0.031	-22.46	22,316	-0.752	0.030	-25.29	6,288
Lcyc	Mcol	Lafr	Mame	0.653	0.038	16.97	22,248	0.676	0.040	16.80	6,014
Lcyc	Mcol	Mpri	Mame	-0.915	0.013	-70.87	38,817	-0.945	0.011	-88.93	11,295
Lafr	Emax	Pant	Mame	0.675	0.038	17.61	43,009	0.716	0.039	18.19	11,766
Lafr	Emax	Lcyc	Mame	0.713	0.030	23.69	58,081	0.725	0.029	25.20	17,275
Lafr	Emax	Mcol	Mame	-0.738	0.030	-24.50	20,295	-0.782	0.031	-25.43	5,662
Lafr	Emax	Mpri	Mame	-0.783	0.023	-33.45	55,309	-0.812	0.023	-35.17	16,102
Lafr	Mpri	Pant	Mame	0.671	0.037	17.93	45,153	0.713	0.039	18.11	11,789
Lafr	Mpri	Emax	Mame	-0.753	0.024	-31.12	57,180	-0.774	0.025	-31.52	16,654
Lafr	Mpri	Lcyc	Mame	0.732	0.027	26.81	58,585	0.761	0.027	28.52	16,371
Lafr	Mpri	Mcol	Mame	-0.920	0.012	-74.60	37,597	-0.946	0.011	-87.43	10,882
Lafr	Mcol	Pant	Mame	0.620	0.043	14.53	16,372	0.659	0.048	13.67	4,245
Lafr	Mcol	Emax	Mame	-0.708	0.032	-21.80	20,293	-0.763	0.030	-25.42	5,708
Lafr	Mcol	Lcyc	Mame	0.706	0.031	23.11	21,396	0.736	0.031	23.48	5,782
Lafr	Mcol	Mpri	Mame	-0.915	0.013	-67.96	36,959	-0.945	0.011	-82.33	10,814
Mpri	Emax	Pant	Mame	-0.036	0.019	-1.90	16,177	-0.006	0.029	-0.22	3,413
Mpri	**Emax**	**Lafr**	**Mame**	**-0.074**	**0.023**	**-3.20**	**18,984**	**-0.100**	**0.027**	**-3.72**	**4,890**
Mpri	**Emax**	**Lcyc**	**Mame**	**-0.114**	**0.021**	**-5.38**	**20,957**	**-0.156**	**0.027**	**-5.81**	**5,720**
Mpri	Emax	Mcol	Mame	0.849	0.021	40.45	25,707	0.886	0.021	42.92	7,331
Mcol	Emax	Pant	Mame	-0.016	0.020	-0.82	5,848	0.025	0.028	0.87	1,193
Mcol	Emax	Lafr	Mame	-0.064	0.029	-2.20	6,904	-0.046	0.044	-1.06	1,648
Mcol	**Emax**	**Lcyc**	**Mame**	**-0.125**	**0.025**	**-4.96**	**7,645**	**-0.145**	**0.033**	**-4.33**	**1,885**
Mcol	Emax	Mpri	Mame	0.821	0.024	34.46	25,631	0.868	0.019	44.60	7,438
Mpri	Mcol	Pant	Mame	-0.022	0.012	-1.75	4,827	-0.027	0.039	-0.69	785
Mpri	Mcol	Emax	Mame	0.092	0.017	5.29	6,939	0.080	0.039	2.06	1,567
Mpri	Mcol	Lafr	Mame	0.035	0.018	1.95	5,184	0.009	0.035	0.26	970

For tests of the form *D* (A_1, A_2; *X, Y*), where A_1, A_2 indicate different individuals within taxon *A,* and *X, Y* indicate different taxa (including one or more individuals), we detect excess genetic

affinity only between *Mammuthus_V* and woolly mammoths. *D (Mammuthus_V, M. columbi_U; M. primigenius$_1$, X*), where *M. primigenius$_1$* stands for all woolly mammoths except for *Mammuthus_V*, and *X* stands for all other proboscidean taxa, ranges from 0.62 to 0.65 ($14 \leq Z \leq 16$), which again indicates that *Mammuthus_V* is genetically a woolly mammoth. However, there is no significant excess genetic affinity between *Mammuthus_V* and *M. columbi_U* nor between *M. primigenius_H* and *M. columbi_U*. Furthermore, there is no significant excess genetic affinity between *P. antiquus* and *L. cyclotis_F* in contrast to the observations from the autosomes.

Finally, there are a few more significant signals in chromosome X but these are not consistent across tests and/or they could be explained by reference bias.

f_4-ratio estimates of ancestry proportions

Given the signals of Columbian mammoth ancestry in *Mammuthus_V* and *M. primigenius_H* described above (Table S11.3), we can infer their proportions using an *f_4*-ratio (25). This is a ratio of two *f_4* statistics (67) *(alpha* [α] = *f_4 (A, O; X, C)/ f_4(A, O; B, C)*) where *X* represents the admixed population, *B* and *C* the source populations or two populations related to the sources, *A* a population related to source population *B* and *O* an outgroup. We computed these ratios in POPSTATS using random allele calls per site for each individual (as described in the *D*-statistics section above) and estimated *f_4*-ratios with *Mammuthus_V* and *M. primigenius_H* in turn as the admixed individual (*X*), *M. primigenius_P* as source *B*, *M. columbi_U* as source *C*, *M. primigenius_G* as the individual related to the woolly mammoth source (*A*), and each of the other proboscidean taxa in turn as the outgroup (*O*; Figure S11.1). Surrogates for source population *B* and population *A* were chosen based on the following statistics: *D* (*M. primigenius_H*/*Mammuthus_V, M. columbi_U; M. primigenius_G, M. primigenius_P*), which are significantly negative ($|Z| = 3.6$), suggesting that *M. primigenius_P* from Oimyakon in northeastern Siberia is genetically closer to the North American mammoths compared to *M. primigenius_G* from the Taimyr peninsula. Using *M. americanum* as the outgroup, the inferred proportion of Columbian mammoth ancestry (1- α) is 8.8 – 11.7% in *Mammuthus_V* and 4.4 – 8.7% in *M. primigenius_H* (mean ± 2 SE, which gives the 95.4% confidence interval; Table S11.7). These ranges become wider when other proboscidean taxa are used as the outgroup but remain lower for *M. primigenius_H* compared to *Mammuthus_V* (4.3 - 8.9 % and 8.7 - 11.9%, respectively).

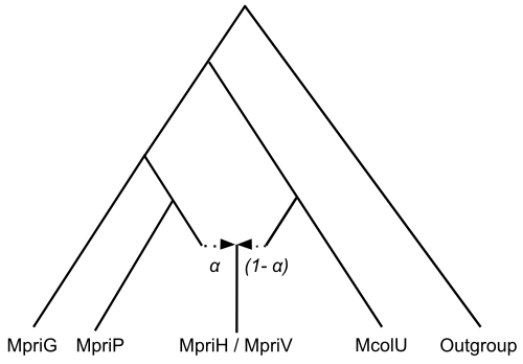

Figure S11.1. Model under which ancestry proportions were estimated in *M. primigenius_H* and *Mammuthus_V* using f_4 ratio tests.

Table S11.7. Inferred ancestry proportions in *M. primigenius_H* and *Mammuthus_V* estimated from the ratio f_4 *(M. primigenius_G, O; X, M. columbi_U) / f_4 (M. primigenius_G, O; M. primigenius_P, M. columbi_U)*, where *O* stands for either of *M. americanum, E. maximus, L. africana, L. cyclotis* or *P. antiquus,* and *X* for *M. primigenius_H* and *Mammuthus_V* in turn. Alpha (α) indicates the estimated woolly mammoth ancestry proportion and (1-α) the Columbian mammoth ancestry proportion in *M. primigenius_H* and *Mammuthus_V*. Min and max values give the 95.4% confidence interval (mean ± 2 SE).

	All sites						Only transversions					
pop*O*	***α***	***SE***	***Z***	**nSNPs**	**Min (1-a)**	**Max (1-a)**	***α***	***SE***	***Z***	**nSNPs**	**Min (1-a)**	**Max (1-a)**
X*: *Mammuthus_V												
Pant	0.867	0.006	143.98	12,681,069	0.121	0.145	0.896	0.007	119.67	4,459,703	0.090	0.119
Emax	0.892	0.006	146.14	13,676,472	0.096	0.120	0.898	0.007	123.69	4,839,966	0.087	0.116
Lafr	0.878	0.006	154.28	13,680,470	0.110	0.133	0.895	0.007	125.51	4,841,098	0.091	0.119
Lcyc	0.883	0.006	151.35	13,670,038	0.106	0.129	0.898	0.007	126.94	4,837,114	0.088	0.116
Mame	0.857	0.006	145.25	12,859,578	0.131	0.155	0.897	0.007	122.21	4,532,035	0.088	0.117
X*: *M. primigenius_H												
Pant	0.931	0.007	126.67	4,599,666	0.054	0.084	0.935	0.011	85.36	1,595,771	0.043	0.087
Emax	0.937	0.007	131.61	4,963,425	0.049	0.077	0.936	0.010	92.62	1,731,820	0.044	0.084
Lafr	0.929	0.007	130.97	4,964,870	0.057	0.085	0.931	0.010	91.63	1,732,203	0.049	0.089
Lcyc	0.929	0.007	131.07	4,960,622	0.057	0.085	0.933	0.010	91.58	1,730,626	0.046	0.087
Mame	0.915	0.007	125.27	4,676,698	0.070	0.099	0.935	0.011	86.46	1,626,373	0.044	0.087

We note that in theory, the *D*-statistics showing excess affinity between North American woolly mammoths (*Mammuthus_V* and *M. primigenius_H*) and Columbian mammoths could also be explained by gene flow in the other direction, i.e., from a North American woolly mammoth source into the ancestors of *M. columbi_U*. Distinguishing between the two possibilities requires two additional mammoth samples with differential relatedness to the potentially admixed individuals, which in this case are available in the form of *M. primigenius_G* and *M.*

primigenius_P (as detailed above). We built admixture graphs (as described in Supplementary Note 12) modeling *Mammuthus_V*, *M. primigenius_H*, *M. columbi_U*, *M. primigenius_G* and *M. primigenius_P* simultaneously, and with either of the possible directions of admixture, and found that indeed the scenario of gene flow from Columbian mammoths into the ancestors of *Mammuthus_V* and *M. primigenius_H* has a significantly better fit. Combined with the mtDNA patterns discussed above, we believe that the history shown in Figure S11.1 is the better justified model.

Based on the asymmetric genetic relatedness between the two forest elephants and straight-tusked elephants (Table S11.2), and assuming that gene flow occurred from a population related to *L. cyclotis_F* into the straight-tusked elephant lineage (see admixture graphs in Supplementary Note 12), we can infer the ancestry proportions in *P. antiquus_N* and *P. antiquus_O* using an f_4-ratio. *L. cyclotis_F* is used as one of the sources of admixture (*B*), *L. cyclotis_A* as the individual related to the West African elephant source (*A*), *M. americanum* as the second source of admixture (*C*), and *L. africana* as population *O* in an unrooted tree (Figure S11.2). Under this configuration, the West African forest elephant related ancestry is inferred to have been 35.1 - 37.3% (mean ± 2 SE) in *P. antiquus_N*, which is similar to the proportions inferred in Supplementary Note 12 from the admixture graphs, and 29.8 – 32.7% in *P. antiquus_O* (Table S11.8). The ancestry proportions appear to be stable so that when we replace *M. americanum* (population *C*) with either *E. maximus* or *M. primigenius* in the test described above, the obtained α ranges do not differ significantly (35.1 – 39.5% in *P. antiquus_N* and 29.8 - 34.1% in *P. antiquus_O*).

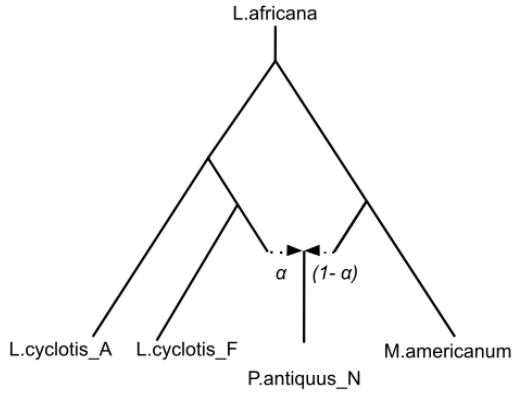

Figure S11.2. Model under which ancestry proportions were estimated in *P. antiquus_N* using the f_4 ratio test. Note that an unrooted tree was assumed in this model.

Table S11.8. Inferred ancestry proportions in *P. antiquus_N* and *P. antiquus_O* estimated from the ratio f_4 *(L. cyclotis_A, L. africana; X, C)* / f_4 *(L. cyclotis_A, L. africana; L. cyclotis_F, C)*, where population *X* stands for *P. antiquus_N* and *P. antiquus_O* in turn, and population *C* for either of *M. americanum, E. maximus* or *M. primigenius*. Alpha (α) indicates the estimated West

African forest elephant-related ancestry proportion in *P. antiquus_N* and *P. antiquus_O*. Min and max values give the 95.4% confidence interval (mean ± 2 SE).

	All sites						Only transversions					
pop *C*	**α**	**SE**	***Z***	**nSNPs**	**min α**	**max α**	**α**	**SE**	***Z***	**nSNPs**	**min α**	**max α**
X*: *P. antiquus_N												
Mame	0.365	0.005	69.80	51,855,611	0.355	0.376	0.362	0.005	66.05	18,282,969	0.351	0.373
Emax	0.380	0.005	73.57	56,091,347	0.369	0.390	0.374	0.005	69.14	19,982,166	0.363	0.385
Mpri	0.385	0.005	75.07	55,965,108	0.375	0.395	0.385	0.005	72.08	19,900,804	0.374	0.395
X*: *P. antiquus_O												
Mame	0.314	0.006	53.13	5,213,441	0.302	0.326	0.312	0.007	42.13	2,000,320	0.298	0.327
Emax	0.328	0.006	55.26	5,621,801	0.316	0.340	0.320	0.007	42.96	2,182,320	0.305	0.335
Mpri	0.330	0.006	56.52	5,610,150	0.319	0.342	0.326	0.007	44.45	2,174,650	0.311	0.341

f_4-ratio tests in chromosome X

Ancestry proportions are expected to be lower in chromosome X than in autosomes only in scenarios of male-biased admixture. Even though we cannot detect significant excess affinity between *M. columbi_U* and either *M. primigenius_H* or *Mammuthus_V* in chromosome X, we computed f_4-ratios as described above for chromosome X. The proportion of Columbian mammoth ancestry in chromosome X is inferred to have been 4.7 – 21.0% in *Mammuthus_V* and 0.0 – 18.3% in *M. primigenius_H* (Table S11.9). These ranges overlap with the ranges inferred from the autosomes but indicate higher uncertainty in the estimates from chromosome X.

Table S11.9. Inferred ancestry proportions of *Mammuthus_V* and *M. primigenius_H* in chromosome X estimated from f_4-ratios. Min and max values give the 95.4% confidence interval (mean ± 2 SE).

	All sites						Only transversions					
pop*O*	**α**	***SE***	***Z***	**nSNPs**	**Min (1-a)**	**Max (1-a)**	**α**	***SE***	***Z***	**nSNPs**	**Min (1-a)**	**Max (1-a)**
X*: *Mammuthus_V												
Pant	0.880	0.022	40.63	114,363	0.077	0.163	0.864	0.037	23.13	41,898	0.061	0.210
Emax	0.907	0.026	35.15	126,353	0.041	0.145	0.883	0.034	25.99	46,527	0.049	0.185
Lafr	0.921	0.026	36.03	126,444	0.028	0.130	0.876	0.036	24.47	46,554	0.053	0.196
Lcyc	0.907	0.026	34.30	126,322	0.040	0.146	0.871	0.038	22.65	46,508	0.052	0.206
Mame	0.878	0.025	35.54	112,077	0.072	0.171	0.875	0.039	22.39	40,859	0.047	0.204
X*: *M. primigenius_H												
Pant	0.972	0.043	22.64	47,274	-0.058	0.114	0.957	0.056	16.98	17,301	-0.069	0.156
Emax	0.935	0.040	23.55	52,250	-0.014	0.145	0.979	0.066	14.82	19,181	-0.111	0.153
Lafr	0.929	0.040	23.33	52,279	-0.009	0.151	0.948	0.066	14.44	19,193	-0.079	0.183
Lcyc	0.932	0.037	24.91	52,220	-0.006	0.143	0.971	0.062	15.77	19,168	-0.095	0.152
Mame	0.922	0.040	22.88	46,400	-0.002	0.159	0.959	0.062	15.45	16,897	-0.083	0.165

Similarly, we estimated the proportion of West African forest elephant related ancestry in *P. antiquus_N* and *P. antiquus_O* on chromosome X. Table S11.10 shows that this ancestry component is inferred to have been 38.2 – 45.8% in *P. antiquus_N* and 31.0 – 43.1% in *P. antiquus_O*. These ranges are only slightly different (higher) from those inferred from the autosomes. Hence, we do not find strong evidence of sex-biased gene flow from the West African forest elephant-related population into straight-tusked elephants nor from the Columbian mammoth into North American woolly mammoths.

Table S11.10. Inferred ancestry proportions of *P. antiquus_N* and *P. antiquus_O* in chromosome X, estimated from f_4-ratio tests. Min and max values give the 95.4% confidence interval (mean ± 2 SE).

	All sites						**Only transversions**					
pop *C*	***α***	**SE**	***Z***	**nSNPs**	**min *α***	**max *α***	***α***	**SE**	***Z***	**nSNPs**	**min *α***	**max *α***
X*: *P. antiquus_N												
M_ame	0.415	0.017	24.86	1,208,778	0.381	0.448	0.417	0.015	28.30	450,989	0.387	0.446
E_max	0.413	0.017	24.91	1,408,160	0.380	0.447	0.416	0.017	24.83	535,334	0.382	0.449
M_pri	0.420	0.016	25.67	1,401,678	0.387	0.453	0.426	0.016	26.29	531,235	0.394	0.458
X*: *P. antiquus_O												
M_ame	0.372	0.021	17.61	134,486	0.330	0.415	0.367	0.028	12.97	55,192	0.310	0.423
E_max	0.394	0.018	21.84	156,161	0.358	0.430	0.384	0.023	16.53	65,345	0.338	0.431
M_pri	0.398	0.017	23.87	155,427	0.365	0.431	0.383	0.022	17.43	64,885	0.339	0.427

Supplementary Note 12

Admixture graph models of elephantid relationships

We combined our observations about population relationships from *D*-statistics and other analyses into a unified framework by constructing admixture graphs, that is, phylogenetic trees augmented with admixture events. We built the models using *qpGraph* (25), which solves for all parameters in an admixture graph (branch lengths and mixture proportions) given a user-defined topology. Model fit can be assessed by comparing the implied values of *f*-statistics (67) among populations in the graph to the corresponding observed values from the data. Large residuals between the fitted and observed statistics indicate subsets of populations (pairs, triples, or quartets) whose relationships are not accurately modeled. All admixture graph results (and all *D*-statistics cited in this note) are based on transversion SNPs (called by sampling a random allele as described in Supplementary Note 8) in order to avoid ancient DNA artifacts and reduce possible instances of recurrent mutation.

Initial model

We began by considering a restricted set of populations consisting of the African forest and savanna elephants (*L. cyclotis* and *L. africana*, each represented by two individuals), straight-tusked elephants (*P. antiquus*, represented by the higher-coverage individual *P. antiquus_N*), and mastodon (*M. americanum*, the outgroup, represented by two individuals). As observed in Supplementary Note 11, these groups do not fit a tree-like topology, as *D (P. antiquus, L. cyclotis; L. africana, M. americanum)* = -0.23 ($|Z|$ = 50) and *D (L. africana, L. cyclotis; P. antiquus, M. americanum)* = -0.33 ($|Z|$ = 58). Moreover, straight-tusked elephants show an excess affinity to the forest elephant individual *L. cyclotis_F* as reflected in the statistic *D (L. cyclotis_A, L. cyclotis_F; P. antiquus, M. americanum)* = -0.04 ($|Z|$ = 9). This signal seems unlikely to be caused by a data-processing artifact given the symmetric comparison to the two forest elephant individuals. Instead, we interpret it as evidence of gene flow from ancestors of *L. cyclotis_F* into the straight-tusked lineage or vice versa. We attempted to build admixture graphs with gene flow in either direction and found that while we obtained a good fit with admixture into the straight-tusked lineage (all *f*-statistics in the model within 2.5 standard errors of the observed values; Figure S12.1a), a graph with admixture from straight-tusked elephants into the *L. cyclotis_F* lineage produced residuals up to $|Z| > 61$ (Figure S12.1b). Thus, the first scenario is the most parsimonious model for this set of populations, although it is still possible that gene flow occurred in both directions but to a higher degree in the direction depicted in the preferred model. This qualification applies to all the admixture events described in what follows; the models we report are the simplest scenarios consistent with the data.

Straight-tusked elephants are inferred to have received 36% of their ancestry from a lineage related to the *L. cyclotis_F* (similar to our f_4-ratio estimate; Table S11.8 that split off only slightly after the divergence of the two forest elephant individuals. Given that this is the deepest

within-species divergence (609,000 - 463,000 years ago based on the assumed mutation rate; see Table S15.2), the implied age of the admixture event (older than 120,000 years ago) appears plausible. The ancestry proportion from *L. cyclotis_F* is inferred to be lower (31%; again similar to our f_4-ratio estimate; Table S11.8) when we use *P. antiquus_O* for the straight-tusked elephant lineage, with the discrepancy possibly due the low coverage of *P. antiquus_O*.

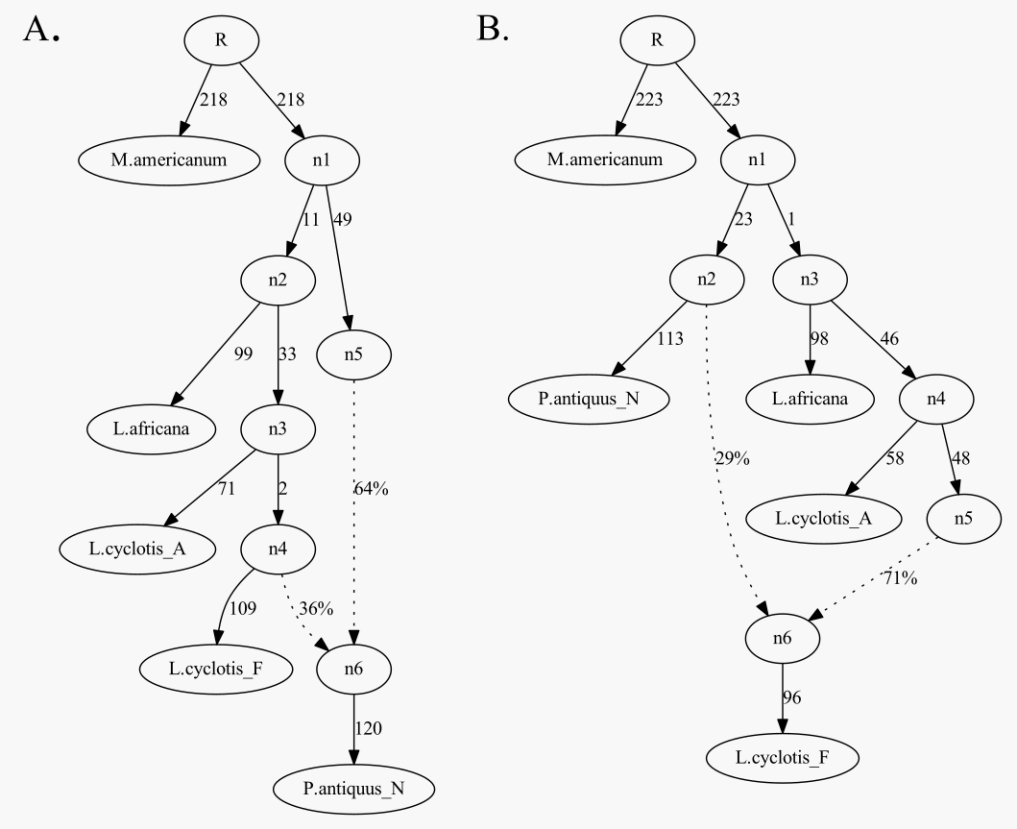

Figure S12.1. Admixture graph models for African forest and savanna elephants, straight-tusked elephants, and mastodon. Dotted lines denote admixture events, with proportions as indicated; branch lengths are shown in units of genetic drift. Terminal branch lengths leading to sampled populations may be inflated. Model (A) provides a good fit to the data (residuals up to $|Z| = 2.5$) whereas model (B) contains residuals up to $|Z| > 61$.

Extended model with Asian elephants and woolly mammoths

Next, we proceeded to extend the model by adding Asian elephants (*E. maximus*, represented by six individuals) and woolly mammoths (*M. primigenius*, represented by six individuals). To a first approximation, these two species form a clade separate from that of African elephants[4] and straight-tusked elephants (Supplementary Note 8), but there are also signals of possible admixture among the different lineages. In particular, as noted in Supplementary Note 11:

a) Asian elephants and woolly mammoths are more closely related to straight-tusked elephants than they are to African elephants: *D (P. antiquus, L. cyclotis/L. africana; E. maximus/M. primigenius, M. americanum)* > 0.02 ($Z > 5$).
b) Straight-tusked elephants are also more closely related to woolly mammoths than they are to Asian elephants: *D (M. primigenius, E. maximus; P. antiquus, M. americanum)* = 0.04 ($Z = 9$).
c) Asian elephants and woolly mammoths are both more closely related to savanna elephants than they are to forest elephants: *D (L. africana, L. cyclotis; E. maximus/M. primigenius, M. americanum)* > 0.04 ($Z > 11$).

For signal (a), the magnitude of the *D*-statistic is approximately twice as large for woolly mammoths compared to Asian elephants, which is consistent with signal (b). These observations could be most parsimoniously explained by gene flow from the woolly mammoth lineage into the straight-tusked elephant lineage but not the reverse. For signal (c), the magnitude of the *D*-statistic is larger for woolly mammoths compared to Asian elephants, but we believe that the apparent relatedness of these taxa to savanna elephants may be due to reference bias, as the reference genome to which all individuals are mapped is one of the two savanna individuals we sequenced (see below).

Guided by the first two signals, we added Asian elephants and woolly mammoths to our initial admixture graph, with admixture from the *M. primigenius* lineage into the straight-tusked lineage (Figure S12.2a). The resulting model has a number of significant residuals, but almost all are potentially related to signal (c), except for 4 statistics that do not involve savanna elephants and indicate an even greater affinity between straight-tusked elephants and *E. maximus/M. primigenius* (residuals up to $Z = 5$). As expected based on the *D*-statistics, if we reverse the direction of the admixture explaining signals (a) and (b) to be from straight-tusked elephants into woolly mammoths instead, the fit is significantly worse, with 36 residuals not involving savanna elephants up to $|Z| = 22$. Similarly, models with admixture from the straight-tusked elephant lineage into the common ancestor of Asian elephants and woolly mammoths, or vice versa, which could explain signal (a) but not signal (b), fit significantly worse than the first model with at least 6 residuals that are not related to reference bias up to $|Z| = 13$. Hence, the first model appears to fit better for this set of populations.

The order in which the *M. primigenius*-related ancestry and *L. cyclotis_F*-related ancestry entered the straight-tusked elephant lineage cannot be determined through our analysis since the two models in Figure S12.2 fit equally well. However, our population split time analyses suggest that gene flow from the woolly mammoth-related lineage into the straight-tusked elephant lineage occurred earlier than the gene flow from the *L. cyclotis_F*-related lineage into the straight-tusked elephant lineage, since the woolly mammoth-related source of admixture splits off deep in the history of the *M. primigenius* lineage (> 80% of the way back to its split from the common ancestor of *E. maximus* and *M. primigenius*, which is inferred to have occurred more than 2 million years ago based on the assumed mutation rate; see Supplementary Notes 16, 17,

18). On the other hand, the *L. cyclotis_F*-related admixture has an upper time limit of 609,000 - 463,000 years ago (the inferred split time of the two forest elephants based on the assumed mutation rate; see Table S15.2). The latter admixture (from the *L. cyclotis_F*-related lineage into the straight-tusked elephant lineage; 36%, or 38% if we reverse the order of the two admixture events; Figure S12.2) has very similar parameters to the initial model, indicating a robust fit. The mixture proportion from the *M. primigenius*-related lineage into straight-tusked elephants is inferred to have been 8% (or 5% if we reverse the order of the two admixture events; in both cases, the final ancestry from each source is the same after the two admixture events).

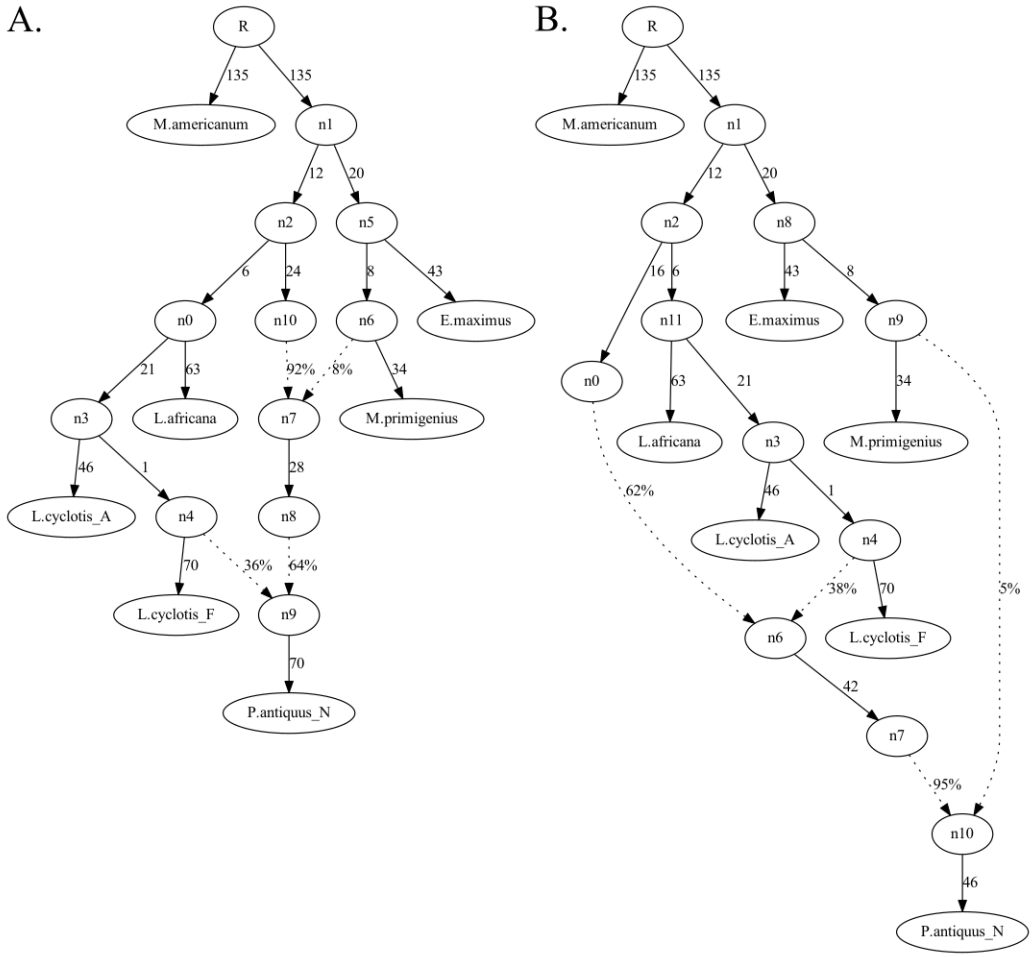

Figure S12.2. Admixture graph model for African forest and savanna elephants, straight-tusked elephants, Asian elephants, woolly mammoths, and mastodon. In graph (A), the straight-tusked elephant lineage receives ancestry first from a lineage related to *M. primigenius* and then from a lineage related to *L. cyclotis_F*, while in graph (B) the reverse temporal order of admixture events is modeled. Both models (A) and (B) fit equally well to the data.

Possible reference bias

We observe a pattern in the data of apparent excess relatedness between African savanna elephants and other taxa (see also Supplementary Note 11). In addition to Asian elephants and woolly mammoths, the Columbian mammoth also exhibits this signal, with a larger magnitude than that observed for woolly mammoths: *D (L. africana, L. cyclotis; M. columbi, M. americanum)* = 0.110 ($Z > 29$). We also find that individuals within taxa show different levels of relatedness to savanna elephants: for example, *D (P. antiquus_N, P. antiquus_O; L. africana, X)* < -0.044 ($|Z| > 3.1$), where *X* stands for all other proboscidean taxa except for *M. columbi*, and *D (M. americanum_I, M. americanum_X; L. africana, Y)* < -0.080 ($|Z| > 3.5$), where *Y* stands for all other proboscidean taxa except for *P. antiquus* (see also statistics in Table S11.5). While the statistics cited as signal (c) could conceivably be due to admixture, it is unlikely that Columbian mammoths would be more closely related to savanna elephants than are woolly mammoths, or that one mastodon or straight-tusked elephant individual would be more closely related to savanna elephants than another. Most of these statistics share a common orientation in which the taxon or individual with lower sequencing coverage or otherwise lower-quality data shows the excess affinity to *L. africana*. From these observations, we conclude that the primary driver of this signal is a reference bias in the mapping/alignment of sequencing reads (*L. africana_C* being the source of the elephant reference genome).

For our *D*-statistic signal (c), we cannot rule out the possibility that a portion of the effect is due to true admixture, but given the evidence of reference bias in our data set, we choose not to make any claims about admixture events based on these statistics. While the Asian elephant and two of the woolly mammoth individuals in our admixture graphs have fairly high coverage, these taxa are affected to some degree by reference bias, and indeed *D (L. africana, L. cyclotis; M. primigenius_P, M. primigenius_Q)* is positive as well (with *M. primigenius_P* having lower coverage), although it does not reach statistical significance. We also note that signals (a) and (b) above are unlikely to be reference-related artifacts: (a) involves an affinity to African elephants in the opposite direction from (c), while (b) does not involve African savanna elephants.

Having chosen to disregard the apparent excess relatedness to savanna elephants in Asian elephants and woolly mammoths, we still wished to ensure that the presence of this bias did not compromise our admixture graph construction (Figure S12.2). While removing *L. africana* from the graph eliminates residuals with $|Z| > 2.3$, doing so leaves us with too few constraints to solve for the remaining parameters in the model. Instead, to control for possible bias, we introduced "dummy" admixture events directly from savanna elephants into the relevant populations (Figure S12.3). The inferred proportions were similar for Asian elephants and woolly mammoths (1.35% and 1.41%, respectively), as expected. For straight-tusked elephants, any signal of reference bias would be confounded with their admixture from forest elephants, so we do not add any additional admixture. With the presence of "dummy" admixture events, the model fit is very good, with only two residuals (up to $|Z| = 3.6$) indicating higher affinity between savanna elephants and woolly mammoths. The resulting graphs (Figure S12.3) are very similar to the

main graphs (Figure S12.2) in all other respects, showing that our results are robust to the possible presence of reference bias.

There is also an alternative model to the ones depicted in Figure S12.3, which can explain signal (c) and which eliminates all remaining significant residuals by adding one additional migration edge from the *M. primigenius* lineage into *L. africana* instead of the two "dummy" migration edges (Figure S12.4). Although this admixture event is in the opposite direction of what would be expected from alignment bias to the savanna elephant reference genome, the presence of reference bias at different levels in each taxon could conceivably create such an effect. From this model, the woolly mammoth-related ancestry in the savanna elephant lineage is inferred to have been 4%. These models have a better fit (residuals up to $|Z| = 2.5$) than those in Figure S12.3 but are similar in all other respects.

Admixture proportions

We estimated standard errors for the mixture proportions inferred by the models depicted in Figure S12.4 by splitting our dataset across the 27 autosomes and re-estimating the graph by dropping one chromosome at a time, computing block jackknife standard errors similar to those in the *D*-statistics. For the graph depicted in Figure S12.4a, the mixture proportion from the *M. primigenius*-related lineage into the straight-tusked elephant lineage is inferred to have been 9.56 ± 0.5% and from the *L. cyclotis_F*-related lineage to 35.29 ± 0.68%. When we reverse the order of the two admixture events (Figure S12.4b), the mixture proportion from the *L. cyclotis_F*-related lineage into the straight-tusked elephant lineage is inferred to have been 37.61 ± 0.72% and from the *M. primigenius*-related lineage 6.19 ± 0.33%. The mixture proportion from the *M. primigenius* lineage into savanna elephants is inferred to have been 4 ± 0.28% in both graphs.

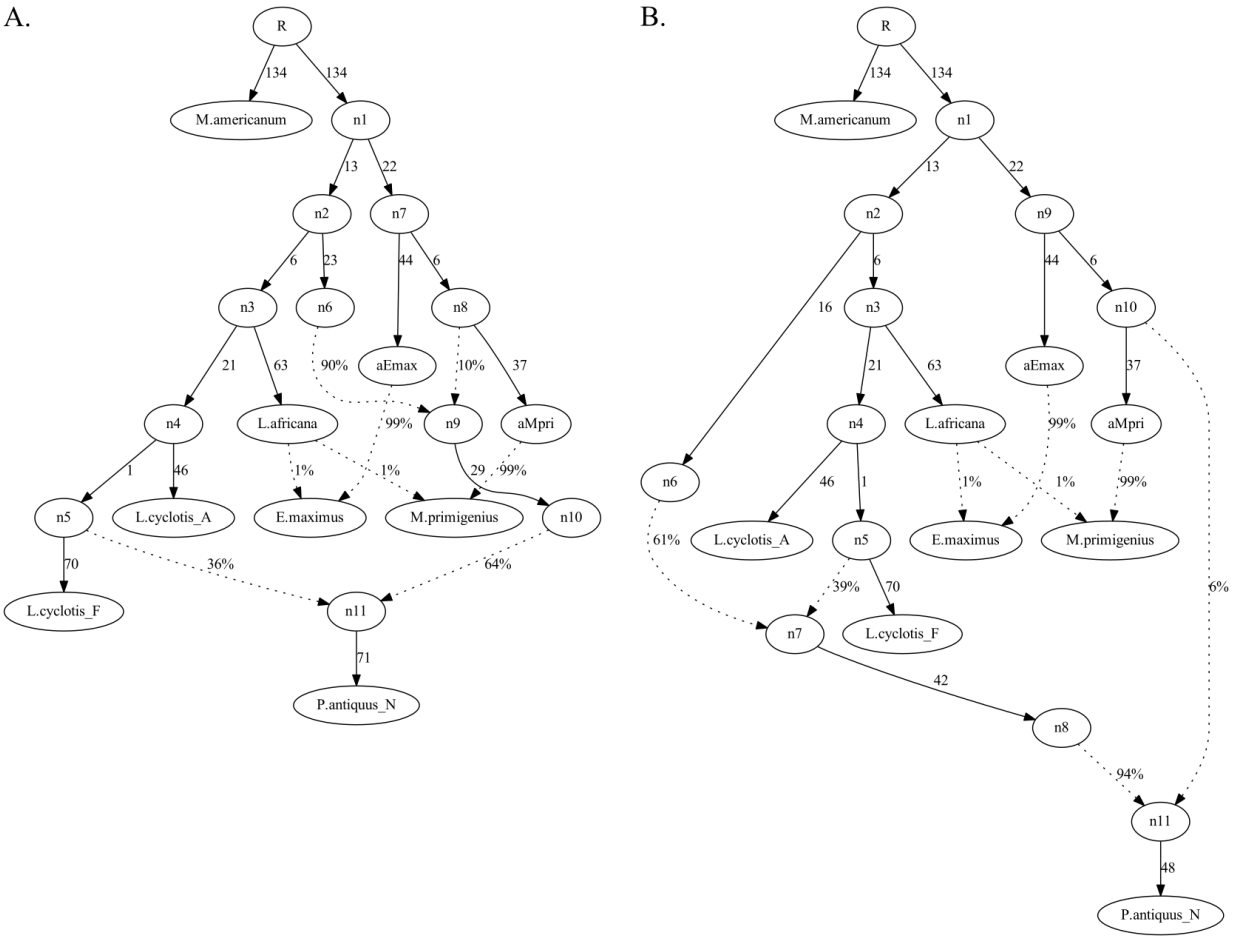

Figure S12.3. Six-taxon admixture graphs as in Figure S12.2 with additional "dummy" admixture from savanna elephants into Asian elephants and woolly mammoths to account for what is likely to be reference bias due to the fact that the *Loxodonta africana* genome is used for mapping.

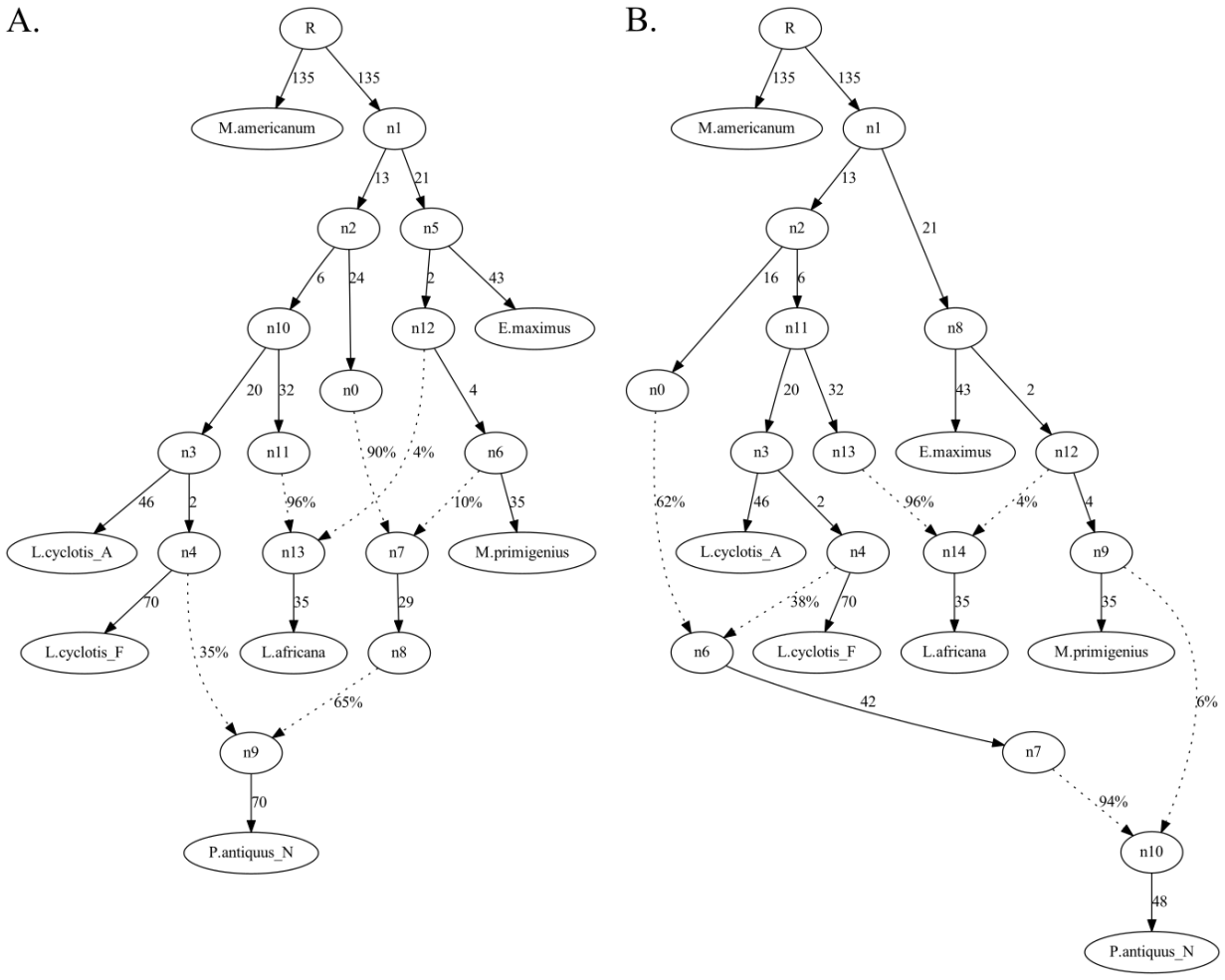

Figure S12.4. Alternative six-taxon admixture graphs with one additional admixture from woolly mammoths into savanna elephants to explain potential reference bias. These models are similar in all other aspects to those in Figure S12.3 but have a moderately better fit to the data.

Supplementary Note 13

Heterozygosity

We estimated heterozygosity across individual genomes with relatively high average coverage (≥ 10x) for which reliable diploid calls could be made. We implemented mlRho (68) v.2.7, which uses a maximum likelihood approach to compute theta ($\theta = 4N_e\mu$), an approximate estimate of expected heterozygosity under the infinite sites model, and epsilon (ε), the associated sequencing error rate. We applied the standard filters described in Supplementary Note 6, including the mappability filter (both 50% and 90% stringency), and excluded sites with minimum read depth below 3. The less stringent mappability filter (50%) results in slightly higher but overall similar heterozygosity estimates (Table S13.1, Figure S13.1).

African forest elephants harbor the highest levels of heterozygosity among living and extinct elephantids. This is in accordance with previous studies that have shown higher genetic diversity in forest elephants compared to African savanna elephants (4, 33, 34, 36). Woolly mammoths, the straight-tusked elephant and Asian elephants have intermediate levels of heterozygosity, approximately half of that in forest elephants, except for *E. maximus_E*, which displays extremely low heterozygosity, consistent with the small size, potential founder effect and insular nature of the Bornean population (61). With the exclusion of *E. maximus_E*, the lowest levels of heterozygosity among all elephantids are found in African savanna elephants, supporting earlier hypotheses about recent founder effects in the history of this taxon, and the established role of male-male competition in lowering effective population size by limiting the proportion of males contributing to the gene pool of each subsequent generation (33, 34).

Sequencing error rates as estimated by mlRho are at least four times lower than heterozygosity estimates for the modern genomes, except for the low-heterozygosity genomes (*L. africana_B, L. africana_C* and *E. maximus_E*), for which the error rates are similar or slightly lower than the respective estimated heterozygosity (Table S13.1). For ancient genomes, the associated sequencing error rates are approximately ½ the estimated heterozygosities, except for the straight-tusked elephant genome (*P. antiquus_N*), for which the error rate is estimated to be ~1.2-fold higher than the heterozygosity. The error estimates from mlRho are generally quite similar and well correlated to those from our simple heuristic method in Supplementary Note 6. The largest differences are the relatively lower estimates for ancient samples in Supplementary Note 6, which we had speculated could be downward-biased as a result of post-mortem DNA damage patterns.

The observed variation in individual heterozygosity within elephantid taxa and in particular within forest elephants is noteworthy. It could either be attributed to individuals from populations with different evolutionary trajectories, or could be owing to differences in depth of coverage and sequencing error. To examine the potential effects of coverage, we subsampled each genome to sequentially lower coverage and estimated autosomal heterozygosity in each

subsample with mlRho. We used the SAMtools v.0.1.19 'view -s' command (19), restricting to reads with mapping quality ≥ 30 for modern DNA data and ≥ 37 for ancient DNA data and excluding sites with read depth below 3, and applied the 90% stringent mappability filter.

For a given individual, estimated heterozygosity is positively correlated with coverage, but the dependence is relatively weak (Figure S13.2), with most of the observed variation among individuals not appearing to be explained by average sequencing depth. Instead, population differences likely explain the within-species variation in heterozygosity; individuals within taxa were sampled from distant geographic locations and potentially represent isolated populations. For instance, as mentioned in Supplementary Note 11, *L. cyclotis_A* originates from the Congolian forest block in Central Africa and *L. cyclotis_F* from the Guinean forest block in western Africa. The population split time between the two forest elephants is the highest among elephantid taxa (609,000 - 463,000 years ago; Table S15.2), suggesting long-term barriers to gene flow between the two populations. Western Africa is currently considered to harbor small isolated populations of forest elephants, which could have been affected by genetic drift and inbreeding induced by recent anthropogenic effects in the absence of gene flow (61). Consistent with this hypothesis, *L. cyclotis_F* displays ~21% lower heterozygosity than *L. cyclotis_A* (Figure S13.1, Table S13.1). Among Asian elephants, *E. maximus_D* from Myanmar displays the highest heterozygosity, followed closely by *E. maximus_Y* from Assam in northeastern India and *E. maximus_L*, which is assumed to originate from India but whose exact geographic origin is unknown. *E. maximus_M* (again of unknown exact origin) and *E. maximus_Z* from the Bandipur National Park in the southern Indian state of Karnataka display lower heterozygosity (~13% - 32% lower) while *E. maximus_E* from Malaysian Borneo exhibits the lowest heterozygosity (~66% - 77% lower), which suggests that this elephant is inbred. The difference in heterozygosity in the woolly mammoths (~20% lower in *M. primigenius_Q* compared to *M. primigenius_P*) has been attributed to the isolation of the ancecstors of *M. primigenius_Q* on Wrangel Island and the associated bottleneck at the Pleistocene/Holocene transition (11) (~11,000 years ago). The two savanna elephants, despite their distant geographic origins in eastern and southern Africa, show similarly low levels of heterozygosity, in agreement with scenarios of a relatively recent founder event, male-biased dispersal, and with population isolation and constrained gene flow occurring only very recently (34).

Table S13.1. Autosomal heterozygosity per 1,000bp (theta; θ) and sequencing error rate per 1,000bp (epsilon; ε) estimated by mlRho with 50% and 90% mappability filters.

Sample	mean theta	CI theta	CI epsilon	mean theta	CI theta	CI epsilon
		Mask 0.5			Mask 0.9	
L. cyclotis_A	3.75	3.74 - 3.75	0.19 - 0.19	3.63	3.63 - 3.64	0.16 - 0.16
L. africana_B	0.91	0.91 - 0.91	0.86 - 0.86	0.88	0.88 - 0.88	0.86 - 0.86

L. africana_C	0.88	0.86 - 0.88	0.71 - 0.71	0.85	0.85 - 0.86	0.71 - 0.71
E. maximus_D	1.46	1.46 - 1.47	0.21 - 0.21	1.36	1.36 - 1.37	0.20 - 0.20
E. maximus_E	0.37	0.37 - 0.38	0.22 - 0.22	0.32	0.32 - 0.32	0.22 - 0.22
L. cyclotis_F	2.93	2.93 - 2.94	0.75 - 0.75	2.85	2.85 - 2.86	0.75 - 0.75
E. maximus_L	1.30	1.30 - 1.30	0.21 - 0.21	1.21	1.21 - 1.21	0.20 - 0.20
E. maximus_M	1.17	1.17 - 1.17	0.21 - 0.21	1.08	1.08 - 1.08	0.21 - 0.21
P. antiquus_N	1.57	1.57 - 1.57	1.83 - 1.83	1.54	1.54 - 1.54	1.83 - 1.83
M. primigenius_P	1.76	1.75 - 1.76	0.76 - 0.76	1.67	1.66 - 1.67	0.73 - 0.73
M. primigenius_Q	1.42	1.42 - 1.42	0.72 - 0.73	1.32	1.32 - 1.32	0.71 - 0.71
E. maximus_Y	1.34	1.34 - 1.34	0.19 - 0.19	1.24	1.24 - 1.25	0.18 - 0.18
E. maximus_Z	0.98	0.98 - 0.98	0.22 - 0.22	0.93	0.93 - 0.93	0.21 - 0.21

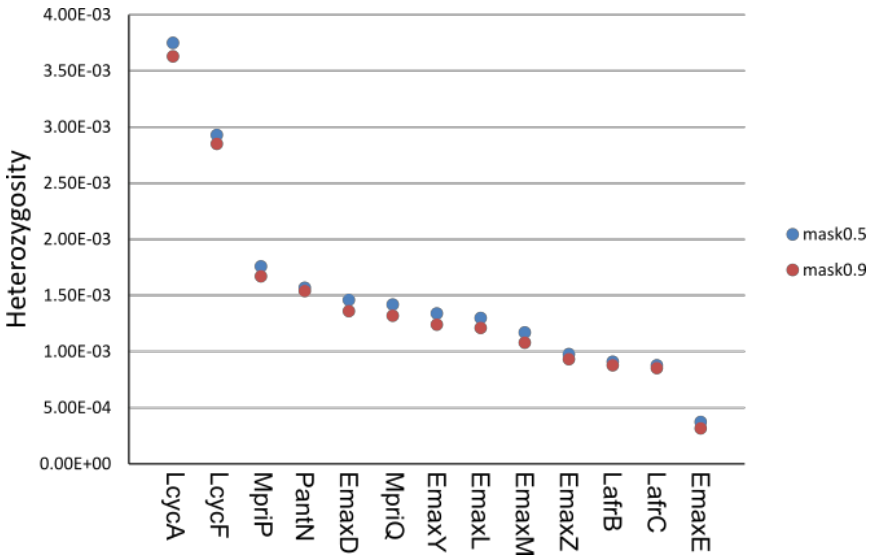

Figure S13.1. Autosomal heterozygosity estimated by mlRho with 50% and 90% mappability filters.

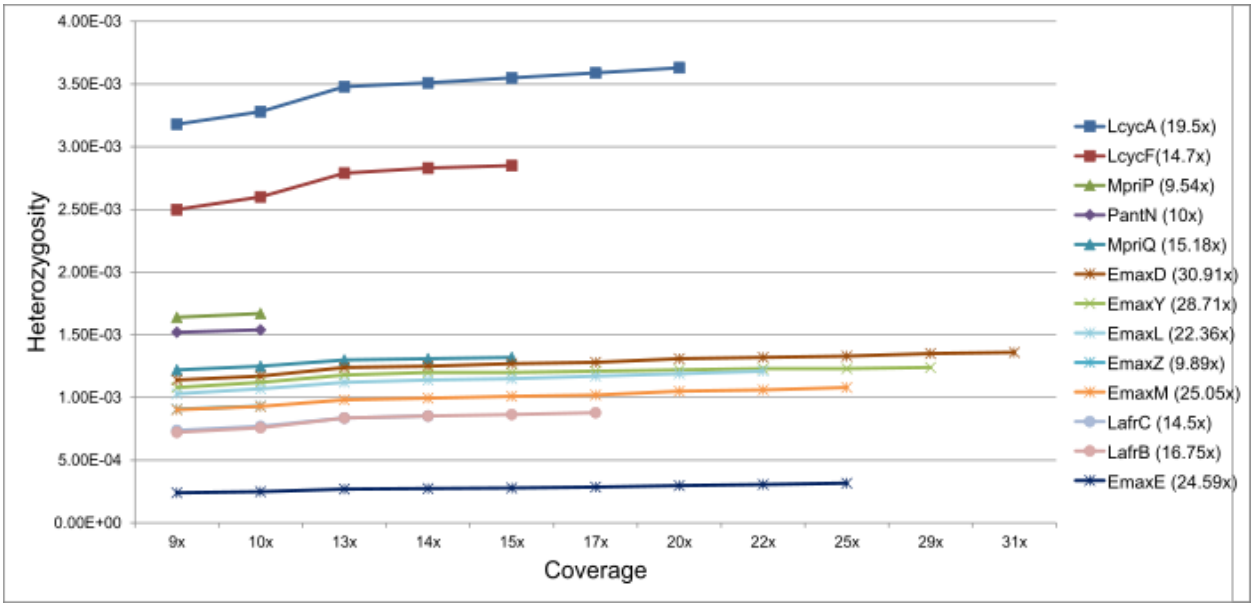

Figure S13.2. Heterozygosity estimated by mlRho from subsampled individual genomes. Full filtered coverage is given in parentheses next to the individual genome abbreviated names and is estimated after restricting to reads with mapping quality ≥ 30 for modern DNA data and mapping quality ≥ 37 for ancient DNA data.

Supplementary Note 14

Population size changes

The Pairwise Sequential Markovian Coalescent method (69) (PSMC) was used to reconstruct the population size history of each elephantid lineage. This method examines heterozygosity across the diploid genome of a single individual to infer the coalescent rate, which is informative about effective population size changes through time. We generated diploid consensus sequences for the autosomes of each genome with relatively high average coverage (≥ 10x) using the SAMtools (19) v.0.1.19 'mpileup' command, bcftools and the 'vcf2fq' command from vcfutils.pl. We applied the standard filtering criteria described in Supplementary Note 6 and excluded sites with root-mean-square mapping quality below 30 and sites within a 5bp window from indels. We further excluded sites with read-depth below 10 (following recommendations by Nadachowska-Brzyska *et al.* (70)) and more than 2-fold the average genome-wide coverage to avoid alignment errors due to segmental duplications and/or copy number variation. We estimated the proportion of sites with missing data under these criteria for each genome and in cases where it exceeded 25%, we reduced the minimum depth of coverage to 1/3 of the average genome-wide coverage. The 90% mappability filter was applied to avoid false heterozygous calls that could be produced by reads (mistakenly) aligned to regions of the genome that show similarity to other regions, even though stringent mappability filters have also been shown to create a bias in PSMC estimates that leads to undererstimates of effective population size at older times due to fragmentation of the data (Pruefer K. personal communication). We ran PSMC with default parameters and performed 100 bootstrap replicates by splitting chromosomes into 50Mbp segments and randomly sampling with replacement from these segments. The PSMC and bootstrap curves for each high-coverage elephantid genome are shown in Figure S14.1.

Effect of average coverage

The population history trajectories of conspecific elephantids appear to be qualitatively similar. However, when plotted together, the PSMC curves of conspecific elephantids do not always line up. This behavior is expected for genomes from temporally different specimens (e.g. the 4,300 year-old and ~45,000 year-old woolly mammoths whose PSMC curves are offset by a fixed amount) but is also observed in the contemporary elephantids. Overall, genomes with higher average coverage or higher individual heterozygosity estimates appear to produce curves with higher effective population sizes (N_e) and that are shifted towards more ancient times (i.e., towards the right of the x-axis; Figure S14.2, left-hand side plots). To evaluate the effect of coverage and associated estimated heterozygosity on the PSMC curves, we subsampled the genomes of elephantids with higher average genome-wide coverage to the lowest coverage of their conspecifics (estimated by restricting to reads with mapping quality ≥ 30 for modern genomes and ≥ 37 for ancient genomes; Table S14.1). We then estimated the PSMC and bootstrap N_e curves of each subsampled genome as described above.

Subsampling higher-coverage genomes to the lowest coverage of their conspecifics resulted in a better fit of the PSMC curves in forest elephants (from the time point when the two curves converge and going further back in time; *L. cyclotis_A* [19.5x] and *L. cyclotis_F* [14.7x]), as well as in woolly mammoths (although the curves are still offset by a fixed amount due to their difference in geological age; *M. primigenius_Q* [15.18x] and *M. primigenius_P* [9.54x]), which exhibit ~21% and ~20% difference in their estimates of individual heterozygosity, respectively (Figure S14.2B, H). In savanna elephants, subsampling of the higher coverage *L. africana_B* genome [16.75x] to the average coverage of *L. africana_C* [14.5x] slightly improves the fit of the curves, although they still do not perfectly align (Figure S14.2D). In Asian elephants, a better fit is observed between the PSMC curve of *E. maximus_Z* [9.89x] and the PSMC curves of the higher coverage genomes (excluding *E. maximus_E* [24.59x]), when the latter are subsampled to the average coverage of the former, which displays ~14-32% lower heterozygosity (Figure S14.2F). However, subsampling to ~10x does not markedly improve the fit of the PSMC curves of *E. maximus_D* [30.91x], *E. maximus_Y* [28.71x], *E. maximus_L* [22.36x], and *E. maximus_M* [25.05x]), which differ ~8-21% in their estimates of individual heterozygosity. Despite the high average coverage of *E. maximus_E* [25x], its PSMC curve does not line up with the curves of the remaining Asian elephants due to its high levels of homozygosity (~66-77% lower heterozygosity). This analysis shows that coverage does have a quantitative effect on the shape of the PSMC curves but that this effect disappears in genomes with average coverage ≥ 17x, most likely because beyond this threshold the number of missing heterozygotes becomes negligible. A similar minimum mean coverage of 18x was recommended by Nadachowska-Brzyska *et al.* (70). Accordingly, we make quantitative interpretations of the PSMC curves obtained from the full data of genomes with average coverage ≥ 17x while only making qualitative interpretations for genomes with lower coverage.

Inference of the population history of elephantid species

Moving forward in time (right-to-left in the plots of Figure S14.1), the N_e plots of forest, savanna and straight-tusked elephants follow a qualitatively similar trajectory up until ~7×10^{-4} divergence units in the past, or ~862,000 years ago assuming a mutation rate of 0.406×10^{-9} per year per site. This mutation rate was estimated in Supplementary Note 16 based on the fossil-calibrated genetic divergence time between *Loxodonta* and *Elephas*, and their estimated divergence per base pair, and is assumed from here on for calibrating time and N_e in the PSMC plots. However, we caution that this estimate is highly uncertain and when better estimates become available, all inferred parameters should be rescaled. Faster or slower mutation rates would shift the time axis to younger and older time estimates, and to lower and higher effective population sizes, respectively. After an initial phase of population growth, during which the forest elephant populations reached their maximum size at ~2×10^{-3} divergence units or ~2.5 million years ago and the savanna elephant populations at ~1.5×10^{-3} divergence units or ~1.8 million years ago, all three elephantid species experienced a severe decline in N_e, which ended at ~7×10^{-4} divergence units or ~862,000 years ago. The amplitude of this evident boom-and-bust cycle seems to have

been larger in savanna elephants, with maximum N_e ~2-fold higher than that inferred in forest elephants and minimum N_e ~3-fold lower that that inferred in Central African forest elephants (assuming no interspecies differences in mutation rate and generation time). An alternative to actual reduction in population size (or increase moving back in time) could be a time period of population separation and admixture (69) within the ancestors of savanna elephants and among the ancestors of forest and straight-tusked elephants. While N_e subsequently remained low in savanna elephants until recently, in forest elephants we observe population recovery at ~4×10^{-4} divergence units or ~493,000 years ago, which is far more pronounced in *L. cyclotis_A* compared to *L. cyclotis_F* (Figure 14.2A). In fact, N_e increased up to its previous peak in *L. cyclotis_A* (67,500 – 105,000) and only 2-fold (31,800 – 41,700) in *L. cyclotis_F*. The PSMC curves of the two forest elephants diverge shortly after their populations began to recover, which likely reflects the time interval during which their ancestral populations split (between 3 – 4×10^{-4} divergence units or ~369,000 – 493,000 years ago, which is younger but overlapping with the population split time inferred by the $F(A|B)$ method; 609,000 - 463,000 years ago; see Table S15.2). A second, more recent and sharp population decline occurred in both forest elephants at ~10^{-4} divergence units or ~123,000 years ago, from which neither of the two bounced back (down to 23,800 – 29,800in *L. cyclotis_A* and ~6,950 in *L. cyclotis_F*). Although population size inference by the PSMC method is less reliable in the recent past (69), the lower N_e in *L. cyclotis_F* compared to *L. cyclotis_A* provides support for the presumed small isolated forest elephant populations in West Africa (61).

In savanna elephants, the PSMC curves overlap across the entire x-axis (Figure 14.2C), suggesting that the two elephants share a common ancestor in the recent past, which is consistent with the young population split time (30,000 – 38,000 years ago) inferred by the $F(A|B)$ method (see Table S15.2). Their recent split together with the historically low population size are consistent with earlier hypotheses of a recent founder event in the history of savanna elephants (33, 34). Following the dramatic ~20-fold population size reduction mentioned above (down to 3,970 – 12,900), which could alternatively reflect ancient population structure not evident in present-day genomes, N_e remained stable for a long time period and then gradually increased at a slow rate. An additional, minor decrease in N_e is observed at ~4×10^{-5} divergence units or ~62,000 years ago, after which N_e grew only slightly in the very recent past, reaching approximately the same size as that observed in *L. cyclotis_F*. The apparent recent population growth could reflect the recent founder event suggested by previous studies, but we are cautious about interpreting population size changes in the very recent past due to the low power of the PSMC method within this time interval.

The N_e curve of the straight-tusked elephant is qualitatively similar to the N_e curves of forest elephants during the ancient past but quantitatively discordant most likely due to the large differences in the coverage of these genomes. In an attempt to line up these curves, we subsampled the genomes of *L. cyclotis_A* and *L. cyclotis_F* to the average coverage of *P.*

antiquus_N (10x) and estimated their population size histories, which we then plotted together with the population history of *P. antiquus_N* (Figure S14.3). Although the straight-tusked elephant is dated to ~120,000 years before present, we did not shift its N_e curve away from the origin of the x-axis to account for branch shortening, since that would result in an empirically worse fit to the forest elephant curves. It is tempting to interpret the increase in population size (going back in time) in all three genomes as a period of separation and admixture between the straight-tusked elephant and forest elephant lineages, particularly in light of the detected signal of excess genetic affinity between *L. cyclotis_F* and *P. antiquus_N* (Table S11.2). However, this population size increase appears to be older than the inferred split between the two forest elephants (reflected by the time point where the green and red curves diverge), suggesting either that this is an actual increase in population size or a more complex history of population structure and admixture between the two species. Even though the coverage of *P. antiquus_N* does not allow us to make quantitative interpretations of its N_e curve, it appears to share the population size peak observed in forest elephants at ~2×10^{-3} divergence units or ~2.5 million years ago, but not the population size increase at ~4×10^{-4} divergence units or ~493,000 years ago, suggesting that the split in the shared ancestry of straight-tusked and forest elephants occurred within this time interval. Following the initial peak and subsequent continuous decline in the population size of *P. antiquus_N*, an extreme inflation in N_e is observed during the most recent past, which is most likely an artifact known to be produced by sequencing and alignment errors (71).

All Asian elephant genomes show evidence of a prolonged period of population decline (or population separation) starting at ~6×10^{-3} divergence units or ~7.4 million years ago (Figure S14.1). This decline appears to have occurred in two steps: an initial ~2-fold reduction at ~2.5×10^{-3} divergence units or ~3.1 million years ago, after which N_e remained relatively stable for a short interval, and a subsequent ~2.5-fold reduction that reached its minimum at ~6×10^{-4} divergence units or 739,000 years ago. A new phase of population expansion and contraction succeeded the initial decline, starting at ~4×10^{-4} divergence units or 493,000 years ago. N_e increased ~3-fold (up to 27,800 – 46,700) by 1.5×10^{-4} divergence units or 185,000 years ago, to a level similar to that observed at the same time in *L. cyclotis_F*, but lower than that observed in *L. cyclotis_A*, assuming no interspecies variation in mutation rates. Then, population size began to drop again at ~10^{-4} divergence units or 123,000 years ago to significantly low levels (at least 10-fold reduction), which are the lowest observed in any of the present-day elephantid species. The most recent inferred N_e in Asian elephants (1,090 – 3,970) is lower than that inferred in savanna elephants, assuming no interspecies variation in mutation rates. Also, as mentioned for the other PSMC plots, this latest population size reduction (or increase moving back in time) could reflect ancestral population divergence and subsequent admixture between Asian elephant lineages as has been suggested by earlier studies (72-75). The nearly identical N_e trajectories for all Asian elephants (Figure S14.2E) together with the relatively short population split times inferred in Supplementary Note 15 (~12,000 – 26,000; Table S15.2), provide support for this hypothesis.

In woolly mammoths, an initial two-step and ~4.5-fold reduction in N_e is revealed by the PSMC curves, which appears to be qualitatively similar to the initial decline observed in Asian elephants. These events could reflect population size changes in the history of the common ancestor of Asian elephants and woolly mammoths or a period of separation and admixture between these lineages. After ~6×10^{-4} divergence units or 743,000 years ago (739,000 years + the calibrated date of *M. primigenius_Q*: 4,300 years), population size in woolly mammoths started to increase, reaching similar or even higher levels than before the initial decline (up to 21,800 – 266,000; note the high uncertainty in the bootstrap N_e curves of *M. primigenius_Q* towards the recent past; Figure S14.1). As originally described in Palkopoulou *et al.* (11), a second, more severe and rapid decline occurred in the history of *M. primigenius_Q*, which is not shared by *M. primigenius_P*. This decline is inferred to have occurred at ~2.5×10^{-5} divergence units or ~35,000 years ago (31,000 years + the calibrated date of *M. primigenius_Q*: 4,300 years), which is older than the Pleistocene/Holocene transition (12,000 years ago) when sea levels rose and the woolly mammoth population became isolated on Wrangel Island.

Table S14.1. Subsampling of high-coverage genomes to the lowest coverage of their conspecifics.

Sample	Filtered coverage*	Subsampled coverage*	% missing data from subsampled genomes
LcycA	19.50	14.7	17.1
LafrB	16.75	14.5	23.4
LafrC	14.50	-	-
EmaxD	30.91	9.89	4.3
EmaxE	24.59	9.89	4.9
LcycF	14.70	-	-
EmaxL	22.36	9.89	4.3
EmaxM	25.05	9.89	4.5
PantN	10.00	-	-
MpriP	9.54	9.54	-
MpriQ	15.18	-	5.1
EmaxY	28.71	9.89	4.7
EmaxZ	9.89	-	-

**Coverage was estimated by restricting to reads with mapping quality ≥ 30 for modern data and ≥ 37 for ancient data. Percentage of missing sites from the subsampled genomes was estimated by applying a minimum depth of 10 reads per site except for the subsampled E. maximus and M. primigenius, for which a minimum depth of 3 reads per site was applied because the proportion of missing sites under the higher coverage filter would exceed 25%.*

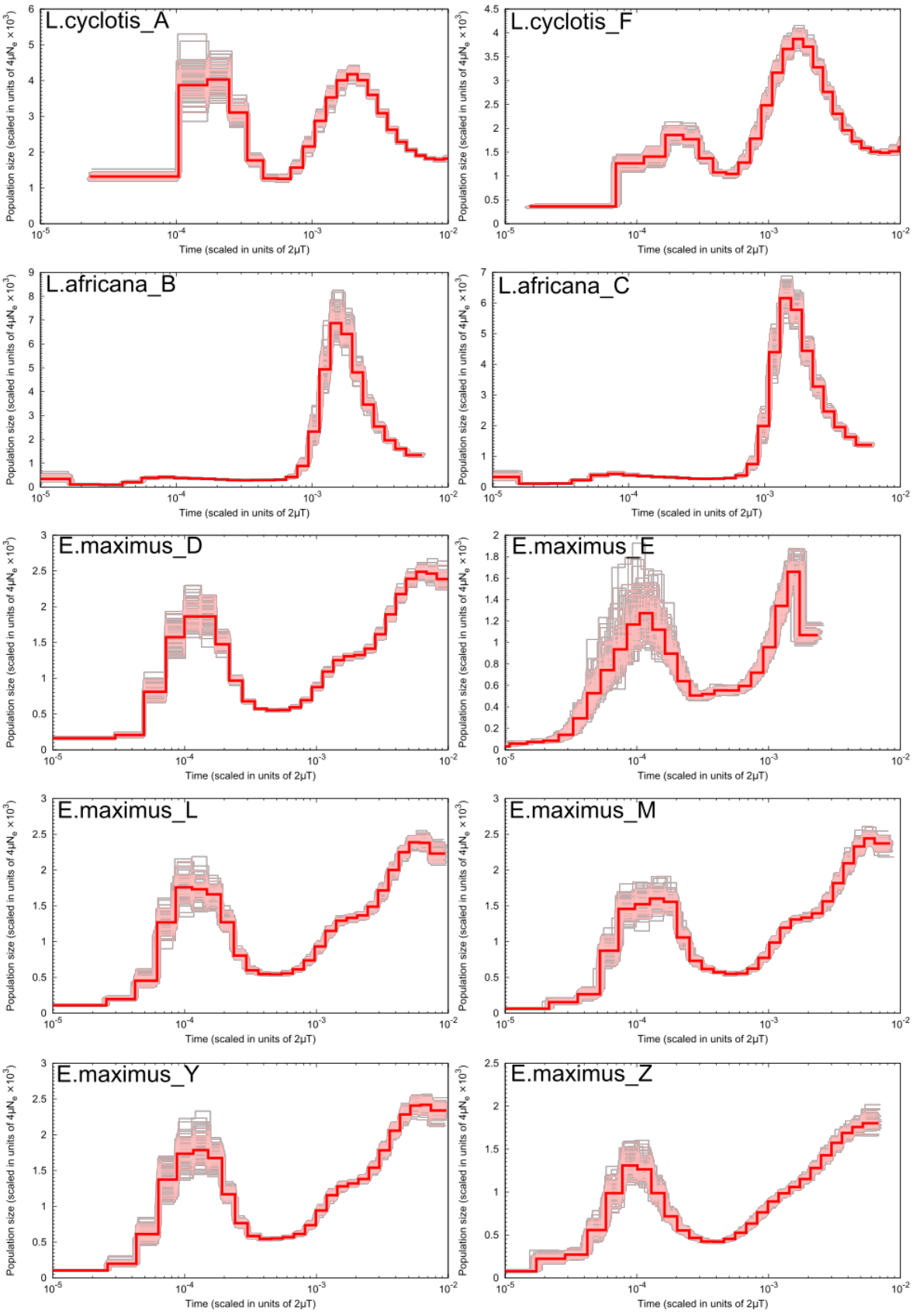
L.cyclotis_A
L.cyclotis_F
L.africana_B
L.africana_C
E.maximus_D
E.maximus_E
E.maximus_L
E.maximus_M
E.maximus_Y
E.maximus_Z
Population size (scaled in units of 4μN$_e$ ×10^3)
Time (scaled in units of 2μT)

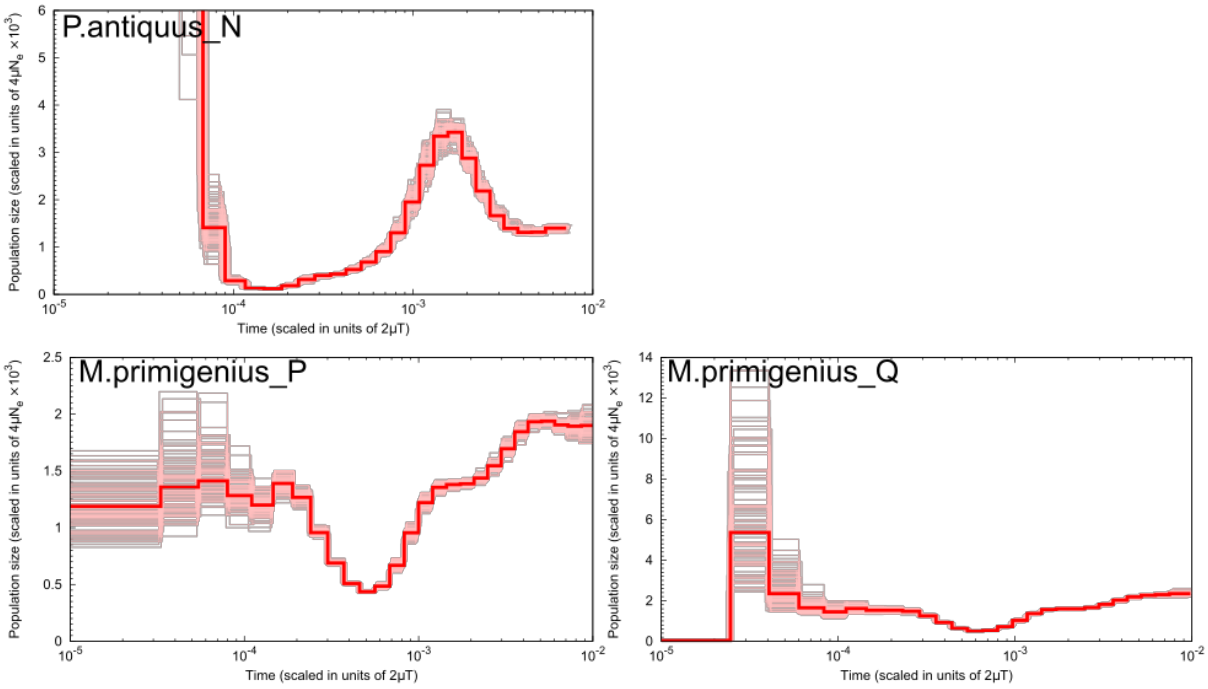

Figure S14.1. Population history inference of individual genomes with average genome-wide coverage ≥10x by the PSMC method. Time is given in units of divergence per base pair on the x-axis. Population size is given in units of $4\mu N_e \times 10^3$ on the y-axis. The PSMC estimate of each genome is shown by the thick red curves and the inference from 100 bootstrap analyses is shown in thin red curves. A minimum coverage depth of 10 reads per site was required for all genomes except for *P. antiquus_N, M. primigenius_P* and *E. maximus_Z*, for which the proportion of missing sites under this coverage filter was higher than 25%. The minimum depth of coverage was hence reduced to 1/3 of the average genome-wide coverage for these three genomes.

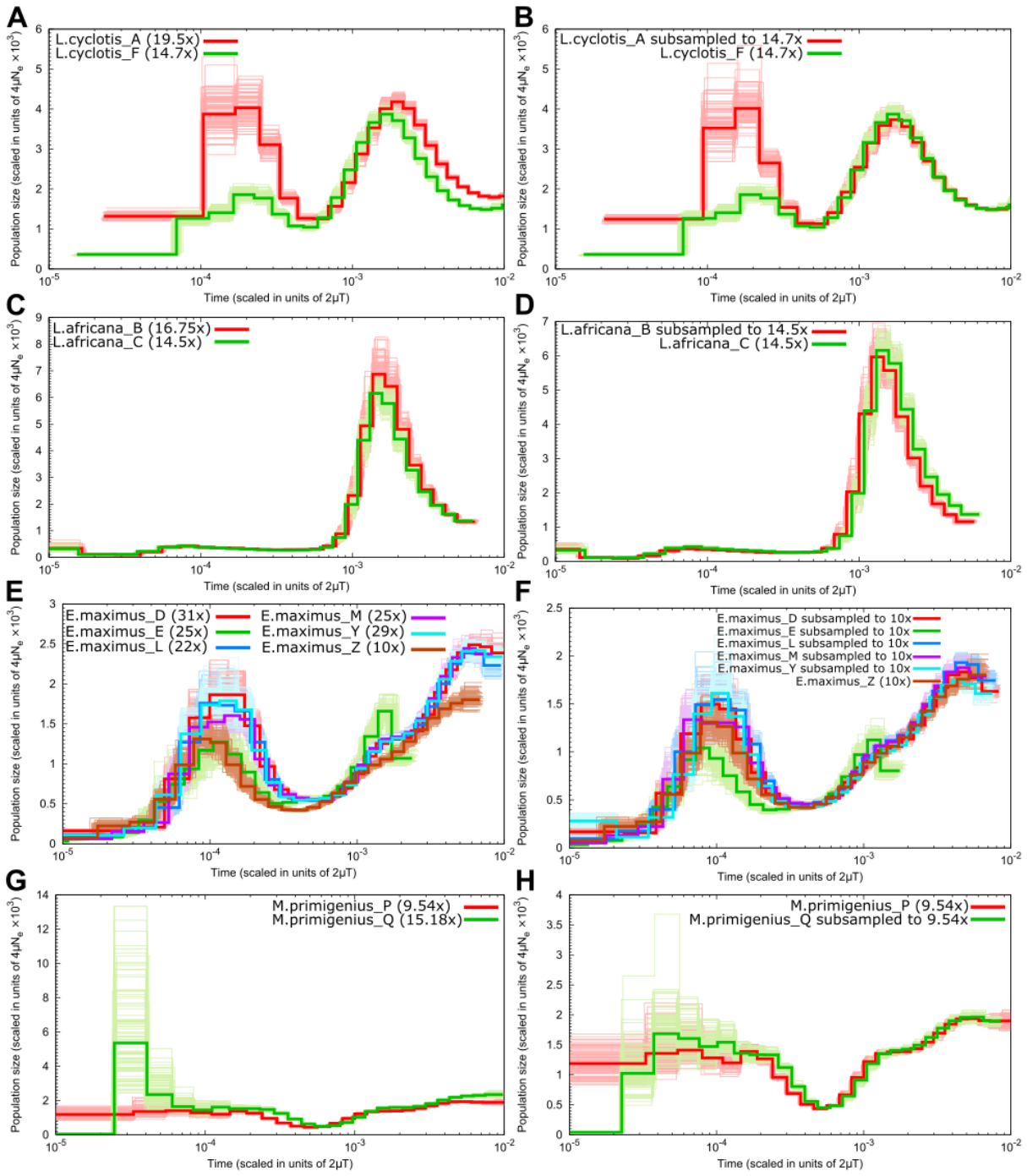

Figure S14.2. Effect of average coverage on PSMC inference. N_e and bootstrap N_e curves are plotted together for conspecific genomes in the left panels: forest elephants (A), savanna elephants (C), Asian elephants (E), woolly mammoths (G). N_e and bootstrap N_e curves inferred from high-coverage genomes that have been subsampled to the lowest average genome coverage of their conspecifics are plotted together in the right panels: *L. cyclotis_A* subsampled to the filtered coverage of *L. cyclotis_F* [14.7x] and *L. cyclotis_F* fully sampled (B), *L. africana_B* subsampled to the filtered coverage of *L. africana_C* [14.5x] and *L. africana_C* fully sampled

(D), *E. maximus_D*, *E. maximus_E*, *E. maximus_L*, *E. maximus*_M and E. max*imus_Y* subsampled to the filtered coverage of *E. maximus_Z* [9.89x] and *E. maximus_Z* fully sampled (F), and *M. primigenius_Q* subsampled to the filtered coverage of *M. primigenius_P* [9.54x] and *M. primigenius_Q* fully sampled (H). Filtered coverage was estimated by restricting to reads with mapping quality ≥ 30 for modern DNA data and ≥ 37 for ancient DNA data and is given in parentheses in the plot legends. A minimum depth of 10 reads per site was required for the forest and savanna elephant genomes in the right panels (B and D). For Asian elephants and woolly mammoths in the right panels, this minimum depth was reduced to 3 reads per site (i.e., 1/3 of the lowest filtered coverage of their conspecific) since the proportion of missing sites under the standard higher coverage filter would exceed 25%. Coverage filters in the left panels are as described in the legend of Figure S14.1. Time is given in units of divergence per base pair on the x-axis. Population size is given in units of $4\mu N_e \times 10^3$ on the y-axis.

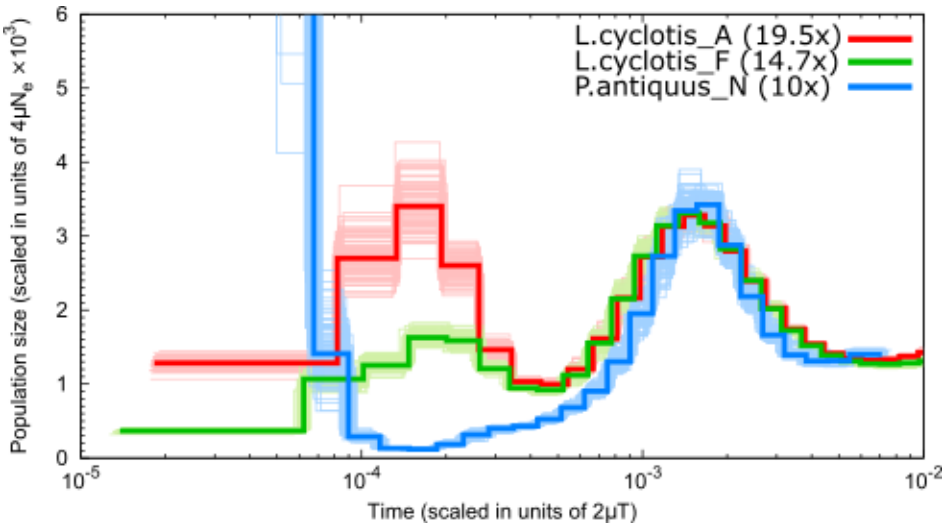

Figure S14.3. Qualitative comparison of the population histories of the straight-tusked elephant (blue curve) and the two forest elephants (red and green curves). Note that the *P. antiquus_N* genome (~120,000 years BP) needs to be shifted away from the origin of the x-axis for an interval corresponding to its age. Time is given in units of divergence per base pair on the x-axis. Population size is given in units of $4\mu N_e \times 10^3$ on the y-axis.

Supplementary Note 15

Estimates of population split times

We inferred population split times using an approach that examines single nucleotide polymorphic (SNP) positions that are heterozygous in an individual from one population and measures the fraction of these sites at which a randomly sampled chromosome from an individual of a second population carries the derived allele ($F(A|B)$), polarized by an outgroup (59). This fraction is expected to be around 1/3 for an individual from the same population, and 0 in an individual from a very distantly related population, since novel mutations accumulate in each population after their split. By taking advantage of the reconstructed population history of the individual in which the SNP is discovered, using the Pairwise Sequential Markovian Coalescent (69) (PSMC), we can infer the functional form of decay with population split time.

We ascertained heterozygous sites in a high-coverage elephantid genome from each taxon (labelled population '*B*') and estimated the proportion of these sites for which a randomly drawn chromosome from a conspecific elephantid (labelled population '*A*') carries the derived allele, and performed simulations to generate the expected decay of $F(A|B)$ as a function of split time. Since we sample a random single allele from population (*A*), genetic drift in this lineage does not need to be taken into account (it will coalesce with the population *B* at a more ancient point than their split time), but we do need to accurately model the demographic history of population (*B*), in which polymorphic sites were ascertained. Taking the inferred population size changes through time from the PSMC method, we simulated models in which population (*B*) splits from population (*A*) given a range of split times. The intersection between the observed $F(A|B)$ estimates and the expected decay of $F(A|B)$ makes it possible to determine a range of population split times that are consistent with the data. We performed this analysis to estimate population split times within species (plus the split between woolly and Columbian mammoths) since very few polymorphisms are expected to be shared across species, given their long divergence times (76).

We generated autosomal diploid calls for genomes with relatively high average coverage (≥ 10x) using the SAMtools (19) v.0.1.19 'mpileup' command, bcftools and the 'vcf2fq' command from vcfutils.pl. Apart from the standard filtering criteria described in Supplementary Note 6, we applied a minimum and maximum read depth of coverage equal to 1/3 of the average genome-wide coverage and 2-fold the average genome-wide coverage respectively, and excluded sites with root-mean-square mapping quality below 30 and sites within 5bp of indels. For genomes that were sequenced at coverage < 10x, such as the outgroup (*M. americanum_I*), the Columbian mammoth (*M. columbi_U*) and the admixed woolly mammoth (*Mammuthus_V*), we sampled a random single allele per site, as described in Supplementary Note 8. We applied the 90% stringent mappability filter to both high- and low-coverage data.

Within each taxon, we discovered heterozygous positions that passed our filters in each high-coverage genome and estimated the proportion of positions for which a randomly chosen chromosome from a conspecific elephantid carried the derived allele, using the mastodon (*M. americanum_I*) sequence to determine the ancestral state. We used the software POPSTATS (https://github.com/pontussk/popstats) to compute the $F(A|B)$ proportion and its standard error using a weighed block jackknife over contiguous blocks of 5Mb either from all substitutions or excluding transitions (Table S15.1). In the analyses that follow, we used empirical values from transversions only to eliminate biases from recurrent mutations as well as residual post-mortem damage in CpG context. We performed these computations for all possible pairs of conspecific genomes using each high-coverage genome interchangeably as population (*A*) or (*B*), with the exception of *E. maximus_E* and *E. maximus_Z*, whose inferred population histories from the PSMC did not converge with those of the remaining Asian elephants due to coverage or heterozygosity differences that can bias inferences as discussed in Supplementary Note 14, and which were therefore only used as samples representing population (*A*). Moreover, for the split between woolly mammoths and *M. columbi_U* and *Mammuthus_V*, the two higher coverage woolly mammoth genomes (*M. primigenius_P* and *M. primigenius_Q*) were interchangeably used as population (*B*) to discover heterozygous sites, and random single alleles were sampled per site from the lower coverage *M. columbi_U* and *Mammuthus_V* to eliminate coverage-related biases as well as sequencing and damage errors.

The proportion of sites for which population (*A*) carries the derived allele is highest in savanna elephants (38-39%), intermediate in Asian elephants (30-38%), lower in woolly mammoths (29-31%), and lowest in forest elephants (29-30%), indicating that within-species splits are oldest among forest elephants (4, 33, 36) (Table S15.1). The theoretical expectation of this proportion, assuming that (*A*) and (*B*) originate from a single constant-size population, is ⅓, but simulations have shown that it deviates under scenarios of population size changes (59). For heterozygous sites discovered within individual woolly mammoths, the Columbian mammoth (*M. columbi_U*) has the derived allele at 22-23% of sites, much lower than ⅓, as expected given that woolly mammoths and Columbian mammoths are different species. The North American (NA) *Mammuthus_V* on the other hand carries the derived allele at 28-30% of sites that are heterozygous in woolly mammoths, a proportion that is closer to that observed in the Eurasian (EA) woolly mammoths (*M. primigenius_P* and *M. primigenius_Q*) but lower (although not significantly so). The reason for this observation is twofold: first, NA *Mammuthus_V* is symmetrically related to the EA mainland *M. primigenius_P* and EA Wrangel Island *M. primigenius_Q* with D (*M. primigenius_P*, *M. primigenius_Q*; *Mammuthus_V*, *X*) consistent with 0, where *X* represents any other non-woolly mammoth proboscidean, indicating a topology in which NA *Mammuthus_V* is placed outside the clade of EA *M. primigenius_P* and *M. primigenius_Q*. Based on this topology, NA *Mammuthus_V* is suggested to have split from the lineage leading to the common ancestor of the two EA mammoths *M. primigenius_P* and *M. primigenius_Q* (i.e., earlier than the split of the latter two), which explains the lower proportion of derived sites carried by NA *Mammuthus_V*. Second, NA *Mammuthus_V* additionally has a

Columbian mammoth ancestry component (8.8 – 11.7%; see the f_4-ratio test in Table S11.7), which violates the model assumption of complete isolation after the initial split. This results in a reduction of the observed proportion of derived sites so that F_{emp} (*Mammuthus_V* | *M. primigenius*) = (α* $F(t_1)$) + ((1 - α) * $F(t_2)$), where F_{emp} is the empirical F (*Mammuthus_V* | *M. primigenius*) estimate, $F(t_1)$ the $F(A|B)$ proportion for the woolly mammoth-related source population of admixture into NA *Mammuthus_V*, $F(t_2)$ $F(A|B)$ the proportion for the Columbian mammoth-related source population of admixture into NA *Mammuthus_V*, and α, (1- α) the mixture proportions from the woolly mammoth-related and Columbian mammoth-related populations, respectively (Figure S11.1). Since we have estimated the mixture proportions of NA *Mammuthus_V*, and we have an empirical estimate for $F(t_2)$ = F_{emp} (*M. columbi_U* | *M. primigenius*), we can solve for $F(t_1)$ in the equation above: $F(t_1)$ = (F_{emp} (*Mammuthus_V* | *M. primigenius*) - ((1 - α) * $F(t_2)$)) / α. Taking the average α = 10.3% (estimated from the f_4-ratio test in Table S11.7), we obtain estimates for $F(t_1)$ of 0.3044 ± 0.0013 and 0.2916 ± 0.0015, using F_{emp} (*Mammuthus_V* | *M. primigenius_P*) and F_{emp} (*Mammuthus_V* | *M. primigenius_Q*) and their standard errors, respectively (Table S15.1), which are slightly lower but overlapping with F_{emp} (*M. primigenius_Q* | *M. primigenius_P*) and F_{emp} (*M. primigenius_P* | *M. primigenius_Q*).

Table S15.1. Proportion of heterozygous sites in population *B* for which population *A* has the derived allele.

		All sites			Transversions		
pop *A*	**pop *B***	***F(A|B)***	**SE**	**nSNPS**	***F(A|B)***	**SE**	**nSNPS**
LcycA	LcycF	0.3033	0.0008	2,844,484	0.2944	0.0009	818,404
LcycF	LcycA	0.2969	0.0007	3,491,761	0.2898	0.0009	998,319
LafrB	LafrC	0.3896	0.0015	660,298	0.3844	0.0018	187,033
LafrC	LafrB	0.3953	0.0017	734,680	0.3877	0.0021	211,341
EmaxD	EmaxL	0.3580	0.0014	1,361,203	0.3533	0.0016	381,777
EmaxD	EmaxM	0.3527	0.0013	1,181,126	0.3471	0.0016	332,339
EmaxD	EmaxY	0.3588	0.0013	1,378,717	0.3526	0.0015	388,996
EmaxE	EmaxD	0.3122	0.0014	1,522,130	0.3050	0.0016	427,801
EmaxE	EmaxL	0.3105	0.0015	1,344,744	0.3037	0.0017	377,098
EmaxE	EmaxM	0.3086	0.0016	1,167,372	0.3008	0.0018	328,591
EmaxE	EmaxY	0.3096	0.0014	1,363,364	0.3014	0.0016	384,647
EmaxL	EmaxD	0.3590	0.0014	1,538,209	0.3523	0.0015	432,198
EmaxL	EmaxM	0.3794	0.0016	1,182,082	0.3735	0.0019	332,599
EmaxL	EmaxY	0.3652	0.0014	1,377,644	0.3580	0.0016	388,641
EmaxM	EmaxD	0.3527	0.0013	1,537,179	0.3473	0.0015	431,830
EmaxM	EmaxL	0.3827	0.0017	1,361,800	0.3793	0.0018	381,822
EmaxM	EmaxY	0.3569	0.0013	1,377,968	0.3515	0.0015	388,684
EmaxY	EmaxD	0.3601	0.0014	1,528,408	0.3542	0.0015	429,218
EmaxY	EmaxL	0.3654	0.0015	1,351,920	0.3610	0.0017	378,826
EmaxY	EmaxM	0.3586	0.0014	1,174,130	0.3530	0.0016	330,225

EmaxZ	EmaxD	0.3455	0.0013	1,287,669	0.3389	0.0015	358,877
EmaxZ	EmaxL	0.3747	0.0020	1,118,271	0.3687	0.0022	310,541
EmaxZ	EmaxM	0.3674	0.0020	972,870	0.3601	0.0023	271,322
EmaxZ	EmaxY	0.3516	0.0015	1,150,746	0.3451	0.0018	321,599
MpriP	MpriQ	0.3030	0.0013	1,450,953	0.2963	0.0015	421,531
MpriQ	MpriP	0.3196	0.0012	1,835,362	0.3121	0.0013	533,927
MpriV	MpriP	0.3044	0.0012	1,685,175	0.2965	0.0014	491,139
MpriV	MpriQ	0.2918	0.0014	1,367,209	0.2842	0.0015	398,759
McolU	MpriP	0.2385	0.0018	1,125,307	0.2276	0.0019	322,198
McolU	MpriQ	0.2308	0.0019	909,444	0.2199	0.0021	260,887
MpriV*	MpriP	0.3119	0.0012	-	0.3044	0.0013	-
MpriV*	MpriQ	0.2988	0.0013	-	0.2916	0.0015	-

*F(*MpriV*|*MpriP) and F(*Mpri*|*MpriQ) have been corrected for the Columbian mammoth-related ancestry in the North American Mammuthus_V as described in the text above.*

To convert $F(A|B)$ estimates to population split times, we used the coalescent simulator *scrm* (77), which is similar to *ms* (78), to model a split between populations (A) and (B) given a range of split times under the history of population (B) inferred from the PSMC (Figure S14.1). We generated datasets of 100 sequences, each of 30Mb in length, and estimated $F(A|B)$ as described above for each simulated dataset. We then plotted the resulting $F(A|B)$ proportions and their standard errors against the simulated split time to calibrate the expected decay of $F(A|B)$. We used the time points at which the empirical values intersected the simulated curve to obtain the inferred range of split time between populations (A) and (B) (Figure S15.1). For the split time between *M. primigenius_P/Q* and *Mammuthus_V*, the estimate $F(t_1)$, which is corrected for the Columbian mammoth-related ancestry in *Mammuthus_V*, was used instead of the empirical value. Table S15.2 lists the inferred population split times (τ) measured in $4N_e \times$ generations units, where N_e is the current or most recent effective population size of population (B). We converted these estimates to years assuming the inferred current or most recent effective population size (scaled in $4\mu N_e \times 10^3$ units, where μ is the mutation rate per site per generation) by the PSMC method, a mutation rate of 0.406×10^{-9} per year per site (as estimated in Supplementary Note 16 based on the fossil-calibrated genetic divergence time between *Loxodonta* and *Elephas* (11), and their estimated divergence per base pair), and a generation time of 31 years (mean estimate from males and females (4)). From here on, we discuss population split times estimated under these assumptions; however, we should note that faster or slower mutation rates would result in younger and older split times, respectively.

The population split time between West and Central African forest elephants is inferred to have occurred ~463,000 – 609,000 years ago (as estimated from the split time of *L. cyclotis_A* and *L. cyclotis_F*; Table S15.2), which falls close to the time interval when the two African forest elephant PSMC curves converge (Figure S14.2A, B). The split time of eastern and southern African savanna elephants is inferred to be at least 10-fold younger (~30,000 – 38,000 years ago), assuming no interspecies variation in the mutation rate. This is in agreement with previous

findings from multiple nuclear loci and from mitochondrial DNA genomes (S clade versus F clade) that the time to the most recent common ancestor (TMRCA) in savanna elephants is more recent than the forest elephant TMRCA (4, 79). However, we should note that in the event of post-split gene flow between the two savanna elephant populations, $F(A|B)$ estimates would be skewed upwards leading to estimates that suggest more recent split times. Our intermediate F_{ST} estimate (0.14; Table S10.1) suggests that eastern and southern savanna elephants are genetically moderately differentiated (consistent with previous findings based on analysis of nuclear loci and microsatellite loci (33, 34)), which together with our inferred recent split time provides support for earlier hypotheses of a recent founder event and only very recent population isolation.

In contrast, the deep split time inferred for the two forest elephant populations suggests that dispersal and gene flow may have been constrained since their initial split. The geographically intervening Dahomey/Benin Gap, which separates the Guinean and Congolian forest blocks in West and Central Africa, respectively, may have acted as a biogeographic barrier to gene flow (61). Even though F_{ST} between the two forest elephants is not especially high (0.18, in agreement with earlier studies that did not detect large genetic differences between the two forest elephant populations (36, 80)), this could be due to large effective population sizes in forest elephants (4, 33) and hence limited genetic drift. Our results demonstrate that there has been substantial separation among these populations, which is confirmed by the asymmetric relatedness of the straight-tusked elephant to the two forest elephants, with excess genetic affinity to the West African forest elephant (Table S11.2), showing that the isolation of these two populations must be at least ~120,000 years old (the date of the straight-tusked elephant sequenced in this study).

Within Asian elephants, inferred population split times are lowest among elephants in India outside Assam (between ~12,000 – 26,000 years ago), intermediate between *E. maximus_D* and *E. maximus_Y* from Myanmar and Assam, respectively, and the other elephants from India (between ~22,000 – 43,000 years ago) and highest between *E. maximus_E* from Malaysian Borneo and all other Asian elephants (at least two times older, between ~103,000 – 190,000 years ago; Table S15.2). Overall, these split time estimates are younger than those in forest elephants, again in agreement with earlier estimates of within-taxon TMRCAs (4, 79), and overlapping but wider than those in savanna elephants. Previous population genetic studies of Asian elephants have identified two highly divergent mitochondrial clades, but the lack of clear phylogeographic structure and nuclear genetic differentiation are indicative of allopatric divergence followed by expansions and subsequent admixture (72-75, 81). Under such a scenario, female philopatry and male-mediated gene flow could explain the apparent incongruence between the deeply diverged mitochondrial clades and the relatively recent nuclear genome-wide estimates of population split times. Notably, genetically divergent and isolated Asian elephant populations have been suggested to inhabit Malaysian Borneo – from whence *E. maximus_E* derives – based on distinct mitochondrial DNA patterns (73). This hypothesis is supported by the older population split time (Table S15.2) and high F_{ST} values (Table S10.1) estimated in this study between *E. maximus_E* and all other Asian elephants. Myanmar, where

both mtDNA clades α and β are present, and from whence *E. maximus_D* derives, has been hypothesized to have been the area of origin of clade α as well as the zone of secondary admixture between clade β haplotypes that were previously isolated in southern regions (75). Secondary admixture between diverged Asian elephant lineages in Myanmar could have produced the observed intermediate split times between *E. maximus_D* and Indian elephants.

In woolly mammoths, the estimated split time between EA *M. primigenius_P* and *M. primigenius_Q*, ~112,000 – 225,000 years ago ([67,000 – 87,000] + the calibrated age of *M. primigenius_P* (44,800); [182,000 – 221,000] + the calibrated age of *M. primigenius_Q*, (4,300)), suggestsa recent split of their ancestral populations (11) despite their deeply divergent mitochondrial lineages (clades I and II/A, respectively; Figure S7.1). The ancestral NA woolly mammoth population (that contributed most of the ancestry of the NA *Mammuthus_V*) is inferred to have split from the EA woolly mammoths (*M. primigenius_P* and *M. primigenius_Q*) at about the same time as the population split of the latter two (~146,000 – 263,000 years ago; [101,000 – 222,000] + 44,800; [251,000 – 259,000] + 4,300). A much older split is estimated between the Columbian mammoth, *M. columbi_U,* and the two EA woolly mammoths (423,000 – 712,000; [378,000 – 408,000] + 44,800; [667,000 – 708,000] + 4,300). This is at least ~2-fold and up to 6-fold older than the split between the two EA woolly mammoths, contrasting with their mtDNA phylogeny, in which the Columbian mammoth falls within the diversity of clade I woolly mammoths (2, 66).

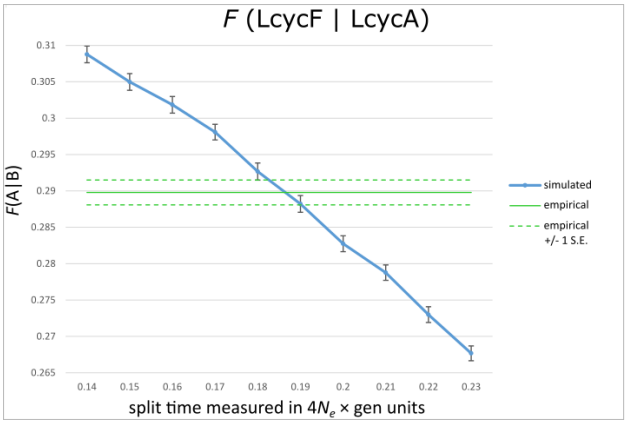

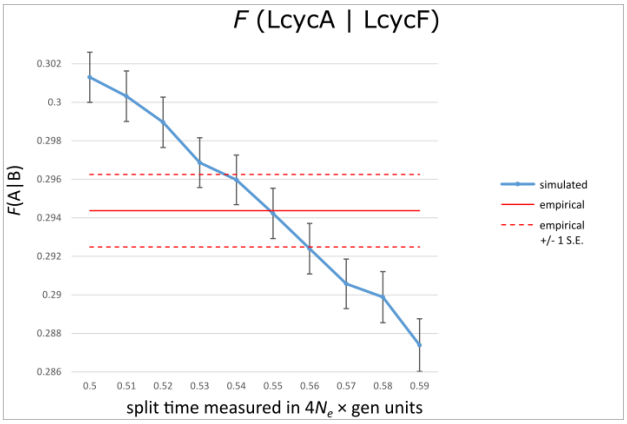

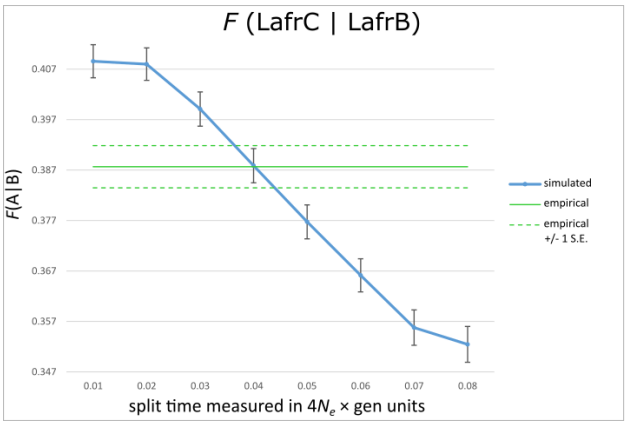
F (LafrC | LafrB)
F(A|B)
0.407
0.397
0.387
0.377
0.367
0.357
0.347
0.01 0.02 0.03 0.04 0.05 0.06 0.07 0.08
split time measured in 4Ne × gen units
simulated
empirical
empirical +/- 1 S.E.

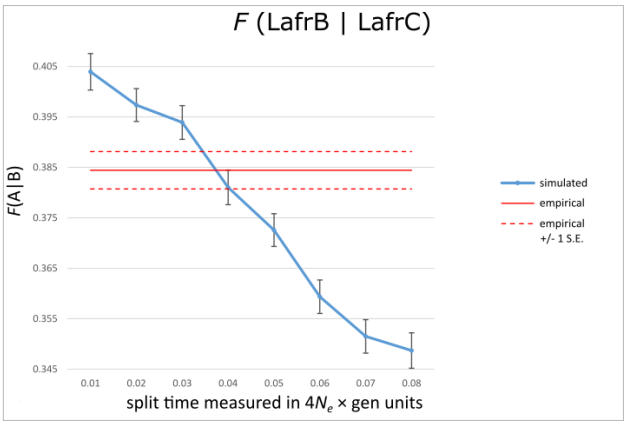
F (LafrB | LafrC)
F(A|B)
0.405
0.395
0.385
0.375
0.365
0.355
0.345
0.01 0.02 0.03 0.04 0.05 0.06 0.07 0.08
split time measured in 4Ne × gen units
simulated
empirical
empirical +/- 1 S.E.

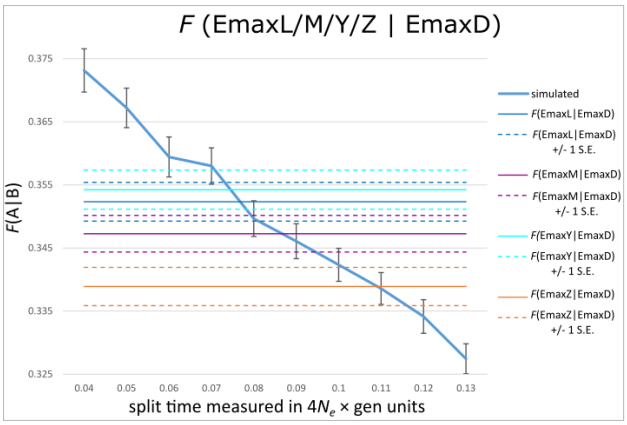
F (EmaxL/M/Y/Z | EmaxD)
F(A|B)
0.375
0.365
0.355
0.345
0.335
0.325
0.04 0.05 0.06 0.07 0.08 0.09 0.1 0.11 0.12 0.13
split time measured in 4Ne × gen units
simulated
F(EmaxL|EmaxD)
F(EmaxL|EmaxD) +/- 1 S.E.
F(EmaxM|EmaxD)
F(EmaxM|EmaxD) +/- 1 S.E.
F(EmaxY|EmaxD)
F(EmaxY|EmaxD) +/- 1 S.E.
F(EmaxZ|EmaxD)
F(EmaxZ|EmaxD) +/- 1 S.E.

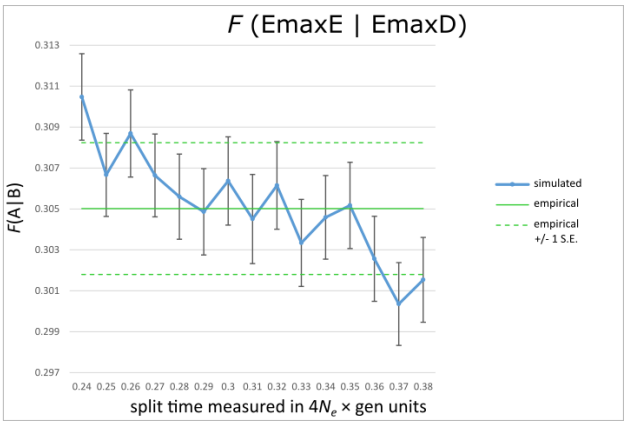
F (EmaxE | EmaxD)
F(A|B)
0.313
0.311
0.309
0.307
0.305
0.303
0.301
0.299
0.297
0.24 0.25 0.26 0.27 0.28 0.29 0.3 0.31 0.32 0.33 0.34 0.35 0.36 0.37 0.38
split time measured in 4Ne × gen units
simulated
empirical
empirical +/- 1 S.E.

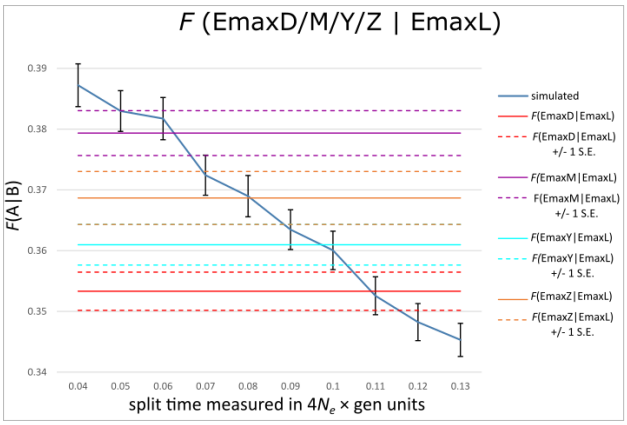
F (EmaxD/M/Y/Z | EmaxL)
F(A|B)
0.39
0.38
0.37
0.36
0.35
0.34
0.04 0.05 0.06 0.07 0.08 0.09 0.1 0.11 0.12 0.13
split time measured in 4Ne × gen units
simulated
F(EmaxD|EmaxL)
F(EmaxD|EmaxL) +/- 1 S.E.
F(EmaxM|EmaxL)
F(EmaxM|EmaxL) +/- 1 S.E.
F(EmaxY|EmaxL)
F(EmaxY|EmaxL) +/- 1 S.E.
F(EmaxZ|EmaxL)
F(EmaxZ|EmaxL) +/- 1 S.E.

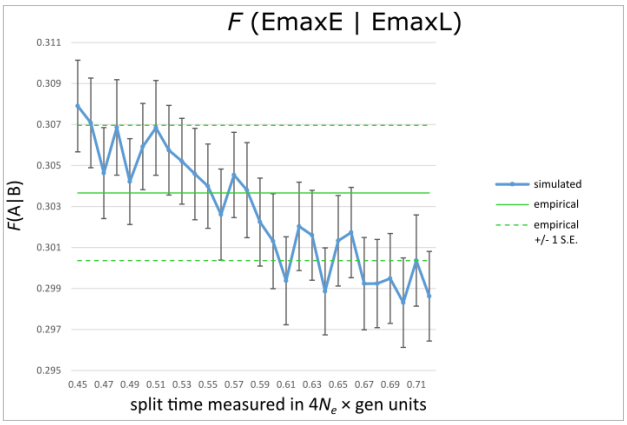
F (EmaxE | EmaxL)
F(A|B)
0.311
0.309
0.307
0.305
0.303
0.301
0.299
0.297
0.295
0.45 0.47 0.49 0.51 0.53 0.55 0.57 0.59 0.61 0.63 0.65 0.67 0.69 0.71
split time measured in 4Ne × gen units
simulated
empirical
empirical +/- 1 S.E.

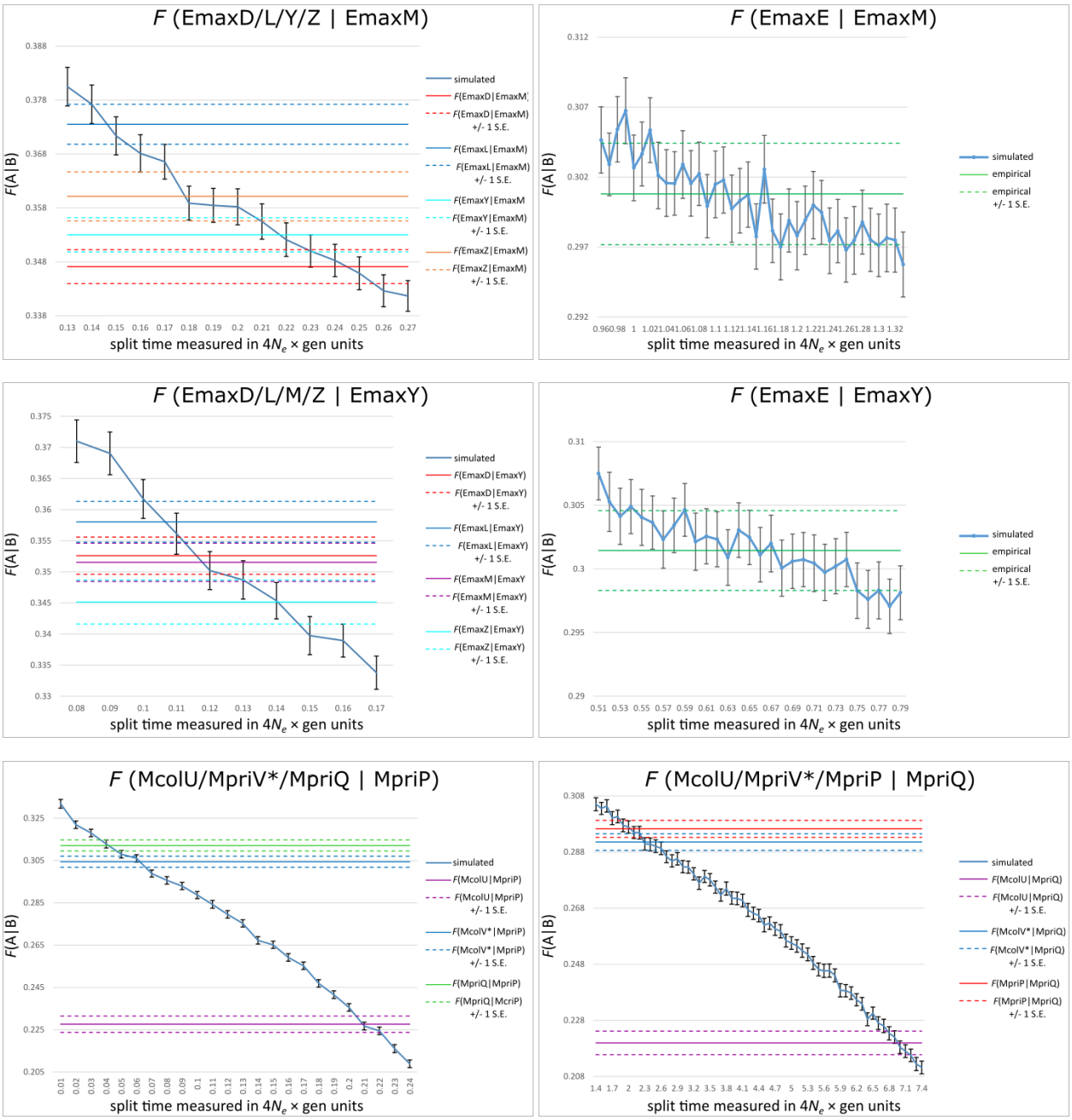

Figure S15.1. Empirical $F(A|B)$ and expected decay of $F(A|B)$ as a function of split time obtained from simulating the population size history of population (B) – as inferred from the PSMC method – given a range of split times from population (A). For F (*MpriV*|MpriP*) and F (*MpriV*|MpriQ*), instead of the empirical $F(A|B)$ values, the estimates corrected for the Columbian mammoth-related ancestry in *Mammuthus_V* are plotted. Time on the x-axis is measured in $4N_e$ × generations units, where N_e is the current or most recent effective population size of population (B). Empirical $F(A|B)$ estimates are indicated by solid lines and $F(A|B)$ ± 2 standard errors by intermittent lines. Error bars in the $F(A|B)$ estimates from the simulations denote ± 2 standard errors. The time points at which empirical $F(A|B)$ values intersect the

expected decay of $F(A|B)$ indicate the range of split times that encompass the observed $F(A|B)$ ± 2 standard errors (95.4% confidence interval).

Table S15.2. Population split times obtained by intersecting empirical $F(A|B)$ values to the expected decay of $F(A|B)$ as a function of split time. τ_{ms} is scaled in units of $4N_e \times$ generations, where N_e is the PSMC-inferred current or most recent effective population size (Pop. size B), which is in turn scaled in $4\mu N_e \times 10^3$ units, where μ is the mutation rate per site per generation. Split time estimates converted into years assume a mutation rate of 0.406×10^{-9} per year per site (as estimated in Supplementary Note 16) and a generation time of 31 years.

$F(A\|B)$	τ_{ms} min	τ_{ms} max	Pop. size (B)	t_{years} min	t_{years} max
F(LcycA|LcycF)	0.5368	0.5595	0.35	462,795	482,337
F(LcycF|LcycA)	0.1826	0.1903	1.30	584,714	609,177
F(LafrB|LafrC)	0.0345	0.0402	0.35	29,732	34,690
F(LafrC|LafrB)	0.0365	0.0439	0.35	31,429	37,881
F(EmaxD|EmaxL)	0.1048	0.1155	0.10	25,812	28,455
F(EmaxD|EmaxM)	0.2287	0.2559	0.05	28,170	31,515
F(EmaxD|EmaxY)	0.1109	0.1240	0.10	27,316	30,545
F(EmaxE|EmaxD)	0.2778	0.3835	0.15	102,623	141,673
F(EmaxE|EmaxL)	0.4605	0.7100	0.10	113,419	174,880
F(EmaxE|EmaxM)	0.9613	1.3219	0.05	118,390	162,795
F(EmaxE|EmaxY)	0.5260	0.7700	0.10	129,563	189,664
F(EmaxL|EmaxD)	0.0640	0.0811	0.15	23,635	29,969
F(EmaxL|EmaxM)	0.1400	0.1548	0.05	17,244	19,063
F(EmaxL|EmaxY)	0.1012	0.1124	0.10	24,933	27,694
F(EmaxM|EmaxD)	0.0791	0.0946	0.15	29,219	34,946
F(EmaxM|EmaxL)	0.0499	0.0665	0.10	12,282	16,384
F(EmaxM|EmaxY)	0.1126	0.1307	0.10	27,725	32,197
F(EmaxY|EmaxD)	0.0708	0.0782	0.15	26,157	28,896
F(EmaxY|EmaxL)	0.0885	0.1032	0.10	21,787	25,428
F(EmaxY|EmaxM)	0.2074	0.2310	0.05	25,537	28,447
F(EmaxZ|EmaxD)	0.1011	0.1161	0.15	37,340	42,902
F(EmaxZ|EmaxL)	0.0693	0.0885	0.10	17,080	21,786
F(EmaxZ|EmaxM)	0.1724	0.2096	0.05	21,236	25,807
F(EmaxZ|EmaxY)	0.1300	0.1467	0.10	32,032	36,129
F(McolU|MpriP)	0.2046	0.2209	0.75	377,953	407,999
F(McolU|MpriQ)	6.7708	7.1837	0.04	667,070	707,754
F(MpriV*|MpriP)	0.0548	0.0659	0.75	101,193	121,669
F(MpriV*|MpriQ)	2.5473	2.6242	0.04	250,963	258,541
F(MpriQ|MpriP)	0.0363	0.0469	0.75	67,064	86,627
F(MpriP|MpriQ)	1.8438	2.2416	0.04	181,659	220,844

*Min and max population split times denote the intersection of the empirical F(A|B) estimates ± 2 S.E. and the expected decay of F(A|B) as a function of time as obtained from simulations. F(*MpriV*|MpriP) and*

*F(*MpriV*|*MpriQ) have been corrected for the Columbian mammoth-related ancestry in the North American Mammuthus_V as described in the text above.*

Supplementary Note 16

Demographic parameter inference using simulations and ABC

We performed coalescent simulations in an Approximate Bayesian Computation (ABC) framework to infer demographic parameters of interest such as ancestral effective population sizes, interspecies split times and migration rates within the family Elephantidae. This approach uses summary statistics to compare data simulated under a range of parameter values, drawn from prior distributions, to the observed data in order to determine posterior distributions of parameters that plausibly fit the data.

We modeled a scenario of four lineages (A, B, C, O, where O is the outgroup) with one diploid individual per lineage related by the basic topology (((A, B), C), O) (Figure S16.1). Starting effective population size (N_e) was the same for each lineage and remained constant within intervals but instantaneously changed following each split. Migration with gene flow in both directions was allowed between all pairs of lineages, excluding the outgroup, during the time interval from the present until the most recent split event (between lineages A and B), moving back in time. The prior distributions used for each parameter in this model are given in Table S16.1.

We used the coalescent simulator *scrm* (77), which uses a syntax compatible with that of *ms* (78), to generate 1,000 diploid sequences of 50,000bp in length per individual under the model described above, assuming an infinite-sites model of mutation. Since it is not possible to infer the proboscidean mutation rate from our data, we fixed it in our simulations to constrain the inference of effective population size and divergence time parameters. Assuming an average genetic divergence time T_{div} = 11.8 million years between *Loxodonta* and *Elephas* (17.4 - 6.2 million years; as inferred from their fossil-calibrated split time at 9 - 4.2 million years ago; see Rohland *et al.* (4) and Palkopoulou *et al.* (11) SI), and taking the average divergence per base pair between the two taxa ($div_{Lox\text{-}Ele}$ = 0.007423; estimated from sequences with randomly-sampled alleles per site with minimum depth of 3 reads), the substitution rate per base pair per year was inferred via the formula $\mu = div_{Lox\text{-}Ele} / (2 \times T_{div(Lox\text{-}Ele)})$ at an average of 0.406×10^{-9} mutations per site per year (range equal to 0.213×10^{-9} – 0.599×10^{-9} mutations per site per year, a wider range that is primarily driven by the wide range of uncertainty for the fossil-calibrated split time). The recombination rate was fixed at a value of 10^{-8} per generation per site, and we assumed a generation time of 31 years to allow comparison to Rohland *et al.* (4), where this value was justified. We ran 100,000 simulations resulting in a total of 5 trillion bp of simulated data.

We randomly sampled one allele per individual and estimated the proportion of unique and shared derived alleles in our simulated data with the ancestral allele polarized by the outgroup. Since we modeled four lineages (including the outgroup) and sampled one random allele per lineage, there are seven possible classes of derived alleles in our four-lineage alignments: unique derived in A, B or C and shared derived in A-B, A-C, B-C or A-B-C. To include information

from linkage disequilibrium, which can be informative for demographic parameters (see Figures S16.2 and S16.3), we examined not only single sites but also pairs of adjacent sites across the autosomes and recorded the transition (i.e. change) from the class of derived alleles at the left-most site to the class of derived alleles at the right-most site of each pair; this is a similar type of data matrix to that described in Rasmussen *et al.* (82). This resulted in a 7x7 matrix of recorded site configuration transitions and we used the proportions of these 49 transitions as summary statistics. We used the program POPSTATS (https://github.com/pontussk/popstats) to compute the counts of 49 site configuration transitions with the option '--sitesconfig pairs'. In addition, we computed three *D*-statistics from the counts of shared derived alleles: $D_1 = (AC-BC) / (AC+BC)$, $D_2 = (AB-BC) / (AB+BC)$, $D_3 = (AB-AC) / (AB+AC)$, where for instance *AC* is the number of shared derived alleles in lineages A and C. We also included divergence per base pair between lineages A and B, A and C, B and C, and A and O as additional summary statistics. Divergence per base pair was estimated as the ratio of the number of sites that differed between the two lineages, again by sampling a random allele per lineage, and the total number of sites.

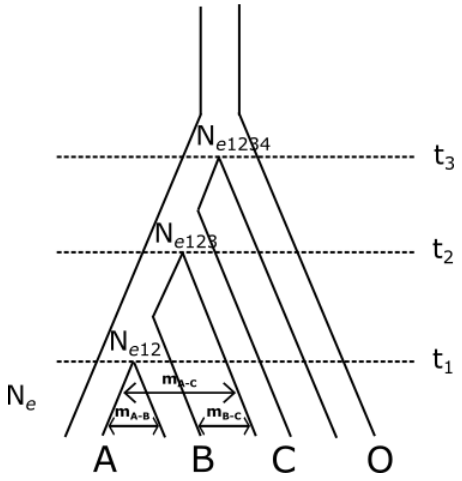

Figure S16.1. Simulated model of four lineages. Effective population size (N_e) remains constant within split intervals but changes instantaneously after each split event. t_1, t_2, t_3 denote split times between lineages A and B, AB and C, and ABC and O, where O is the outgroup. m_{A-B}, m_{A-C}, m_{B-C} indicate bidirectional gene flow between lineages A and B, A and C, and B and C.

Table S16.1. Prior distributions of parameter values used in the simulated data.

Parameter	Prior distribution
N_e	Uniform: [1000-500,000]
N_{e12}	Uniform: [0.01-2]* N_e
N_{e123}	Uniform: [0.01-2]* N_e
N_{e1234}	Uniform: [0.01-2]* N_e
t_1	Uniform: [1,000,000-10,000,000]

t_2	Uniform: [1.01-5]*t_1
t_3	Uniform: [1.01-5]* t_2
m_{A-B}	Exponential: [$\lambda = 2\times10^{-7}$]
m_{A-C}	Exponential: [$\lambda = 2\times10^{-7}$]
m_{B-C}	Exponential: [$\lambda = 2\times10^{-7}$]
% recur	Uniform: [0-0.1]
μ	Fixed: 0.406×10^{-9}
r	Fixed: 1×10^{-8}
gen time	Fixed: 31

Ancestral effective population sizes (N_{e12}, N_{e123}, N_{e1234}) are scaled by current or most recent effective population size (N_e).
The prior distribution of the most recent split time (t_1) is given in years.
Older split times (t_2, t_3) are scaled by the most recent split time (t_1).
m_{i-j} denotes the fraction of migrants in lineage i received from lineage j per generation and vice versa.
% recur denotes the proportion of polymorphic positions on all lineages that owe their origin to > 1 mutations.
μ is the mutation rate per site per generation, estimated as described above and fixed in all simulations.
r is the recombination rate per site per generation and was fixed in all simulations.
The generation time is given in years and is based on the average of estimates for males and females from African savanna and Asian elephants (Rohland et al. (4)).

Given the long divergence times within *Proboscidea* (37), recurrent mutations (e.g., homoplasies) are expected to have occurred on all branches, with most of them occurring on the lineage leading to the outgroup (mastodon). This process needs to be taken into account in our simulations since it inflates the counts and proportions of shared derived mutations, including those of sites suggesting incomplete lineage sorting (i.e., shared derived character states in lineages A and C, and shared derived in lineages B and C, assuming the topology mentioned above). Since we used the infinite-sites model, which does not allow for recurrent mutations, we collapsed pairs of sites to imitate the process of recurrent mutations for a proportion of sites sampled from a prior uniform distribution [0-10%]. The proportion of collapsed sites was then inferred from the simulated data along with other parameters of interest.

As described above for the simulated data, we computed the proportions of 49 site configuration transitions, three *D*-statistics and divergence per base pair in our empirical data. We created four-taxon alignments including one randomly selected high-coverage individual from each taxon: *L. africana_B* for the savanna elephant lineage; *Lcyclotis_A* and *L. cyclotis_F* for the forest elephant lineage (both forest elephants were analyzed because of the excess genetic affinity between *L. cyclotis_F* and *P. antiquus*); *E. maximus_D* for the Asian elephant lineage; *P. antiquus_N* for the straight-tusked elephant lineage; and *M. primigenius_Q* for the woolly mammoth lineage. From taxa that lacked high-coverage genomes, we analyzed the individual with the highest sequencing depth: *M. columbi_U* for the Columbian mammoth lineage and *M. americanum_I* for the mastodon lineage (outgroup). For these alignments, we assumed the topology suggested by the admixture graphs in Supplementary Note 12, in which the ancestral *P. antiquus* lineage splits off from the common ancestor of *Loxodonta* (forest and savanna elephants). To calculate the proportions of 49 site configuration transitions, the three *D*-statistics

and sequence divergence, we included chromosomes 1-27 in the alignments and sampled a random allele per site as described in Supplementary Note 8 but excluding sites with minimum read depth below 3. Sequence divergence per bp between lineages A and B, A and C, B and C, and A and O was estimated as the number of different sites divided by the total number of sites.

Parameter inference was performed with the ABC package (83) in R (R development Core Team 2011). This package computes the Euclidean distance (*d*) between the summary statistics of the simulated data and the observed data, and retains simulations for which *d* is lower than a given threshold. This threshold is defined by the tolerance rate, i.e., the percentage of accepted simulations, which is set by the user. The neural networks regression algorithm was employed for posterior distribution inference from the parameter values of the accepted simulations. This method accounts for the non-linearity of the regression function as well as the collinearity among summary statistics by reducing the number of correlated variables (84). A correction for heteroscedasticity was applied and all parameters were log-transformed prior to estimation and back-transformed to their original scale after the regression estimation, except for the migration rates. A tolerance ratio of 0.01 was used for inference of posterior distributions.

We initially assessed the accuracy of our model for parameter inference using the cross-validation function implemented in the ABC package in R. This approach randomly picks a simulated dataset to be considered as the 'true' data and uses the remaining simulations for posterior inference. We performed cross-validation for 100 iterations and measured the correlation between a point estimate of the inferred posterior distribution (median) and the 'true' parameter value, using Pearson's correlation coefficient. We also evaluated the sensitivity of three different tolerance rates: 0.01, 0.005 and 0.001.

Posterior inference performs well for ancestral effective population sizes (N_{e123}, N_{e1234}), older split times (t_2, t_3) and proportion of recurrent mutations (Pearson's correlation coefficient > 0.95, p-value < 2.2×10^{-16} with 0.01 tolerance rate; Figure S16.2). However, inference is less accurate for current or more recent ancestral effective population sizes (N_e, N_{e12}), the most recent split time (t_1) and migration rates between lineages A and C, and B and C (Pearson's correlation coefficient = 0.90 – 0.92, p-value < 2.2×10^{-16} with 0.01 tolerance rate), and non-informative for migration rate between lineages A and B (Pearson's correlation coefficient = 0.29, p-value = 0.006 with 0.01 tolerance rate). For migration rates between lineage A and C, and between B and C, cross-validation shows that for 'true' migration rates > 2×10^{-7}, the estimated migration rate is always > 0. The least stringent tolerance rate (0.01) was therefore used for inference from the empirical data, as this not only produced the most accurate estimates but also allowed us to use the largest number of simulations.

In addition, we performed a cross-validation analysis using the proportions of single derived sites (7 classes) instead of the 49 proportions of site configuration transitions of adjacent pairs of derived sites (7x7 matrix) to verify that linkage disequilibrium information improves parameter inference. Indeed, accuracy increases for all estimated parameters when using pairs of sites

compared to single sites with the proportion of recurrent mutations showing the largest improvement in accuracy (Figure S16.3).

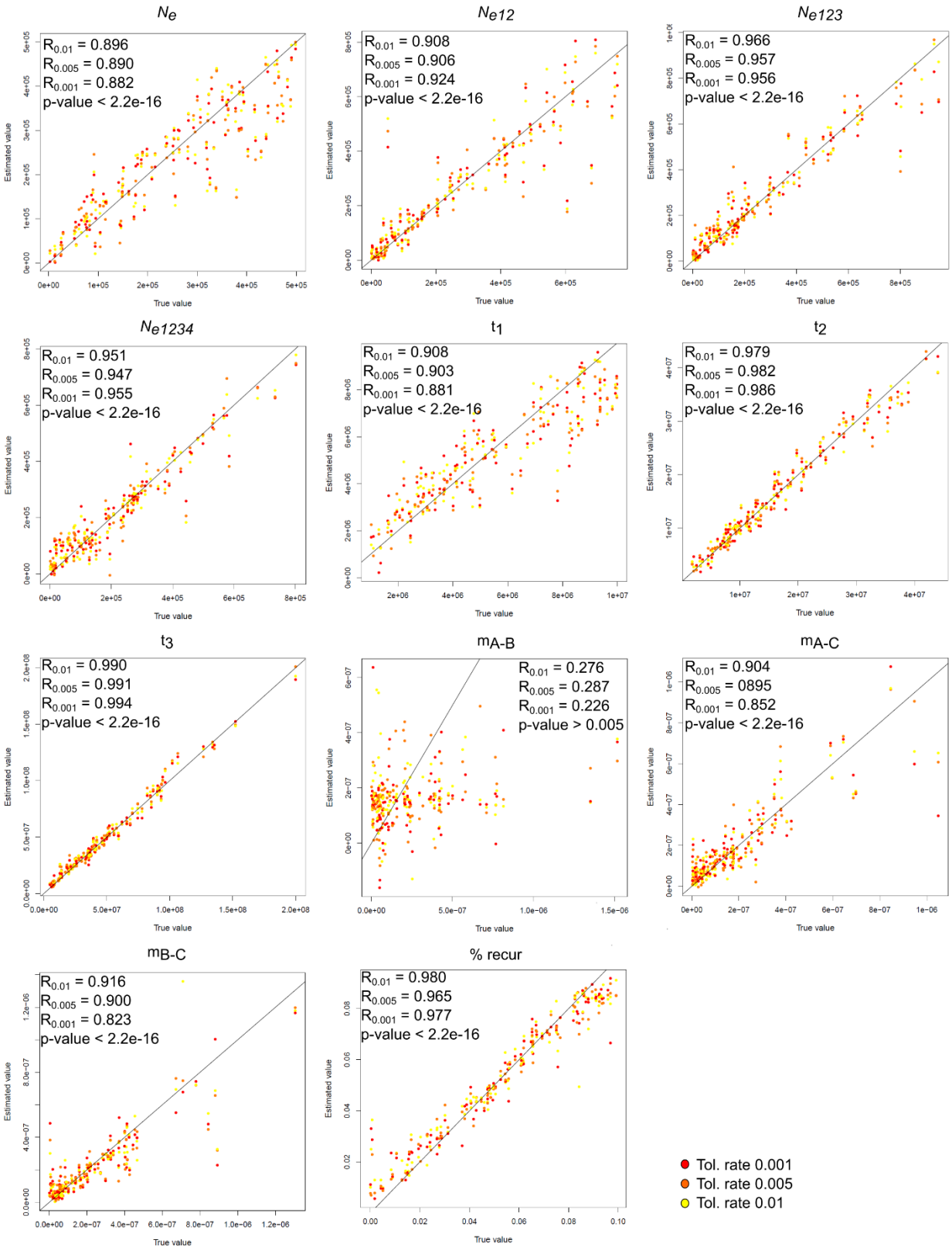

Figure S16.2. Cross-validation of parameter inference from 100 iterations. The following summary statistics were used: 49 proportions of derived site transitions, three *D*-statistics and

four divergence rate estimates. Colored dots from red to yellow represent increasing tolerance rates of 0.001, 0.005 and 0.01. Pearson's correlation coefficient (R) and significance (p-value) are given inside each plot for the three tolerance rates tested.

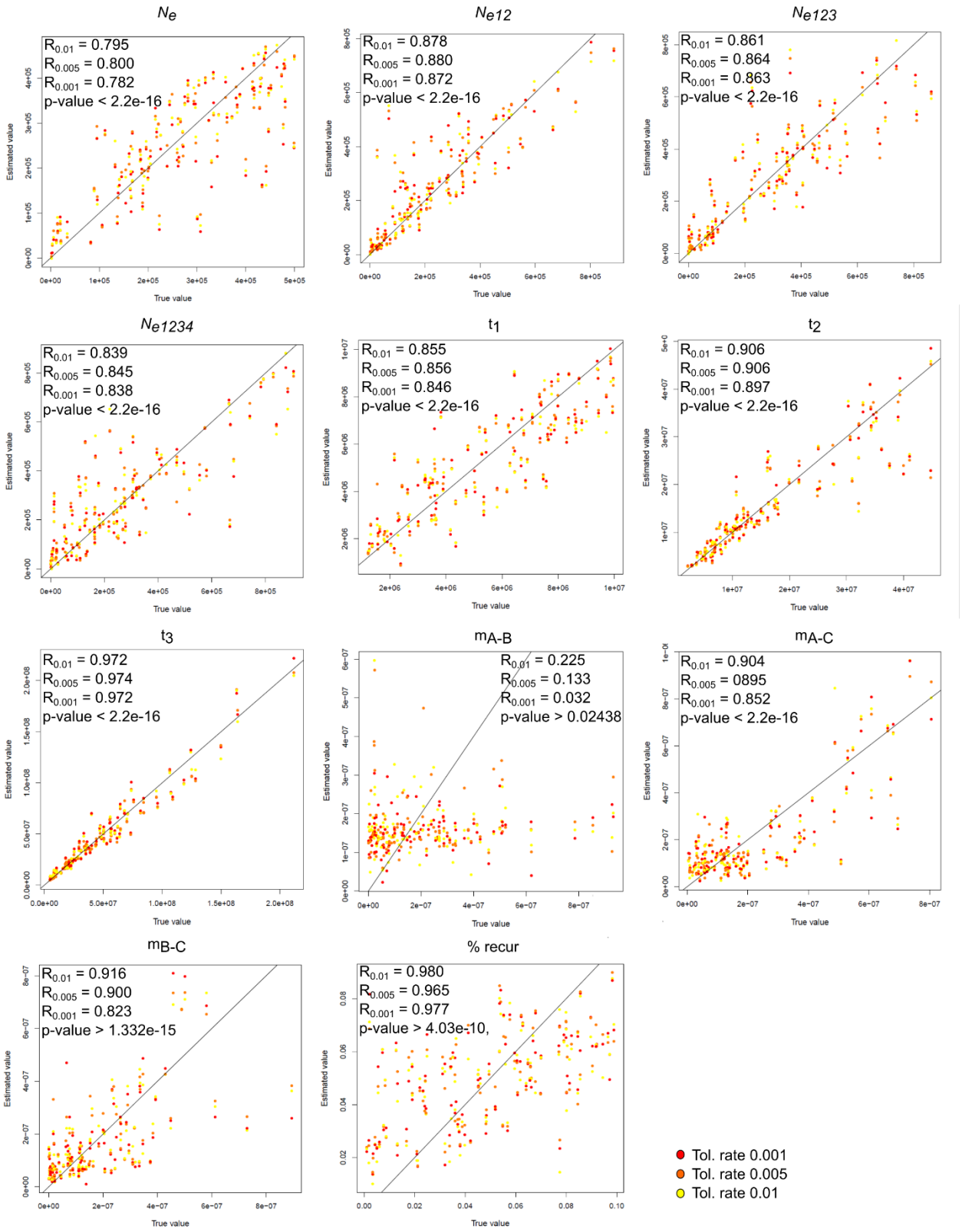

Figure S16.3. Cross-validation analysis exploring the accuracy of parameter inference under a different set of summary statistics: 7 proportions of single derived sites, three *D*-statistics, and

four divergence rate estimates. Results from 100 iterations are shown. Colored dots from red to yellow represent increasing tolerance rates of 0.001, 0.005 and 0.01. Pearson's correlation coefficient (R) and significance (p-value) are given inside each plot for the three tolerance rates tested.

We inferred posterior distributions for all parameters using the observed summary statistics from each four-taxon alignment (Table S16.2). Current or most recent N_e ranges from ~10,000 to 240,000 individuals (combined 95% highest credible intervals [CI]). Ancestral N_{e12} for *L. cyclotis* and *L. africana* ranges from ~13,300 to 229,000 individuals or 0.14 – 2.87 × N_e (95% CI of the N_{e12}/N_e ratio; Figure S16.4). N_{e123} for *L. cyclotis*, *L. africana* and *P. antiquus,* or N_{e12} for *L. cyclotis* and *P. antiquus* or *L. africana* and *P. antiquus* ranges from ~36,600 to 233,000 or 0.04 – 7.71 × N_e. Ancestral N_{e12} for *M. primigenius* and *M. columbi* ranges from ~7,600 to 29,900 individuals (0.22 – 2.26 × N_e), while N_{e123} for *M. columbi, M. primigenius* and *E. maximus,* or N_{e12} for the latter two ranges from ~10,300 to 130,000 (0.18 – 4.05 times N_e). N_{e123} for any three of *P. antiquus, L. africana*, *L. cyclotis* and *E. maximus* or *M. primigenius* ranges from ~6,650 to 105,000 individuals (0.06 – 2.64 × N_e). Ancestral N_{e1234} for all taxa including the outgroup *M. americanum* ranges from ~1,880 to 204,000 (0.05 – 18.51 × N_e).

The split time (t_1) between *L. cyclotis* and *L. africana* is estimated to have occurred ~5.11 - 1.98 million years ago (Mya) from the alignment of *L. africana_B, L. cyclotis_A/F, E. maximus_D/M. primigenius_Q, M. americanum,* and 8.96 - 3.71 Mya from the alignment of *L. africana_B, L. cyclotis_A/F, P. antiquus_N, M. americanum* (Table S16.2). The common ancestor of savanna and forest elephants is estimated to have split from *P. antiquus* (t_2) ~20.9 - 7.68 Mya or 1.12 – 4.59 × t_1 (95% CI of the t_2/t_1 ratio). However, when we infer the split time between *P. antiquus* and *L. africana* (t_2) we obtain more recent time ranges between ~5.24 - 2.09 Mya that overlap almost entirely the estimated split time between *L. cyclotis* and *L. africana* (t_1), and even more recent time ranges ~3.08 - 1.39 Mya for the split between *P. antiquus* and *L. cyclotis* (t_2). The discrepancy between the above estimates could at least partially be explained by the complex admixture history between these taxa (as suggested by the admixture graphs in Supplementary Note 12) as well as the fact that our inference is largely dependent on the assumed mutation rate and generation time. An accurate estimate of the proboscidean mutation rate is still lacking and both mutation rate and generation time could vary across lineages. Our parameter estimates are therefore associated with uncertainty, and although we cannot account for differences in mutation rate and generation time across lineages, we integrate out the uncertainty introduced by the assumed mutation rate by looking at ratios of parameters inferred from each alignment (e.g. t_2/t_1 and N_{e12}/N_e as reported above) and not only on direct estimates (Figure S16.4).

The split time between *M. columbi* and *M. primigenius* (t_3) is inferred to have occurred ~1.52 - 0.65 Mya and that between their common ancestor and *E. maximus* (t_4) to ~4.71 - 3.0 Mya or 2.16 – 6.21 × t_3. The inferred split time range between *M. primigenius* and *E. maximus* (t_4; ~5.16 - 2.18 Mya) is wider but consistent with the above range. The split time between the common ancestors of *P. antiquus*, *L. cyclotis*, *L. africana*, and *E. maximus*,*M. primigenius* (t_5) is estimated

to have occurred ~10.4 - 4.54 Mya or 1.31 – 4.14 × t_1 (where t_1 is the split time between *L. cyclotis* and *L. africana*), 1.28 – 5.35 × t_2 (where t_2 is the split time between *P. antiquus*, *L. cyclotis* and *L. africana*), and 1.20 – 3.92 × t_4 (where t_4 is the split time between *M. columbi, M. primigenius* and *E. maximus*; Figure S16.4).

The common ancestor of all elephantids is estimated to have split from *M. americanum* (t_6) ~28.4 - 10.4 Mya (except for the ranges obtained from the alignments of *L. africana_B, L. cyclotis_A/F, P. antiquus_N, M. americanum*, which are much older at ~59.2 - 16.7 Mya). This split time is 2.74 – 5.33 × t_4 (where t_4 is the split time between *M. columbi, M. primigenius* and *E. maximus*), 1.34 – 5.42 × t_2 (where t_2 is the split time between *P. antiquus*, *L. cyclotis* and *L. africana*), and 1.47 – 4.85 × t_5 (where t_5 is the split time between the common ancestor of *P. antiquus*, *L. cyclotis* and *L. africana* and the common ancestor of *E. maximus* and *M. primigenius*).

Our estimate of the elephantid-mastodon split time (~28.4 - 10.4 Mya) encompasses the age of the earliest known mammutid fossil remain (85) (28 – 24 Mya), although the lower bound of our range is much younger. The split between *Loxodonta*, *Elephas* and *Mammuthus*, dated to 9 - 4.2 Mya based on the fossil record (as justified in Rohland *et al.* (4)), largely overlaps the range inferred by our model (10.4 - 4.54 Mya). Compared to the ratios of population divergence times estimated from MCMCcoal by Rohland *et al.* (4), our estimated ratios have wider ranges but almost entirely encompass them. For instance, the ratio of the split time between forest and savanna elephant (t_2), and the split time between forest-savanna and Asian-mammoth (t_5) is estimated to be 0.45 – 0.79 (90% CI) by Rohland *et al.* (4) compared to ~0.24 – 0.77 (95% CI) by our model (Table S16.2). Similarly, the ratio of the split time between Asian elephant and woolly mammoth (t_4) and the split between forest-savanna and Asian-mammoth (t_5) is estimated to be 0.46 – 0.74 by Rohland *et al.* (4) compared to ~0.25 – 0.71 by our model.

Although we would expect to obtain estimates with more narrow ranges since we use a larger genome-wide dataset than that in Rohland *et al.* (4), the inclusion of migration rate parameters in our models could result in higher uncertainty in the inference of all other parameters, including split times. Given that the ABC analysis simultaneously tries to fit all parameters of the model to the observed data, uncertainty in the inference of migration rates may have an effect on the estimation of split times and effective population sizes. We plotted the joint posterior distribution of migration rates and split times (τ) measured in $4N_e$ × generation time units to test this effect. We find weak positive or no significant correlation between split times (τ) and migration rate between lineages A and B (|Pearson's correlation coefficient| < 0.18; p-value = 5.75×10^{-9}; Figure S16.5). Migration rate between lineages A and C, and B and C on the other hand, are as expected negatively correlated to split times (τ), since older split times generate more divergence while higher migration rates create the opposite effect, and the degree of correlation depends on the inferred migration rate, with higher estimates exhibiting increased correlation coefficients. For instance, the migration rate between *P. antiquus_N* and *M. primigenius_Q* (95% CI: 2.06×10^{-7} – 6.09×10^{-7}; proportion of migrants per generation, as estimated from the alignment of *P.*

antiquus_N, L. cyclotis_A, M. primigenius_Q, M. americanum) is negatively correlated to τ_1, τ_2 and τ_3 (|Pearson's correlation coefficient| > 0.35; p-value < 2.2×10^{-16}), whereas the migration rate between *L. cyclotis_A* and *M. primigenius_Q* (95% CI: 9.52×10^{-10} – 2.7×10^{-07}) is still negatively correlated to τ_1, τ_2 and τ_3 but not as strongly (|Pearson's correlation coefficient| < 0.15; p-value < 1.94×10^{-3}; Figure S16.5).

The effect of migration rates between lineages A and C, and B and C on the inference of split times could explain the wide ranges obtained for the latter parameters. As shown in Figures S16.6 – S16.22, the posterior distributions obtained for the migration rate between lineages A and B in the four-taxon alignments do not differ substantially from the prior distribution, suggesting that our summary statistics are non-informative for this particular parameter (also shown from the cross-validation analysis in Figure S16.2). This could potentially also add uncertainty in the inference of all other parameters, although we find only weak or no significant bias introduced by this parameter. Due to this, we restrain from making inferences for gene flow between lineages A and B.

The highest migration (i.e. gene flow) rates are inferred between *L. cyclotis_F* and *P. antiquus_N* (95% CI: 5.89×10^{-7} – 1.49×10^{-6} proportion of migrants per generation; Table S16.2), and *L. cyclotis_A* and *P. antiquus_N* (4.88×10^{-7} – 1.23×10^{-6}). Possible gene flow is also inferred between *P. antiquus_N* and *E. maximus_D* (1.32×10^{-7} – 5.71×10^{-7}), and between *P. antiquus_N* and *M. primigenius_Q* (1.84×10^{-7} – 6.44×10^{-7}). However, posterior distributions of migration rates inferred from different four-taxon alignments are rather wide. For instance, the migration rate between *P. antiquus_N* and *M. primigenius_Q* is estimated to have been 2.45×10^{-7} – 6.41×10^{-7} from the alignment of *P. antiquus_N, L. cyclotis_F, M. primigenius_Q, M. americanum*, and 0 – 2.91×10^{-7} from the alignment of *E. maximus_D, M. primigenius_Q, P. antiquus_N, M. americanum*. We do not consider the migration rate ranges inferred for all other pairs of taxa as 'true' gene flow since their median estimates are below 2.0×10^{-7}, the threshold above which our model can detect migration based on the cross-validation analysis (Figure S16.2).

Recurrent mutations comprise 2.11 – 7.04% of polymorphic sites in our four-taxon alignments.

We performed posterior predictive checks to test whether the obtained posterior distributions fit our data. We used estimates from the weighted distribution of all parameters from each four-taxon alignment as priors to simulate 1,000 datasets under the model described in Figure S16.1, and computed their summary statistics. We then plotted the distribution of summary statistics from the simulated datasets together with the observed summary statistic estimates for each of the four-taxon alignments. Figures S16.23 – S16.39 show that the observed summary statistic estimates fall within the posterior distribution of summary statistics in the majority of the four-taxon alignments, confirming that the estimated parameter ranges fit our data. There are three alignments for which observed estimates for some of the summary statistics do not fit well with the distribution of simulated summary statistics, but they are still overlapping (*L. africana_B, L.*

cyclotis_A/F, P. antiquus_N, M. americanum and *M. columbi_U, M. primigenius_Q, E. maximus_D, M. americanum*; Figures S16.33, S16.36, S16.39).

Table S16.2. Posterior distributions estimated from neural networks regression analysis on the observed data from the four-taxon alignments. The 95% highest density of the posterior distributions is given. The *N* parameters are effective population sizes (effective number of individuals in this time interval). The *t* parameters are split times in years. The *m* parameters are the proportion of migrants per generation in a bidirectional gene flow model. We assumed a mutation rate of 0.406×10^{-9} per site per year and 31 years per generation.

Parameter	N_e	N_{e12}	N_{e123}	N_{e1234}	t_1	t_2	t_3	m_{A-B}	m_{A-C}	m_{B-C}	% recur
1. P. antiquus_N, L. africana_B, E. maximus_D, M. americanum											
Weighted 2.5% perc.	45,479	40,486	14,244	9,460	2,184,620	5,479,117	11,888,200	4.63E-09	1.39E-07	5.03E-10	0.021
Weighted median	98,589	127,818	44,708	87,016	3,131,726	7,433,611	18,861,770	1.77E-07	2.81E-07	1.13E-07	0.033
Weighted mean	107,145	132,423	42,811	82,794	3,282,708	7,552,918	19,285,450	2.40E-07	2.94E-07	1.43E-07	0.033
Weighted mode	75,754	121,977	49,096	101,029	2,990,429	7,431,814	18,231,640	1.82E-07	3.25E-07	7.05E-08	0.033
Weighted 97.5% perc.	240,011	233,443	63,145	160,495	5,241,125	10,093,200	27,948,060	7.99E-07	5.57E-07	4.33E-07	0.047
2. P. antiquus_N, L. africana_B, M. primigenius_Q, M. americanum											
Weighted 2.5% perc.	38,092	36,561	8,651	7,198	2,088,031	5,399,129	12,221,630	1.61E-08	1.84E-07	2.82E-08	0.024
Weighted median	84,169	112,678	41,986	65,666	2,963,813	7,273,619	17,818,450	2.01E-07	3.56E-07	1.30E-07	0.033
Weighted mean	91,191	115,488	40,072	61,215	3,100,757	7,406,388	18,269,440	2.60E-07	3.69E-07	1.58E-07	0.034
Weighted mode	65,441	106,543	47,116	76,922	2,815,607	6,806,324	17,002,740	1.89E-07	4.01E-07	1.01E-07	0.033
Weighted 97.5% perc.	198,456	206,393	65,187	112,810	4,732,511	10,248,100	25,935,280	8.00E-07	6.44E-07	4.33E-07	0.047
3. P. antiquus_N, L. cyclotis_A, E. maximus_D, M. americanum											
Weighted 2.5% perc.	37,698	54,957	32,810	7,187	1,466,400	4,537,565	12,645,770	3.38E-08	1.32E-07	0.0E-00	0.021
Weighted median	81,940	97,858	72,096	68,351	2,000,684	6,066,246	17,700,230	2.07E-07	2.90E-07	8.33E-08	0.027

Weighted mean	91,710	96,933	70,120	66,729	2,050,557	6,109,506	17,987,490	2.70E-07	3.00E-07	9.89E-08	0.027
Weighted mode	69,177	108,828	80,118	73,046	1,977,158	5,485,069	17,302,380	8.09E-07	1.28E-07	5.42E-08	0.028
Weighted 97.5% perc.	208,694	141,751	102,377	124,776	2,842,287	8,064,117	24,307,050	8.18E-07	5.23E-07	2.76E-07	0.035
4. P. antiquus_N, L. cyclotis_A, M. primigenius_Q, M. americanum											
Weighted 2.5% perc.	36,324	49,200	34,881	7,110	1,518,353	4,962,507	13,363,120	4.03E-08	2.06E-07	9.52E-10	0.022
Weighted median	81,449	81,463	69,405	59,802	2,088,877	6,453,907	19,372,000	2.19E-07	3.69E-07	8.42E-08	0.028
Weighted mean	89,420	80,469	67,170	57,406	2,148,542	6,509,632	19,594,320	2.89E-07	3.80E-07	9.89E-08	0.028
Weighted mode	69,168	89,887	76,502	64,120	2,040,668	5,899,741	19,094,730	8.14E-07	2.34E-07	6.72E-08	0.029
Weighted 97.5% perc.	199,250	112,665	92,938	111,162	3,079,093	8,443,047	26,563,230	8.82E-07	6.09E-07	2.70E-07	0.036
5. P. antiquus_N, L. cyclotis_F, E. maximus_D, M. americanum											
Weighted 2.5% perc.	38,576	54,324	35,455	7,322	1,391,308	4,653,519	12,072,680	4.03E-08	1.85E-07	0.0E-00	0.023
Weighted median	80,254	96,802	73,061	66,299	1,886,638	6,118,503	17,551,060	2.12E-07	3.41E-07	8.52E-08	0.029
Weighted mean	89,416	95,885	70,342	63,676	1,932,520	6,162,743	17,846,820	2.78E-07	3.50E-07	1.01E-07	0.029
Weighted mode	68,513	108,365	80,489	71,838	1,774,473	5,651,941	16,809,190	8.18E-07	1.90E-07	6.38E-08	0.029
Weighted 97.5% perc.	199,156	140,719	97,284	121,037	2,719,947	7,969,187	24,957,740	8.39E-07	5.71E-07	2.77E-07	0.038
6. P. antiquus_N, L. cyclotis_F, M. primigenius_Q, M. americanum											
Weighted 2.5% perc.	33,899	52,944	35,346	7,264	1,388,644	4,703,446	14,172,020	5.89E-08	2.45E-07	0.0E-00	0.023
Weighted median	74,758	96,219	74,560	54,508	1,936,300	6,382,742	19,700,730	2.49E-07	4.07E-07	8.59E-08	0.030
Weighted mean	82,603	96,130	72,420	52,464	1,990,134	6,425,157	19,963,050	3.10E-07	4.17E-07	1.01E-07	0.030
Weighted	63,441	106,212	84,914	59,214	1,877,473	6,789,319	18,756,630	8.79E-07	2.64E-07	6.90E-08	0.030

mode											
Weighted 97.5% perc.	187,204	144,694	104,891	99,367	2,885,743	8,664,375	27,502,780	8.57E-07	6.41E-07	2.86E-07	0.039
7. E. maximus_D, M. primigenius_Q, P. antiquus_N, M. americanum											
Weighted 2.5% perc.	32,703	23,341	6,786	3,103	2,564,472	5,796,275	14,012,630	2.69E-09	0.0E-00	0.0E-00	0.025
Weighted median	73,892	65,303	45,388	52,890	3,563,074	7,635,082	20,927,730	1.39E-07	6.63E-08	7.24E-08	0.035
Weighted mean	85,966	65,910	44,784	53,370	3,646,926	7,720,262	21,057,950	1.98E-07	8.55E-08	8.25E-08	0.035
Weighted mode	58,665	76,741	48,117	53,188	3,329,987	7,286,226	19,073,510	3.97E-08	1.56E-07	8.16E-08	0.035
Weighted 97.5% perc.	213,767	117,577	78,184	116,175	5,164,588	10,056,920	28,361,500	7.05E-07	2.91E-07	2.34E-07	0.047
8. E. maximus_D, M. primigenius_Q, L. africana_B, M. americanum											
Weighted 2.5% perc.	37,039	24,736	18,111	4,124	2,356,605	5,986,299	12,850,350	0.0E-00	0.0E-00	0.0E-00	0.025
Weighted median	77,519	71,083	44,946	53,315	3,238,927	7,919,292	20,042,050	1.42E-07	7.22E-08	7.95E-08	0.035
Weighted mean	91,412	71,851	43,630	51,960	3,322,753	8,006,050	20,308,030	2.08E-07	9.27E-08	9.29E-08	0.035
Weighted mode	63,680	61,961	47,396	59,826	3,028,804	7,392,929	17,960,490	2.23E-09	1.64E-07	9.33E-08	0.032
Weighted 97.5% perc.	217,609	128,972	61,085	107,581	4,638,494	10,398,070	28,052,550	7.96E-07	3.26E-07	2.93E-07	0.048
9. E. maximus_D, M. primigenius_Q, L. cyclotis_A, M. americanum											
Weighted 2.5% perc.	37,720	24,594	21,623	3,719	2,175,564	5,865,429	12,677,450	2.31E-09	0.0E-00	0.0E-00	0.028
Weighted median	78,511	70,663	44,167	53,970	2,997,542	7,576,180	19,234,660	1.47E-07	3.64E-08	2.56E-08	0.039
Weighted mean	93,038	71,196	43,008	51,485	3,096,104	7,650,378	19,482,090	2.11E-07	5.57E-08	3.55E-08	0.039
Weighted mode	64,684	82,283	46,680	61,148	2,886,956	7,403,180	17,364,780	2.51E-08	1.15E-07	3.56E-08	0.037
Weighted 97.5% perc.	230,628	124,545	57,240	105,131	4,403,303	9,773,308	26,865,450	7.81E-07	2.78E-07	2.24E-07	0.054

10. E. maximus_D, M. primigenius_Q, L. cyclotis_F, M. americanum

Weighted 2.5% perc.	37,289	26,450	23,026	3,894	2,193,573	5,857,843	13,449,270	1.15E-08	0.0E-00	0.0E-00	0.027
Weighted median	78,484	70,535	43,681	53,464	3,019,282	7,494,946	19,711,730	1.44E-07	5.46E-08	5.00E-08	0.037
Weighted mean	92,222	71,233	42,633	51,193	3,114,582	7,562,489	19,813,260	2.08E-07	7.22E-08	6.23E-08	0.038
Weighted mode	63,811	83,008	46,125	59,252	2,902,313	7,084,693	17,748,840	4.32E-08	1.27E-07	6.12E-08	0.035
Weighted 97.5% perc.	223,456	129,611	55,769	104,762	4,403,938	9,584,226	26,204,620	7.60E-07	2.93E-07	2.56E-07	0.051

11. *L. africana_B, L. cyclotis_A, P. antiquus_N, M. americanum*

Weighted 2.5% perc.	41,736	23,690	6,731	3,198	3,712,808	7,848,476	16,807,390	4.14E-08	0.0E-00	4.88E-07	0.039
Weighted median	79,229	91,300	72,759	73,530	6,232,371	11,190,990	33,087,750	1.97E-07	8.95E-08	7.51E-07	0.054
Weighted mean	82,830	92,275	72,227	80,238	6,165,562	11,815,050	34,700,110	2.48E-07	1.08E-07	7.76E-07	0.055
Weighted mode	72,676	98,557	83,827	25,916	6,752,823	10,259,360	25,484,800	2.62E-07	7.87E-08	9.62E-07	0.052
Weighted 97.5% perc.	148,332	174,297	157,821	203,036	8,333,199	18,078,250	59,176,740	7.20E-07	3.26E-07	1.23E-06	0.070

12. L. africana_B, L. cyclotis_A, E. maximus_D, M. americanum

Weighted 2.5% perc.	40,232	34,410	7,369	6,471	2,325,976	5,721,849	11,052,440	0.0E-00	3.58E-08	2.55E-10	0.033
Weighted median	85,495	90,904	34,633	77,410	3,312,314	7,660,807	17,160,810	1.52E-07	1.56E-07	1.07E-07	0.043
Weighted mean	97,349	92,115	33,097	73,081	3,386,543	7,842,574	17,486,850	2.12E-07	1.69E-07	1.28E-07	0.043
Weighted mode	69,114	89,264	43,650	89,714	3,292,393	7,448,751	16,166,520	1.60E-07	1.78E-07	4.69E-08	0.044
Weighted 97.5% perc.	228,545	159,078	54,046	139,067	5,114,276	10,437,390	23,945,050	7.96E-07	3.92E-07	3.65E-07	0.052

13. L. africana_B, L. cyclotis_A, M. primigenius_Q, M. americanum

Weighted 2.5% perc.	34,675	29,339	7,195	6,494	2,176,373	5,159,273	10,643,290	0.0E-00	2.97E-08	2.11E-09	0.031

Weighted median	75,170	82,237	33,595	70,410	3,096,413	7,075,420	16,516,000	1.59E-07	1.58E-07	1.14E-07	0.040
Weighted mean	85,857	83,790	32,431	66,323	3,166,898	7,213,332	16,807,050	2.19E-07	1.69E-07	1.33E-07	0.040
Weighted mode	60,881	79,128	41,795	78,694	3,069,228	6,933,846	15,632,890	1.66E-07	1.78E-07	5.03E-08	0.041
Weighted 97.5% perc.	203,594	150,471	52,711	125,305	4,849,201	9,722,495	23,028,830	7.93E-07	3.91E-07	3.86E-07	0.049
14. *L. africana_B, L. cyclotis_F, P. antiquus_N, M. americanum*											
Weighted 2.5% perc.	31,850	14,123	4,966	2,160	3,557,391	7,676,109	18,323,400	5.49E-08	0.0E-00	5.89E-07	0.037
Weighted median	68,207	88,248	65,993	68,710	6,495,954	11,832,580	32,622,900	1.90E-07	9.36E-08	9.03E-07	0.053
Weighted mean	73,225	93,909	65,545	75,433	6,429,358	12,571,900	33,231,020	2.37E-07	1.16E-07	9.38E-07	0.053
Weighted mode	62,178	64,357	67,985	22,207	7,034,961	10,718,030	28,195,090	2.43E-07	8.66E-08	1.14E-06	0.050
Weighted 97.5% perc.	145,816	228,958	140,953	204,274	8,964,653	20,897,130	50,942,650	6.91E-07	3.50E-07	1.49E-06	0.069
15. L. africana_B, L. cyclotis_F, E. maximus_D, M. americanum											
Weighted 2.5% perc.	38,799	34,582	10,060	7,209	2,102,554	5,467,218	10,441,520	0.0E-00	1.25E-08	0.0E-00	0.036
Weighted median	84,194	93,023	31,665	79,232	3,034,260	7,359,742	16,749,120	1.63E-07	1.51E-07	1.10E-07	0.046
Weighted mean	95,724	95,795	30,331	75,615	3,118,336	7,513,906	17,151,510	2.24E-07	1.65E-07	1.28E-07	0.046
Weighted mode	69,228	86,465	37,875	89,669	3,023,420	7,135,684	15,689,110	1.68E-07	1.94E-07	3.69E-08	0.046
Weighted 97.5% perc.	220,423	175,150	44,926	149,548	4,877,184	10,166,330	24,899,390	8.01E-07	4.34E-07	3.83E-07	0.060
16. L. africana_B, L. cyclotis_F, M. primigenius_Q, M. americanum											
Weighted 2.5% perc.	36,616	33,657	6,647	6,768	1,980,542	5,132,266	10,596,290	0.0E-00	2.66E-08	2.66E-10	0.036
Weighted median	78,424	88,474	31,405	67,592	2,851,071	6,917,917	15,999,630	1.73E-07	1.55E-07	1.19E-07	0.045
Weighted	88,983	90,900	30,532	64,599	2,920,715	7,086,958	16,354,780	2.33E-07	1.69E-07	1.36E-07	0.045

mean											
Weighted mode	64,963	80,489	34,734	71,298	2,806,816	6,736,908	14,910,660	1.66E-07	1.88E-07	4.51E-08	0.045
Weighted 97.5% perc.	200,799	161,832	50,700	123,022	4,496,703	9,578,250	23,020,070	7.99E-07	3.99E-07	3.74E-07	0.055
17. M. columbi_U, M. primigenius_Q, E. maximus_D, M. americanum											
Weighted 2.5% perc.	9,999	7,596	10,253	1,876	653,956	2,998,074	11,462,370	0.0E-00	4.89E-08	6.33E-08	0.021
Weighted median	21,692	22,003	25,472	13,291	965,518	3,799,964	15,770,090	1.20E-07	1.63E-07	1.83E-07	0.029
Weighted mean	25,166	20,923	25,036	13,829	1,005,156	3,806,179	15,735,640	1.95E-07	1.74E-07	1.89E-07	0.029
Weighted mode	19,142	23,252	27,816	13,984	917,991	3,811,833	14,836,830	4.77E-07	1.60E-07	1.49E-07	0.028
Weighted 97.5% perc.	61,800	29,934	39,343	28,252	1,518,831	4,714,653	19,621,340	7.89E-07	3.63E-07	3.65E-07	0.038

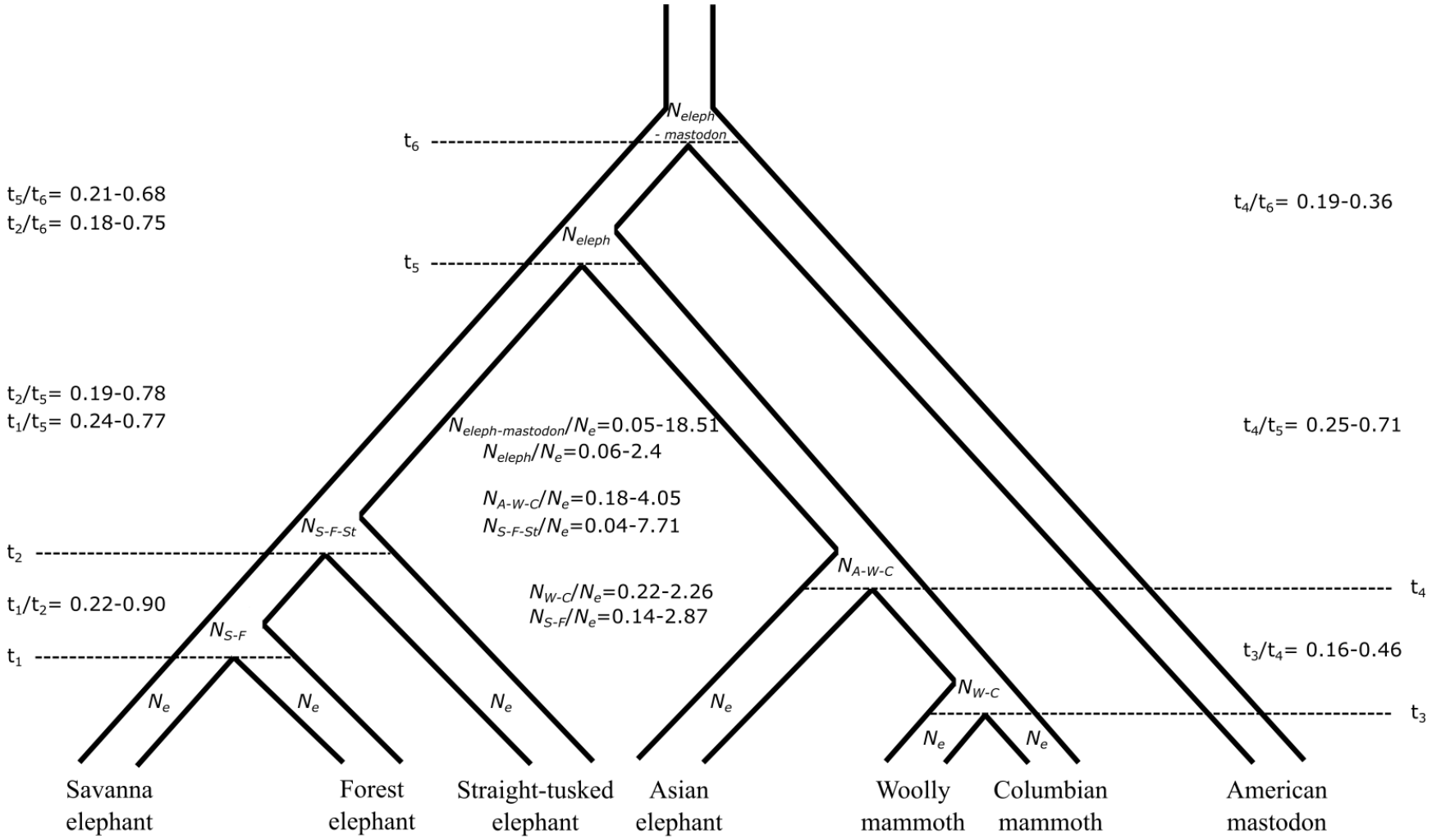
N_{eleph} - mastodon
t_6
t_5/t_6= 0.21-0.68
t_2/t_6= 0.18-0.75
t_4/t_6= 0.19-0.36
N_{eleph}
t_5
t_2/t_5= 0.19-0.78
t_1/t_5= 0.24-0.77
t_4/t_5= 0.25-0.71
$N_{eleph-mastodon}/N_e$=0.05-18.51
N_{eleph}/N_e=0.06-2.4
N_{A-W-C}/N_e=0.18-4.05
N_{S-F-St}/N_e=0.04-7.71
N_{S-F-St}
t_2
N_{A-W-C}
t_4
N_{W-C}/N_e=0.22-2.26
N_{S-F}/N_e=0.14-2.87
t_1/t_2= 0.22-0.90
N_{S-F}
t_3/t_4= 0.16-0.46
t_1
N_{W-C}
t_3
N_e
N_e
N_e
N_e
N_e
N_e
Savanna elephant
Forest elephant
Straight-tusked elephant
Asian elephant
Woolly mammoth
Columbian mammoth
American mastodon

Figure S16.4. Posterior distributions of effective population size and split time parameter ratios from all four-taxon alignments. The 95% highest density of the union of posterior distribution ratios is shown. N_e indicates current or most recent effective population size. Remaining *N* parameters in this figure indicate effective population size of ancestral populations, for example $N_{S\text{-}F}$ indicates the effective population size of the ancestral population of savanna and forest elephants, and N_{eleph} refers to the effective population size of the ancestral populations of all elephantids. Population split times are indicated by t, for example t_1 indicates the split time between savanna and forest elephants.

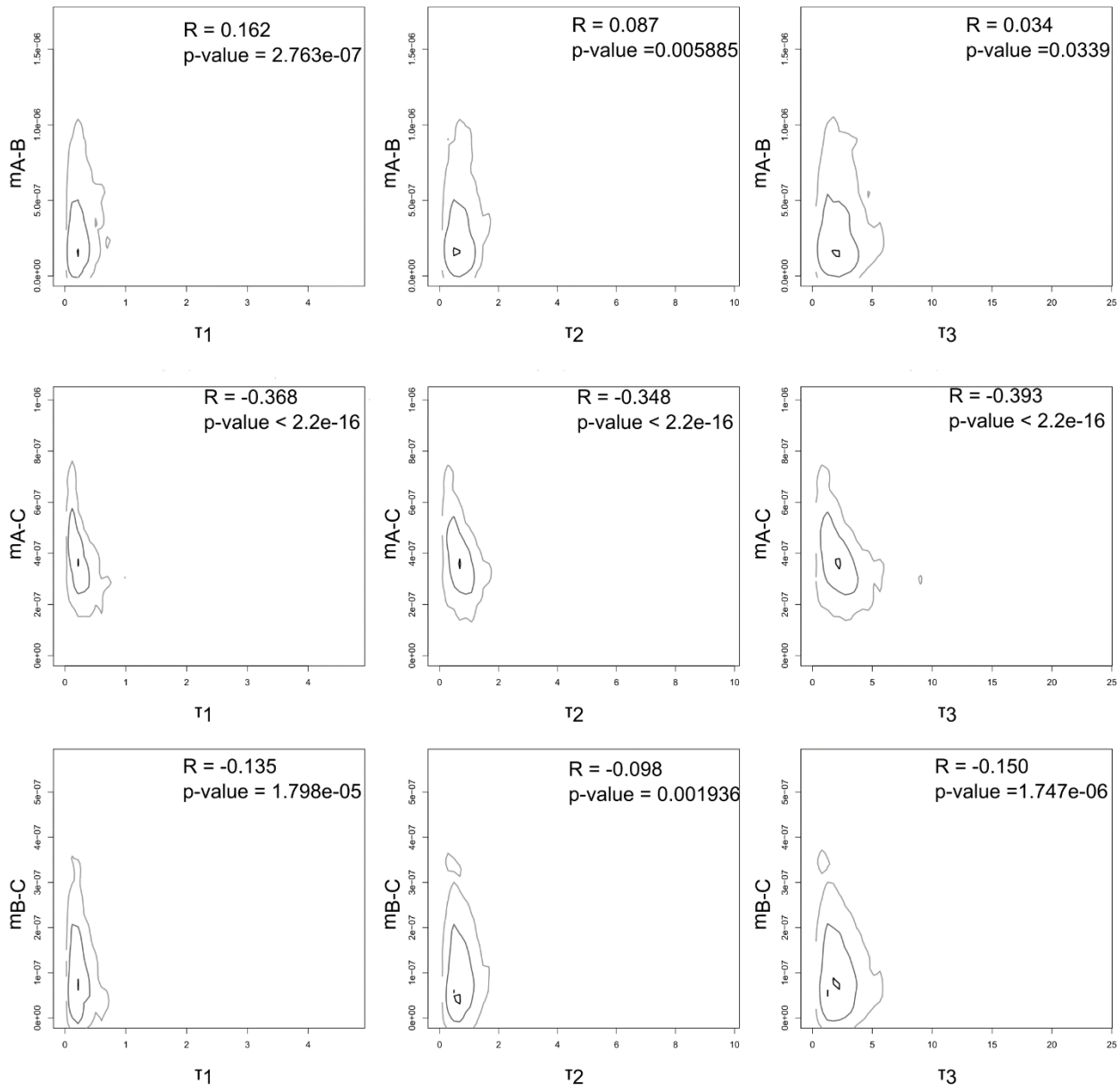

Figure S16.5. Joint posterior distributions of migration rates and split times (measured in 4*N_e*generation time units) as estimated from the alignment of *P. antiquus_N, L. cyclotis_A, M. primigenius_Q, M. americanum* (respectively A, B, C, O). $m_{A\text{-}B}$ indicates migration rate between taxa A and B, and τ_1 , τ_2, τ_3, split times measured in 4*N_e*generation time units between taxa A and B, A and C, B and C, respectively. Light gray, gray and black curves correspond to the 95%, 70% and 5% of the highest marginal posterior density of the bivariate region.

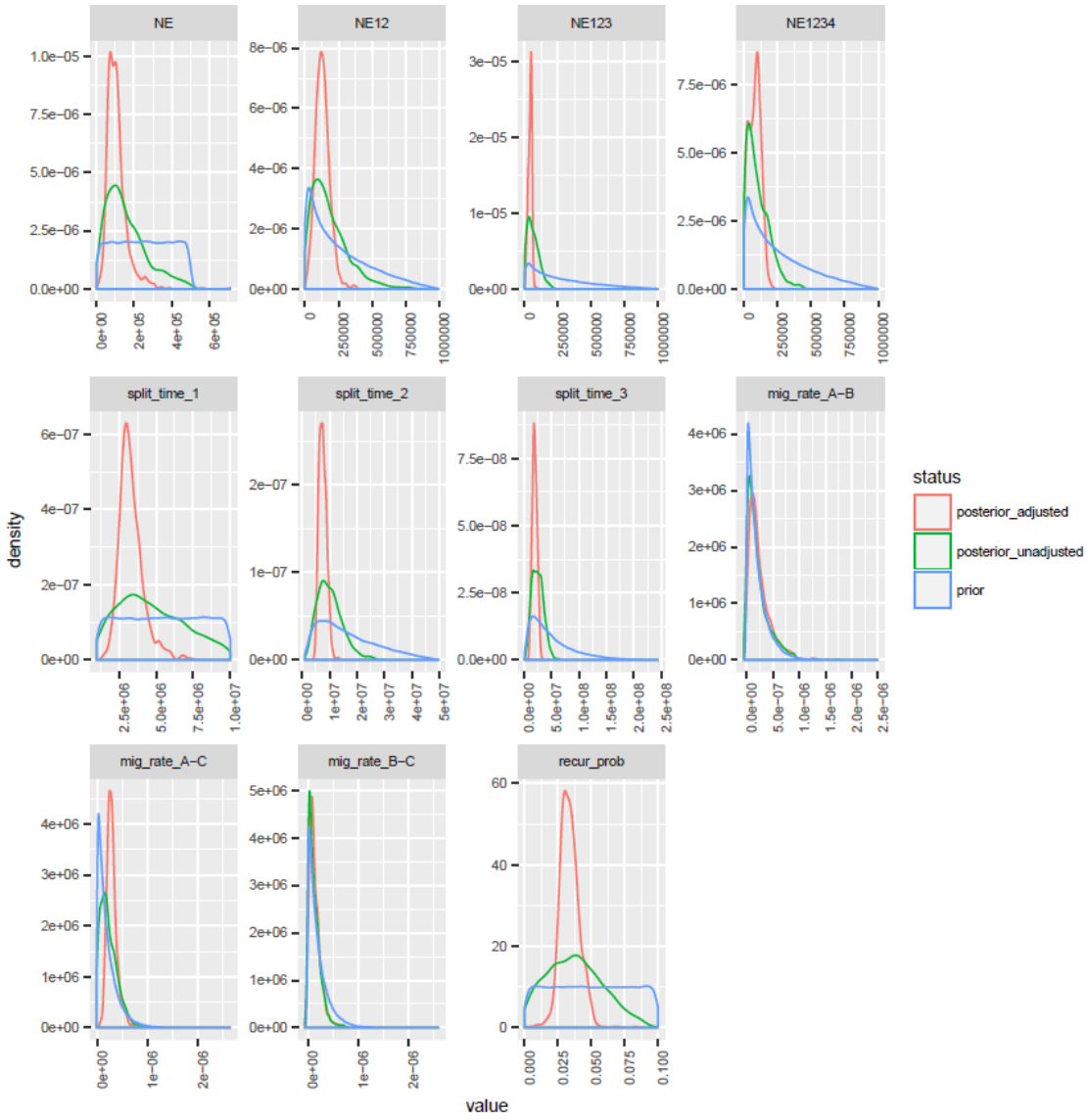

Figure S16.6. Posterior distributions of parameters inferred from the alignment of *P. antiquus_N, L. africana_B, E. maximus_D, M. americanum*. Prior distributions of parameter values are shown in blue. Posterior distributions without correction from the regression analysis are shown in green. Posterior distributions of parameter values adjusted by the regression analysis are shown in pink.

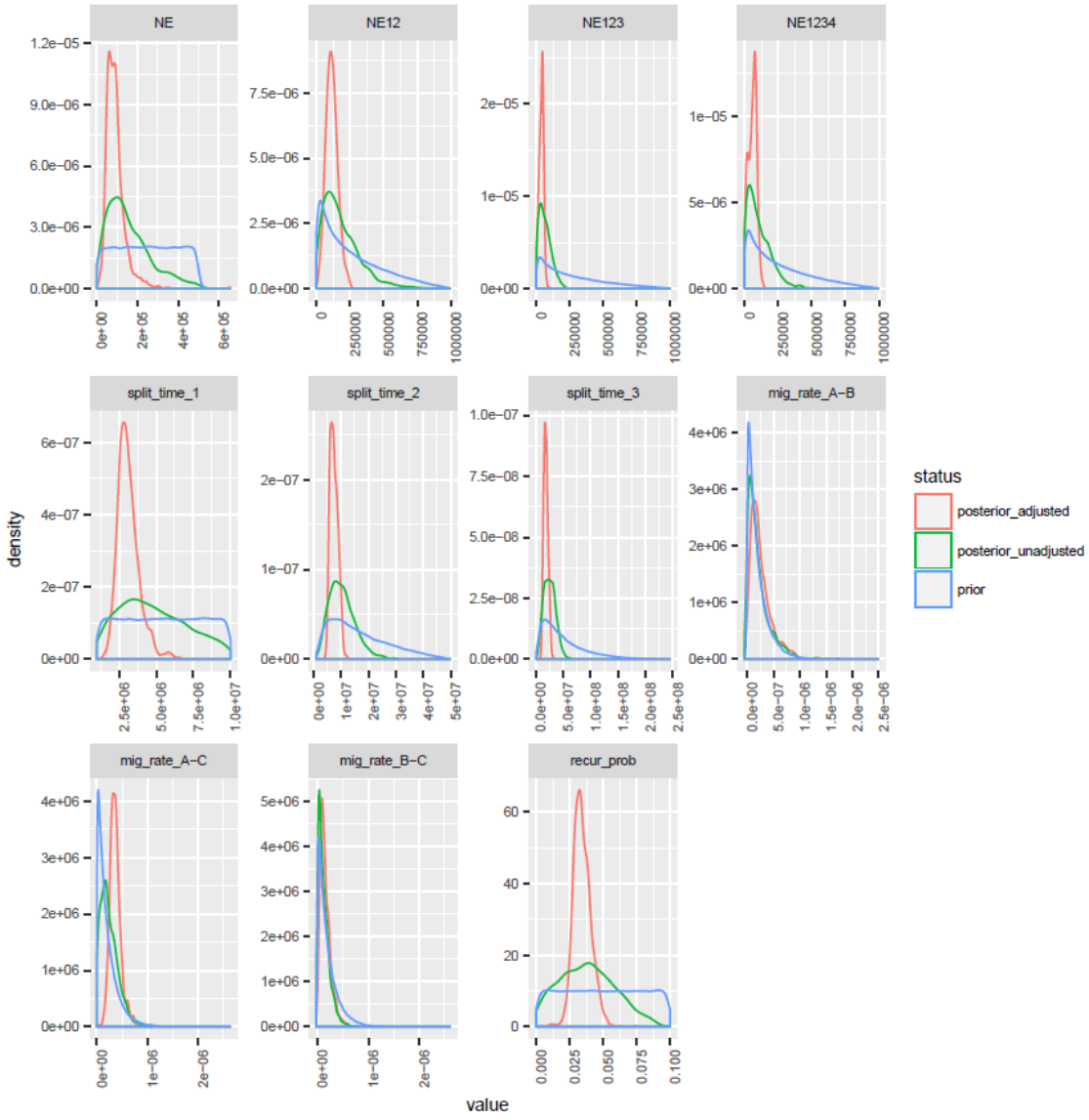

Figure S16.7. Posterior distributions of parameters inferred from the alignment of *P. antiquus_N, L. africana_B, M. primigenius_Q, M. americanum*. Prior and posterior distributions are as described in Figure legend S16.6.

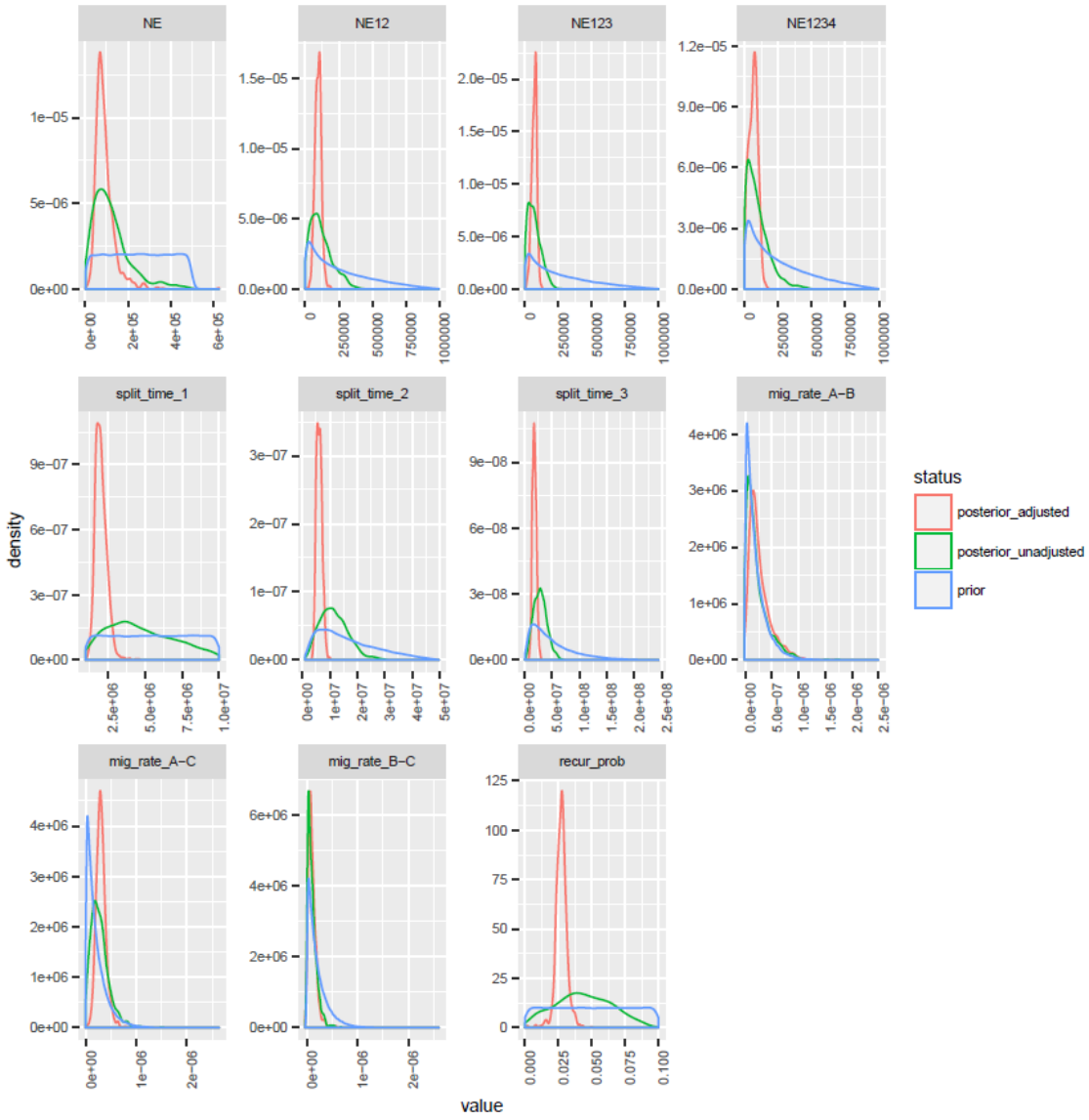

Figure S16.8. Posterior distributions of parameters inferred from the alignment of *P. antiquus_N, L. cyclotis_A, E. maximus_D, M. americanum*. Prior and posterior distributions are as described in Figure legend S16.6.

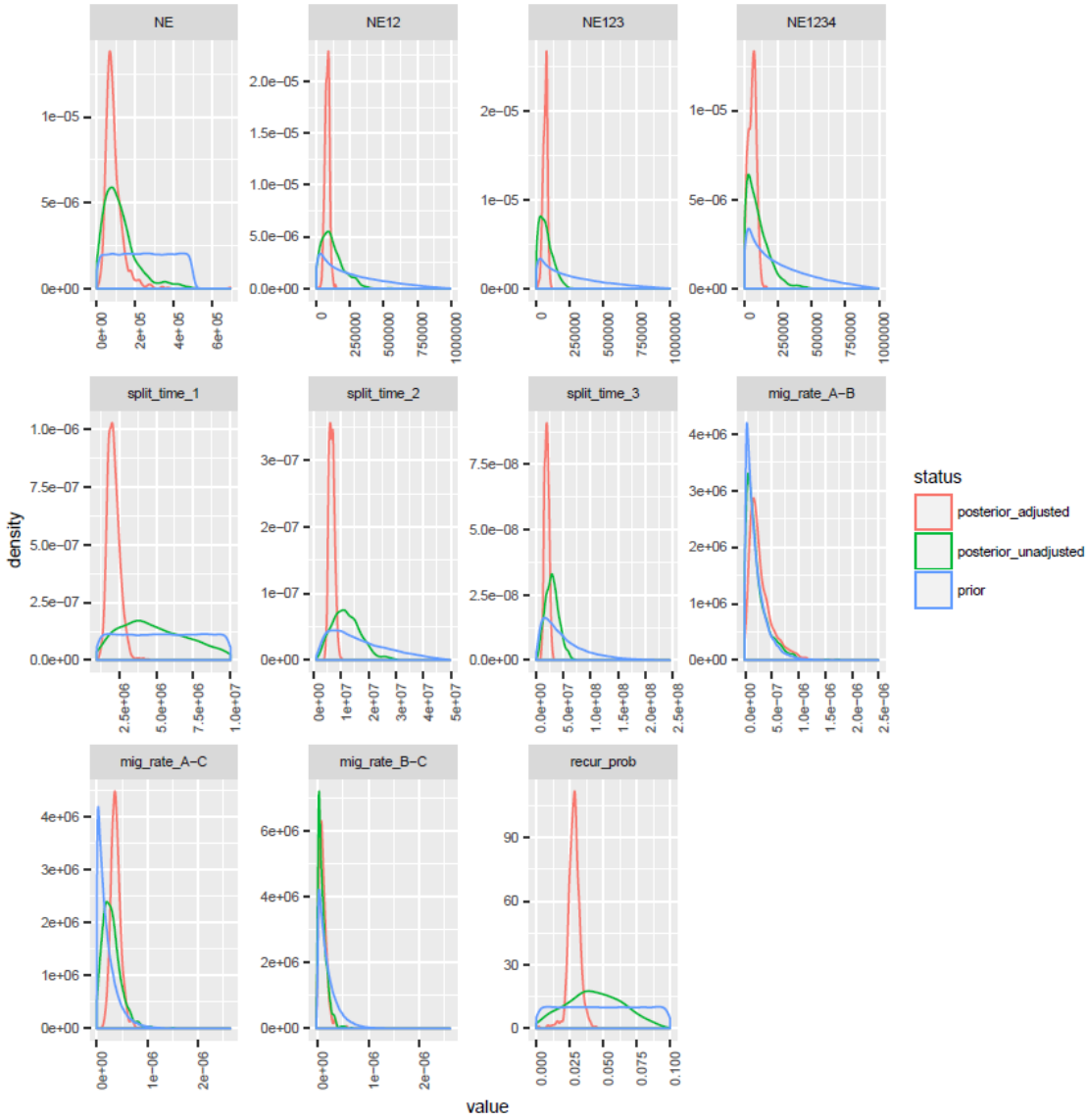

Figure S16.9. Posterior distributions of parameters inferred from the alignment of *P. antiquus_N, L. cyclotis_F, M. primigenius_Q, M. americanum*. Prior and posterior distributions are as described in Figure legend S16.6.

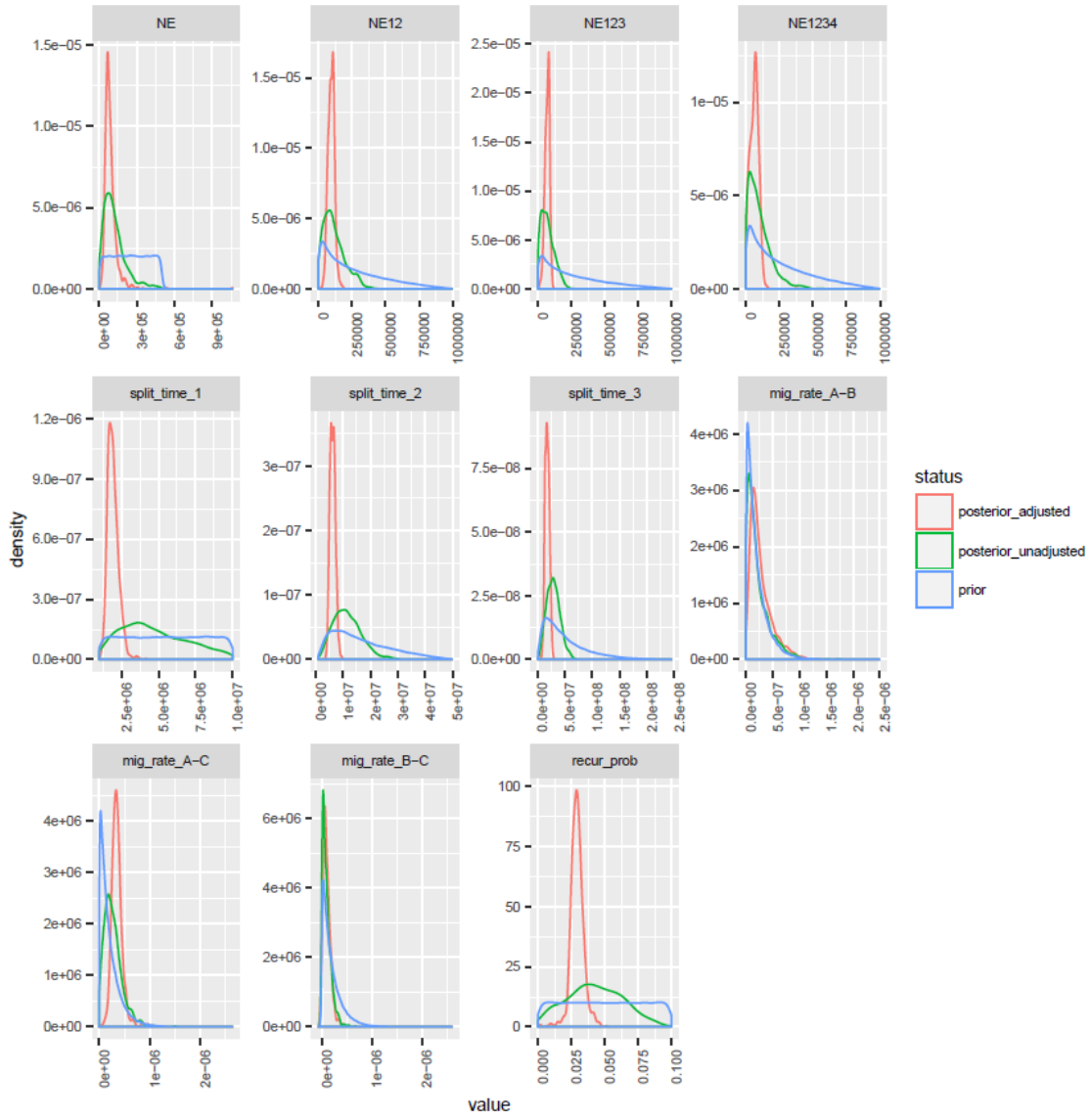

Figure S16.10. Posterior distributions of parameters inferred from the alignment of *P. antiquus_N, L. cyclotis_F, E. maximus_D, M. americanum*. Prior and posterior distributions are as described in Figure legend S16.6.

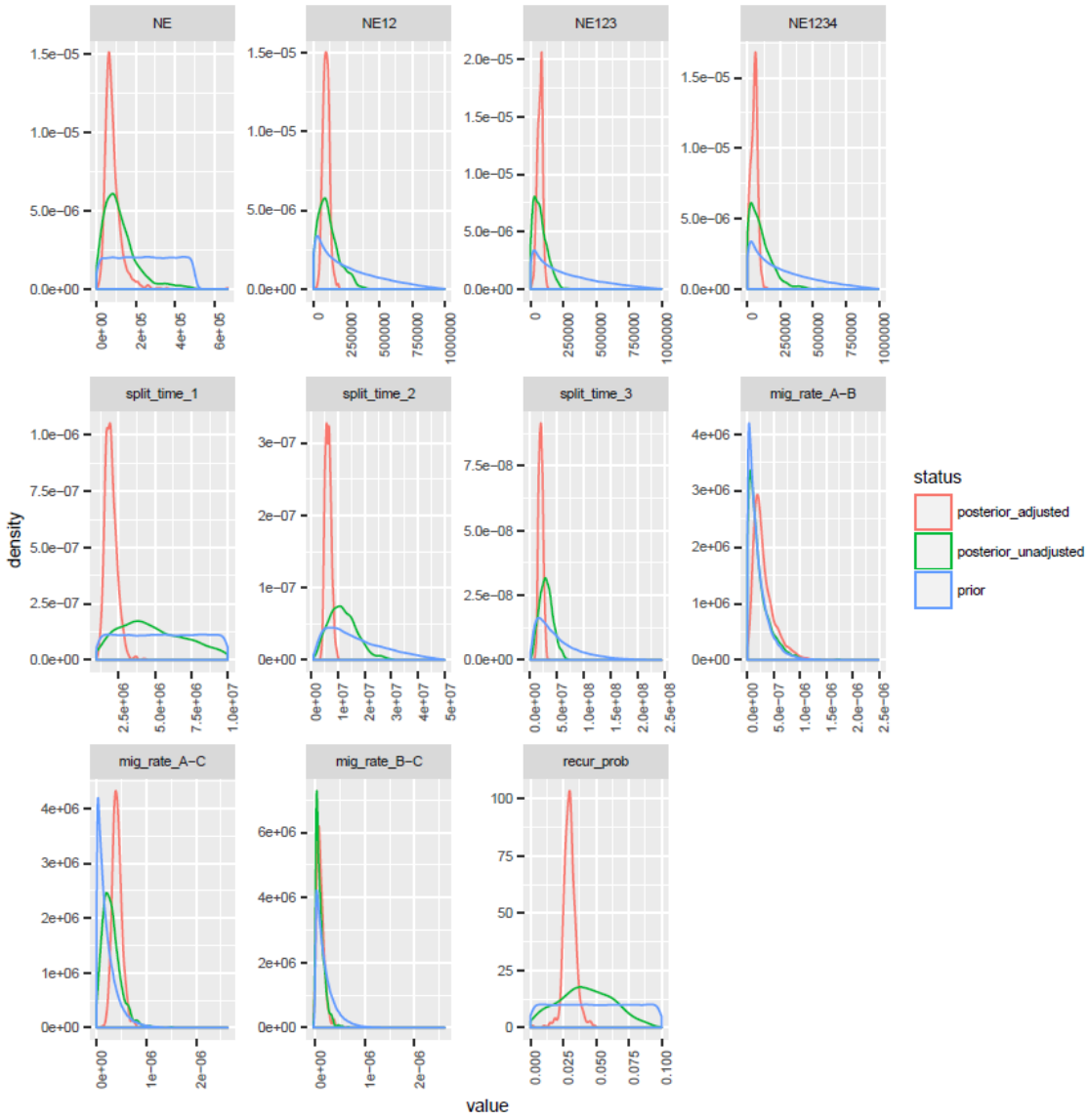

Figure S16.11. Posterior distributions of parameters inferred from the alignment of *P. antiquus_N, L. cyclotis_F, M. primigenius_Q, M. americanum*. Prior and posterior distributions are as described in Figure legend S16.6.

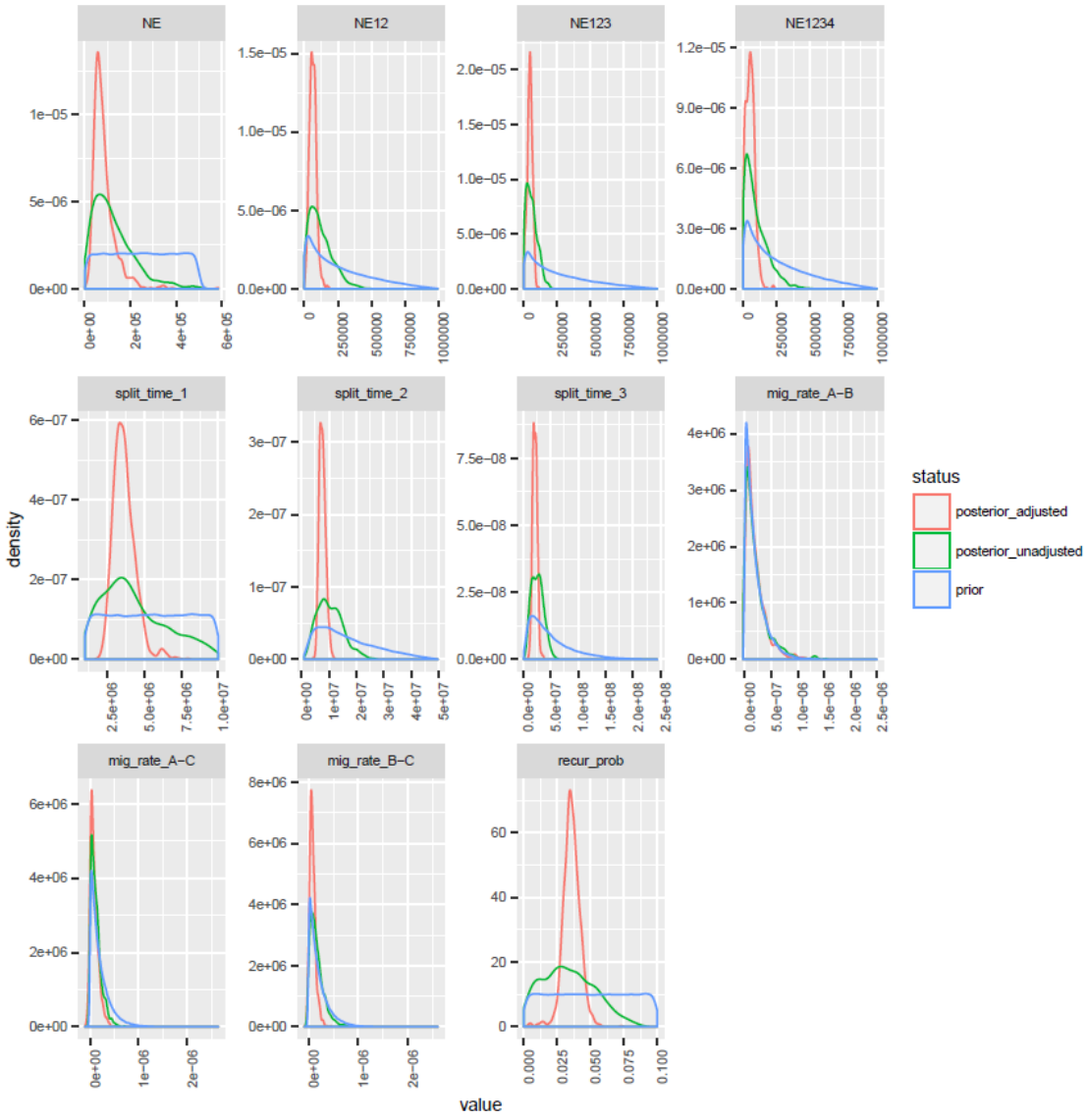

Figure S16.12. Posterior distributions of parameters inferred from the alignment of *E. maximus_D, M. primigenius_Q, P. antiquus_N, M. americanum*. Prior and posterior distributions are as described in Figure legend S16.6.

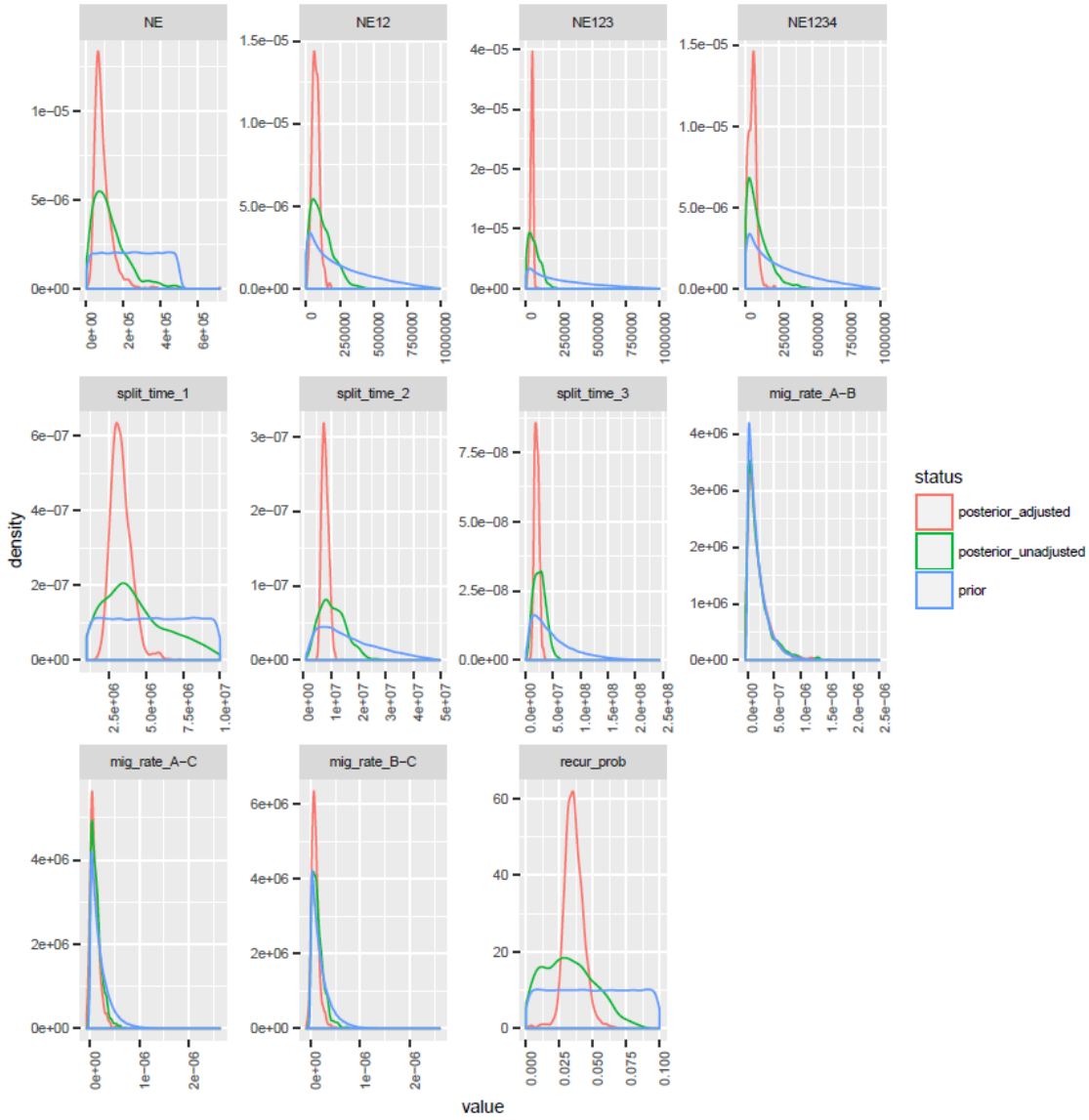

Figure S16.13. Posterior distributions of parameters inferred from the alignment of *E. maximus_D, M. primigenius_Q, L. africana_B, M. americanum*. Prior and posterior distributions are as described in Figure legend S16.6.

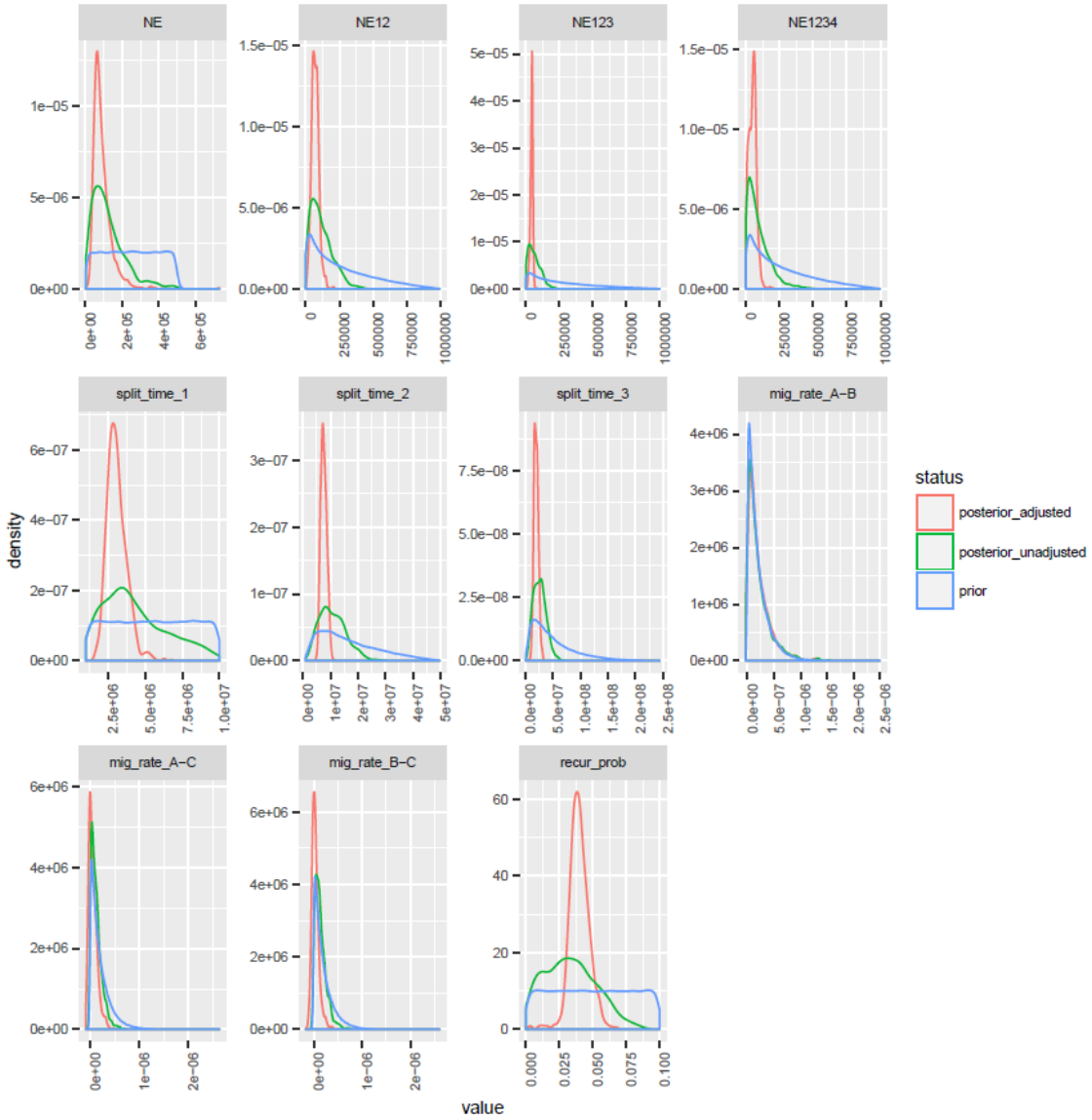

Figure S16.14. Posterior distributions of parameters inferred from the alignment of *E. maximus_D, M. primigenius_Q, L. cyclotis_A, M. americanum*. Prior and posterior distributions are as described in Figure legend S16.6.

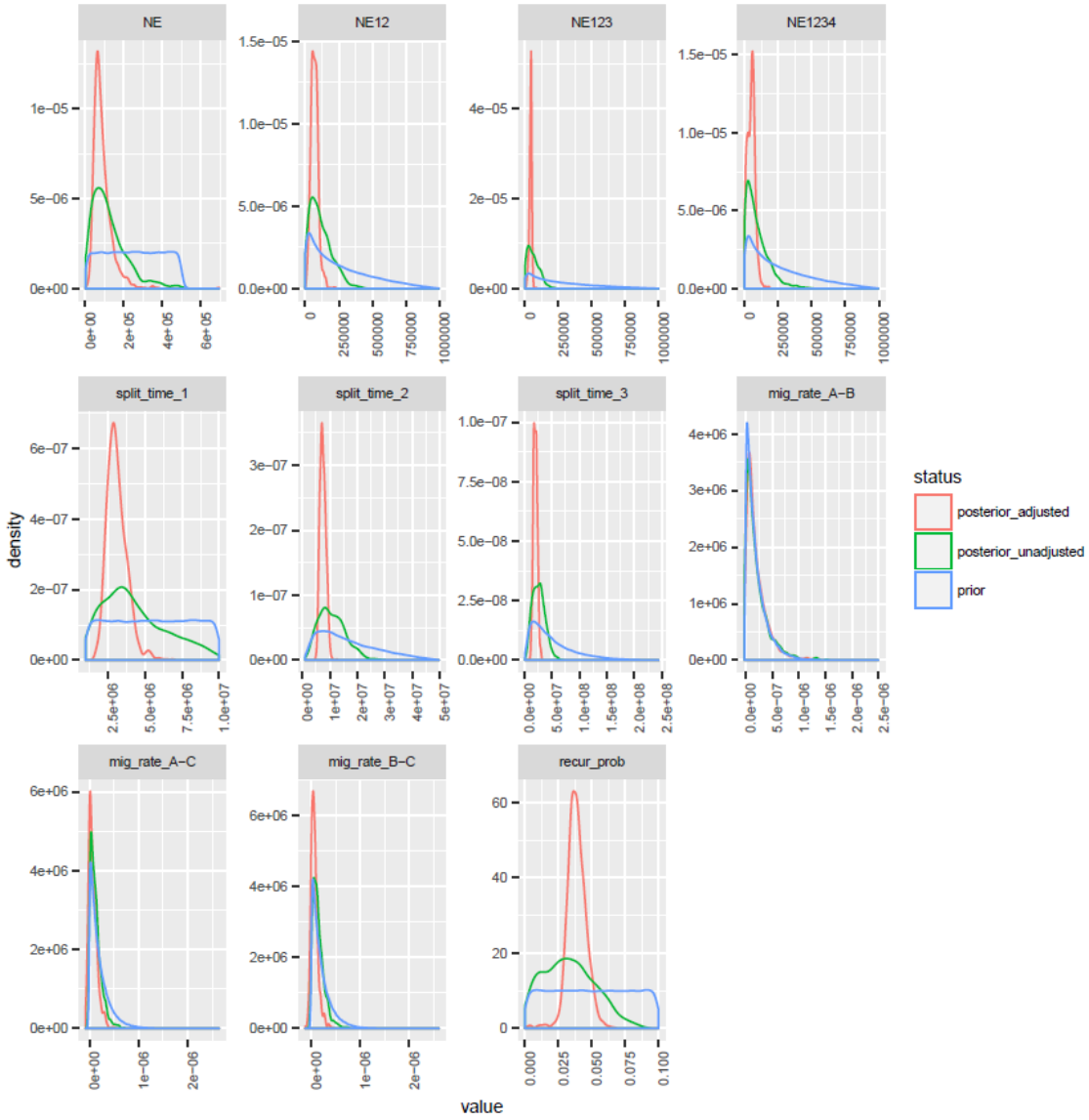

Figure S16.15. Posterior distributions of parameters inferred from the alignment of *E. maximus_D, M. primigenius_Q, L. cyclotis_F, M. americanum*. Prior and posterior distributions are as described in Figure legend S16.6.

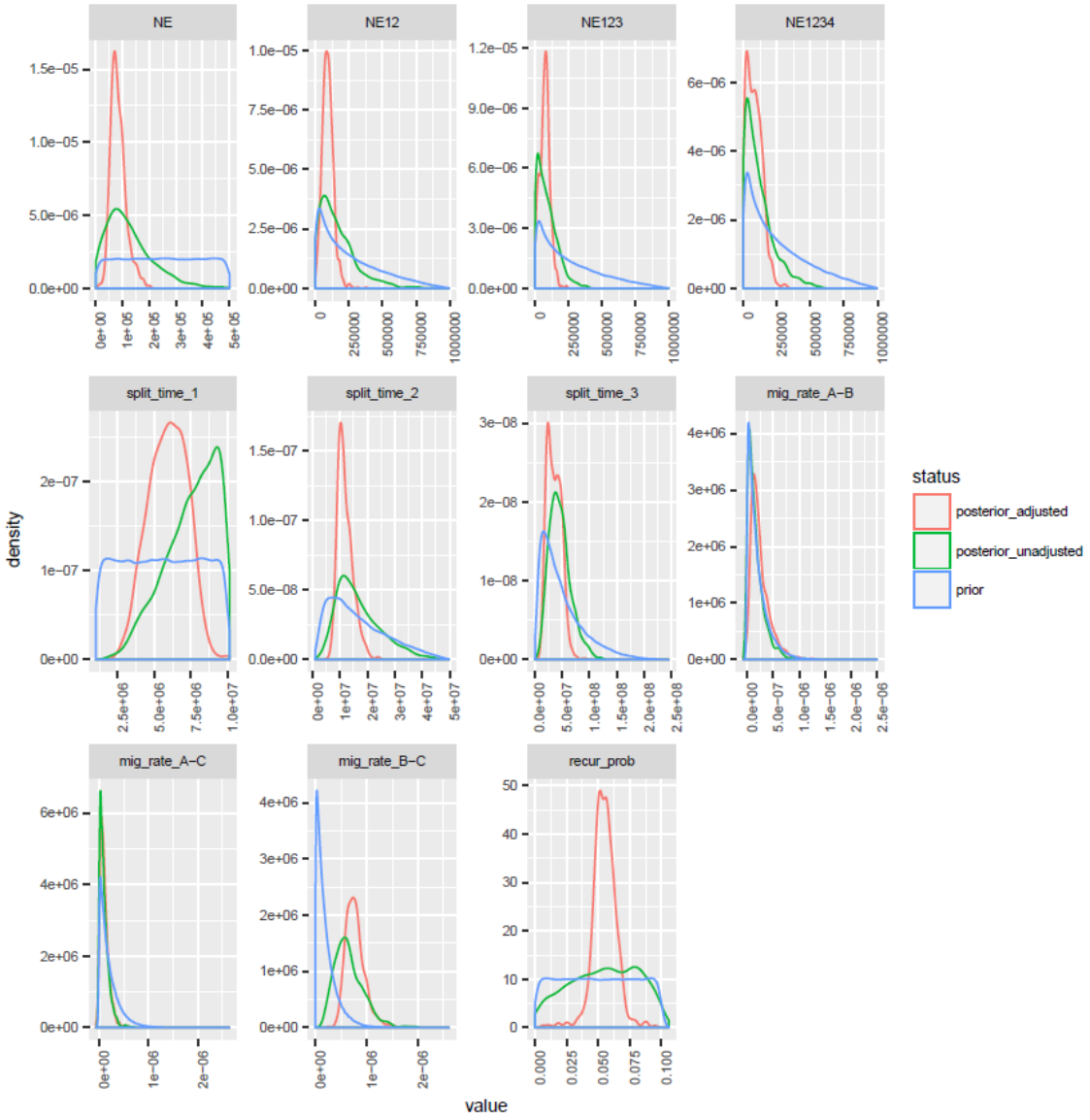

Figure S16.16. Posterior distributions of parameters inferred from the alignment of *L. africana_B, L. cyclotis_A, P. antiquus_N, M. americanum*. Prior and posterior distributions are as described in Figure legend S16.6.

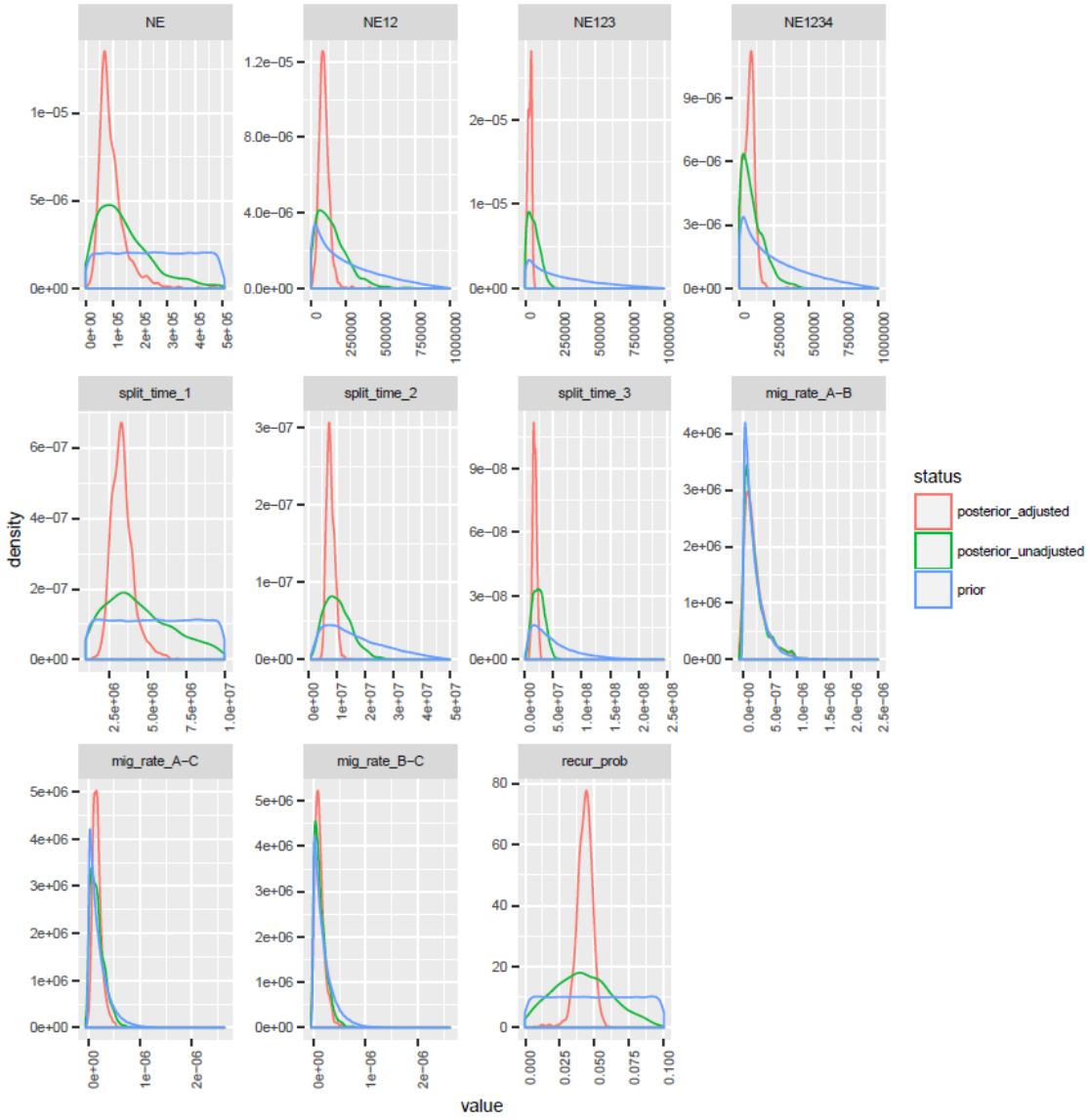

Figure S16.17. Posterior distributions of parameters inferred from the alignment of *L. africana_B, L. cyclotis_A, E. maximus_D, M. americanum*. Prior and posterior distributions are as described in Figure legend S16.6.

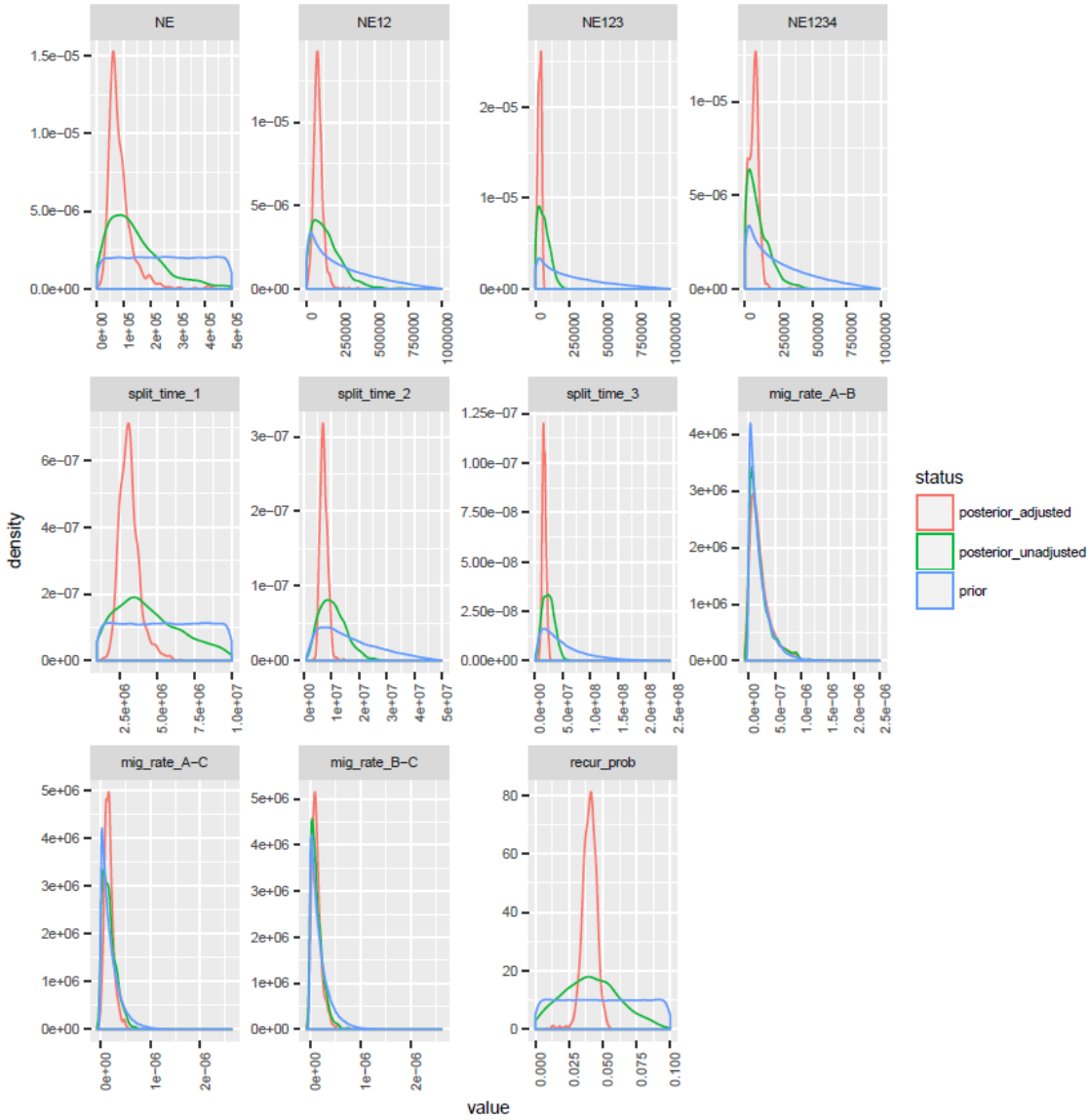

Figure S16.18. Posterior distributions of parameters inferred from the alignment of *L. africana_B, L. cyclotis_A, M. primigenius_Q, M. americanum*. Prior and posterior distributions are as described in Figure legend S16.6.

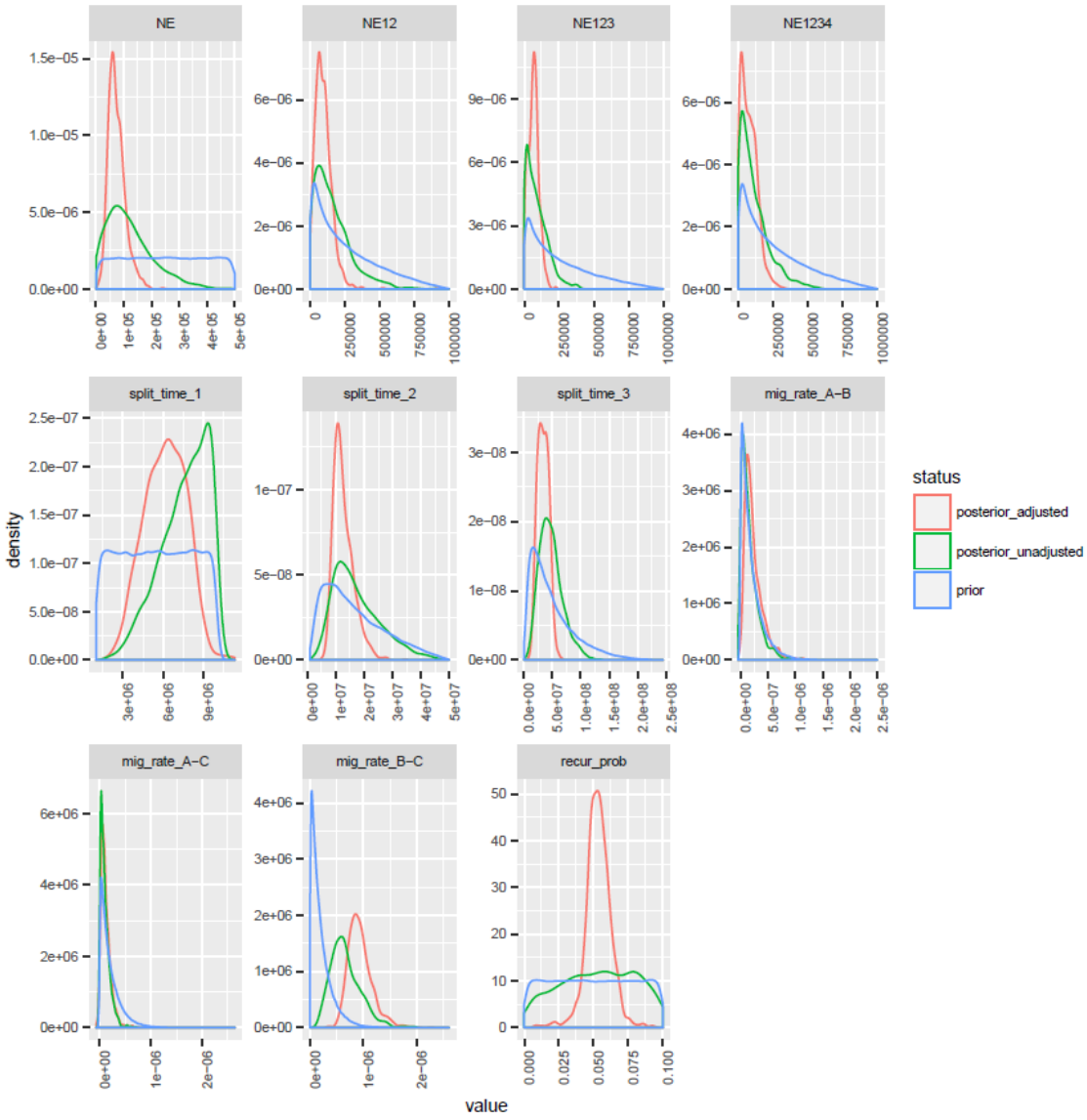

Figure S16.19. Posterior distributions of parameters inferred from the alignment of *L. africana_B, L. cyclotis_F, P. antiquus_N, M. americanum*. Prior and posterior distributions are as described in Figure legend S16.6.

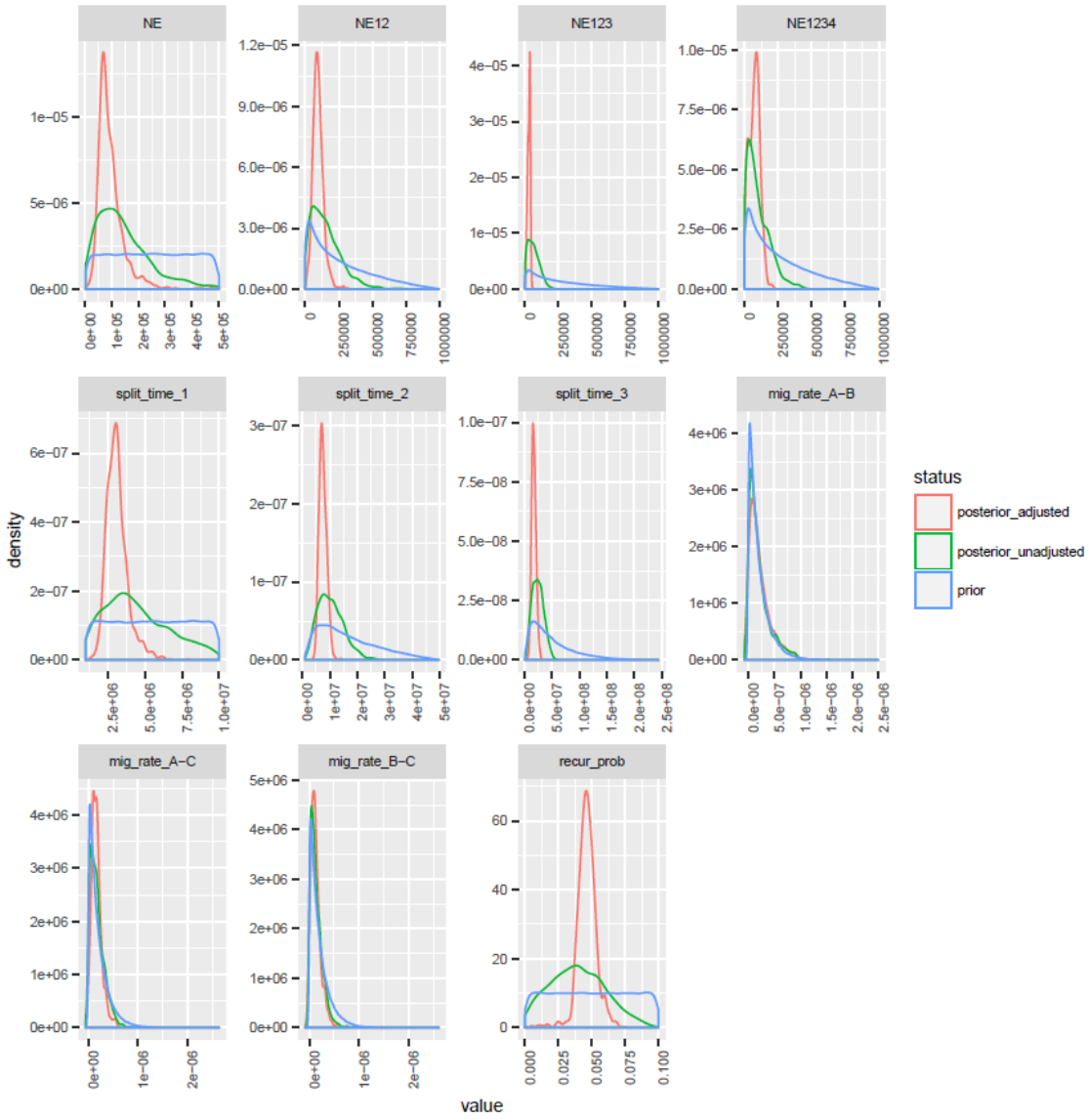

Figure S16.20. Posterior distributions of parameters inferred from the alignment of *L. africana_B, L. cyclotis_F, E. maximus_D, M. americanum*. Prior and posterior distributions are as described in Figure legend S16.6.

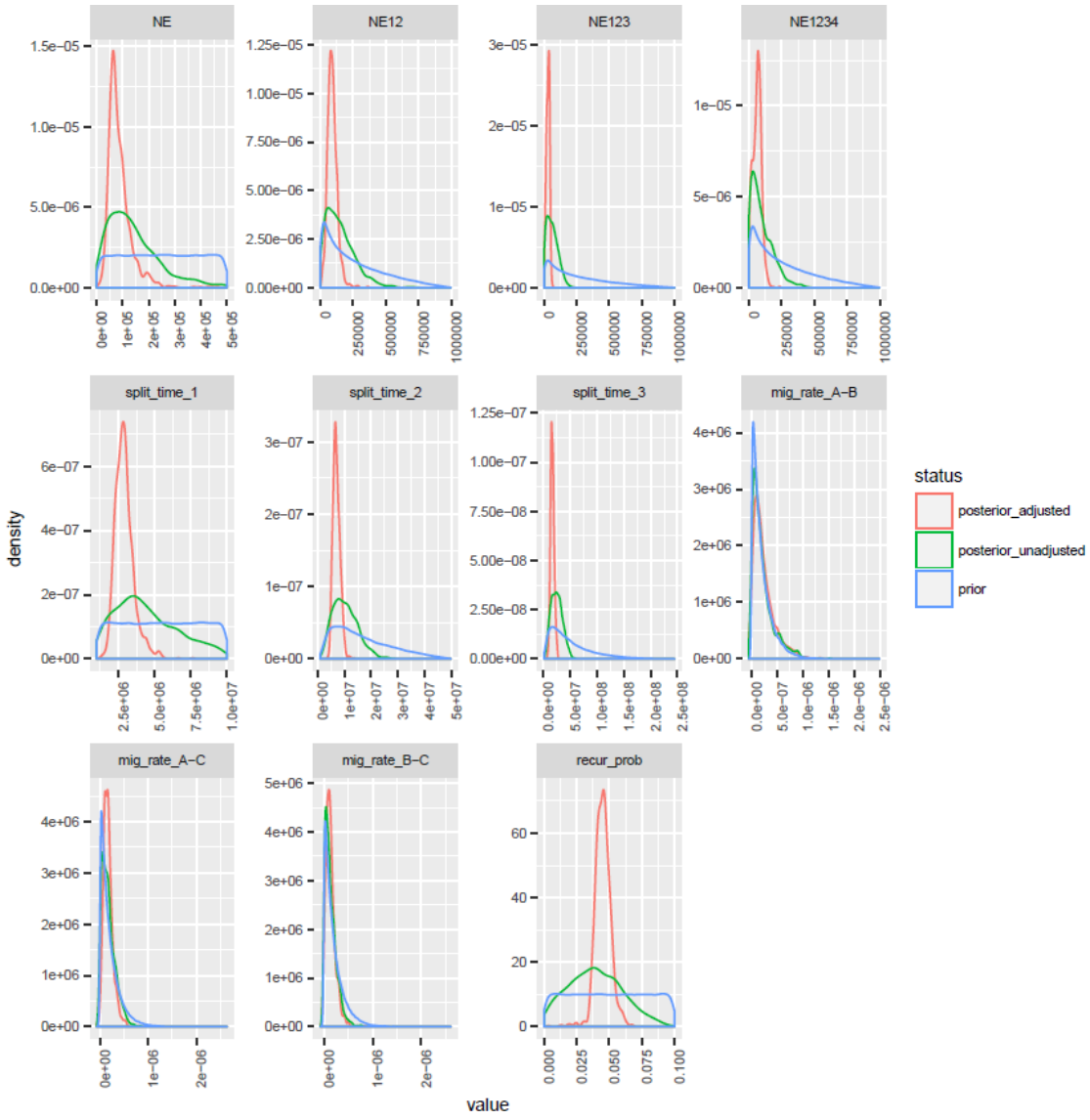

Figure S16.21. Posterior distributions of parameters inferred from the alignment of *L. africana_B, L. cyclotis_F, M. primigenius_Q, M. americanum*. Prior and posterior distributions are as described in Figure legend S16.6.

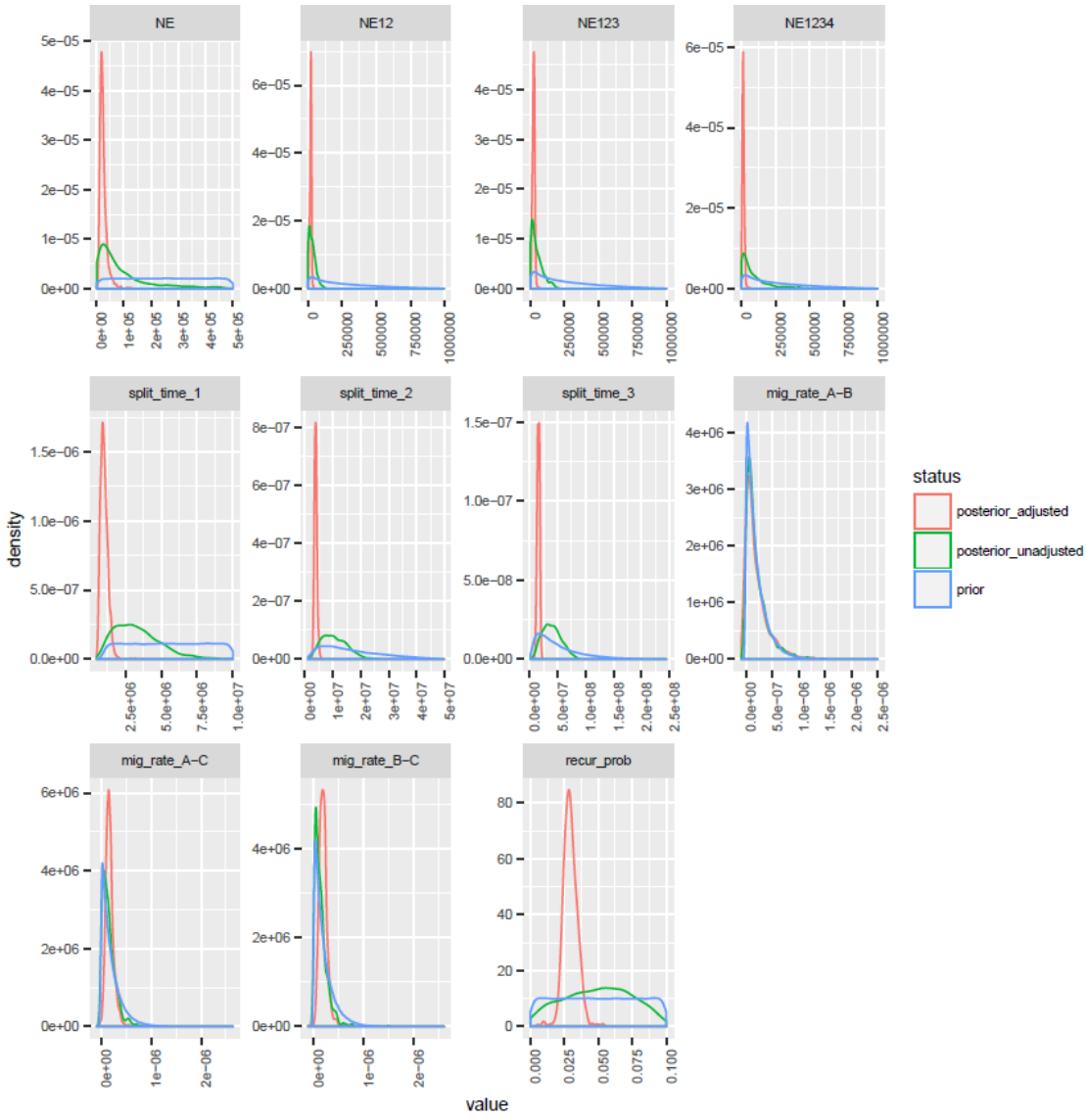

Figure S16.22. Posterior distributions of parameters inferred from the alignment of *M. columbi_U, M. primigenius_Q, E. maximus_D, M. americanum*. Prior and posterior distributions are as described in Figure legend S16.6.

Figure S16.23. Posterior predictive checks for the alignment of *P. antiquus_N, L. africana_B, E. maximus_D, M. americanum*. The posterior distribution of summary statistics is plotted against the summary statistics estimated from the four-taxon alignment, shown in red vertical lines. The first 49 plots show the proportions of the 49 site configuration transitions. For example, "0010-0110" indicates the proportion of site-pairs in which the left-most site is unique derived in taxon C (*E. maximus_D* in the empirical data) and the right-most site is shared derived in taxa B and C (*L. africana_B and E. maximus_D*). "div12", "div13", "div23", "div14" indicates the divergence rate between taxa A and B, A and C, B and C, and A and outgroup, respectively. "*D*1", "*D*2" and "*D*3" indicate the three *D*-statistics from the counts of shared derived alleles. A similar description applies to figures S16.24-S16.39, for various sets of taxa.

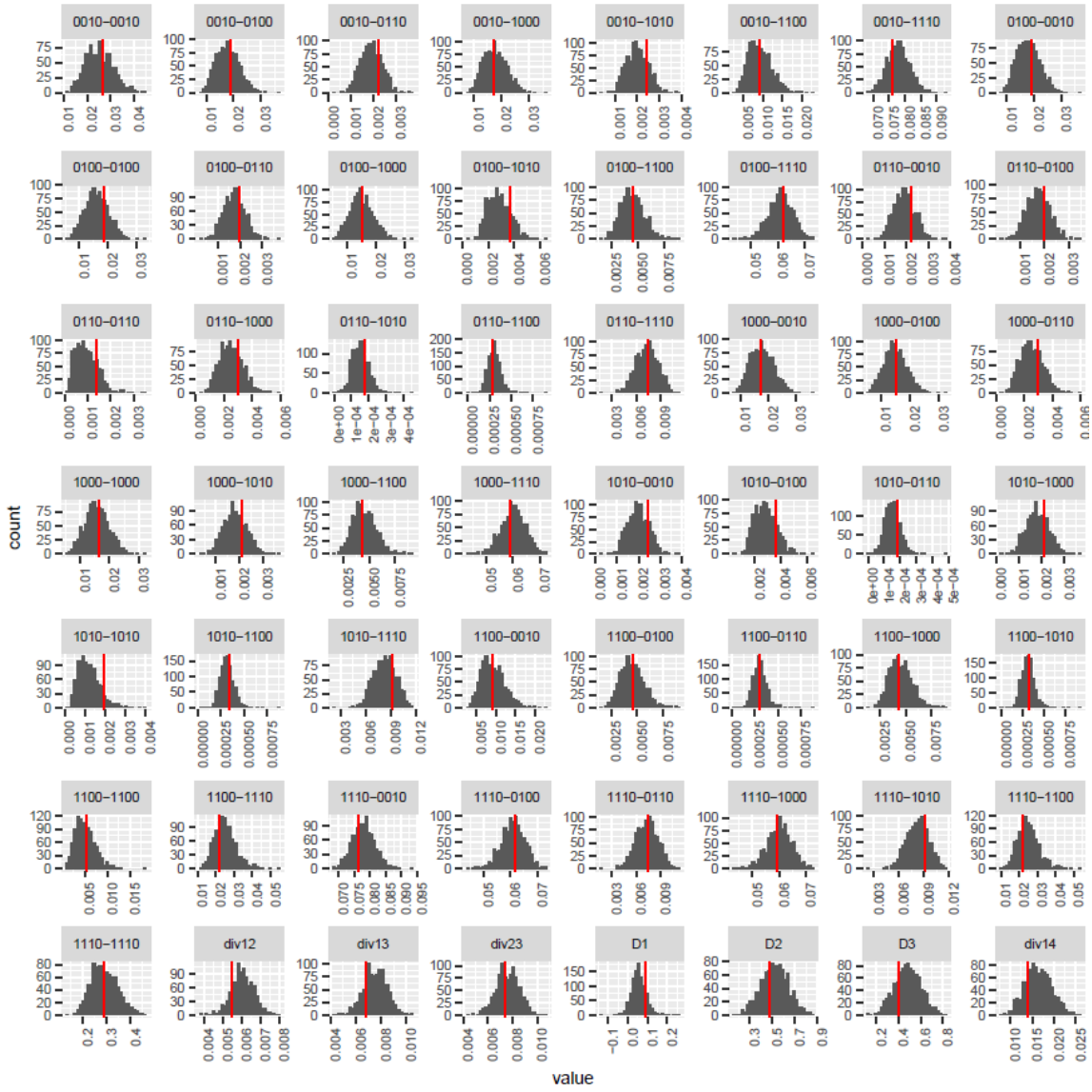

Figure S16.24. Posterior predictive checks for the alignment of *P. antiquus_N, L. africana_B, M. primigenius_Q, M. americanum*. For details see legend to Figure S16.23.

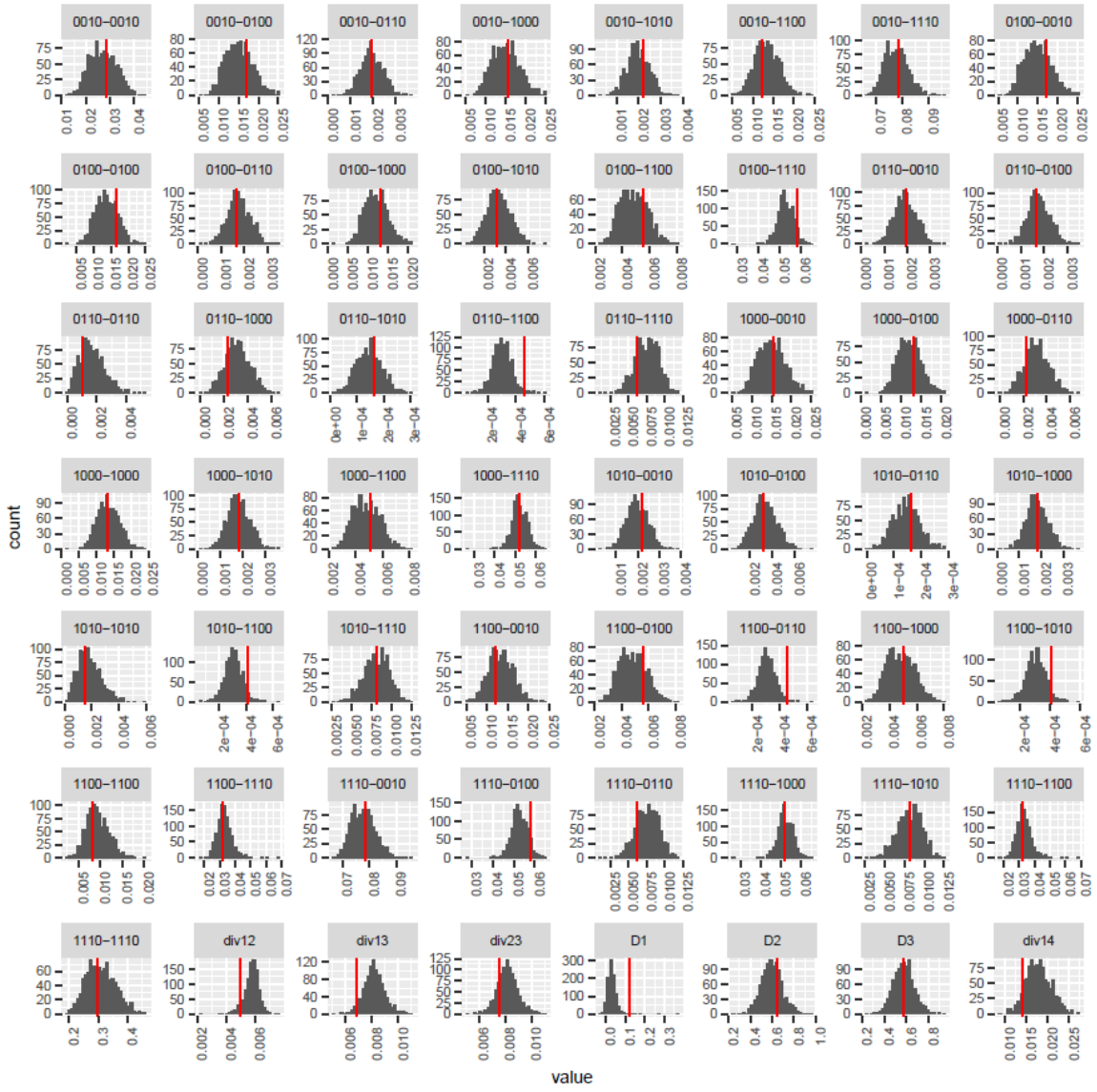

Figure S16.25. Posterior predictive checks for the alignment of *P. antiquus_N, L. cyclotis_A, E. maximus_D, M. americanum*. For details see legend to Figure S16.23.

Figure S16.26. Posterior predictive checks for the alignment of *P. antiquus_N, L. cyclotis_A, M. primigenius_Q, M. americanum*. For details see legend to Figure S16.23.

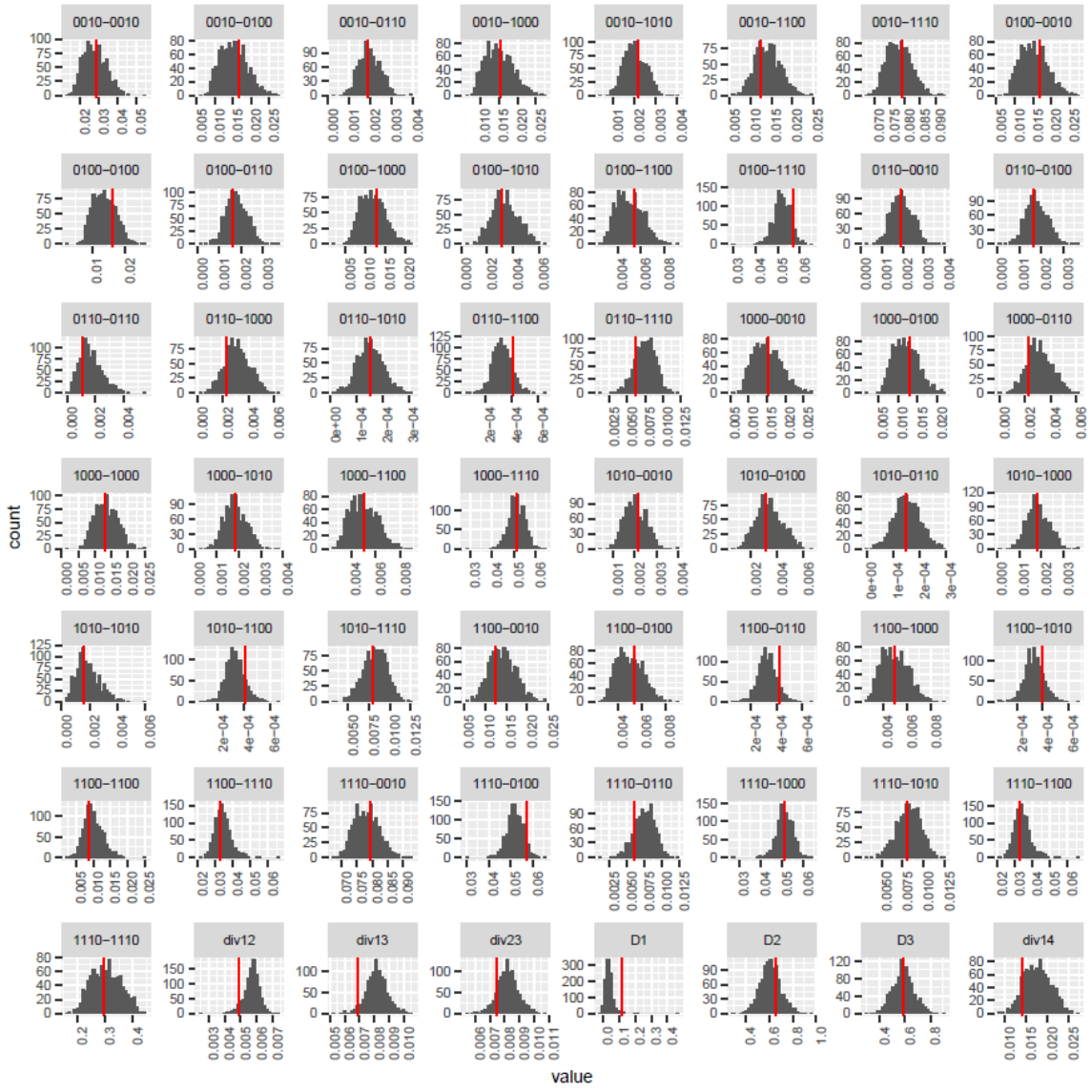

Figure S16.27. Posterior predictive checks for the alignment of *P. antiquus_N, L. cyclotis_F, E. maximus_D, M. americanum*. For details see legend to Figure S16.23.

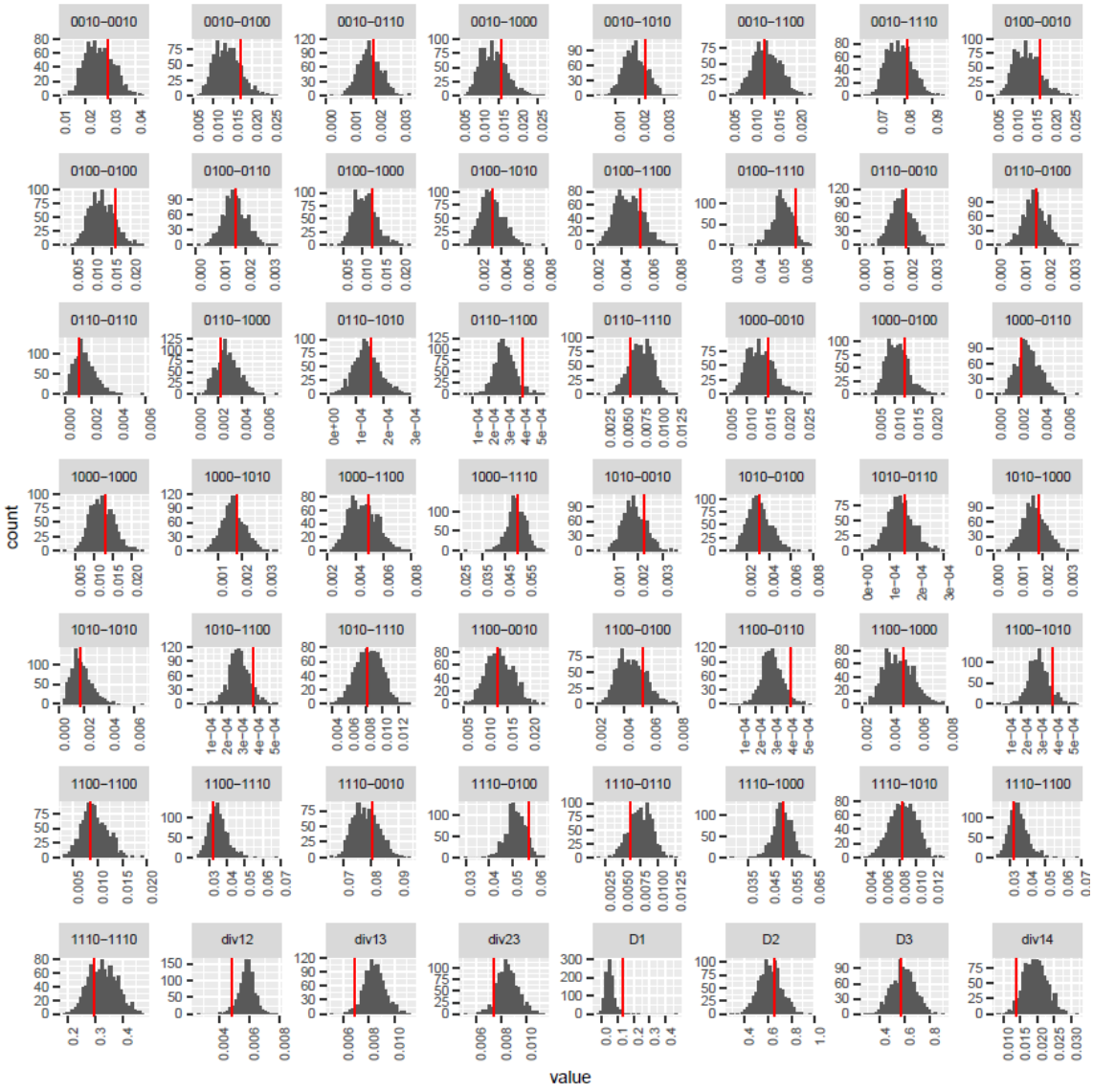

Figure S16.28. Posterior predictive checks for the alignment of *P. antiquus_N, L. cyclotis_F, M. primigenius_Q, M. americanum*. For details see legend to Figure S16.23.

Figure S16.29. Posterior predictive checks for the alignment of *E. maximus_D, M. primigenius_Q, P. antiquus_N, M. americanum*. For details see legend to Figure S16.23.

Figure S16.30. Posterior predictive checks for the alignment of *E. maximus_D, M. primigenius_Q, L. africana_B, M. americanum*. For details see legend to Figure S16.23.

Figure S16.31. Posterior predictive checks for the alignment of *E. maximus_D, M. primigenius_Q, L. cyclotis_A, M. americanum*. For details see legend to Figure S16.23.

Figure S16.32. Posterior predictive checks for the alignment of *E. maximus_D, M. primigenius_Q, L. cyclotis_F, M. americanum*. For details see legend to Figure S16.23. For details see legend to Figure S16.23.

Figure S16.33. Posterior predictive checks for the alignment of *L. africana_B, L. cyclotis_A, P. antiquus_N, M. americanum*. For details see legend to Figure S16.23.

Figure S16.34. Posterior predictive checks for the alignment of *L. africana_B, L. cyclotis_A,E. maximus_D, M. americanum*. For details see legend to Figure S16.23.

Figure S16.35. Posterior predictive checks for the alignment of *L. africana_B, L. cyclotis_A, M. primigenius_Q, M. americanum*. For details see legend to Figure S16.23.

Figure S16.36. Posterior predictive checks for the alignment of *L. africana_B, L. cyclotis_F, P. antiquus_N, M. americanum*. For details see legend to Figure S16.23.

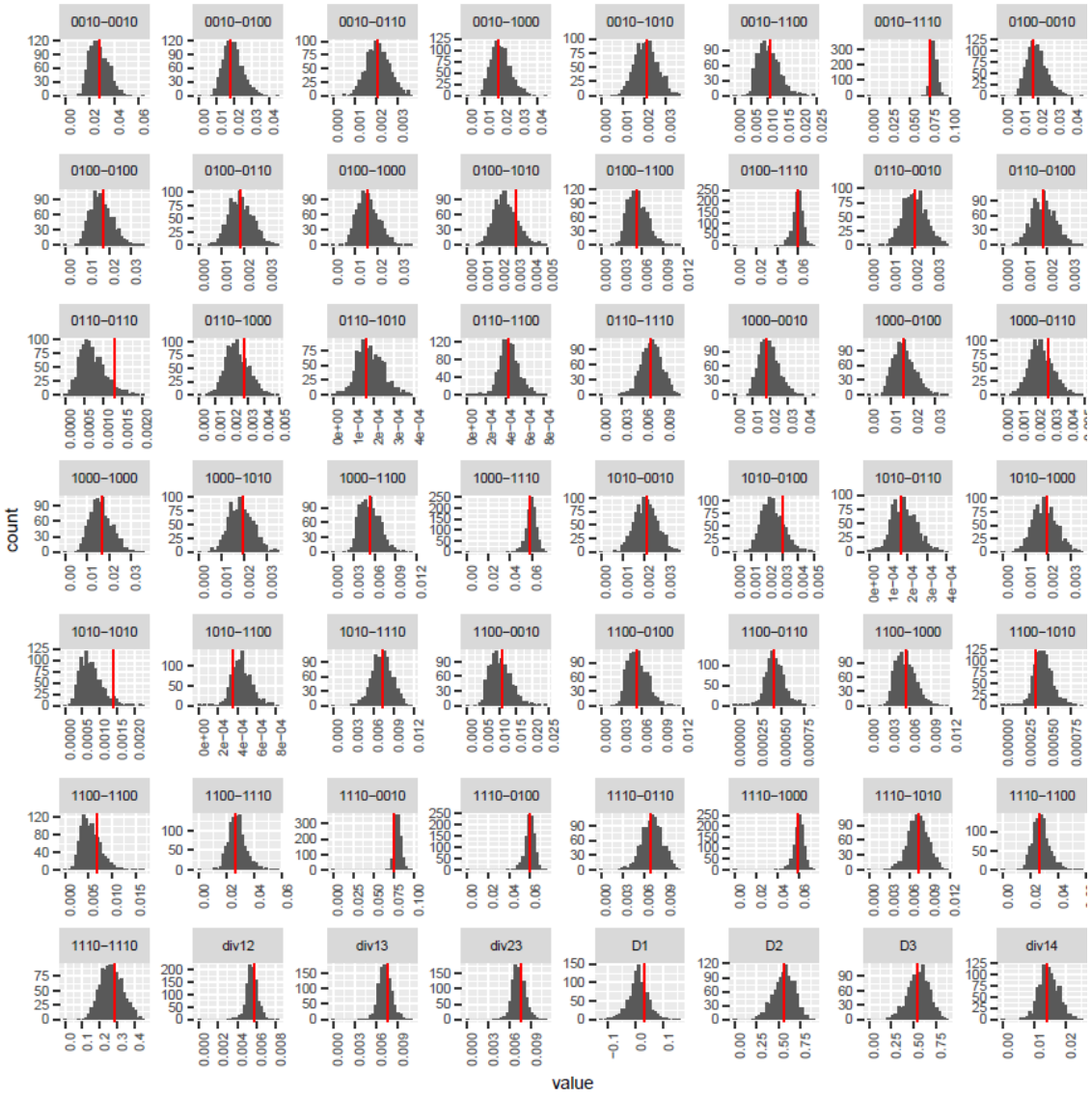

Figure S16.37. Posterior predictive checks for the alignment of *L. africana_B, L. cyclotis_F,E. maximus_D, M. americanum*. For details see legend to Figure S16.23.

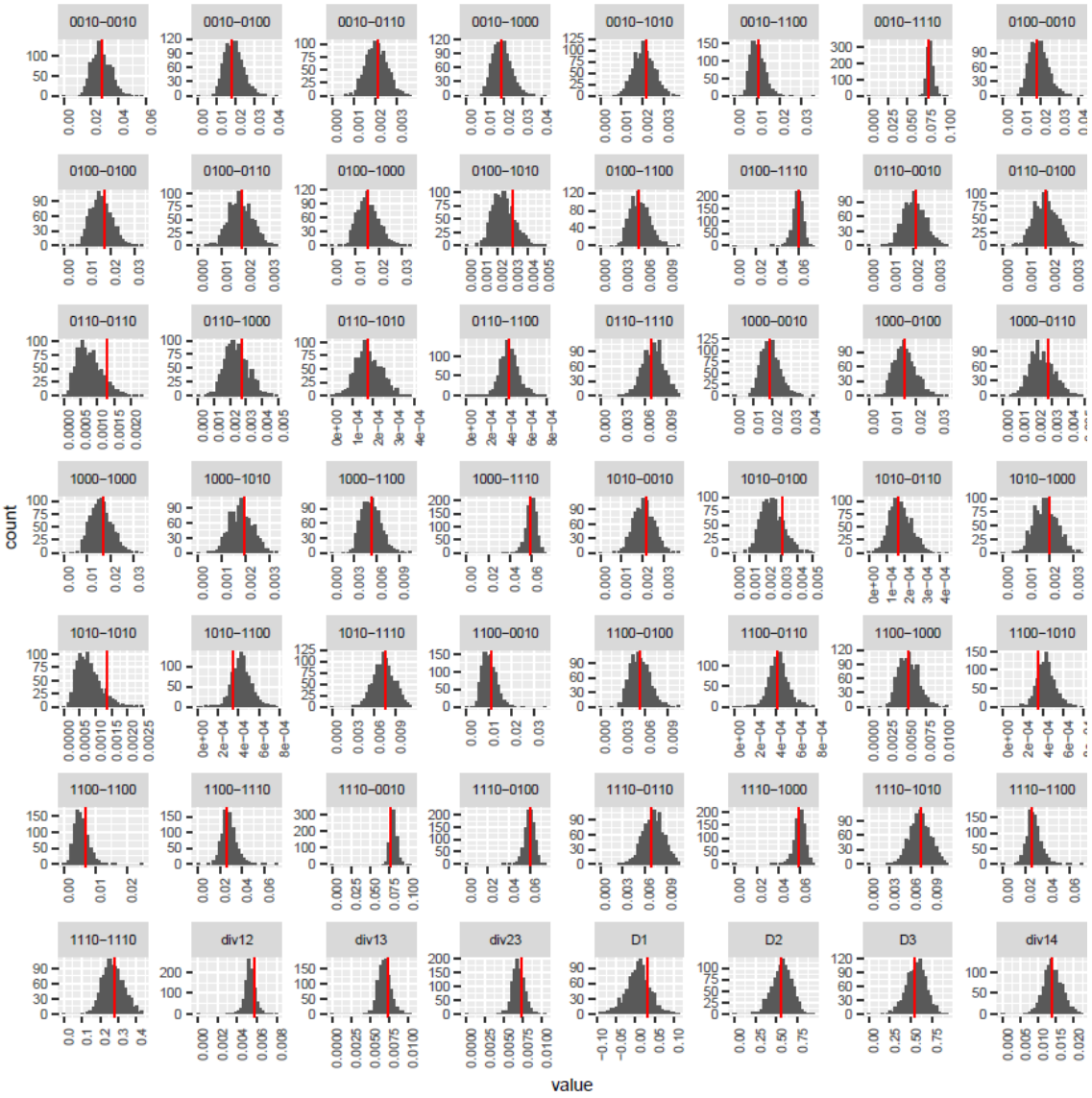

Figure S16.38. Posterior predictive checks for the alignment of *L. africana_B, L. cyclotis_F, M. primigenius_Q, M. americanum*. For details see legend to Figure S16.23.

Figure S16.39. Posterior predictive checks for the alignment of *M. columbi_U, M. primigenius_Q, E. maximus_D, M. americanum*. For details see legend to Figure S16.23.

Supplementary Note 17

CoalHMM analysis of incomplete lineage sorting among species trios

The demographic model applied in this analysis is an isolation model with no gene flow following species' splits, with population sizes assumed to be constant along each branch of the species tree. As shown in Figure S17.1, parameters of this model include the two split times (T_1 and T_{12}) and the effective sizes of the two ancestral populations (Ne_{12} and Ne_{123}).

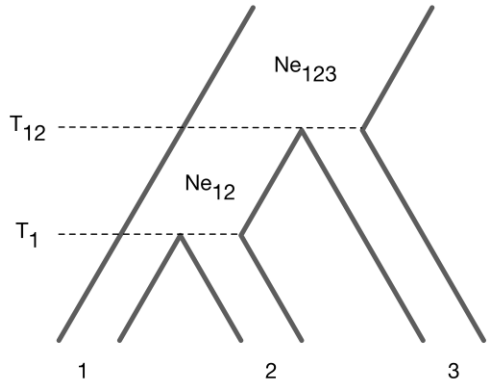

Figure S17.1. Isolation model used in the analysis. T_1: speciation time of species 1 and 2. T_{12}: speciation time of species 1 and 3. Ne_{12}: effective population size of the population ancestral to species 1 and 2. Ne_{123}: effective population size of the ancestor to all three species.

In a genomic alignment of three species, divergence between species pairs will vary along the alignment as a result of ancestral polymorphism. Recombination events in the genealogical history of aligned sequences allow the coalescence times of individual gene trees to vary along the alignment. The coalescence rate in the population ancestral to species 1 and 2 is inversely proportional to Ne_{12}. This means that if Ne_{12} is sufficiently large and/or the time between T_1 and T_{12} is sufficiently small, the lineages from species 1 and 2 may not have coalesced at time T_{12}. At that time, coalescence of each pair of lineages (1,2 or 1,3 or 2,3) is equally likely. This means that the probability that any gene tree along the alignment has a topology different from the species tree is:

$$P_{ILS} = 2/3 \times \exp[-(T_{12} - T_1)/(g \times 2Ne_{12}]$$

where g is the generation time. This phenomenon is called incomplete lingeage sorting (ILS) and is – along with sequence divergence – informative of ancestral demography of the species in our model. The coalescent hidden Markov model (86) we applied approximates the ancestral recombination graph as a sequential Markov coalescent (SMC). The model has four hidden states, which each correspond to a gene tree as shown in Figure S17.2. Two states represent the cases where species 1 and 2 coalesce first in either the more recent (bottom left tree) or the less recent (bottom right tree) ancestral populations. The two different cases of incomplete lineage sorting are represented by the two remaining states (top left and right trees). Arrows denote

transitions (i.e. changes) between hidden states parameterized using coalescent theory. The probability of emitting an alignment column from a state is calculated as the probability of the underlying tree given the four bases. The likelihood of the model given the model parameters is calculated using the forward algorithm. The likelihood is maximized using a modified Newton-Raphson algorithm.

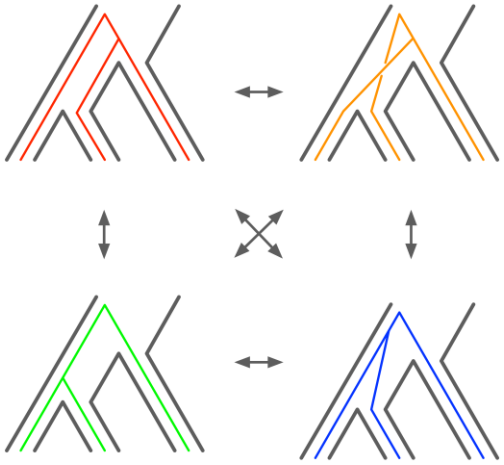

Figure S17.2. Outline of the four states in the HMM. The four states correspond to the four different trees describing the ancestry of an alignment column. Arrows indicate allowed transitions between hidden states.

Using this framework, we performed separate analyses of four species trios with mastodon (*M. americanum_I*) as outgroup. The species listed in each trio are applied as species 1, 2, and 3 in our demographic model.

- forest elephant (*L. cyclotis_A*), savanna elephant (*L. africana_B*), Asian elephant (*E. maximus_D*)
- Asian elephant (*E. maximus_D*), woolly mammoth (*M. primigenius_P*), straight-tusked elephant (*P. antiquus_N*)
- forest elephant (*L. cyclotis_A*), straight-tusked elephant (*P. antiquus_N*), Asian elephant (*E. maximus_D*)
- forest elephant (*L. cyclotis_F*), straight-tusked elephant (*P. antiquus_N*), Asian elephant (*E. maximus_D*)

The two analyses that differ only in the choice of sample for forest elephant are performed to investigate whether *L. cyclotis_F* is more closely related to the straight-tusked elephant than is *L. cyclotis_A*, as suggested by other analyses.

Preparation of genomic alignments

Pseudo-haploid sequences with random allele calls, generated as described in Note 8 but excluding sites with read depth below 3, were analyzed in each trio and filtered with the

mappability filter with 90% stringency. We split each alignment into segments at base positions where all ingroup species have 'N'. Resulting segments with an N-content larger than 50% were discarded. Segments separated by not more than 100bp were assembled into chunks honoring reference coordinates. Chunks shorter than 500bp were discarded. For the four trios listed above this resulted in alignments covering respectively 1,595.795, 1,653.713, 1,508.074 and 1,358.555 megabases of the reference genome.

CoalHMM analysis

Parameter estimates were produced for separate coalHMM analyses on approximately 1Mb of alignment blocks, restarting the HMM between alignment blocks more than 100bp apart. The resulting estimates are associated with a known bias that was corrected as described by Dutheil *et al.* (86). Briefly, we simulated 100 alignments of 1Mb in length for relevant combinations of model parameter values. We ran a coalHMM analysis on each of these data sets and recorded the estimated model parameters. We then computed the bias on model parameters in each analysis as the deviation of the estimate from the true value used for the simulation. A linear model that explains the bias from known values of parameters and their interaction was then fitted. The fitted model was then used to correct the bias on the parameters estimated from each analysis of empirical data. Estimates were rescaled using a mutation rate per year of 0.406×10^{-9} and a generation time of 31 years to be able to compare with the simulation analyses in Note 16 (but note that the assumed mutation rate is uncertain). Tables S17.1 – S17.4 list medians, means and standard errors for parameters estimated across analyses on autosomes. To address the effect of outliers on mean estimates, we evaluated the use of a mahalanobis distance of 5 as a filtering criterion for parameter estimates from each coalHMM analysis (Figures S17.3 – S17.6 and Figures S17.7 – S17. 10 for raw and corrected unscaled parameter estimates).

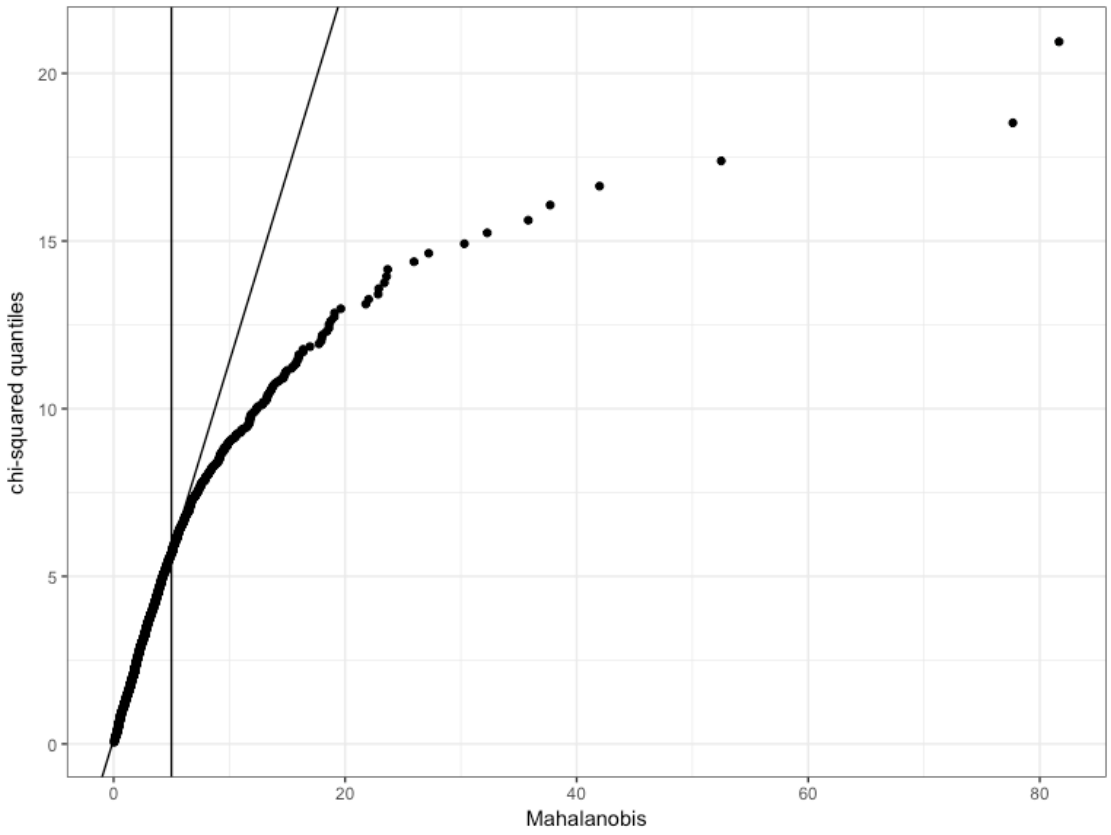

Figure S17.3. qqplot of chi-square distribution vs. mahalanobis distances for the savanna, forest, Asian elephant trio.

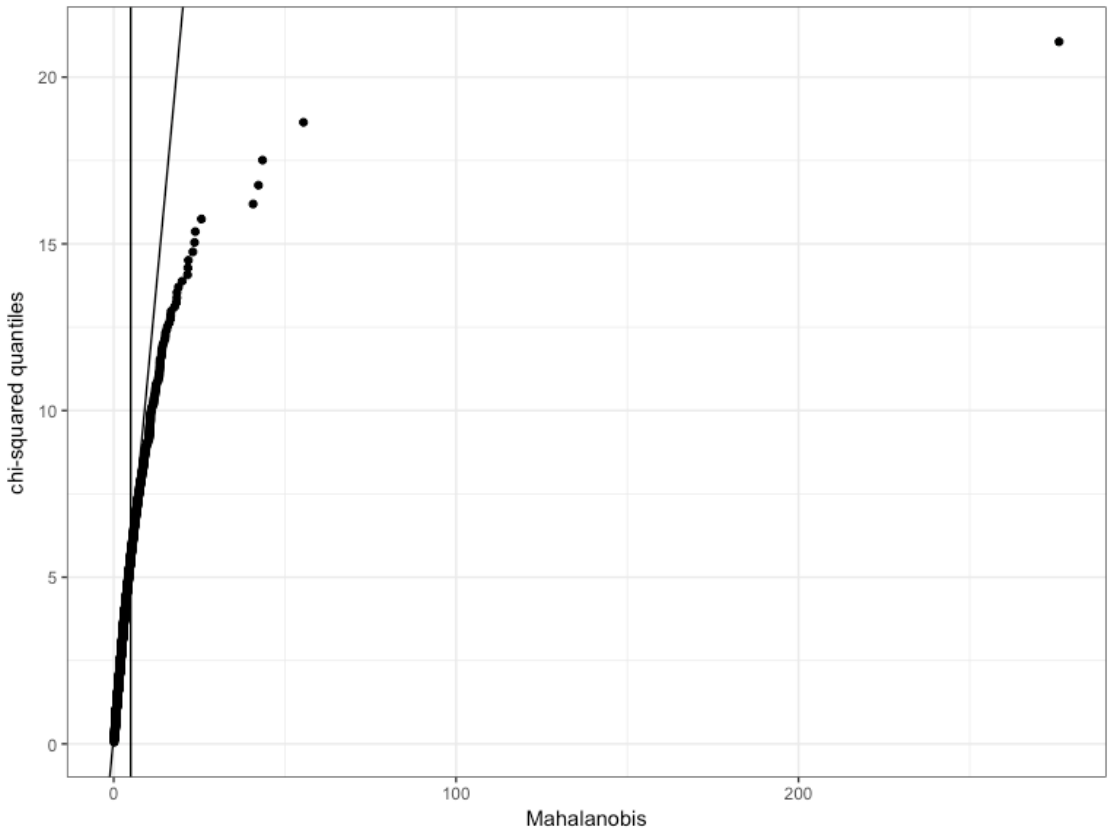

Figure S17.4. qqplot of chi-square distribution vs. mahalanobis distances for the Asian elephant, woolly mammoth, straight-tusked elephant trio.

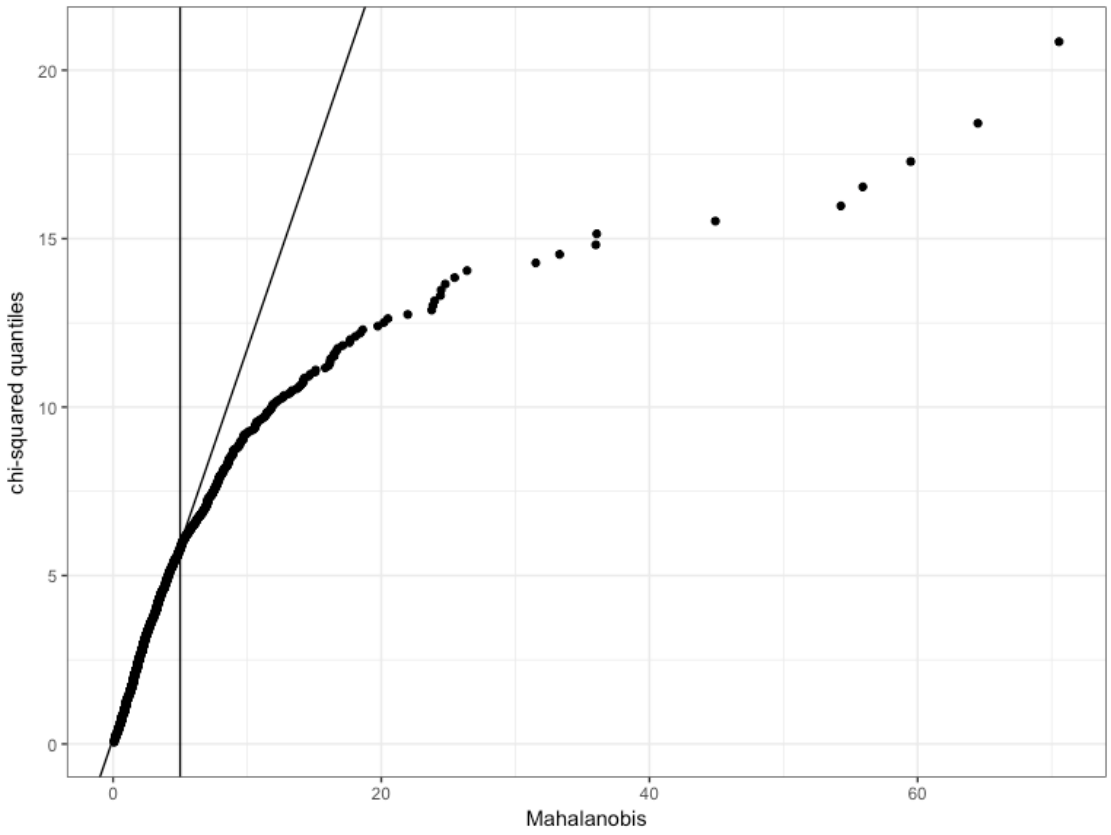

Figure S17.5. qqplot of chi-square distribution vs. mahalanobis distances for the forest (*L. cyclotis_A*), straight-tusked, Asian elephant trio.

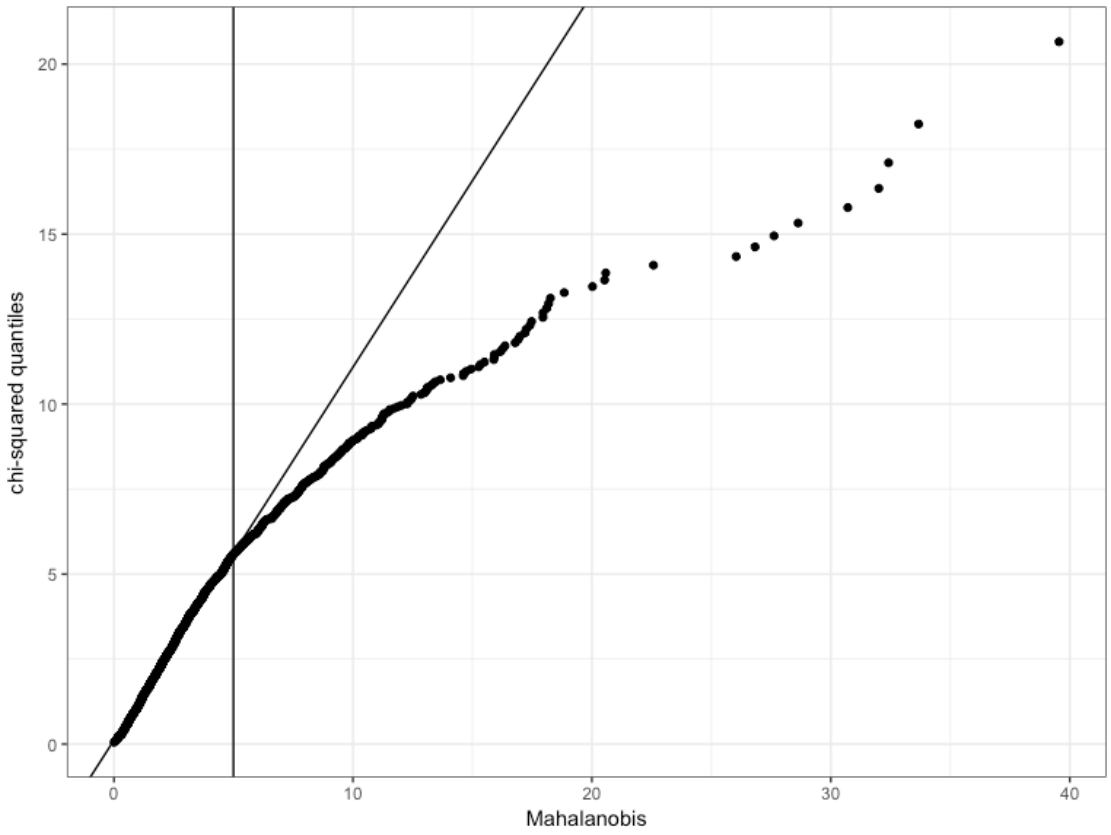

Figure S17.6. qqplot of chi-square distribution vs. mahalanobis distances for the forest (*L. cyclotis_F*), straight-tusked, Asian elephant trio.

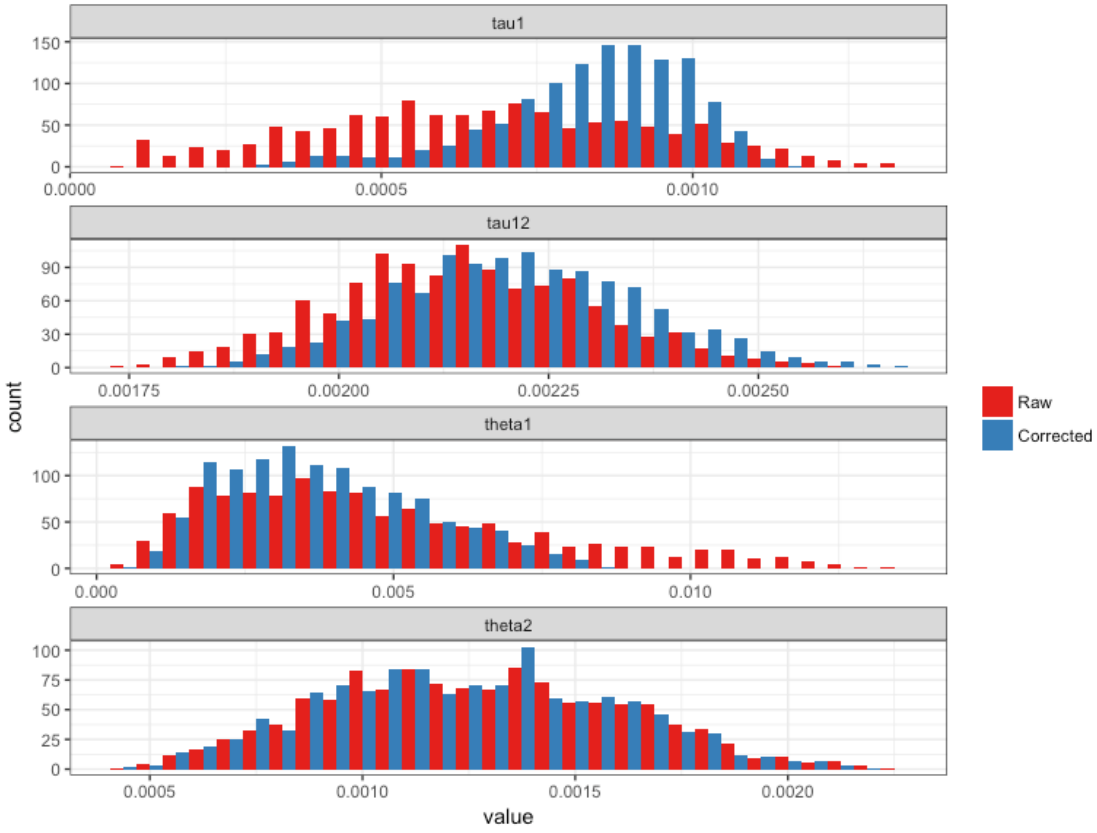

Figure S17.7. Raw and corrected unscaled parameter estimates, outliers removed for the savanna, forest, Asian elephant trio.

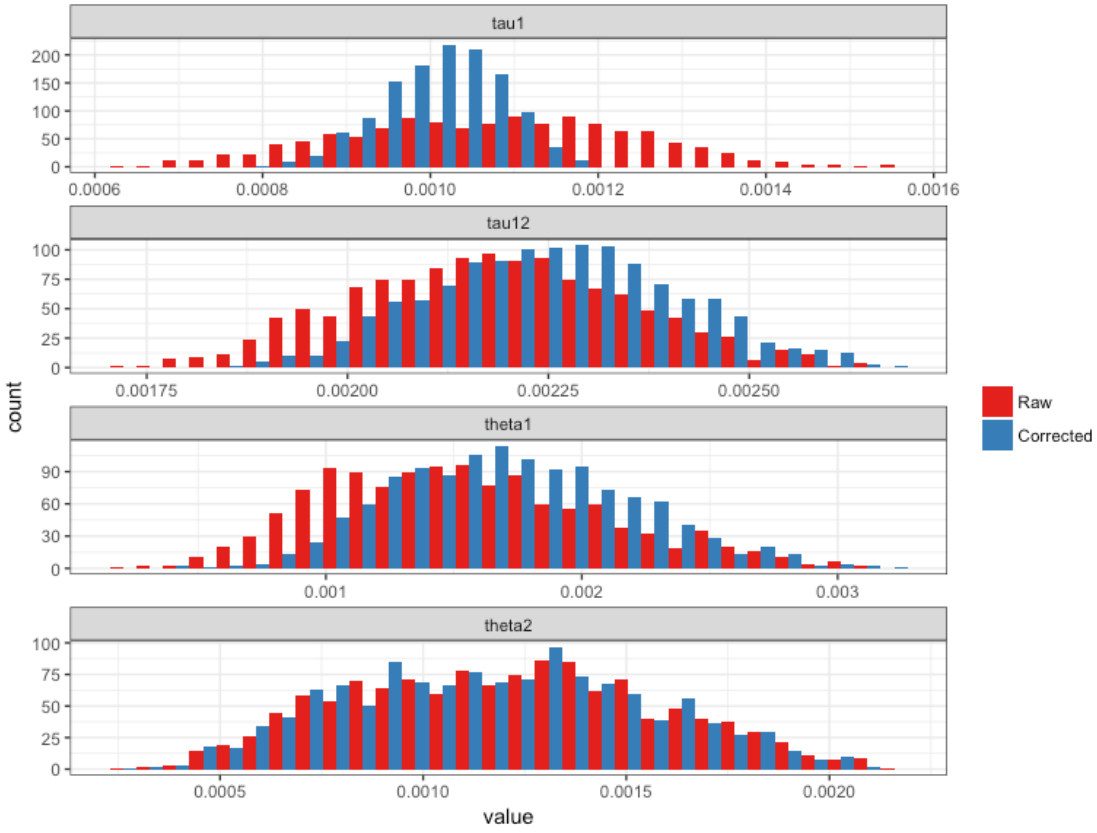

Figure S17.8. Raw and corrected unscaled parameter estimates, outliers removed for the Asian elephant, woolly mammoth, straight-tusked elephant trio.

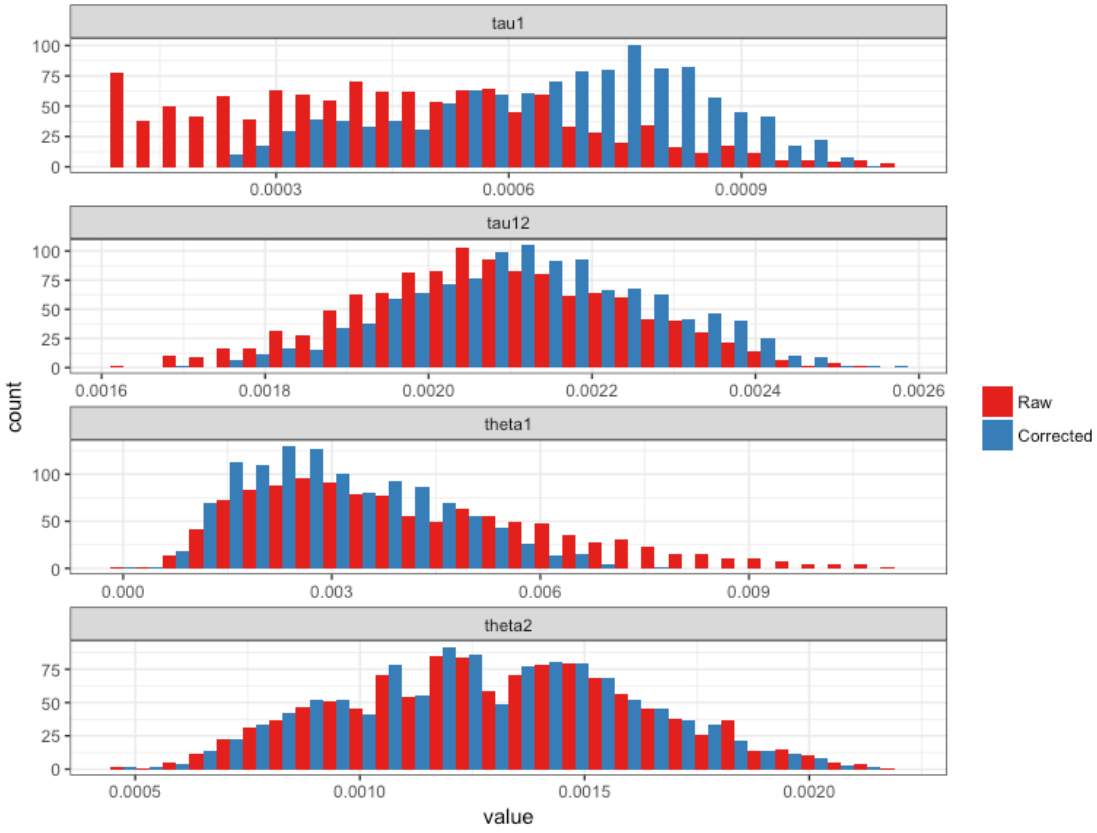

Figure S17.9. Raw and corrected unscaled parameter estimates, outliers removed for the forest (*L. cyclotis_A*), straight-tusked, Asian elephant trio.

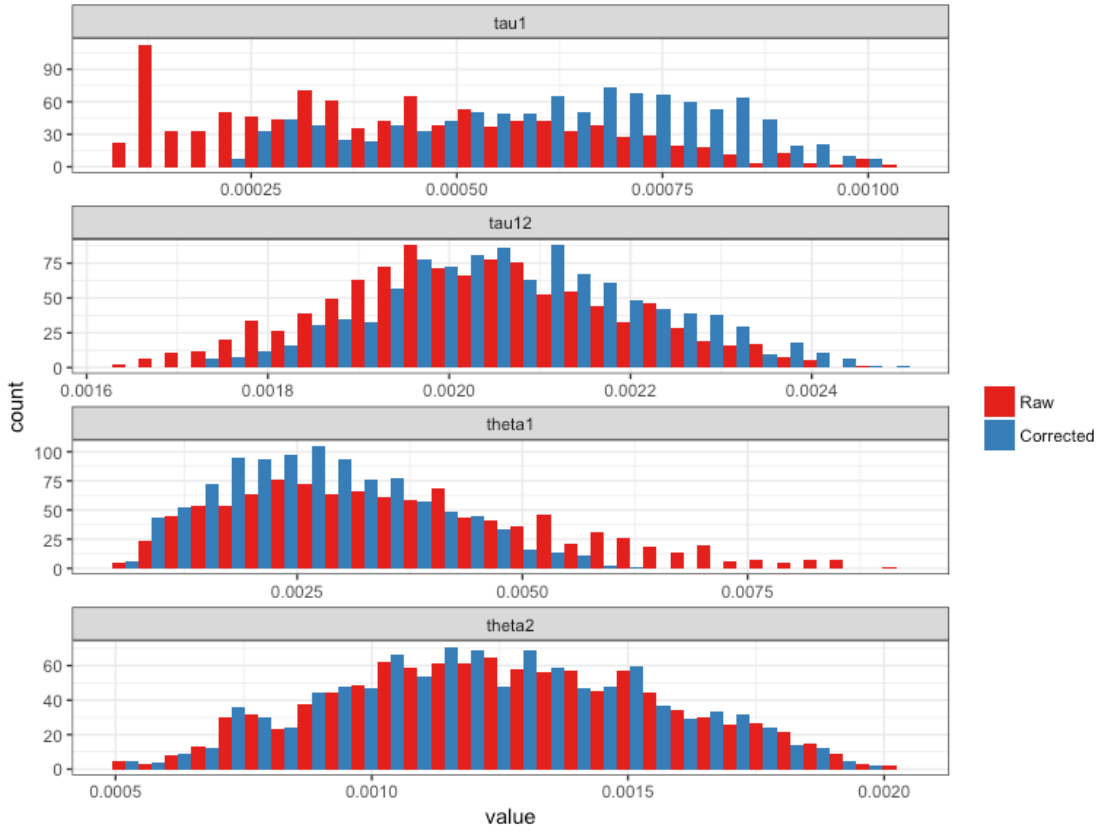

Figure S17.10. Raw and corrected unscaled parameter estimates, outliers removed for the forest (*L. cyclotis_F*), straight-tusked, Asian elephant trio.

The age of the split between forest and savanna elephants is estimated to have occurred approximately 2,000,000 years with an ancestral effective population size of ~165,000 (Table S17.1). The split between Asian elephant and woolly mammoth is estimated at approximately 2,500,000 years with an ancestral effective population size of ~72,000 (Table S17.3). The age of the split between Asian and African elephants is estimated to have occurred between 5,000,000 and 5,600,000 across the four analyses and ancestral effective population size is estimated at 48,000 to 53,000. We caution that the split time between forest and straight-tusked elephants (aproximately 1,700,000 for *L. cyclotis_A* and 1,600,000 for *L. cyclotis_F*; Tables S17.5, S17.7) cannot be meaningfully estimated as a single event given the complicated admixture history, and the estimated effective size of the population ancestral to forest and straight-tusked elephants likely reflects strong population structure as inferred by the admixture graph (Figures S12.1 – S12.4).

Table S17.1. Corrected parameter estimates for the savanna, forest, Asian elephant trio.

parameter	N (Mb)	median	mean	standard error
N_{e12}	1,540	148,829	165,246	2,431
N_{e123}	1,540	51,969	52,054	388

T_1	1,540	2,147,266	2,040,274	45,360
T_{12}	1,540	5,401,241	5,422,989	60,093

Table S17.2. Corrected parameter estimates (outliers removed) for the savanna, forest, Asian elephant trio.

parameter	N (Mb)	median	mean	standard error
N_{e12}	1,194	140,505	149,809	1,935
N_{e123}	1,194	49,344	49,513	393
T_1	1,194	2,110,017	2,055,838	10,971
T_{12}	1,194	5,384,903	5,386,399	10,838

Table S17.3. Corrected parameter estimates for the Asian elephant, woolly mammoth, straight-tusked elephant trio.

parameter	N (Mb)	median	mean	standard error
N_{e12}	1,626	69,630	72,429	621
N_{e123}	1,626	47,843	48,008	423
T_1	1,626	2,510,263	2,505,216	5,196
T_{12}	1,626	5,586,478	5,583,249	11,474

Table S17.4. Corrected parameter estimates (outliers removed) for the Asian elephant, woolly mammoth, straight-tusked elephant trio.

parameter	N (Mb)	median	mean	standard error
N_{e12}	1,253	67,582	68,669	517
N_{e123}	1,253	47,027	46,790	410
T_1	1,253	2,498,909	2,490,799	4,787
T_{12}	1,253	5,571,006	5,559,600	9,532

Table S17.5. Corrected parameter estimates for the forest (*L. cyclotis_A*), straight-tusked, Asian elephant trio.

parameter	N (Mb)	median	mean	standard error
N_{e12}	1,473	121,351	136,560	2,029
N_{e123}	1,473	53,339	53,311	395
T_1	1,473	1,748,010	1,737,179	34,312
T_{12}	1,473	5,169,767	5,220,825	32,530

Table S17.6. Corrected parameter estimates (outliers removed) for the forest (*L. cyclotis_A*), straight-tusked, Asian elephant trio.

parameter	N (Mb)	median	mean	standard error
N_{e12}	1,156	115,129	123,741	1,697
N_{e123}	1,156	50,660	51,045	376
T_1	1,156	1,688,063	1,625,728	12,994
T_{12}	1,156	5,127,024	5,130,204	11,575

Table S17.7. Corrected parameter estimates for the forest (*L. cyclotis_F*), straight-tusked, Asian elephant trio.

parameter	N (Mb)	median	mean	standard error
N_{e12}	1,352	109,238	120,973	1,705
N_{e123}	1,352	50,538	51,043	383
T_1	1,352	1,632,616	1,589,713	14,571
T_{12}	1,352	5,010,859	5,023,484	14,005

Table S17.8. Corrected parameter estimates (outliers removed) for theforest (*L. cyclotis_F*), straight-tusked, Asian elephant trio.

parameter	N (Mb)	median	mean	standard error
N_{e12}	1,038	106,811	110,531	1,347
N_{e123}	1,038	48,474	49,017	386
T_1	1,038	1,579,592	1,526,665	14,999
T_{12}	1,038	4,987,047	4,993,639	12,724

Patterns of ILS

We called hidden states along the genomic alignment with highest posterior probability and computed the proportion of analyzed sites assigned to each state in non-overlapping 1Mb windows. We only consider windows where more than 30% is covered by the analyzed alignment in all four analyses. Confidence intervals for each proportion of ILS were computed as the mean +/- 1.96 times the standard error obtained from bootstrapping. Among savanna, forest and Asian elephants, the total proportion of ILS is 40.8%-42.0%; among Asian elephant, woolly mammoth and straight-tusked elephant it is 26.4%-27.2%; and in the two analyses of forest, straight-tusked and Asian elephants it is 35.2%-36.4% when using *L. cyclotis_A* for forest elephant and 34.3%-35.5% when using *L. cyclotis_F*. The difference in proportion of ILS between the two latter analyses is significant (paired t-test p-value $< 2.2\times10^{-16}$), and is consistent with a closer relationship of straight-tusked elephants to *L. cyclotis_F* than to *L. cyclotis_A* (as indicated by *D*-statistics analyses; Table S11.2).

In each trio, the proportions of the two different ILS topologies are expected to be the same assuming that the mutation rate has been constant across the species tree. However, the inferred proportions of each kind of ILS will differ if the two most closely related species in a trio have admixed with the third species to different extents. Among savanna, forest and Asian elephants the two proportions are: ((*L. cyclotis*, *E. maximus*), *L. africana*): 22.0%-22.6%; ((*L. africana*, *E. maximus*), *L. cyclotis*): 18.8%-19.4%. Among Asian elephants, woolly mammoth and straight-tusked elephants they are: ((*E. maximus*, *P. antiquus*), *M. primigenius*): 12.9%-13.4%; ((*M. primigenius*, *P. antiquus*), *E. maximus*): 13.4%-13.9%. Among forest, straight-tusked and Asian elephants they are: ((*L. cyclotis_A*, *E. maximus*), *P. antiquus*): 15.4%-16.0%, ((*P. antiquus*, *E. maximus*), *L. cyclotis_A*): 19.7%-20.5% and ((*L. cyclotis_F*, *E. maximus*), *P. antiquus*): 15.3%-15.9%, ((*P. antiquus*, *E. maximus*), *L. cyclotis_F*): 18.8%-19.6%. Although all differences are significant (paired t-test p-values < 0.0001), the effect sizes range from almost perfect ILS symmetry in the case of Asian elephants, woolly mammoth and straight-tusked elephants to substantial asymmetries for forest, straight-tusked and Asian elephants. The latter is consistent with the computed *D*-statistics, which indicate excess genetic affinity between straight-tusked elephants and Asian elephants compared to forest elephants (Table S11.1), as well as the inferred admixture graph (Figure S12.2 – S12.4), where estimated admixture proportions suggest that 6 - 10% of the straight-tusked elephant sequence is more closely related to a woolly mammoth-related population, which splits off from the ancestral Asian elephant lineage, than to forest elephants. ILS proportions among savanna, forest and Asian elephants become symmetric after applying more stringent filters, suggesting that these apparent differences are driven by data quality issues. Figures S17.11 – S17.18 show the distributions of ILS proportions in each analyzed trio.

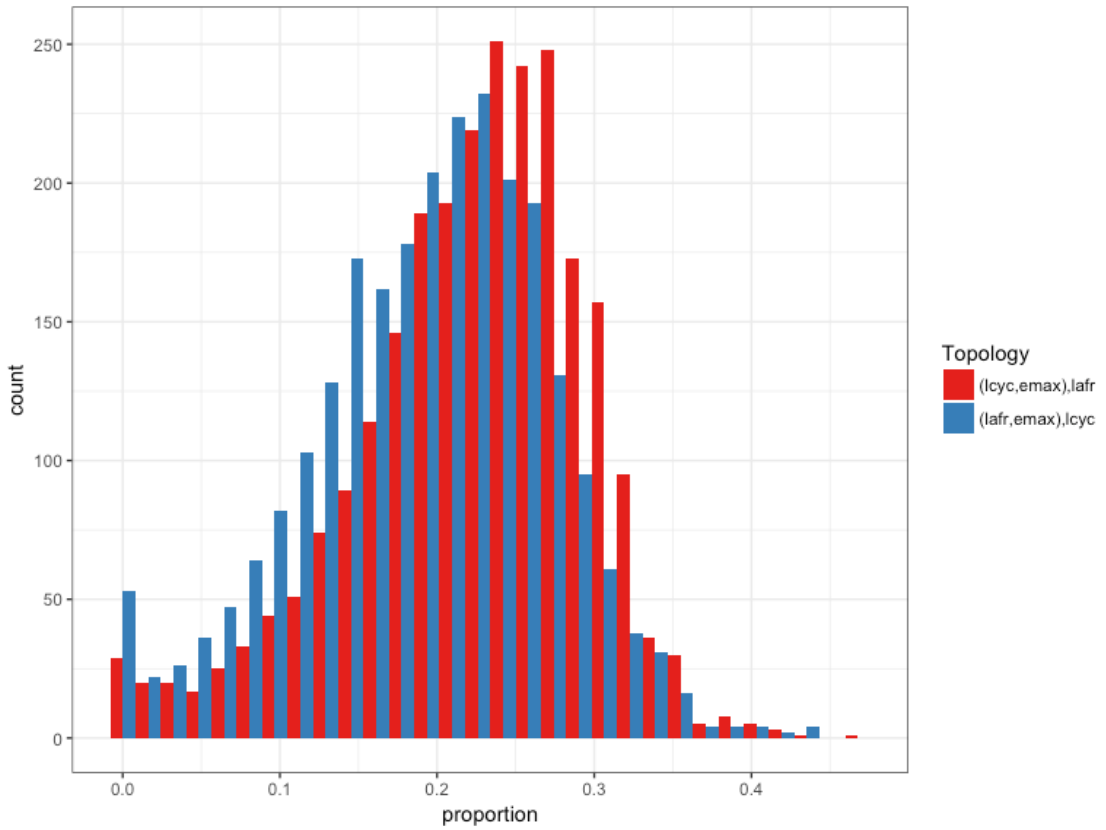

Figure S17.11. Distribution of ILS proportions in 1Mb windows along autosomes for savanna, forest, Asian elephants.

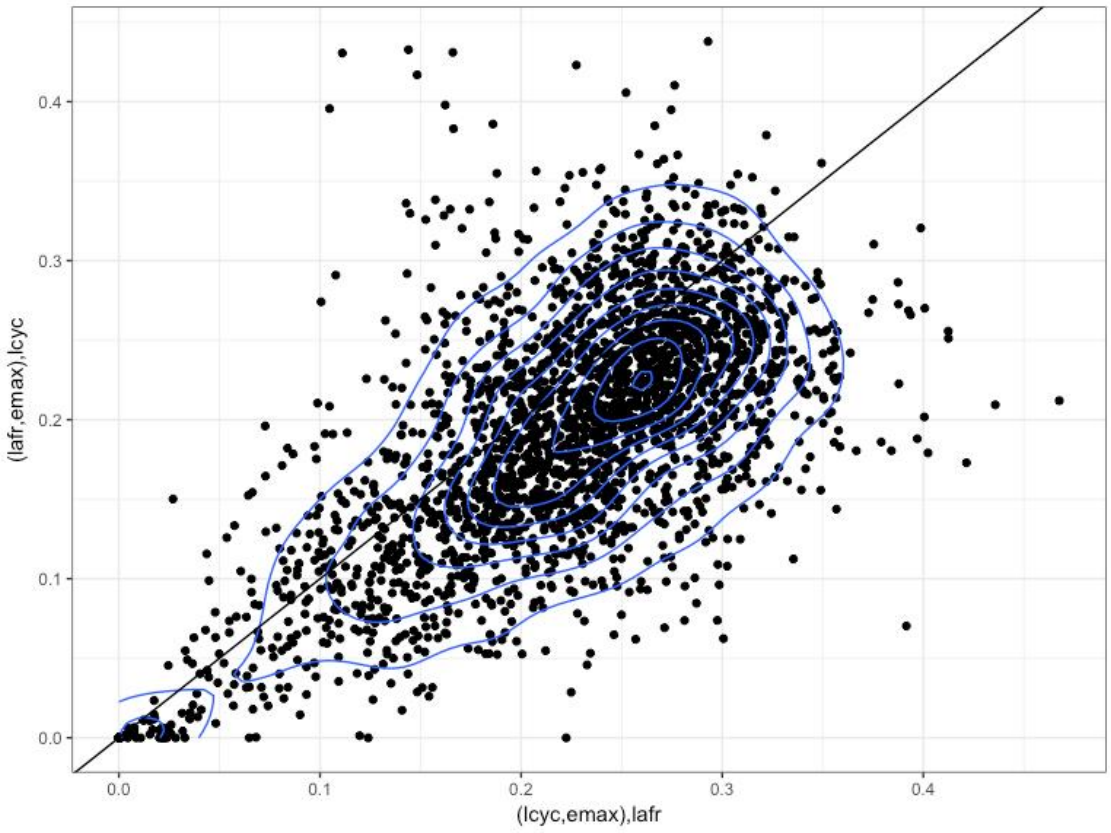

Figure S17.12. Individual ILS proportions of 1Mb windows along autosomes for savanna, forest, Asian elephants.

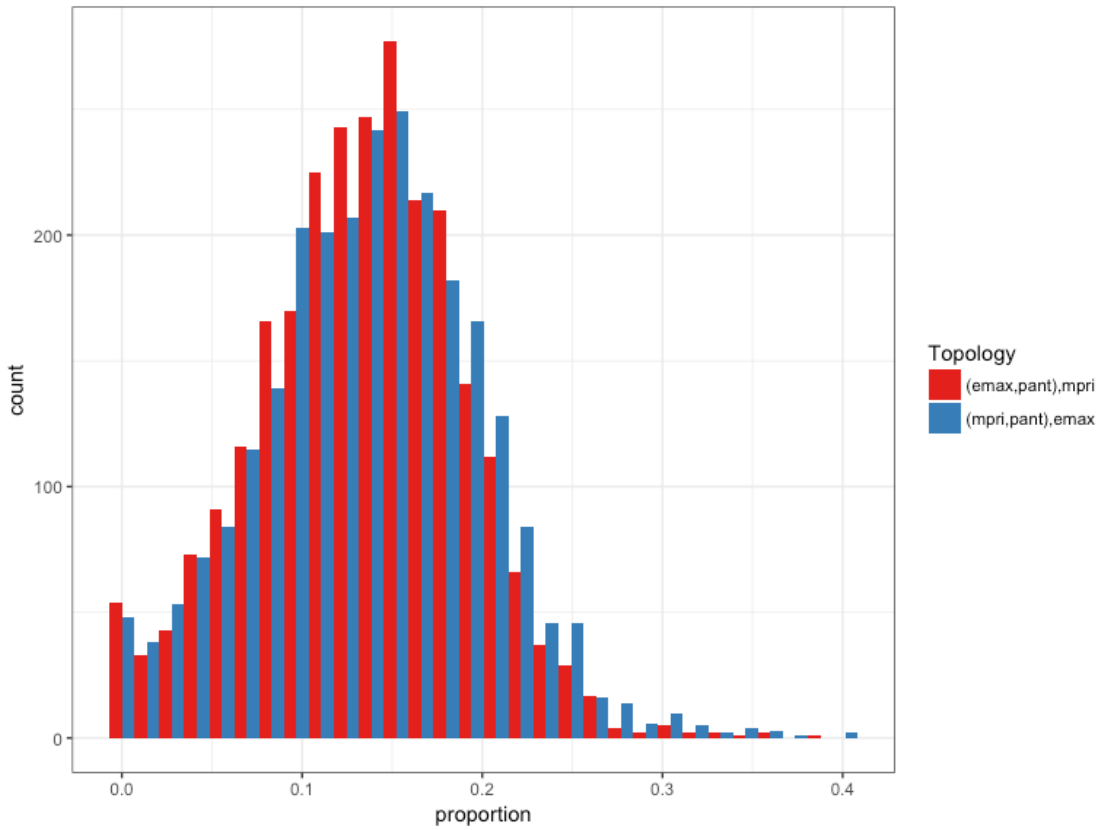

Figure S17.13. Distribution of ILS proportions in 1Mb windows along autosomes for Asian elephant, woolly mammoth, straight-tusked elephant.

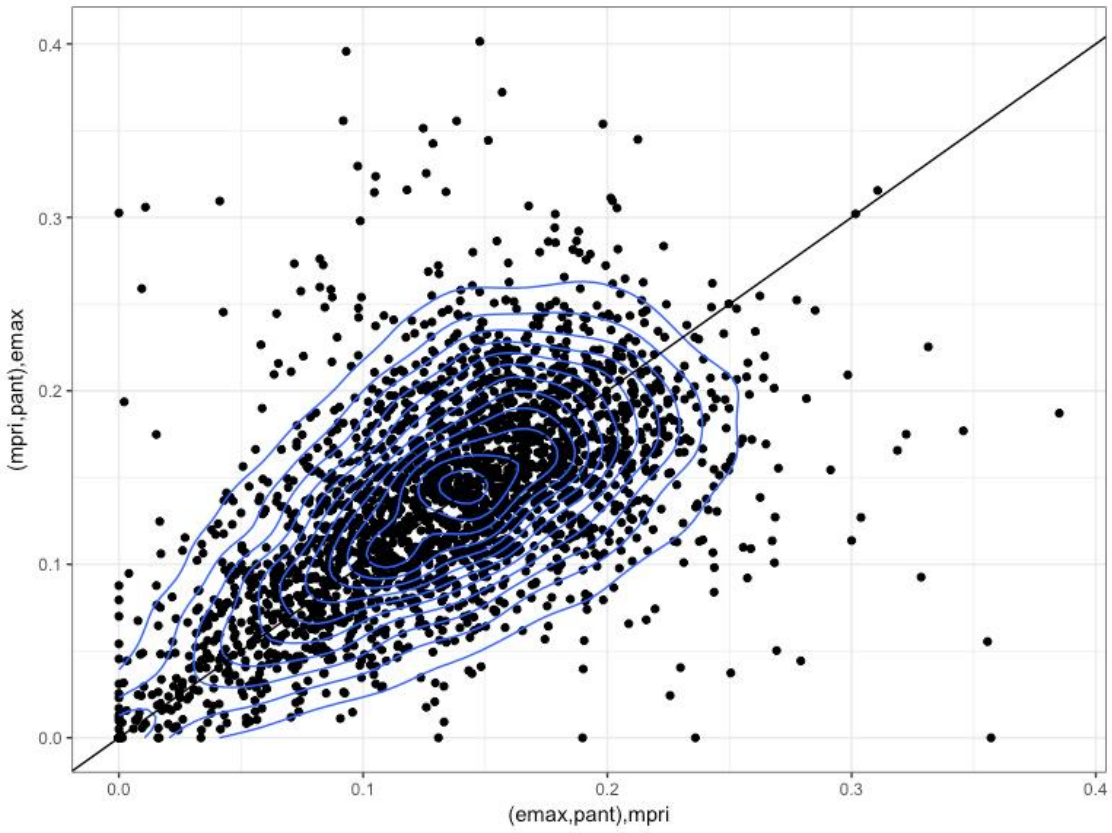

Figure S17.14. Individual ILS proportions of 1Mb windows along autosomes for Asian elephants, woolly mammoth, straight-tusked elephants.

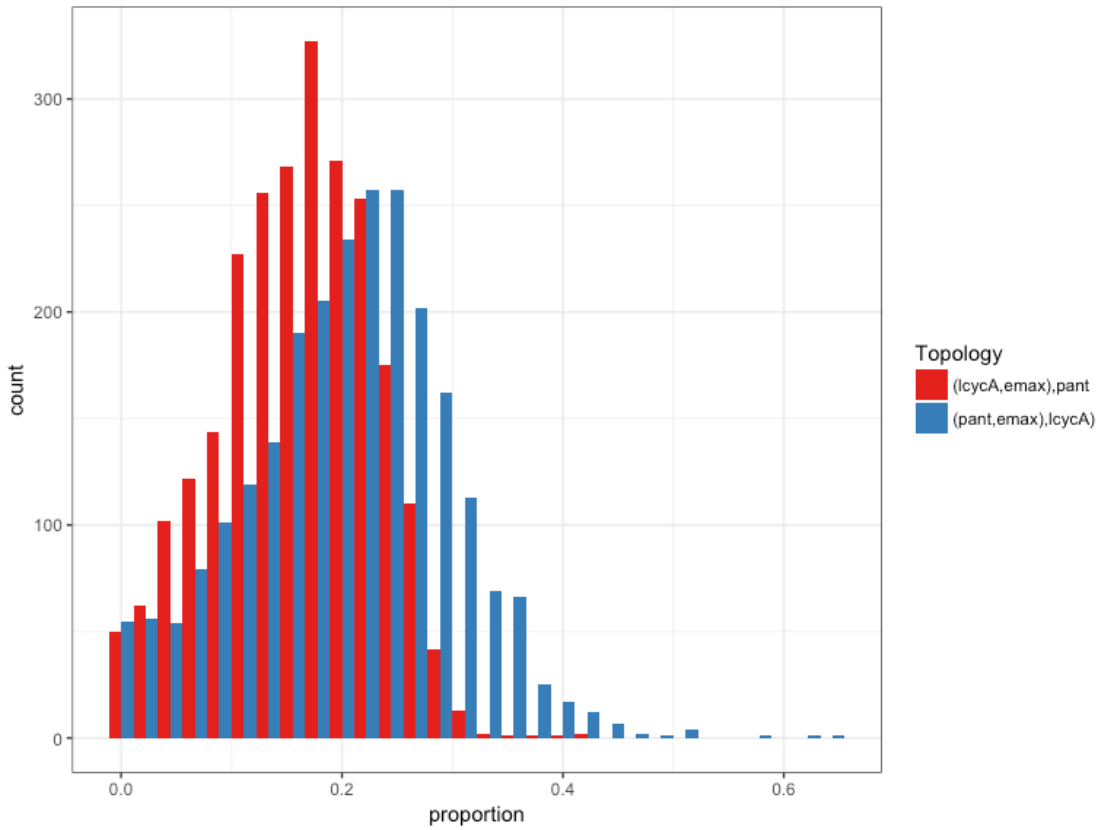

Figure S17.15. Distribution of ILS proportions in 1Mb windows along autosomes for forest (*L. cyclotis_A*), straight-tusked, Asian elephants.

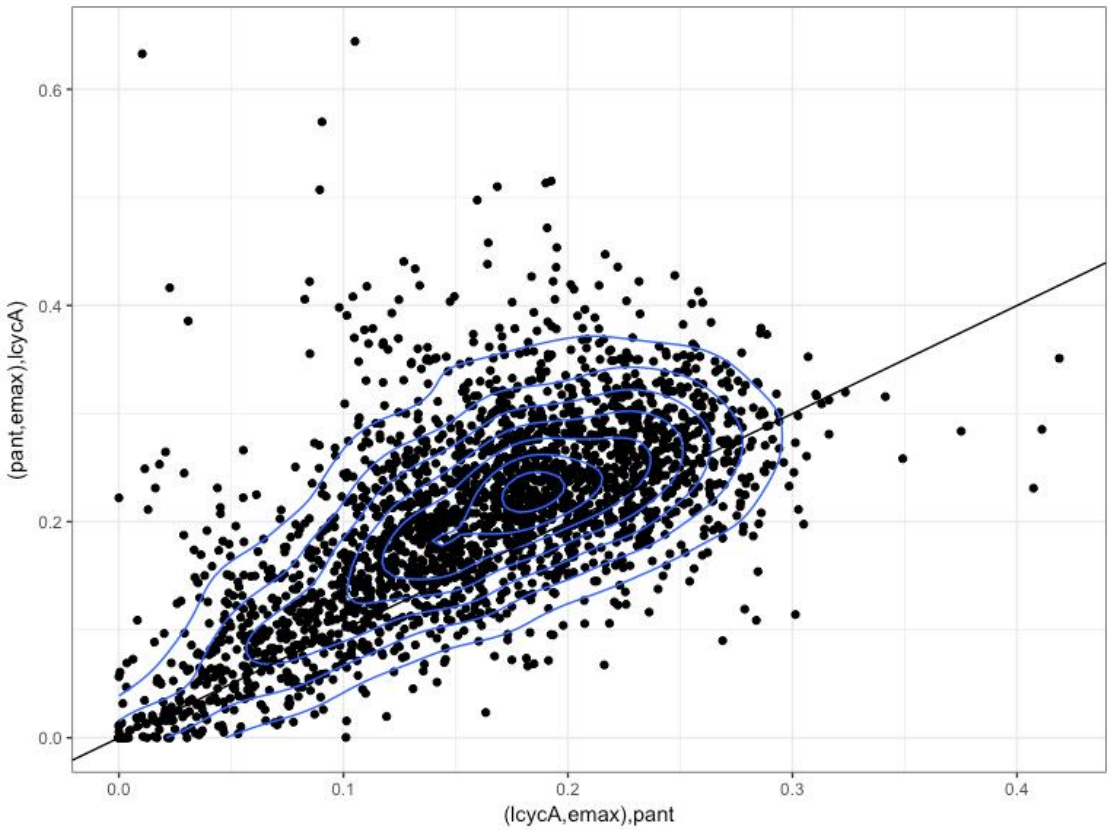

Figure S17.16. Individual ILS proportions of 1Mb windows along autosomes for forest (*L. cyclotis_A*), straight-tusked, Asian elephants.

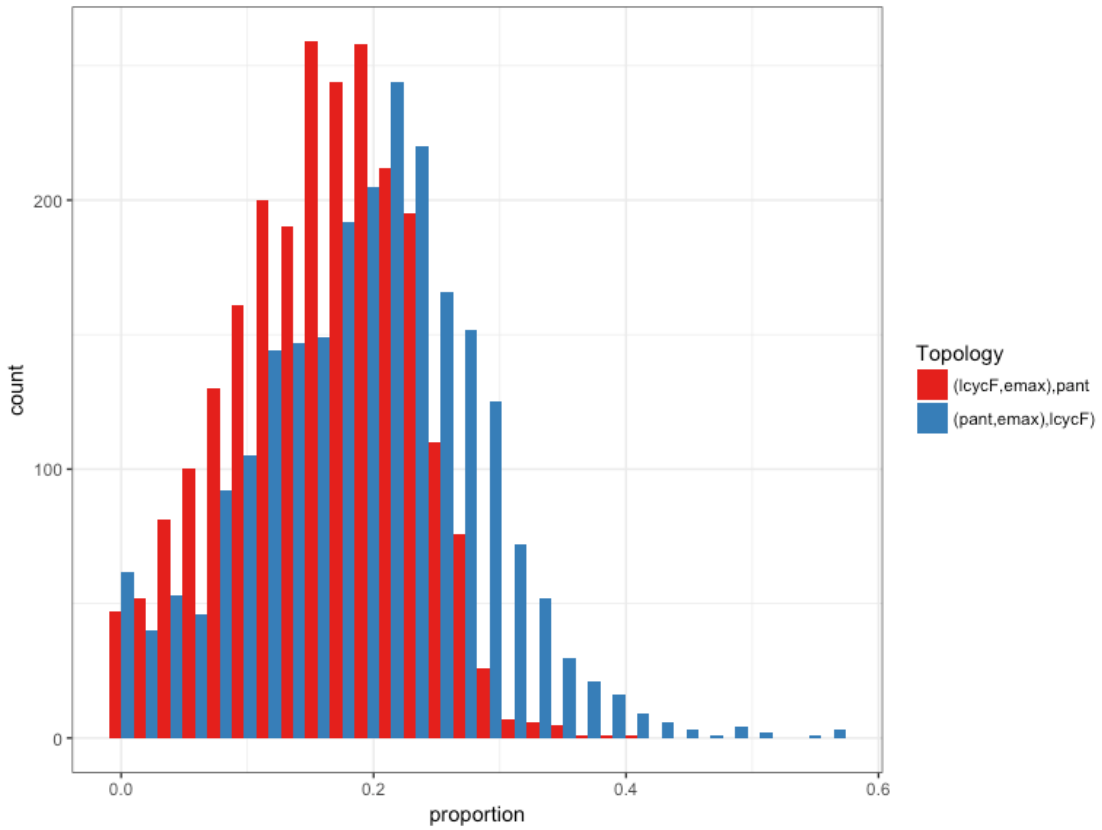

Figure S17.17. Distribution of ILS proportions in 1Mb windows along autosomes for forest (*L. cyclotis_F*), straight-tusked, Asian elephants.

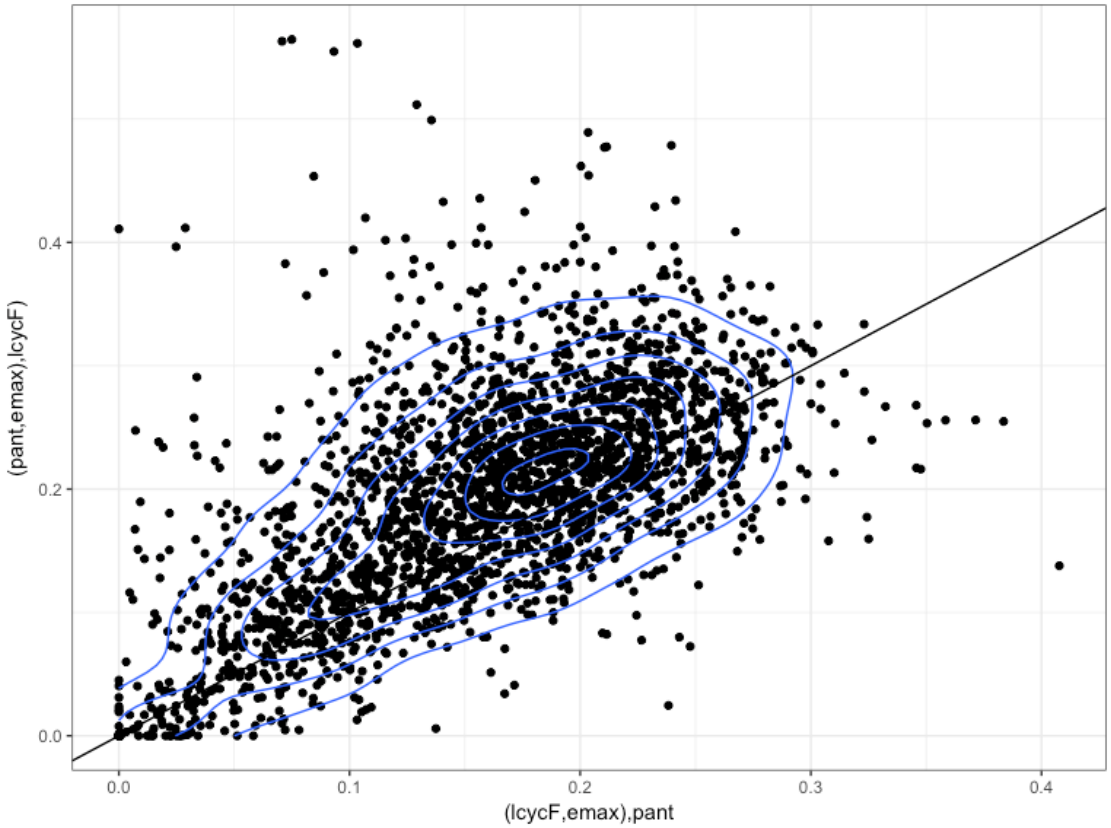

Figure S17.18. Individual ILS proportions of 1Mb windows along autosomes for forest (*L. cyclotis_F*), straight-tusked, Asian elephants.

X chromosome

Here we discuss the results of ILS analyses for the X chromosome. We excluded the *L. cyclotis_F*, straight-tusked elephant and Asian elephants trio due to lack of sufficient sequence to reliably estimate demographic parameters and ILS proportions.

The age of the split between forest and savanna elephants is estimated to have occurred approximately 2,000,000 years with an ancestral effective population size of ~88,000 (Table S17.9). The split between Asian elephant and woolly mammoth is estimated to have occurred approximately 2,300,000 years with an ancestral effective population size of ~45,000 (Table S17.11). We caution that the split time between forest and straight-tusked elephants (approximately 1,700,000 for *L. cyclotis_A*; Table S17.13), represents the combined effect of two different splits in the admixture graph (Figures S12.1 – S12.4). The age of the split between Asian and African elephants is estimated to have occurred between 4,500,000 and 5,100,000 years across the three analyses. The effective size of the population ancestral to all six elephantids is estimated to have been between 28,000 and 31,000.

The ancestral effective population sizes of chromosome X relative to those of the autosomes (A) are 0.53 for forest and savanna elephants, 0.62 for Asian elephant and woolly mammoth, and between 0.56 and 0.58 for the population ancestral to Asian and African elephants. These values are all considerably lower than the expected 0.75 assuming neutrality, equal sex ratios and similar male and female patterns of reproductive success. Linked selection (87, 88), population size change (89), sex-biased migration (90) and differences in the variance of reproductive success between the sexes (91, 92) will affect the X/A ratio. Whereas increased linked selection on the X chromosome is expected to decrease the X/A ratio, the matrilocal social structure and higher variance in male reproductive success in elephants (61) are expected to increase rather than decrease the X/A ratio. Higher variance in male reproductive success (than female), is expected to lower the male effective population size relative to that of females and therefore diversity in chromosome X is expected to be higher relative to the autosomes, increasing the X/A ratio. However, the isolation model used for this analysis does not model gene flow after an initial split and any such gene flow will to some extent be interpreted by the model as ancestral population structure, thus inflating the estimate of ancestral effective population size. Sex-biased gene flow is expected to affect autosomal- and chromosome X- estimates differentially. It is thus possible that male-biased gene flow, which affects the autosomes more than the X chromosomes since males carry only one chromosome X, would inflate the estimated ancestral effective population size of the autosomes relative to that of the X chromosome, and thus decrease the inferred X/A ratio.

Table S17.9. Corrected X chromosome parameter estimates for savanna, forest, Asian elephants.

variable	N (Mb)	median	mean	se_mean
N_{e12}	46	67,808	88,350	8,874
N_{e123}	46	27,435	29,225	1,818
T_1	46	2,104,917	2,042,825	45,425
T_{12}	46	4,764,860	4,712,802	62,548

Table S17.10. Corrected X chromosome parameter estimates (outliers removed) for savanna, forest, Asian elephants.

variable	N (Mb)	median	mean	se_mean
N_{e12}	23	78,717	98,802	10,698
N_{e123}	23	28,587	30,706	1,690
T_1	23	2,088,439	2,008,179	50,878
T_{12}	23	4,863,442	4,881,518	47,560

Table S17.11. Corrected X chromosome parameter estimates for Asian elephant, woolly mammoth, straight-tusked elephant.

variable	N (Mb)	median	mean	se_mean
N_{e12}	33	38,578	44,907	4,471
N_{e123}	33	22,203	27,758	3,791
T_1	33	2,255,851	2,272,937	40,528
T_{12}	33	5,030,025	5,089,240	83,185

Table S17.12. Corrected X chromosome parameter estimates (outliers removed) for Asian elephant, woolly mammoth, straight-tusked elephant.

variable	N (Mb)	median	mean	se_mean
N_{e12}	17	41,522	43,922	2,386
N_{e123}	17	22,900	25,875	2,583
T_1	17	2,339,073	2,332,835	46,063
T_{12}	17	5,126,057	5,172,511	75,642

Table S17.13. Corrected X chromosome parameter estimates for forest (*L. cyclotis_A*), straight-tusked, Asian elephants.

variable	N (Mb)	Median	mean	se_mean
N_{e12}	34	49,680	63,798	9,073
N_{e123}	34	27,265	30,620	2,889
T_1	34	1,489,738	1,466,194	58,683
T_{12}	34	4,612,520	4,509,853	106,167

Table S17.14. Corrected X chromosome parameter estimates (outliers removed) for forest (*L. cyclotis_A*), straight-tusked, Asian elephants.

variable	N (Mb)	median	mean	se_mean
N_{e12}	20	58,487	69,686	8,992
N_{e123}	20	26,882	29,610	2,026
T_1	20	1,483,055	1,459,541	69,483
T_{12}	20	4,728,344	4,696,346	59,623

Table S17.15. Corrected X chromosome parameter estimates for forest (*L. cyclotis_F*), straight-tusked, Asian elephants.

variable	N (Mb)	Median	mean	se_mean
N_{e12}	3	154,051	122,196	29,092

N_{e123}	3	76,594	73,742	17,239
T_1	3	2,041,363	1,782,388	329,178
T_{12}	3	5,686,853	5,377,762	288,643

Table S17.16. Corrected X chromosome parameter estimates (outliers removed) for forest (*L. cyclotis_F*), straight-tusked, Asian elephants.

variable	N (Mb)	median	mean	se_mean
N_{e12}	2	102,869	102,869	36,380
N_{e123}	2	56,324	56,324	14,277
T_1	2	1,652,900	1,652,900	475,141
T_{12}	2	5,167,171	5,167,171	367,916

Patterns of ILS on chromosome X

As for autosomes, we only considered windows where more than 30% was covered by the analyzed alignment in the remaining three trio analyses. Among savanna, forest and Asian elephants, the total proportion of ILS is 28.9%-35.8% (mean +/- 1.96 SE); among Asian elephant, woolly mammoth and straight-tusked elephant, it is 11.7%-15.8%; and in the analysis of forest, straight-tusked and Asian elephants, it is 16.5%-23.1% when using *L. cyclotis_A*. These proportions of ILS tend to be smaller than those expected from the ¾ effective population size of the X chromosome (35.2%, 19.59% and 28.91% respectively); possibly the result of stronger linked selection on the X chromosome.

The relative proportions of the two different types of ILS are potentially informative of admixture characteristics unique to the X chromosome. In contrast to the autosomes, the X chromosome shows highly asymmetric proportions of the two types of ILS among savanna, forest and Asian elephants: ((*L. cyclotis*, *E. maximus*), *L. africana*): 18.4%-22.4%; ((*L. africana*, *E. maximus*), *L. cyclotis*): 10.3%-13.5%. This suggests that exchange of X chromosomes was less restricted between forest and Asian elephants than between savanna and Asian elephants. This could result from different extents of sex-bias on migration between forest and Asian and between savanna and Asian elephants, or could be the result of stronger selection against exchange of X chromosomes between savanna and Asian than between forest and Asian elephants. However, high ILS asymmetry on chromosome X could be driven by data quality issues, such as those observed in the autosomes of this trio.

Asian elephants, woolly mammoths and straight-tusked elephants, which show ILS symmetry on autosomes, also show symmetric ILS on chromosome X: ((*E. maximus*, *P. antiquus*), *M. primigenius*): 6.1%-8.4%; ((*M. primigenius*, *P. antiquus*), *E. maximus*): 5.4%-7.7%. The ILS symmetry on both X and autosomes is inconsistent with the computed *D*-statistics that indicate

stronger genetic affinity between straight-tusked elephants and woolly mammoths than between straight-tusked and Asian elephants (Table S11.1), as well as the inferred admixture graph, in which straight-tusked elephants receive between 6 to 10% of their ancestry from a population most closely related to woolly mammoths (Figures S12.2 – S12.4). However, as depicted in the admixture graph, the woolly mammoth-related source of admixture splits off only shortly after the split of Asian elephants and woolly mammoths and therefore has not experienced sufficient drift to produce asymmetric ILS proportions between straight-tusked elephants and Asian elephants vs. woolly mammoths. Forest (*L. cyclotis_A*), straight-tusked and Asian elephants show ILS symmetry on the X chromosome: ((*L. cyclotis_A*, *E. maximus*), *P. antiquus*): 8.2%-11.5%; ((*P. antiquus*, *E. maximus*), *L. cyclotis_A*): 8.2%-11.7%. This could be reconciled with the observed asymmetry on the autosomes either through lack of statistical power (the X-chromosome confidence intervals are relatively wide) or by reduced gene flow on the X.

Supplementary Note 18

Isolation with Migration CoalHMM analysis

We fitted the *isolation* and the *isolation-with-initial-migration* coalescent hidden Markov models from Mailund *et al.* (93) to selected pairs of genome sequences. These models exploit patterns of divergence along a pairwise sequence alignment to infer the variation in coalescence times caused by the recombination process and fit this variation to expectations under a clean split isolation process, and under a speciation process with an initial period of constant gene flow between the emerging species. With the isolation model we can infer the time of the split between two species and the effective population size in the ancestral species. With the initial-migration model we can infer two time points: when the ancestral population split and when gene flow between the two resulting populations ended, in addition to the effective population size in the ancestral population and level of gene flow between the two populations during the speciation. This migration is assumed to be constant over time and symmetric between the two populations.

We generated pseudo-haploid sequences with random allele calls per site with minimum depth of 3 reads (as described in Supplementary Notes 16, 17) for the following individuals: *L. cyclotis_A* (A)*, L. africana_B* (B)*, L. africana_C* (C)*, E. maximus_D* (D)*, E. maximus_E* (E)*, L. cyclotis_F* (F)*, M. americanum_I* (I)*, P. antiquus_N* (N)*, M. primigenius_P* (P)*, M. primigenius_Q* (Q). All sequences were masked with the 90% stringent mappability filter and sequences from different taxa were pairwise aligned. Since the X chromosome often behaves differently from the autosomes, both when it comes to selection and gene flow, we separated all data into X chromosomes and autosomes, and analysed these data sets separately.

Model selection

Since the isolation and migration models have different numbers of parameters (3 and 5, respectively), and are not nested models, we used the Akaike Information Criterion (AIC) to choose the preferred model. Figures S18.1, S18.2 show the relative AIC for the two models, that is, the AIC for the isolation model minus the AIC for the migration model. Since the preferred model is the one with the smallest AIC value, positive numbers indicate a preference for the migration model and negative numbers a preference for the clean isolation model. For autosomes, all pairs of samples have a preference for the migration model, except for the savanna elephant (*L. africana_B*) and woolly mammoth (*M. primigenius_P*), for which the relative AIC is close to zero (Figure S18.1). In contrast, for the X chromosome, a large number of pairs prefer the clean isolation model (Figure S18.2). Specifically, for Asian elephants and woolly mammoths, as well as for straight-tusked elephants and woolly mammoths, none of the pairs of samples have a preference for the migration model, providing no evidence for gene flow on the X chromosome for these pairs of taxa. However, we caution that this could be due to insufficient power to detect gene flow since data are far more limited on the X chromosome. With the exception of savanna and Asian elephants, savanna elephants and mastodon, and Asian

elephants and mastodon, for which all pairs of samples prefer the migration model, and savanna and straight-tusked elephants, for which the relative AIC is close to zero, all other pairs of taxa show either a preference for the isolation model or a preference for the migration model on chromosome X, depending on the analyzed pair of samples.

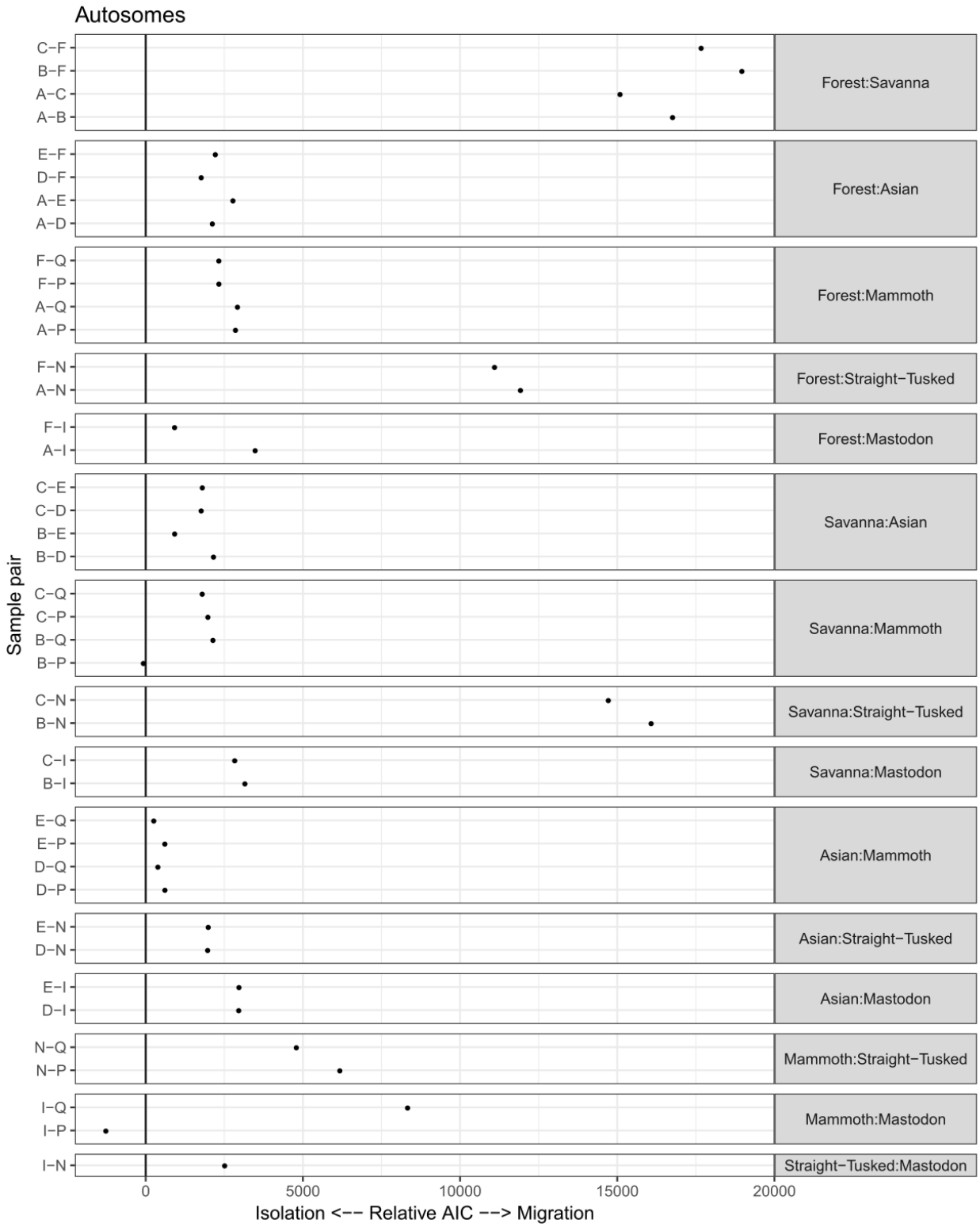

Figure S18.1. Relative AIC for model selection on autosomes. Positive numbers indicate a preference for the migration model and negative numbers a preference for the strict isolation model.

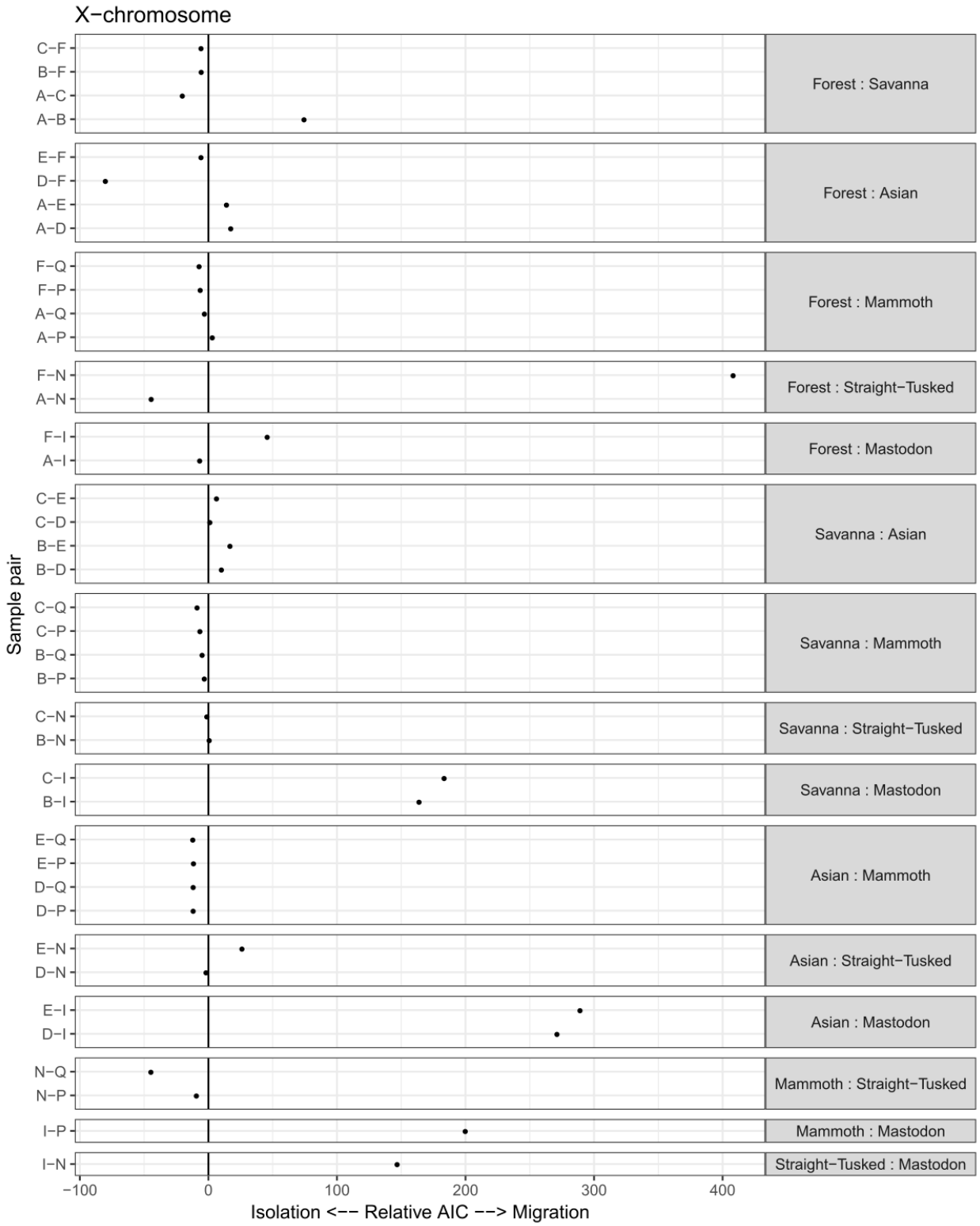

Figure S18.2. Relative AIC for model selection on X chromosomes. Positive numbers indicate a preference for the migration model and negative numbers a preference for the strict isolation model.

Parameter estimation

As part of fitting the models we obtain maximum likelihood estimates of the various demographic parameters, including ancestral effective population sizes, migration rates, and split times. In Figures S18.3 – S18.4, when the migration model is preferred , the initial split is shown at the high end of a range with the end of gene flow at the low end and the migration rate shown in square brackets following the interval. Time points are measured as the expected number of substitutions at a given time in the past and migration rates as the expected number of migrations a lineage will have seen per substitution. In Tables S18.1 – S18.2, *mig-period* refers to the time when the migration period ends and *split-time* to the initial population split. Time intervals have been rescaled using a per-year substitution rate of 0.406×10^{-9} (to enable comparison to the simulation analyses in Note 16 but note that the assumed mutation rate is uncertain), and the effective population size is computed using the estimated coalescence rate, the substitution rate mentioned above, and a generation time of 31 years. The migration rate is shown as two numbers: *m* refers to the fraction of migrants per generation and *M* to the total number of migrants per generation (assuming that the effective population size matches the actual population size). When the isolation model is preferred, we show the split time only and have set *M*, *m*, and *mig-period* to *NA*.

From the analysis of autosomes, forest and savanna elephants are inferred to have initiated splitting ~5.3 Mya (confidence interval [CI] obtained from 100 or 40 bootstrap replicates: 5.5 – 2.6 Mya for pairs including *L. cyclotis_A* and 5.6 – 4.7 Mya for pairs including *L. cyclotis_F*) and exchanged gene flow until ~1.3 Mya (CI: 3.0 – 1.1 Mya for pairs including *L. cyclotis_A*) or more recently (CI: 1.4 – 0.1 Mya for pairs including *L. cyclotis_F*) with 5.33×10^{-6} migrants per lineage per generation (CI: 3.15×10^{-14} – 1.21×10^{-4}), and ancestral N_e of 43,500 – 69,000 individuals (Table S18.1). The split between straight-tusked and forest/savanna elephants is estimated to have begun at ~5.9 Mya (CI: 6.0 – 5.6 Mya) with gene flow continuing until ~1.2 Mya (CI: 1.3 – 1.0 Mya) with forest and ~1.6 Mya (CI: 1.7 – 1.6 Mya) with savanna elephants. The inferred migration rate between forest and straight-tusked elephants (CI: 1.00×10^{-5} – 1.49×10^{-5}) is approximately two-fold higher than that inferred between savanna and straight-tusked elephants (CI: 5.17×10^{-6} – 6.00×10^{-6}), consistent with the findings from the ABC analysis, and their ancestral N_e is estimated at 46,400 – 52,800 individuals. The initial split between Asian elephants and woolly mammoths is estimated at ~3 Mya (but note wide CI: 19.3 – 2.9 Mya) with gene flow of 1.61×10^{-6} migrants per generation (CI: 1.35×10^{-7} – 4.10×10^{-5}) continuing until ~1.5 Mya (CI: 2.8 – 0.6 Mya) and ancestral N_e between 26,600 – 60,000 individuals. The straight-tusked and African elephants are estimated to have began splitting from Asian elephants and woolly mammoths ~5.8 Mya (combined CI: 6.1 – 5.0 Mya). Gene flow between African elephants and Asian elephants/woolly mammoths ceased already at ~3.8 Mya (combined CI: 4.8 – 3.4 Mya), while between straight-tusked elephants and Asian elephants/woolly mammoths continued until 1.6 Mya (CI: 3.7 – 1.3 Mya), consistent with the finding of woolly mammoth-related admixture into the straight-tusked elephant lineage (Figure

S12.2). The migration rate between these two major lineages is estimated to have been 2.72×10^{-07} – 1.04×10^{-05} (combined CIs) and ancestral N_e between 53,600 – 68,500 individuals (combined CIs). All elephantids began splitting from the mastodon ~15 Mya (CI: 24.2 – 13.0 Mya) with gene flow of 2.8×10^{-6} migrants per generation (CI: 2.65×10^{-8} – 2.16×10^{-5}) until ~11.1 Mya (CI: 12.5 – 2.9 Mya). Their ancestral N_e is inferred to have been 36,500 – 76,800 individuals. However, we are cautious about these latter parameter estimates (from species' pairs including the mastodon) since the mastodon genome is sequenced only at ~4-fold coverage and therefore of low quality.

Overall, younger split times are inferred from the analyses of X chromosomes. When comparing ancestral N_e estimates from autosomes (A) and X chromosomes, the X/A ratio is usually lower than the expected ¾ ratio assuming panmictic ancestral populations (similar to the pattern observed in the ILS analyses in Note 17). For the few pairs of samples for which migration was the preferred model, the inferred migration rate ranges are considerably wider than those for the autosomal data (Table S18.2).

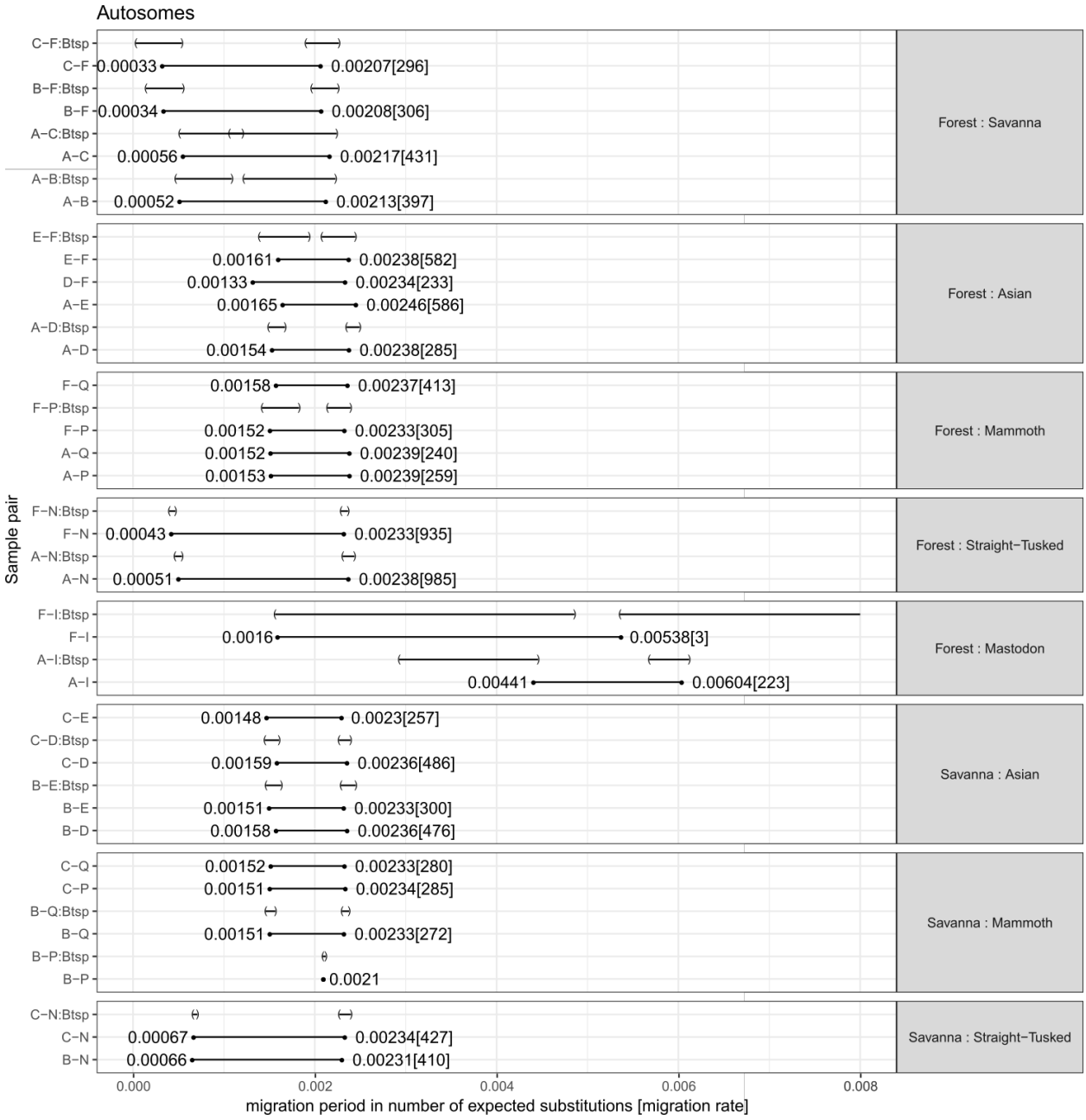
Autosomes
C−F:Btsp
C−F
0.00033
0.00207[296]
B−F:Btsp
B−F
0.00034
0.00208[306]
A−C:Btsp
A−C
0.00056
0.00217[431]
A−B:Btsp
A−B
0.00052
0.00213[397]
Forest : Savanna
E−F:Btsp
E−F
0.00161
0.00238[582]
D−F
0.00133
0.00234[233]
A−E
0.00165
0.00246[586]
A−D:Btsp
A−D
0.00154
0.00238[285]
Forest : Asian
F−Q
0.00158
0.00237[413]
F−P:Btsp
F−P
0.00152
0.00233[305]
A−Q
0.00152
0.00239[240]
A−P
0.00153
0.00239[259]
Forest : Mammoth
F−N:Btsp
F−N
0.00043
0.00233[935]
A−N:Btsp
A−N
0.00051
0.00238[985]
Forest : Straight−Tusked
Sample pair
F−I:Btsp
F−I
0.0016
0.00538[3]
A−I:Btsp
A−I
0.00441
0.00604[223]
Forest : Mastodon
C−E
0.00148
0.0023[257]
C−D:Btsp
C−D
0.00159
0.00236[486]
B−E:Btsp
B−E
0.00151
0.00233[300]
B−D
0.00158
0.00236[476]
Savanna : Asian
C−Q
0.00152
0.00233[280]
C−P
0.00151
0.00234[285]
B−Q:Btsp
B−Q
0.00151
0.00233[272]
B−P:Btsp
B−P
0.0021
Savanna : Mammoth
C−N:Btsp
C−N
0.00067
0.00234[427]
B−N
0.00066
0.00231[410]
Savanna : Straight−Tusked
0.000
0.002
0.004
0.006
0.008
migration period in number of expected substitutions [migration rate]

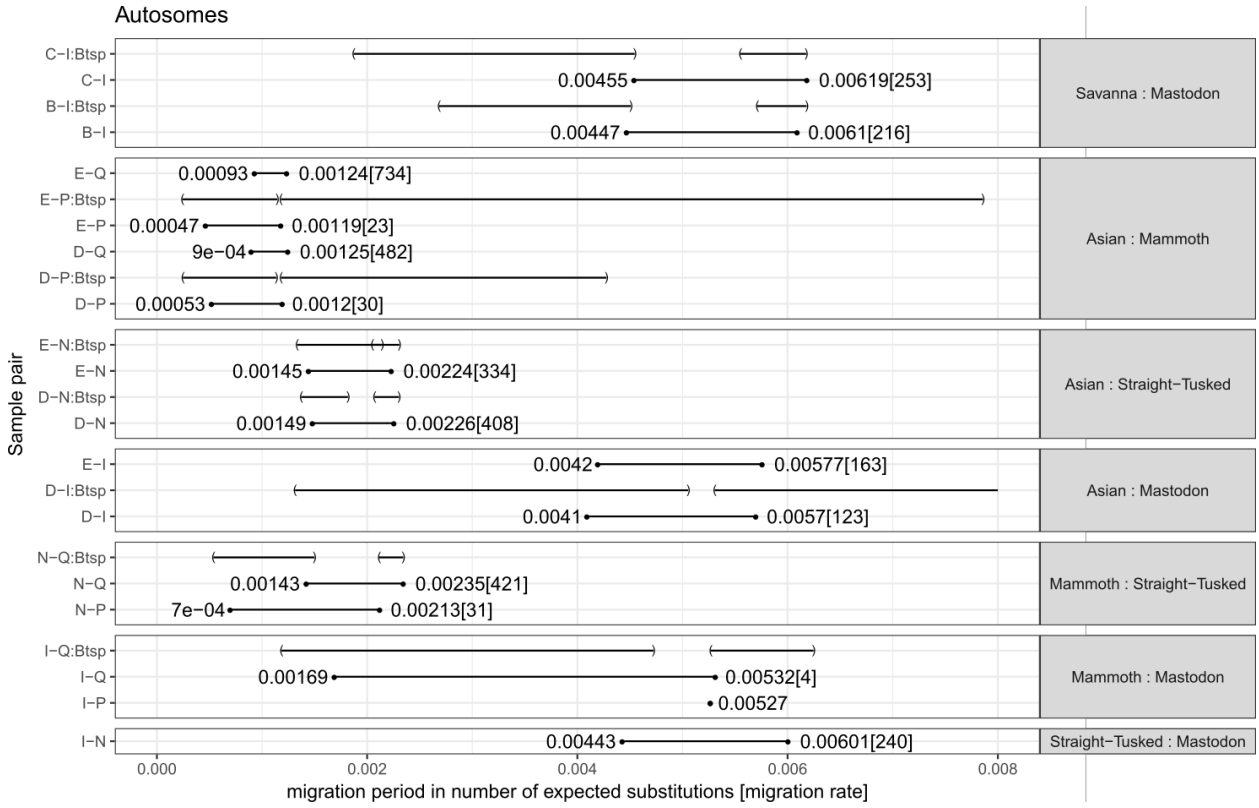

Figure S18.3. Parameter estimates from isolation and migration CoalHMM analysis on autosomes. When the strict isolation model is the preferred model, the split time is shown as a dot. When the migration model is preferred, the initial split is shown at the high end of a range with the end of gene flow at the low end and the migration rate is shown in square brackets following the interval. Lower and upper confidence intervals for the initial split and end of gene flow obtained from bootstrap analyses are given on top of the respective dots. Times are given in units of substitutions and migration rates as the expected number of migrants per lineage per substitution.

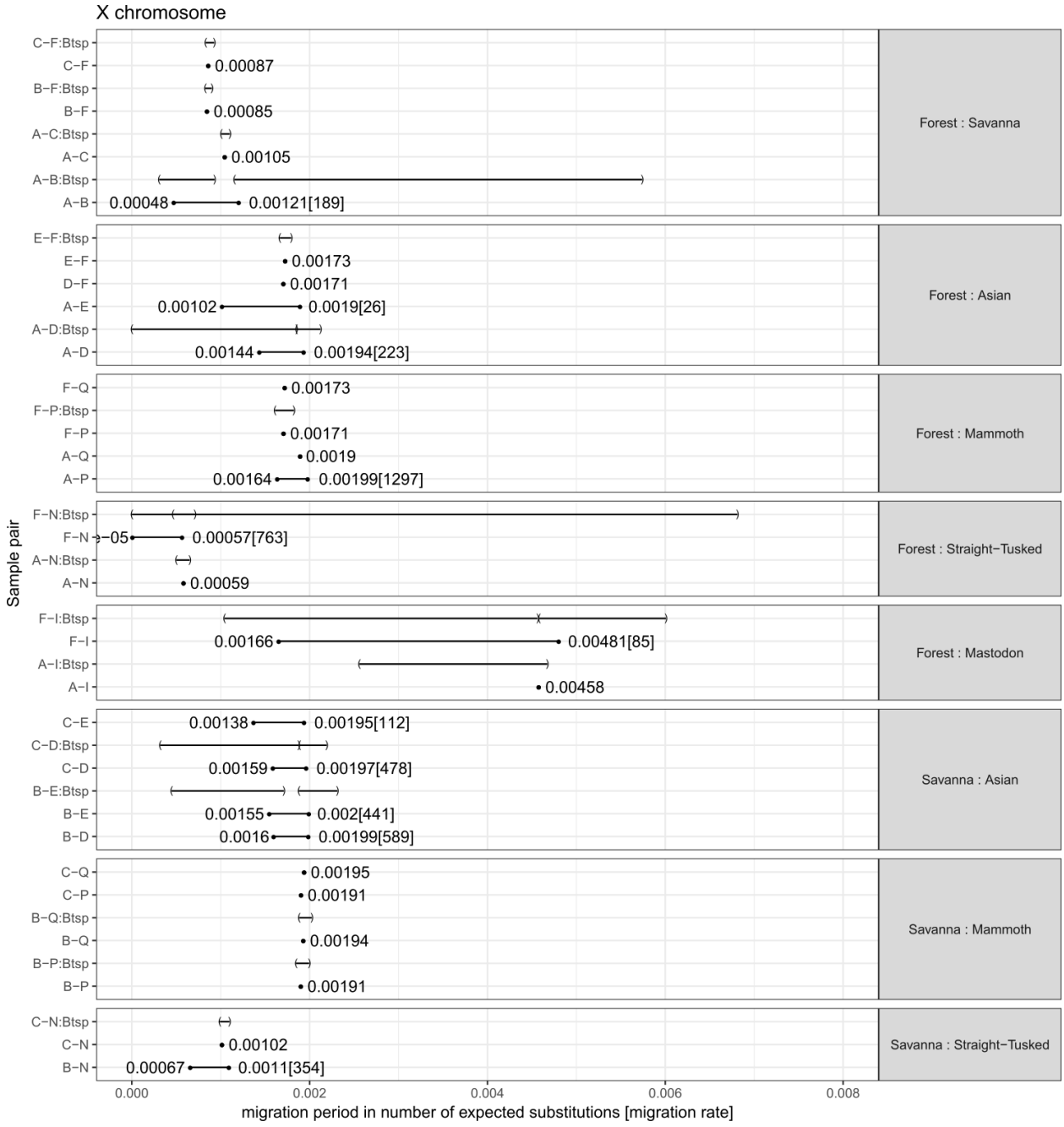
X chromosome
C−F:Btsp
C−F
0.00087
B−F:Btsp
B−F
0.00085
A−C:Btsp
A−C
0.00105
A−B:Btsp
A−B
0.00048
0.00121[189]
Forest : Savanna
E−F:Btsp
E−F
0.00173
D−F
0.00171
A−E
0.00102
0.0019[26]
A−D:Btsp
A−D
0.00144
0.00194[223]
Forest : Asian
F−Q
0.00173
F−P:Btsp
F−P
0.00171
A−Q
0.0019
A−P
0.00164
0.00199[1297]
Forest : Mammoth
F−N:Btsp
F−N
−05
0.00057[763]
A−N:Btsp
A−N
0.00059
Forest : Straight−Tusked
F−I:Btsp
F−I
0.00166
0.00481[85]
A−I:Btsp
A−I
0.00458
Forest : Mastodon
C−E
0.00138
0.00195[112]
C−D:Btsp
C−D
0.00159
0.00197[478]
B−E:Btsp
B−E
0.00155
0.002[441]
B−D
0.0016
0.00199[589]
Savanna : Asian
C−Q
0.00195
C−P
0.00191
B−Q:Btsp
B−Q
0.00194
B−P:Btsp
B−P
0.00191
Savanna : Mammoth
C−N:Btsp
C−N
0.00102
B−N
0.00067
0.0011[354]
Savanna : Straight−Tusked
Sample pair
0.000
0.002
0.004
0.006
0.008
migration period in number of expected substitutions [migration rate]

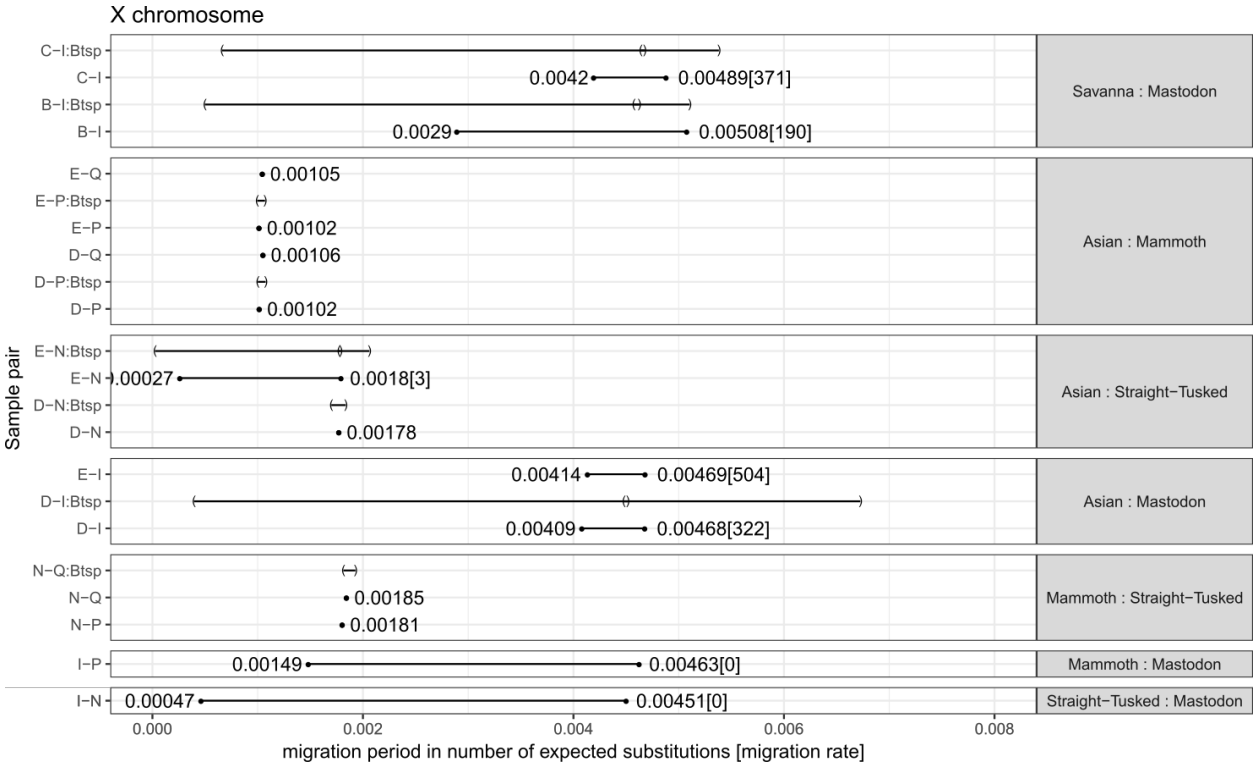

Figure S18.4. Parameter estimates from isolation and migration CoalHMM analysis on the X chromosome. When the strict isolation model is the preferred model, the split time is shown as a dot. When the migration model is preferred, the initial split is shown at the high end of a range with the end of gene flow at the low end and the migration rate is shown in square brackets following the interval. Lower and upper confidence intervals for the initial split and end of gene flow obtained from bootstrap analyses are given on top of the respective dots. Times are given in units of substitutions and migration rates as the expected number of migrants per lineage per substitution.

Table S18.1. Parameter estimates for autosomes from isolation and migration CoalHMM analysis. Lower and upper confidence intervals are obtained from bootstrap analyses (100 or 40 replicates, the latter shown in italics). *split time* refers to the initial population split and *mig period* to the time when the migration period ends. Time intervals have been rescaled using a per-year substitution rate of 0.406×10^{-9}, the effective population size is computed using the estimated coalescence rate, the substitution rate mentioned above, and a generation time of 31 years. The migration rate is shown as two numbers, *m* refers to the fraction of migrants per lineage per generation and *M* to the total number of migrants per generation assuming that the effective population size matches the actual population size. When the strict isolation model is preferred, the *split time* is only shown and *M*, *m*, and *mig period* are set to *NA*.

	N_e lower	N_e	N_e upper	*M* lower	*M*	*M* upper	*m* lower	*m*	*m* upper	mig period lower	mig period	mig period upper	split time lower	split time	split time upper
Forest - Savanna															
AB	55,045	56,237	64,925	0.473	0.583	2.864	4.20E-06	5.19E-06	2.55E-05	1,154,187	1,304,187	2,676,847	2,998,522	5,279,064	5,485,468
AC	54,884	56,152	69,037	0.000	0.599	13.643	3.15E-14	5.33E-06	1.21E-04	1,261,330	1,354,433	2,969,951	2,612,315	5,296,552	5,515,764
BF	43,459	46,345	48,135	0.261	0.375	0.531	2.82E-06	4.05E-06	5.73E-06	350,493	882,759	1,357,635	4,837,931	5,120,690	5,557,882
CF	44,434	46,049	48,878	0.223	0.371	0.500	2.42E-06	4.02E-06	5.43E-06	77,586	922,906	1,323,153	4,682,020	5,194,089	5,580,296
Forest - Asian															
AD	57,663	59,093	60,313	0.352	0.424	0.975	2.98E-06	3.58E-06	8.25E-06	3,672,167	3,788,177	4,119,458	5,784,729	5,852,956	6,142,611
EF	53,633	54,610	58,074	0.190	0.484	1.137	1.74E-06	4.44E-06	1.04E-05	3,421,675	3,819,212	4,770,690	5,114,286	5,712,562	6,022,906
Forest - Mammoth															
FP	55,085	56,519	58,877	0.197	0.441	0.768	1.74E-06	3.90E-06	6.79E-06	3,497,044	3,766,256	4,498,522	5,267,980	5,768,719	5,893,842
Forest - Straight-tusked															
AN	50,657	51,790	52,473	1.037	1.190	1.513	1.00E-05	1.15E-05	1.46E-05	1,132,759	1,250,246	1,327,340	5,681,034	5,926,355	5,999,507
FN	*46,363*	*47,722*	*48,919*	*0.956*	*1.110*	*1.421*	*1.00E-05*	*1.16E-05*	*1.49E-05*	*982,020*	*1,056,650*	*1,146,798*	*5,636,453*	*5,742,118*	*5,828,571*
Forest - Mastodon															
AI	66,651	67,593	71,582	0.167	0.378	0.415	1.24E-06	2.79E-06	3.07E-06	7,212,315	10,880,788	10,974,384	13,987,931	14,885,714	15,068,473
FI	45,894	66,598	72,656	0.005	0.282	1.641	3.98E-08	2.12E-06	1.23E-05	3,844,828	10,444,828	11,961,576	13,196,059	14,386,700	20,219,704
Savanna - Asian															
BE	60,148	61,121	62,715	0.376	0.462	0.979	3.08E-06	3.78E-06	8.01E-06	3,601,970	3,709,113	4,017,734	5,635,714	5,730,542	6,033,744
CD	61,348	63,020	64,288	0.330	0.434	0.837	2.61E-06	3.45E-06	6.64E-06	3,570,690	3,685,961	3,956,404	5,580,542	5,669,951	5,893,103
Savanna - Mammoth															
BP	64,919	66,506	67,978	NA	NA	NA	NA	NA	NA	NA	NA	NA	5,143,596	5,181,034	5,220,936

BQ	*64,298*	*66,151*	*68,473*	*0.359*	*0.432*	*0.632*	*2.71E-06*	*3.27E-06*	*4.78E-06*	*3,595,567*	*3,704,187*	*3,856,650*	*5,662,562*	*5,726,601*	*5,852,956*
Savanna - Straight-tusked															
CN	51,794	52,499	52,840	0.543	0.564	0.630	5.17E-06	5.38E-06	6.00E-06	1,621,429	1,650,000	1,742,857	5,588,177	5,746,305	5,904,433
Savanna - Mastodon															
BI	62,945	63,914	67,829	0.092	0.330	0.367	7.20E-07	2.58E-06	2.87E-06	6,613,547	11,000,000	11,102,956	14,068,473	15,003,941	15,224,138
CI	61,894	63,279	69,146	0.007	0.332	0.386	5.74E-08	2.62E-06	3.05E-06	4,612,069	11,071,429	11,195,320	13,673,892	15,066,256	15,212,315
Asian - Mammoth															
DP	41,405	56,660	60,200	0.032	0.183	2.432	2.78E-07	1.61E-06	2.15E-05	609,852	1,515,025	2,796,305	2,910,345	2,974,631	10,532,020
EP	26,593	56,356	59,111	0.015	0.040	4.617	1.35E-07	3.58E-07	4.10E-05	600,246	1,254,926	2,817,734	2,906,404	2,937,931	19,351,970
Asian - Straight-tusked															
DN	57,143	57,870	60,770	0.326	0.508	0.913	2.82E-06	4.39E-06	7.89E-06	3,382,512	3,606,158	4,476,601	5,100,000	5,519,458	5,671,182
EN	54,944	57,796	59,397	0.278	0.488	0.852	2.41E-06	4.22E-06	7.37E-06	3,285,468	3,666,256	5,276,355	5,050,246	5,494,828	5,678,818
Asian-Mastodon															
DI	*36,447*	*74,410*	*76,232*	*0.006*	*0.010*	*3.221*	*3.95E-08*	*6.83E-08*	*2.16E-05*	*3,236,453*	*4,940,640*	*12,448,030*	*13,070,936*	*13,251,478*	*24,231,034*
Mammoth-Straight-tusked															
NQ	*60,017*	*61,276*	*63,175*	*0.033*	*0.048*	*0.729*	*2.72E-07*	*3.91E-07*	*5.95E-06*	*1,325,369*	*1,636,700*	*3,688,916*	*5,210,345*	*5,290,394*	*5,771,921*
Mammoth-Mastodon															
IQ	*65,325*	*74,122*	*76,770*	*0.004*	*0.007*	*2.082*	*2.65E-08*	*4.71E-08*	*1.40E-05*	*2,919,704*	*4,174,384*	*11,633,744*	*12,979,064*	*13,103,695*	*15,385,961*

Table S18.2. Parameter estimates for X chromosomes from isolation and migration CoalHMM analysis. Lower and upper confidence intervals are obtained from bootstrap analyses (100 or 40 replicates, the latter shown in italics). *split time* refers to the initial population split and *mig period* to the time when the migration period ends. Time intervals have been rescaled using a per-year substitution rate of 0.406×10^{-9}, the effective population size is computed using the estimated coalescence rate, the substitution rate mentioned above, and a generation time of 31 years. The migration rate is shown as two numbers, *m* refers to the rate of migrations per lineage per generation and *M* to the number of migrations in total per generation assuming that the effective population size matches the actual population size. When the strict isolation model is preferred, the split time is only shown and *M*, *m*, and *mig period* are set to NA.

	***N_e* lower**	***N_e***	***N_e* upper**	***M* lower**	***M***	***M* upper**	***m* lower**	***m***	***m* upper**	**mig period lower**	**mig period**	**mig period upper**	**split time lower**	**split time**	**split time upper**
Forest - Savanna															

AB	17,263	39,866	45,088	0.095	0.435	7.331	1.19E-06	5.46E-06	9.19E-05	756,897	1,588,916	2,291,379	2,843,103	3,188,916	14,137,685
AC	31,833	39,649	56,468	NA	NA	NA	NA	NA	NA	NA	NA	NA	2,478,079	2,602,217	2,715,517
BF	17,960	30,476	34,779	NA	NA	NA	NA	NA	NA	NA	NA	NA	2,035,468	2,120,936	2,218,227
CF	16,469	29,354	41,574	NA	NA	NA	NA	NA	NA	NA	NA	NA	2,045,813	2,156,650	2,281,773
Forest - Asian															
AD	27,535	35,291	45,469	0.006	0.358	461.163	8.86E-08	5.08E-06	6.53E-03	-	3,693,350	4,564,286	4,560,099	4,848,030	5,225,862
EF	19,039	30,572	48,200	NA	NA	NA	NA	NA	NA	NA	NA	NA	4,097,044	4,258,128	4,416,256
Forest - Mammoth															
FP	21,691	51,321	60,514	NA	NA	NA	NA	NA	NA	NA	NA	NA	3,964,778	4,099,507	4,488,670
Forest - Straight-tusked															
AN	30,443	36,225	50,900	NA	NA	NA	NA	NA	NA	NA	NA	NA	1,232,266	1,462,562	1,605,419
FN	*667*	*34,481*	*55,113*	*0.046*	*0.596*	*3.692*	*6.71E-07*	*8.65E-06*	*5.35E-05*	-	*1,131,527*	*1,747,291*	*1,142,365*	*1,656,158*	*16,775,616*
Forest - Mastodon															
AI	38,640	99,575	116,081	NA	NA	NA	NA	NA	NA	NA	NA	NA	6,302,709	6,370,936	11,508,128
FI	1,949	33,656	45,187	0.000	0.108	0.409	5.87E-12	1.61E-06	6.08E-06	2,565,517	7,562,562	11,242,118	11,288,424	11,861,084	14,794,089
Savanna - Asian															
BE	28,867	36,153	50,816	0.008	0.103	0.974	1.17E-07	1.42E-06	1.35E-05	1,099,754	3,264,039	4,209,606	4,629,310	4,863,054	5,693,350
CD	28,911	36,884	48,528	0.002	0.329	8.784	3.32E-08	4.46E-06	1.19E-04	786,453	3,914,039	4,622,167	4,647,291	4,841,379	5,396,305
Savanna - Mammoth															
BP	26,230	42,349	61,531	NA	NA	NA	NA	NA	NA	NA	NA	NA	4,550,493	4,712,315	4,916,749
BQ	*27,644*	*42,333*	*51,760*	*NA*	*NA*	*NA*	*NA*	*NA*	*NA*	*NA*	*NA*	*NA*	*4,635,714*	*4,808,374*	*4,985,222*
Savanna - Straight-tusked															
CN	29,865	41,292	57,979	NA	NA	NA	NA	NA	NA	NA	NA	NA	2,435,714	2,552,463	2,705,419
Savanna - Mastodon															
BI	27,652	37,053	40,265	0.000	0.010	0.355	7.54E-12	1.32E-07	4.79E-06	1,228,079	6,687,685	11,392,118	11,264,778	11,772,660	12,571,675
CI	26,790	35,824	44,440	0.000	0.015	0.637	5.03E-15	2.08E-07	8.89E-06	1,631,034	6,956,650	11,517,241	11,428,079	11,739,901	13,254,926
Asian - Mammoth															
DP	20,652	37,464	54,777	NA	NA	NA	NA	NA	NA	NA	NA	NA	2,464,778	2,547,291	2,649,754
EP	22,521	37,651	48,246	NA	NA	NA	NA	NA	NA	NA	NA	NA	2,450,985	2,509,113	2,634,236
Asian - Straight-tusked															

DN	25,312	39,071	54,817	NA	NA	NA	NA	NA	NA	NA	NA	NA	4,185,961	4,398,030	4,522,414
EN	23,018	38,034	55,669	0.003	0.291	387.773	3.48E-08	3.83E-06	5.10E-03	60,591	3,533,990	4,405,911	4,363,054	4,525,123	5,077,340
Asian - Mastodon															
DI	*24,346*	*39,258*	*54,604*	*0*	*0.104*	*1.18*	*6.29E-15*	*1.33E-06*	*1.50E-05*	*972,660*	*9,149,015*	*11,122,167*	*11,033,005*	*11,493,596*	*16,566,256*
Mammoth - Straight-Tusked															
NQ	*22,966*	*44,063*	*61,421*	*NA*	*NA*	*NA*	*NA*	*NA*	*NA*	*NA*	*NA*	*NA*	*4,468,966*	*4,589,901*	*4,750,493*

References

1. Debruyne R*, et al.* (2008) Out of America: ancient DNA evidence for a New World origin of Late Quaternary woolly mammoths. *Current Biology* 18(17):1320.
2. Enk J*, et al.* (2016) *Mammuthus* Population Dynamics in Late Pleistocene North America: Divergence, Phylogeography, and Introgression. *Frontiers in Ecology and Evolution* 4(42).
3. Rohland N*, et al.* (2007) Proboscidean Mitogenomics: Chronology and Mode of Elephant Evolution Using Mastodon as Outgroup. *Plos Biology* 5(8):e207.
4. Rohland N*, et al.* (2010) Genomic DNA sequences from mastodon and woolly mammoth reveal deep speciation of forest and savanna elephants. *PLoS Biol* 8.
5. Meyer M*, et al.* (2017) Palaeogenomes of Eurasian straight-tusked elephants challenge the current view of elephant evolution. *eLife* 6:e25413.
6. Fisher DC*, et al.* (2012) Anatomy, death, and preservation of a woolly mammoth (Mammuthus primigenius) calf, Yamal Peninsula, northwest Siberia. *Quaternary International* 255:94-105.
7. Haynes CV, Surovell TA, & Hodgins GWL (2013) The U.P. Mammoth Site, Carbon County, Wyoming, USA: More Questions than Answers. *Geoarchaeology* 28(2):99-111.
8. Claesson S, Baleka S, Hofreiter M, & Widga C (2017) The contribution of Late Pleistocene megafauna finds to submerged archaeology and the interpretation of ancient coastal landscapes. *Journal of Archaeological Science: Reports* 15:290-298.
9. Lynch Vincent J*, et al.* (2015) Elephantid Genomes Reveal the Molecular Bases of Woolly Mammoth Adaptations to the Arctic. *Cell Reports* 12(2):217-228.
10. Reddy PC*, et al.* (2015) Comparative sequence analyses of genome and transcriptome reveal novel transcripts and variants in the Asian elephant *Elephas maximus*. *Journal of Biosciences* 40(5):891-907.
11. Palkopoulou E*, et al.* (2015) Complete Genomes Reveal Signatures of Demographic and Genetic Declines in the Woolly Mammoth. *Current Biology* (25):1-6.
12. Bronk Ramsey C (2016) Bayesian Analysis of Radiocarbon Dates. *Radiocarbon* 51(1):337-360.
13. Reimer PJ*, et al.* (2013) *IntCal13 and Marine13 Radiocarbon Age Calibration Curves 0–50,000 Years cal BP*.
14. Meyer M & Kircher M (2010) Illumina sequencing library preparation for highly multiplexed target capture and sequencing. *Cold Spring Harbor Protocols* 2010(6):pdb. prot5448.
15. Kircher M, Sawyer S, & Meyer M (2012) Double indexing overcomes inaccuracies in multiplex sequencing on the Illumina platform. *Nucleic Acids Research* 40(1):e3-e3.
16. Karpinski E, Mead JI, & Poinar HN (2017) Molecular identification of paleofeces from Bechan Cave, southeastern Utah, USA. *Quaternary International* 443:140-146.
17. Li H & Durbin R (2009) Fast and accurate short read alignment with Burrows–Wheeler transform. *Bioinformatics* 25(14):1754-1760.

18. Kircher M (2012) Analysis of high-throughput ancient DNA sequencing data. *Ancient DNA*, (Springer), pp 197-228.
19. Li H*, et al.* (2009) The sequence alignment/map format and SAMtools. *Bioinformatics* 25(16):2078-2079.
20. Rogers RL & Slatkin M (2017) Excess of genomic defects in a woolly mammoth on Wrangel island. *PLOS Genetics* 13(3):e1006601.
21. Skoglund P*, et al.* (2014) Separating endogenous ancient DNA from modern day contamination in a Siberian Neandertal. *Proceedings of the National Academy of Sciences*.
22. Briggs AW*, et al.* (2010) Removal of deaminated cytosines and detection of in vivo methylation in ancient DNA. *Nucleic acids research* 38(6):e87-e87.
23. Meyer M*, et al.* (2012) A High-Coverage Genome Sequence from an Archaic Denisovan Individual. *Science* 338(6104):222-226.
24. Prufer K*, et al.* (2014) The complete genome sequence of a Neanderthal from the Altai Mountains. *Nature* 505(7481):43-49.
25. Patterson N*, et al.* (2012) Ancient admixture in human history. *Genetics* 192(3):1065-1093.
26. Katoh K, Misawa K, Kuma K, & Miyata T (2002) MAFFT: a novel method for rapid multiple sequence alignment based on fast Fourier transform. *Nucleic Acids Res* 30.
27. Katoh K & Standley DM (2013) MAFFT Multiple Sequence Alignment Software Version 7: Improvements in Performance and Usability. *Molecular Biology and Evolution* 30(4):772-780.
28. Stamatakis A (2014) RAxML version 8: a tool for phylogenetic analysis and post-analysis of large phylogenies. *Bioinformatics* 30(9):1312-1313.
29. Palkopoulou E*, et al.* (2013) Holarctic genetic structure and range dynamics in the woolly mammoth. *Proceedings of the Royal Society B: Biological Sciences* 280(1770).
30. Chang D*, et al.* (2017) The evolutionary and phylogeographic history of woolly mammoths: a comprehensive mitogenomic analysis. *Scientific Reports* 7:44585.
31. Krause J*, et al.* (2010) A Complete mtDNA Genome of an Early Modern Human from Kostenki, Russia. *Current biology : CB* 20(3):231-236.
32. Felsenstein J (1989) PHYLIP - Phylogeny Inference Package (Version 3.2). *Cladistics* 5:164-166.
33. Roca AL, Georgiadis N, Pecon-Slattery J, & O'Brien SJ (2001) Genetic Evidence for Two Species of Elephant in Africa. *Science* 293(5534):1473-1477.
34. Comstock KE*, et al.* (2002) Patterns of molecular genetic variation among African elephant populations. *Molecular Ecology* 11(12):2489-2498.
35. Roca AL, Georgiadis N, & O'Brien SJ (2007) Cyto-nuclear genomic dissociation and the African elephant species question. *Quaternary International* 169:4-16.
36. Ishida Y*, et al.* (2011) Reconciling Apparent Conflicts between Mitochondrial and Nuclear Phylogenies in African Elephants. *PLoS ONE* 6(6):e20642.

37. Shoshani J*, et al.* (2007) Relationships within the Elephantinae using hyoid characters. *Quaternary International* 169–170:174-185.
38. Todd NE (2010) New Phylogenetic Analysis of the Family Elephantidae Based on Cranial-Dental Morphology. *The Anatomical Record: Advances in Integrative Anatomy and Evolutionary Biology* 293(1):74-90.
39. Roca AL, Georgiadis N, & O'Brien SJ (2005) Cytonuclear genomic dissociation in African elephant species. *Nat Genet* 37(1):96-100.
40. Debruyne R (2005) A case study of apparent conflict between molecular phylogenies: the interrelationships of African elephants. *Cladistics* 21(1):31-50.
41. Landegren U, Nilsson M, & Kwok P-Y (1998) Reading Bits of Genetic Information: Methods for Single-Nucleotide Polymorphism Analysis. *Genome Research* 8(8):769-776.
42. Rishishwar L, Tellez Villa CE, & Jordan IK (2015) Transposable element polymorphisms recapitulate human evolution. *Mobile DNA* 6(1):21.
43. Kortschak RD, Adelson, D. L (bíogo: a simple high-performance bioinformatics toolkit for the Go language. *bioRxiv*.
44. Edgar RC & Myers EW (2005) PILER: identification and classification of genomic repeats. *Bioinformatics* 21(suppl_1):i152-i158.
45. Edgar RC (2004) MUSCLE: a multiple sequence alignment method with reduced time and space complexity. *BMC Bioinformatics* 5(1):113.
46. Edgar RC (2004) MUSCLE: multiple sequence alignment with high accuracy and high throughput. *Nucleic Acids Res* 32.
47. Kohany O, Gentles AJ, Hankus L, & Jurka J (2006) Annotation, submission and screening of repetitive elements in Repbase: RepbaseSubmitter and Censor. *BMC Bioinformatics* 7(1):474.
48. Gish W (1996-2004) *WU BLAST*.
49. Wheeler DL*, et al.* (2007) Database resources of the National Center for Biotechnology Information. *Nucleic Acids Research* 35(suppl_1):D5-D12.
50. Jurka J*, et al.* (2005) Repbase Update, a database of eukaryotic repetitive elements. *Cytogenet Genome Res* 110.
51. Altschul SF, Gish W, Miller W, Myers EW, & Lipman DJ (1990) Basic local alignment search tool. *Journal of Molecular Biology* 215(3):403-410.
52. Quinlan AR & Hall IM (2010) BEDTools: a flexible suite of utilities for comparing genomic features. *Bioinformatics* 26(6):841-842.
53. Swofford DL (2001) *Paup*: Phylogenetic analysis using parsimony (and other methods) 4.0.b5*.
54. Kuritzin A, Kischka T, Schmitz J, & Churakov G (2016) Incomplete Lineage Sorting and Hybridization Statistics for Large-Scale Retroposon Insertion Data. *PLOS Computational Biology* 12(3):e1004812.

55. Ivancevic AM, Walsh AM, Kortschak RD, & Adelson DL (2013) Jumping the fine LINE between species: Horizontal transfer of transposable elements in animals catalyses genome evolution. *BioEssays* 35(12):1071-1082.
56. Walsh AM, Kortschak RD, Gardner MG, Bertozzi T, & Adelson DL (2013) Widespread horizontal transfer of retrotransposons. *Proceedings of the National Academy of Sciences* 110(3):1012-1016.
57. Adelson DL, Raison JM, & Edgar RC (2009) Characterization and distribution of retrotransposons and simple sequence repeats in the bovine genome. *Proceedings of the National Academy of Sciences* 106(31):12855-12860.
58. Bhatia G, Patterson N, Sankararaman S, & Price AL (2013) Estimating and interpreting FST: The impact of rare variants. *Genome Research* 23(9):1514-1521.
59. Green RE*, et al.* (2010) A Draft Sequence of the Neandertal Genome. *Science* 328(5979):710-722.
60. Prufer K*, et al.* (2012) The bonobo genome compared with the chimpanzee and human genomes. *Nature* 486(7404):527-531.
61. Roca AL*, et al.* (2015) Elephant Natural History: A Genomic Perspective. *Annual Review of Animal Biosciences* 3(1):139-167.
62. Eggert LS, Rasner CA, & Woodruff DS (2002) The evolution and phylogeography of the African elephant inferred from mitochondrial DNA sequence and nuclear microsatellite markers. *Proceedings of the Royal Society of London Series B-Biological Sciences* 269(1504):1993-2006.
63. Eggert LS, Eggert JA, & Woodruff DS (2003) Estimating population sizes for elusive animals: the forest elephants of Kakum National Park, Ghana. *Molecular Ecology* 12(6):1389-1402.
64. Hoyle BG*, et al.* (2004) Late Pleistocene mammoth remains from Coastal Maine, USA. *Quaternary Research* 61(3):277-288.
65. Lister AM & Sher AV (2015) Evolution and dispersal of mammoths across the Northern Hemisphere. *Science* 350(6262):805-809.
66. Enk J*, et al.* (2011) Complete Columbian mammoth mitogenome suggests interbreeding with woolly mammoths. *Genome Biology* 12(5):1-8.
67. Reich D, Thangaraj K, Patterson N, Price AL, & Singh L (2009) Reconstructing Indian population history. *Nature* 461(7263):489-494.
68. Haubold B, Pfaffelhuber P, & Lynch M (2010) mlRho–a program for estimating the population mutation and recombination rates from shotgun-sequenced diploid genomes. *Molecular ecology* 19(s1):277-284.
69. Li H & Durbin R (2011) Inference of human population history from individual whole-genome sequences. *Nature* 475(7357):493-496.
70. Nadachowska-Brzyska K, Burri R, Smeds L, & Ellegren H (2016) PSMC analysis of effective population sizes in molecular ecology and its application to black-and-white Ficedula flycatchers. *Molecular Ecology* 25(5):1058-1072.

71. Fu Q*, et al.* (2014) Genome sequence of a 45,000-year-old modern human from western Siberia. *Nature* 514(7523):445-449.
72. Fernando P, Pfrender ME, Encalada SE, & Lande R (2000) Mitochondrial DNA variation, phylogeography and population structure of the Asian elephant. *Heredity* 84(3):362-372.
73. Fleischer RC, Perry EA, Muralidharan K, Stevens EE, & Wemmer CM (2001) Phylogeography of the Asian elephant (*Elephas maximus*) based on mitochondrial DNA. *Evolution* 55(9):1882-1892.
74. Vidya TNC & Sukumar R (2005) Social organization of the Asian elephant (Elephas maximus) in southern India inferred from microsatellite DNA. *J Ethol* 23.
75. Vidya TNC, Sukumar R, & Melnick DJ (2009) Range-wide mtDNA phylogeography yields insights into the origins of Asian elephants. *Proc R Soc B Biol Sci* 276.
76. Shoshani J & Tassy P (1996) *The Proboscidea: Evolution and Palaeoecology of Elephants and Their Relatives* (Oxford University Press, Oxford; New York).
77. Staab PR, Zhu S, Metzler D, & Lunter G (2015) scrm: efficiently simulating long sequences using the approximated coalescent with recombination. *Bioinformatics* 31(10):1680-1682.
78. Hudson RR (2002) Generating samples under a Wright-Fisher neutral model of genetic variation. *Bioinformatics* 18(2):337-338.
79. Brandt AL, Ishida Y, Georgiadis NJ, & Roca AL (2012) Forest elephant mitochondrial genomes reveal that elephantid diversification in Africa tracked climate transitions. *Molecular Ecology* 21(5):1175-1189.
80. Wasser SK, Shedlock AM, Comstock KE, Ostrander EA, & Mutayoba B (2004) Assigning African elephant DNA to geographic region of origin: applications to the ivory trade. *PNAS* 101.
81. Lei R, Brenneman RA, Schmitt DL, & Louis EE (2012) Genetic diversity in North American captive Asian elephants. *Journal of Zoology* 286(1):38-47.
82. Rasmussen M*, et al.* (2011) An Aboriginal Australian genome reveals separate human dispersals into Asia. *Science* 334(6052):94-98.
83. Csillery K, Francois O, & Blum MGB (2012) abc: an R package for approximate Bayesian computation (ABC). *Methods in Ecology and Evolution*:doi: 10.1111/j.2041-1210X.2011.00179.x.
84. Blum MGB & Francois O (2010) Non-linear regression models for Approximate Bayesian Computation. *Statistics And Computing* 20(1):63-73.
85. Sanders W.J. GE, Harris J.M., Saegusa H., Delmer C. (2010) *Proboscidea. In Cenozoic Mammals of Africa* (eds. L Werdelin, WJ Sanders. Berkeley: Univ. Calif. Press).
86. Dutheil JY*, et al.* (2009) Ancestral Population Genomics: The Coalescent Hidden Markov Model Approach. *Genetics* 183(1):259-274.

87. Aquadro CF, Begun DJ, & Kindahl EC (1994) Selection, Recombination, and DNA Polymorphism in Drosophila. *Non-Neutral Evolution: Theories and Molecular Data*, ed Golding B (Springer US, Boston, MA), pp 46-56.
88. Charlesworth B (2009) Background selection and patterns of genetic diversity in Drosophila melanogaster. *Genetical Research* 68(2):131-149.
89. Pool JE & Nielsen R (2007) Population size changes reshape genomic patterns of diversity. *Evolution* 61(12):3001-3006.
90. Laporte V & Charlesworth B (2002) Effective population size and population subdivision in demographically structured populations. *Genetics* 162(1):501-519.
91. Caballero A (1995) On the Effective Size of Populations with Separate Sexes, with Particular Reference to Sex-Linked Genes. *Genetics* 139(2):1007-1011.
92. Charlesworth B (2001) The effect of life-history and mode of inheritance on neutral genetic variability. *Genetical Research* 77(2):153-166.
93. Mailund T*, et al.* (2012) A New Isolation with Migration Model along Complete Genomes Infers Very Different Divergence Processes among Closely Related Great Ape Species. *PLoS Genet* 8(12):e1003125.